ANTI-INFLAMMATORY AND NEUROPROTECTIVE MECHANISMS OF REGULATOR OF G PROTEIN SIGNALING 10 (RGS10) IN MICROGLIA

by

MENBERE YISFASHEWA WENDIMU

(Under the Direction of Shelley B. Hooks)

ABSTRACT

Neurodegenerative diseases affect millions of people worldwide and are the leading cause of disability in older adults. Chronic neuroinflammation is an underlying mechanism for the initiation and progression of many neurodegenerative diseases, including Alzheimer's disease and Parkinson's disease. One of the key drivers of inflammatory response in the central nervous system is chronic activation of microglia cells. Activated microglia produce several neurotoxic factors, including prostaglandins, pro-inflammatory cytokines, and reactive oxygen species. Therefore, anti-inflammatory mechanisms that regulate microglia activation are therapeutic targets for neurodegenerative diseases. The Regulator of G protein signaling 10 (RGS10) is expressed in microglia, and loss of its expression during inflammation is associated with dysregulation of the microglial pro-inflammatory response and an increased risk of age-related neurodegeneration. However, the anti-inflammatory effect of RGS10 is mediated by an unknown mechanism, independent of its canonical role in G protein regulation. Therefore, while the protective functions of RGS10 position it as an anti-inflammatory target for neurodegenerative diseases, the lack of

information on its molecular mechanism limits its therapeutic potential. In this study, we used a combination of proteomics and signaling approaches and identified a biochemical and functional interaction between RGS10 and the endoplasmic reticulum (ER)-localized calcium sensor STIM2, which is an essential component of the store-operated calcium entry (SOCE) machinery. Furthermore, we determined that the SOCE pathway is required for the induction of pro-inflammatory genes in microglia and that the anti-inflammatory effects of RGS10 require a functional interaction with the SOCE machinery. In addition to its anti-inflammatory role, transcriptome analysis showed that RGS10 regulates a wide range of genes involved in stress response pathways and innate immune and viral defense processes, further suggesting additional neuroprotective functions. Overall, our study provides information on the protective mechanisms of RGS10, which has implications for many neurodegenerative diseases associated with chronic neuroinflammation.

INDEX WORDS: Microglia, Neuroinflammation, Neurodegenerative diseases (NDs), Regulator of G protein Signaling (RGS), G protein Signaling, G protein coupled receptors (GPCR), GTPase-activating proteins (GAP)s, Cyclooxygenase-2 (COX-2), Tumor-necrosis factor alpha (TNFα), Stromal Interaction Molecule 2 (STIM2), Store-operated calcium entry (SOCE)

ANTI-INFLAMMATORY AND NEUROPROTECTIVE MECHANISMS OF REGULATOR OF G PROTEIN SIGNALING 10 (RGS10) IN MICROGLIA

by

MENBERE YISFASHEWA WENDIMU

BS., Colby-Sawyer College, 2016

A Dissertation Submitted to the Graduate Faculty of The University of Georgia in Partial Fulfillment of the Requirements for the Degree

DOCTOR OF PHILOSOPHY

ATHENS, GEORGIA

2022

ANTI-INFLAMMATORY AND NEUROPROTECTIVE MECHANISMS OF REGULATOR OF G PROTEIN SIGNALING 10 (RGS10) IN MICROGLIA

by

MENBERE YISFASHEWA WENDIMU

Major Professor:	Shelley B. Hooks
Committee:	Eileen Kennedy
	James Franklin
	Walter Schmidt
	Jae-Kyung Lee

Electronic Version Approved:

Ron Walcott
Vice Provost for Graduate Education and Dean of the Graduate School
The University of Georgia
May 2022

DEDICATION

To my father

Yisfashewa Wendimu

1953-2016

Thank you, Dad, for your endless love and support. I would not be here if it weren't for your constant prayers and emotional and financial support for my education. I am grateful for all the special memories we shared together. The words of wisdom you shared with me have kept me motivated throughout this difficult but rewarding journey. I wish you were physically present to celebrate this milestone, but I am sure you’re proud of everything we accomplished together. I am forever grateful to God for giving me such a strong and supportive father. Rest in Peace!

ACKNOWLEDGEMENTS

The completion of this dissertation would not have been possible without the guidance and expertise of my excellent Ph.D. supervisor, Dr. Shelley Hooks. She exemplifies what it means to be an excellent mentor by remaining patient, empathetic, and optimistic throughout the ups and downs of my research career. I would also like to express my gratitude to the members of my dissertation committee, Dr. Eileen Kennedy, Dr. James Franklin, Dr. Walter Schmidt, and Dr. Jae-Kyung Lee, for providing constructive feedback and for supporting me with my career transition.

I am grateful to the members of Hooks Lab, past and present, for their kindness and support, especially Mohammed, Ellen, and Faris, who have made significant contributions to my research. I also thank our collaborators in the Grimsey Lab, Moreno Lab, Yao Lab, and Wohlschlegal Lab who have assisted me with experiments. I also acknowledge the Graduate School, the PBS department, Molly Blank Foundation and the LaRocca family for their monetary assistance, and the PBS administrative staff, Julie, and others, for their administrative support. Also, special thanks to my graduate school friends Lishann, Lillie, Wided, Chelsea, and Rajani for being there for me.

There are many people I am grateful for outside of UGA; in particular, my undergraduate biology professor Bill Thomas encouraged me to apply for a Ph.D. program and believed in my scientific potential. Thank you to my family and friends who supported me from afar; especially my amazing mom Mulumebet Demma, my siblings – Bilen, Kidest, Brucktawit, Michael, and Fikerte, my uncle Meheret's family, and my friends Nahom, Rackeb, Ramsha, Amna, and many others in the US and abroad. Thank you all for your love and support. Above all, I would like to thank God, whose endless love, guidance, and blessing has made me who I am today.

TABLE OF CONTENTS

Page

LIST OF TABLES

Page

LIST OF FIGURES

Page

CHAPTER 1

MICROGLIA PHENOTYPES IN AGING AND NEURODEGENERATIVE DISEASES [1]

[1] **Wendimu, Menbere Y**., Hooks, Shelley. B. Submitted to *Cells,* April 15, 2022

Abstract

Neuroinflammation is a hallmark of many neurodegenerative diseases (NDs) and plays a fundamental role in mediating the onset and progression of disease. Microglia, which function as first-line immune guardians of the central nervous system (CNS), are the central drivers of neuroinflammation. Numerous human postmortem studies and in vivo imaging analyses have shown chronically activated microglia in patients with various acute and chronic neuropathological diseases. While microglial activation is a common feature of many NDs, the exact role of microglia in various pathological states is complex and often contradictory. However, there is a consensus that microglia play a biphasic role in pathological conditions, with both detrimental (M1-like) and protective (M2-like) phenotypes, and the overall response of microglia and the activation of different phenotypes depends on the nature and duration of the inflammatory insult, as well as the stage of disease development. This review provides a comprehensive overview of current research on the various microglia phenotypes and inflammatory responses in health, aging, and NDs, with a special emphasis on the heterogeneous phenotypic response of microglia in acute and chronic diseases such as hemorrhagic stroke (HS), Alzheimer's disease (AD), and Parkinson's disease (PD). The primary focus is on translational research in preclinical animal models and bulk/single-cell transcriptome studies in human postmortem samples. Additionally, this review covers key microglial receptors and signaling pathways that are potential therapeutic targets for modulating microglial inflammatory responses during aging and in NDs. Additionally, age, sex, and species-specific microglial differences will be briefly reviewed.

1.1. Microglia in physiology

Microglia origin, development, and maturation

Microglia are resident immune cells of the central nervous system (CNS) with specialized macrophage-like functions. After decades of controversy, a series of parabiosis, transplantation, and lineage tracing experiments have confirmed that microglia and blood monocytes have distinct developmental origins (Ajami et al., 2007; Alliot et al., 1999; Ginhoux et al., 2010; Goldmann et al., 2016) (For historical reviews, see (Ginhoux & Garel, 2018)). Unlike circulating monocytes with blood-derived myeloid lineages (Fogg et al., 2006), microglia and most tissue macrophages emerge exclusively from erythromyeloid progenitors in the yolk sac (YS) that differentiate into YS macrophages during embryonic development (Alliot et al., 1999; Goldmann et al., 2016). These precursor YS macrophages migrate to/and colonize the CNS parenchyma prior to the maturation of the blood-brain barrier and subsequently differentiate to microglia (Ginhoux et al., 2010; Goldmann et al., 2016; Gomez Perdiguero et al., 2015; Monier et al., 2007).

After colonizing the CNS, microglia maintain their population through self-renewal and become ubiquitously distributed in nonoverlapping fields (Ajami et al., 2007; Monier et al., 2007), accounting for 0.5-16% and 5-12% of total cells in mouse and human brains, respectively (Lawson et al., 1990; Mittelbronn et al., 2001). Microglia maintain a steady number of cells during lifetime by a dynamic and finely regulated balance between local proliferation and apoptosis, without the contribution of peripheral progenitors (Askew et al., 2017). According to some studies, microglia exhibit regional heterogeneity within the CNS and are abundant in some anatomical regions, including the hippocampus, basal ganglia, and substantia nigra, but are sparse in brain stem cells and cerebellum (Lawson et al., 1990; Mittelbronn et al., 2001). The relative density of microglia

in the white and gray matter has been observed to vary between species; white matter of the human cortex exhibits higher microglia density than gray matter (Mittelbronn et al., 2001), while gray matter of the mouse cortex has higher density of microglia (Lawson et al., 1990). Dos Santos et al. (2020) recently challenged the idea that microglia have species-specific distribution, demonstrating that microglia density differs little across different brain structures and mammalian species (Dos Santos et al., 2020).

As microglia mature in the CNS, they exhibit some characteristics that distinguish them from precursor cells, such as downregulation of certain cell surface proteins, such as cluster of differentiation 45 (CD45) and MHC class II molecules (MHCII), and expression of unique microglia signature genes, including transmembrane protein 119 (TMEM119), P2Y purinergic receptor 12 (P2RY12), and Sal-like protein (SALL1) (Bennett et al., 2016; Butovsky et al., 2014; Buttgereit et al., 2016; Li & Barres, 2018). Microglia development, differentiation, and maintenance in the CNS are regulated by a variety of factors, such as cell-cell interaction between microglia and neurons. Interactions between the microglial colony stimulating factor-1 receptor (CSF1R) and neuron-derived secreted ligands, IL-34 and CSF-1, are critical for microglial development and survival (Easley-Neal et al., 2019; Elmore et al., 2014; Wang et al., 2012), while interaction between the microglial CX3-chemokine receptor 1 (CX3CR1) and the neuronal ligand CX3CL1 regulates their proliferation and activation (Hatori et al., 2002; Pawelec et al., 2020).

Microglia functions in physiology

Microglia are the immune guardians of the brain that play a critical role in providing host defense against pathogens and CNS disorders (Nimmerjahn et al., 2005). Additionally, microglia perform essential housekeeping functions, such as maintaining CNS homeostasis during

development, adulthood, and aging (Schwartz et al., 2013). During development, they play an essential role in the regulation of neurogenesis and neuronal survival by phagocytosing newborn apoptotic cells, removing excess synaptic connections, and secreting neurotrophic mediators such as insulin-like growth factor-1 (IGF-1), transforming growth factor- β (TGF-β), and brain-derived neurotrophic factor (BDNF) (Parkhurst et al., 2013; Ueno et al., 2013). Microglia are also essential for maintaining brain homeostasis in the adult brain; They provide neuronal support, promote oligodendrocyte development and myelination, phagocytose excess metabolic products and damaged tissues, and play a critical role in learning by regulating synaptic pruning and remodeling of neuronal circuits (Butovsky & Weiner, 2018).

Microglia morphologies

In a healthy brain and under normal conditions, microglia exhibit a ramified morphology with numerous long, thin, and highly branched processes (Boche et al., 2013). Ramified microglia were long thought to be in a 'resting state' until advances in molecular tools such as in vivo two-photon imaging revealed the highly motile nature of microglial protrusions with unique abilities to extend and retract, allowing them to actively survey, detect, and respond to environmental aberrations (Davalos et al., 2005; Nimmerjahn et al., 2005) Transcriptome analysis demonstrated that microglia with ramified morphology largely express genes associated with steady-state brain functions such as synaptic integrity, neuronal maturation, and overall maintenance of cell homeostasis (Parakalan et al., 2012). The branched processes of microglia enable them to perform these essential functions, as they allow microglia to constantly interact with neurons and other glial cells, either through direct contact or through secreted mediators (Cserep et al., 2020; Davalos et al., 2005; Nimmerjahn et al., 2005). Upon detecting environmental changes, microglia rapidly

migrate toward the triggering stimuli via their branched processes, aided by chemotactic cues (Boche et al., 2013). Microglial activation is commonly accompanied by a morphological transformation from a ramified state to an amoeboid state, characterized by an enlarged cell body, shorter processes, and the presence of numerous cytoplasmic vacuoles (Kaur et al., 1985; Madore et al., 2013; Nimmerjahn et al., 2005). Morphological transformation in activated microglia also accompany functional responses such as migration, antigen presentation, and phagocytosis (Parakalan et al., 2012).

Along with the well-known ramified and amoeboid morphologies, other microglia phenotypes have been characterized through ultrastructural studies (Savage et al., 2018; Sierra et al., 2016). A biopolar/rod-shaped morphology is described as a transition state between ramified and amoeboid states (Au & Ma, 2017), and this microglia phenotype exhibits distinct transcriptome profiles and a high proliferative and phagocytic ability (Tam & Ma, 2014; Ziebell et al., 2012). Activated microglia with these morphological features have been characterized mostly in the aged brain and in neuropathological conditions where they closely align with and surround injured axons, generally assuming neuroprotective roles (Bachstetter et al., 2017; Bachstetter et al., 2015; Taylor et al., 2014; Ziebell et al., 2012). Additionally, bipolar/rod-shaped microglia are involved in other essential functions such as synaptic stripping, which supports rewiring of neuronal circuits (Au & Ma, 2017). Other microglial morphologies have also been reported, including hypertrophic microglia, dystrophic (senescent) microglia, satellite microglia, gitter cell-like microglia, and dark microglia (Savage et al., 2018).

1.2. Microglia activation and polarization

Microglia express various immune pattern recognition receptors (PRRs), including toll-like receptors (TLRs), nucleotide-binding oligomerization domain (NOD)-like receptors (NLRs), and scavenger receptors (SRs)(Doens & Fernandez, 2014). PRRs recognize exogenous pathogenic molecules known as pathogen-associated molecular patterns (PAMPs) or endogenous host-derived molecules known as damage-associated molecular patterns (DAMPs) (Ransohoff & Brown, 2012; Zindel & Kubes, 2020). PAMPs and DAMPs have distinct responses; PAMPs induce an antimicrobial response and inflammation in response to infection, while DAMPs drive sterile inflammation in response to CNS injuries such as trauma, hypoxia, and NDs (Broggi & Granucci, 2015). When microglial PRRs interact with PAMP/DAMPs, a variety of intracellular cascades, kinases, and downstream transcription factors are activated, ultimately leading to the synthesis of molecular mediators of inflammation and other cellular responses (Broggi & Granucci, 2015; Ransohoff & Brown, 2012).

Microglia activation is associated with changes in the expression of cell surface receptors, unique polarization responses, and the release of a variety of inflammatory mediators that contribute to either a tissue reparative protective role or a detrimental neurotoxic response. Although oversimplified, activation of microglia is frequently defined in terms of two broad polarization states: a classically activated M1-like phenotype or an alternatively activated M2-like phenotype. These polarization states differ in the triggering stimuli, expression of phenotypic markers, and secreted mediators, all of which determine the overall outcome. In general, the classically activated M1 phenotype is associated with pro-inflammatory and neurotoxic responses,

while the M2 phenotype mostly mediates anti-inflammatory and neuroprotective functions (Tang & Le, 2016). (**Figure 1.1**).

The M1 microglia phenotype is induced in vitro by interferon-γ (IFNγ) and/or the gram-negative bacterial endotoxin lipopolysaccharide (LPS). LPS is a ligand for Toll-like receptor 4 (TLR4) which couples with coreceptors to activate various pro-inflammatory transcription factors including NFκB, AP1, STAT5 and IRFs, via TIR domain-containing adapter inducing IFNβ (TRIF) and myeloid differentiation primary response protein 88 (MyD88)-dependent pathways (Goulopoulou et al., 2016; Platanitis & Decker, 2018). IFNγ acts on IFNγ receptors 1 and 2 (IFNγR 1/2) and activates the JAK/STAT pathway that leads to the phosphorylation and nuclear translocation of STAT1 and other IRFs (Ivashkiv, 2018) Transcription factors activated by M1 microglia trigger upregulation of pro-inflammatory cell surface markers, such as MHCII and the cluster of differentiation marker 86 (CD86)(Boche et al., 2013; Chhor et al., 2013) Additionally, they induce the production of a variety of pro-inflammatory mediators, including cytokines, such as tumor necrosis factor-α (TNFα) and interleukins (IL-1β, IL-6, IL-12, IL-17, IL-18, IL-23), chemokines such as CCL12 and CXCL10, and other pro-inflammatory mediators, including reactive oxygen and nitrogen species (ROS and RNS), inducible nitric oxide synthase (iNOS) and cyclooxygenase-2 (COX-2)(Chauhan et al., 2021; Chhor et al., 2013; Franco & Fernandez-Suarez, 2015; Nakagawa & Chiba, 2015). M1 microglia play an important role in eliciting innate immune responses to combat foreign pathogens and trigger the adaptive immune response (Lehnardt, 2010). However, chronic activation in pathological conditions contributes to neuroinflammation, oxidative stress, and neurotoxicity (Lehnardt, 2010; Song & Suk, 2017) (**Figure 1.1**; left side).

M2 polarized microglia can assume an ‘alternatively activated,’ or ‘acquired deactivation’ state, and are often associated with functions such as immune resolution and tissue repair through the secretion of anti-inflammatory and neurotrophic factors (Song & Suk, 2017; Subramaniam & Federoff, 2017; Tang & Le, 2016). M2 microglia can be activated by four major anti-inflammatory cytokines, IL-4, IL-10, IL-13, and TGF-β. IL-4 and IL-13 promote the alternative activation state, and generally function to antagonize M1 pro-inflammatory responses such as the production of TNFα, IL-6, and iNOS (Gadani et al., 2012; Jurga et al., 2020). The multifunctional cytokine TGF-β plays a pivotal role in angiogenesis, immunoregulation, and tissue repair, and together with IL-10, it induces the acquired deactivation state (Tang & Le, 2016). The M2 phenotypes are subclassified into three states, M2a, M2b, and M2c, which have overlapping biochemical roles but differ in the activating stimuli, marker expression, and mechanism of actions (Franco & Fernandez-Suarez, 2015). (**Figure 1.1**; right side).

M2a is considered an anti-inflammatory, phagocytic, and wound healing phenotype, and is activated upon stimulation with IL-4 or IL-13 cytokines (Song & Suk, 2017). This is accompanied by the activation of the JAK1/3-STAT6 pathway leading to the upregulation of cell surface markers CD206 (mannose receptor), Arg1 (arginase-1), YM1 (chitinase-like protein), Fizz1 (found in inflammatory zone 1), and different scavenger receptors (SRs)(Boche et al., 2013; Nakagawa & Chiba, 2015). The M2a phenotype is involved in immunity against parasites, collagen formation, and tissue repair (Chhor et al., 2013). M2b microglia, also known as type II, is generally characterized as an inflammation regulatory phenotype, and is activated by fusion of TLRs and FCγ receptors, and subsequent interaction of these receptors with B cell-derived IgG (Anderson & Mosser, 2002; Clynes et al., 1999; Swisher et al., 2014). M2b polarized microglia

share similar characteristics as M1 microglia in that both can be activated by TLR agonists and are characterized by the expression of COX-2 and M1-associated cell surface proteins CD86 and MHCII(Edwards et al., 2006; Mosser & Edwards, 2008). However, M2b microglia also have different responses, such as the recruitment of regulatory T cells and the release of the anti-inflammatory cytokine IL-10 (Edwards et al., 2006). IL-10, along with TGF-β and glucocorticoids, triggers the activation of the immunosuppressive M2c phenotype (Chhor et al., 2013; Mecha et al., 2015). M2c polarized microglia exhibit an 'acquired deactivation' state and play a prominent role in matrix remodeling, tissue repair, and immunoregulation (Boche et al., 2013; Chhor et al., 2013). IL-10-induced M2c polarization is mediated by interaction with the IL-10R1 and IL-10R2 receptors and subsequent activation of the JAK1/STAT3 pathway. This leads to the upregulation of the cell surface marker CD163, and TGF-β and IL-10 cytokines, and inhibition of M1-associated pro-inflammatory cytokines (Chhor et al., 2013; Franco & Fernandez-Suarez, 2015).

Microglia are capable of dynamically shifting polarization states between M1 and M2 phenotypes. Rather than employing two distinct activated states, the M1 and M2 represents a continuous spectrum of various activation phenotypes, and the different phenotypic markers can co-exist together, suggesting several intermediate phenotypes (Song & Suk, 2017). Advances in genome-wide expression profiling studies have further elucidated the biological complexity of microglial polarization response in which mixed phenotypes with simultaneous expression of M1 and M2 markers are evident, prominently in aging and pathological disease models (Chiu et al., 2013; Grabert et al., 2016; Wes et al., 2016). For example, the presence of a mixed transitional phenotype known as Mtran has been demonstrated in a traumatic brain injury (TBI) model in which a significant proportion of TGF-β (M2 marker)-positive microglia also coexpressed the M1

marker CD16/32 (Kumar et al., 2016). An intermediate polarization state termed 'M1 ½' has also been reported in rd1 retinal degeneration mouse model (Zhou et al., 2017). Recently, an atypical M2d phenotypic state has been described which is induced by transforming the M1 phenotype into a pro-angiogenic/anti-inflammatory M2 activated phenotypic state, and this phenotypic switch is mediated by coactivation with TLR ligands and the adenosine A2A receptor (A2AR)(Ferrante & Leibovich, 2012; Ferrante et al., 2013). This polarization phenotype is explored primarily in tumor-associated macrophages and its significance in microglia is unclear.

The highlighted studies demonstrated that the oversimplified M1/M2 paradigm, which was largely understood through in vitro assays, does not accurately model the complexity of microglia phenotypes in vivo, where the response of microglia is dictated by intricate interaction with the brain microenvironment. However, the broad binary characterization of microglia phenotypes still provides valuable insight into the pro-inflammatory and anti-inflammatory nature of microglia with both beneficial and neurotoxic functions. The overall contribution of microglia in the normal and diseased brain and the transition between different phenotypic states depend on the activating mechanism, the duration of the signal, and the regulatory signaling molecules (L'Episcopo et al., 2018; Zhang, 2019) . A select few modulatory factors are discussed in Section 7.

1.3. Microglia phenotypes in aging

In recent years, there has been increasing interest in identifying aging-associated changes in microglial activation, function, and molecular signatures. There are limited aging studies in human microglia, as there is shortage of postmortem human brain samples and lack of noninvasive imaging and genetic manipulation tools to visualize and characterize live human microglia. Additionally, aging research is expensive and time-consuming due to the long waiting period for

the natural aging process to take place in preclinical models. Therefore, despite recent advances in transcriptomics and live imaging methodologies (Eme-Scolan & Dando, 2020; Gerrits et al., 2020), our current understanding of microglial responses in aging is largely derived from studies using transgenic model organisms with accelerated ageing to mimic the natural process of aging.

Growing evidence suggests that during aging, microglia undergo a morphological transition from a ramified state to a spheroid-activated phenotype with abnormal cytoplasmic structure and fragmented processes associated with microglial dystrophy (Koellhoffer et al., 2017; Spittau, 2017; Streit et al., 2004). In vivo positron emission tomography (PET) imaging of human brains using the PET ligand (R)-[11C]PK11195 showed a widespread distribution of activated microglia in human cortical and subcortical regions during healthy aging (Schuitemaker et al., 2012). Aged microglia also exhibit an inflammatory hypersensitive phenotype, often referred to as 'primed microglia'(Holtman et al., 2015; Norden & Godbout, 2013). Primed microglia are overreactive to inflammatory and neurotoxic insults, and produce large amounts of pro-inflammatory cytokines, chemokines, and reactive species (Norden & Godbout, 2013) (**Figure 1.2**).

Some studies have also examined microglial polarization responses associated with age. Recently, Wang et al. (2019) compared microglial M1/M2 markers in 2, 6, 18 and 28-month-old rat brains, and observed an age-dependent increase in transcript and protein levels of M1 markers (TNFα and IL-1β) and an opposite trend in M2 marker expression (Arg1 and IL-10)(Wang et al., 2019). The observed increase in M1/M2 marker ratio also correlated with age-induced DA neuronal loss. Relative loss of the M2 phenotype has also been reported in aging mice, as demonstrated by suppressed anti-inflammatory IL-4/IL-13 signaling (Lee et al., 2013). Increased M1-microglia responses such as upregulation of TLRs, various activation markers (MHCII, CD68,

and CD86), and microglia/macrophage-specific inflammatory receptors CD11b are also evident in aged brains of rodents, canines, humans, and non-human primates (Frank et al., 2006; Godbout et al., 2005; Hart et al., 2012; Letiembre et al., 2007; Norden & Godbout, 2013; Streit et al., 2004; VanGuilder et al., 2011). These results suggest that aged microglia have a predominant M1 phenotype associated with neurotoxic responses.

Age-associated loss of endogenous microglia regulatory pathways has been implicated as a mechanism for the presence of reactive microglia in the aged brain. For example, impaired TGFβ-signaling, a pathway that promotes microglia quiescence, has been reported in the aged brain and is associated with a reduction in the protective function of microglia (Tichauer et al., 2014; Zoller et al., 2018). Furthermore, downregulation of microglial receptors involved in microglia-neuron interactions is prominent in the aged brain, such as the P2Y purinergic receptor 12 (P2Y12R), which is a key regulator of microglial activation and phenotypic transformation (Lopes et al., 2022). Similarly, age-related neurodegeneration leads to the loss of neuron-derived immunomodulatory molecules, such as the CX3CL1 ligand, which keeps microglia in a quiescent state (Bachstetter et al., 2011). These alterations in endogenous regulatory factors contribute to chronic activation, microglial dystrophy, and neurodegeneration ***(*Figure 1.2)**.

Transcriptome studies have allowed researchers to characterize global gene expression changes associated with aging. A recent postmortem study by Soreq et al. (2017) analyzed the transcriptome profiles of glial and neuronal cell types in different regions of the human brain in 480 subjects aged 16 to 106 years and observed an increase in microglia-specific genes in all regions of the brain that strongly predict biological aging, such as upregulation of complement molecules and inflammatory responses (Soreq et al., 2017). A separate study also identified

signature genes involved in normal aging, such as high expression of genes encoding TNF family ligands, vesicle release proteins, and the pro-inflammatory cytokine high mobility group box 1 (HMGB1)(Orre et al., 2014). HMGB1 mediates microglia priming in aged brain, and its inhibition is known to desensitize aged microglia to an inflammatory insult .

A transcriptomic coexpression meta-analysis by Holtman et al. (2015) also examined changes in microglia signatures in four mouse models of aging and NDs (Holtman et al., 2015). They compared normal aged mice, $Ercc1^{ko}$ accelerated aging mice with loss of DNA repair mechanism, and transgenic models of Alzheimer's disease (AD) and Amyotrophic Lateral Sclerosis (ALS). Their study identified common microglial inflammatory gene networks shared across normal aging and in pathological models that mediate age-associated microglial priming. Unlike LPS-induced upregulated acute inflammatory gene networks, such as activation of NFκB signaling, primed microglia of these aging models displayed upregulated expression of MHCII and other pro-inflammatory genes encoding cell surface markers CD11c integrins and CXC-chemokine receptor 4 (CXCR4). Most of these signature primed microglia gene networks were involved in functions related to lysosome, phagosome, oxidative phosphorylation, and antigen presentation, indicating that aged microglia have impaired immune regulation and phagocytosis response.

In a healthy developing brain, one of the main housekeeping functions of microglia is the pruning of synapses through a phagocytic clearance process. This is mediated primarily through a mechanism involving the recognition of complement proteins on synapses via microglial complement receptors (Stevens et al., 2007). However, it is known that complement-mediated clearance mechanisms are normally lost in healthy adult microglia but later reemerge during the aging process, leading to a dysfunctional microglial phenotype that can contribute to synaptic loss

and neurodegeneration (Schartz & Tenner, 2020) ***(*Figure 1.2)**. For example, C1q and C3 complement proteins are evident in the aging brain and are deposited on synapses and can activate C1qR and C3R phagocytic complement receptors expressed on microglia and subsequently trigger clearance of healthy synapses (Reichwald et al., 2009; Rupprecht et al., 2021; Rutar et al., 2014; Stephan et al., 2013). These findings implicate a detrimental role for complement-mediated phagocytosis in aging that can contribute to neurodegeneration.

Age-associated functional change in the brain is also associated with dysregulation of calcium signaling(Chandran et al., 2019; Olmedillas Del Moral et al., 2019), which can lead to a variety of neuropathological conditions. Calcium homeostasis is impaired in the aged brain due to age-dependent deregulation of important calcium channels and dysfunction in mitochondria and the endoplasmic reticulum (ER)(Chandran et al., 2019). Microglia express various plasma membrane ionotropic and metabotropic receptors that are coupled to changes in intracellular calcium levels $[Ca^{2+}]_i$, including two main classes of nucleotide receptors, purinergic P2X receptors and P2Y receptors (Eyo et al., 2013; Koizumi et al., 2007). Changes in Ca^{2+} response triggered either by activation of these receptors or indirectly by other signaling pathways play an essential role in regulating various executive functions of microglia such as phagocytosis and inflammatory responses (Brawek & Garaschuk, 2013; Farber & Kettenmann, 2006). Visualization of live microglial Ca^{2+} dynamics is increasingly being used to study functional and morphological changes in the intact brain (Brawek et al., 2017; Eichhoff et al., 2011; Olmedillas Del Moral et al., 2019). Recently, Olmedillas del Moral et al. (2019) used high-resolution two-photon microscopy and in vivo Ca^{2+} imaging to compare changes in the functional properties of cortical microglia in three different cohorts of mice: young (2-4 months old), middle-aged (9-11 months old), and old

(18–21 months old)(Olmedillas Del Moral et al., 2019). Their study revealed two distinct phenotypes of aging microglia. Middle-aged microglia exhibited a reactive 'immune-alert' phenotype, characterized by normal process motility and increased spontaneous $[Ca^{2+}]_i$ signaling, while microglia from older mice showed a reduced Ca^{2+} response and disorganized motility, resembling a dysfunctional/senescent phenotype. In addition to alterations in Ca^{2+} responses in the aging brain, Ca^{2+} dysregulation is also prominent in response to injury, inflammation, and neurodegenerative diseases (Brawek et al., 2014; Pozner et al., 2015). Overall, the evidence reviewed here suggests that age-associated impairment of microglial responses throughout life contributes to the development of neurodegenerative diseases **(Figure 1.2)**.

1.4. Microglia in acute and chronic neurodegenerative diseases

The next sections will review the complex microglial phenotypes and functions in three neurodegenerative diseases, hemorrhagic stroke, Alzheimer's disease, and Parkinson's disease, focusing on the specific microglial response that is shaped by the underlying pathology.

1.4.1. Microglia in Hemorrhagic Stroke

Hemorrhagic stroke (HS) is primarily caused by a rupture of blood vessels that results in bleeding within or surrounding the brain parenchyma (Lan et al., 2017; Montano et al., 2021). There are two main subtypes of HS: intracerebral hemorrhage (ICH-within the brain) and subarachnoid hemorrhage (SAH-surrounding the brain). HS is known for its high mortality and morbidity, with more than 50,000 annual deaths reported in the US (Unnithan & Mehta, 2022). In particular, ICH has the highest mortality rate: approximately 30-50% of patients die within the first month, and most of the surviving patients experience long-term disability (Montano et al., 2021; Unnithan & Mehta, 2022). The incidence of HS increases with age as the two main

predisposing factors, chronic hypertension and amyloid angiopathy, are more prominent in the elderly (Hemphill et al., 2001; Unnithan & Mehta, 2022).

Although HS is considered a cerebrovascular disease, it can cause acute tissue destruction, hematoma formation, and elevation of intracranial pressure, which can lead to brain damage (Aronowski & Zhao, 2011; Chen et al., 2014). Immediate neuronal death in the acute phase of injury subsequently triggers secondary brain damage. Currently, there is no cure for hemorrhagic stroke, and treatment options are limited primarily to supportive care (Hemphill et al., 2015; Thabet et al., 2017). Therefore, there is an urgent need to characterize the molecular mechanism of HS and identify therapeutic targets underlying early and delayed brain injury. In HS, one of the key players in secondary neurodegeneration is chronic neuroinflammation, and therefore promising immunotherapeutic approaches have been considered to mitigate inflammation-induced neurodegeneration (Tschoe et al., 2020).

Microglia activation in HS

Microglia and infiltrating macrophages are one of the first immune respondents after ICH, and thus play a fundamental role in disease progression (Taylor & Sansing, 2013). In the hemorrhagic brain, numerous molecular mediators trigger microglial activation, including complement components, coagulation factors, and blood-derived hematoma products (Babu et al., 2012; Zhou et al., 2014). Microglia activation is a prominent feature of HS, and its activation response has been studied in patients and experimental models. Studies in a collagenase-injection ICH model demonstrated an increased in microglia/macrophage population in the acute stage of injury (days 1-3) and a gradual decline to baseline levels after 21 days (Wang et al., 2003; Wang & Tsirka, 2005). Activated microglia populations were observed as early as 1 hour after ICH and this

activation response is prominent in the perihematomal region surrounding the injury site (Wang & Dore, 2007). In an autologous blood injection model of ICH, microglia activation is evident beginning at 4 h after insult and persisted up to 4 weeks, with a peak density observed 2-3 days after injury (Xue & Del Bigio, 2000, 2003; Zhou et al., 2014). A contrasting finding using the same ICH model showed a delayed peak in maximal activation which occurs in the subacute stage of injury around days 7-10 (d7-10) (Gong et al., 2000). Although the use of specific microglial markers and experimental models has led to discrepancies in observations, collective evidence suggests an early microglial recruitment and activation response in HS that changes throughout the course of the disease.

Microglia activation by components of hematoma

HS induces the lysis of red blood cells (RBCs) and the release of hemoglobin, accompanied by the subsequent production of free heme (Babu et al., 2012; Zhou et al., 2014). In the brain, elevated concentrations of hemoglobin, heme, and its oxidized form hemin trigger brain injury by inducing microglial activation, neuroinflammation, oxidative stress, and edema formation (Aronowski & Zhao, 2011; Babu et al., 2012; Righy et al., 2018; Robinson et al., 2009). Heme metabolism in microglia plays a diverse role in HS. Phagocytic microglia can help sequester large amounts of extracellular heme (Fang et al., 2014; Li et al., 2021; Yang et al., 2015), thereby limiting its neurotoxic effect to other cell types. However, uptake of excess heme/hemin can cause accumulation of toxic heme degradation products in microglia that can exacerbate HS injury (Babu et al., 2012; Robinson et al., 2009). Hematoma components modulate microglia activity by activating specific receptors and inflammatory pathways. In particular, heme-induced inflammatory damage is believed to occur primarily through TLR4, and this receptor is

upregulated in microglia in response to ICH and exogenous heme treatment (Lin et al., 2012; Teng et al., 2009) (Lin et al., 2012; Teng et al., 2009). Heme-induced TLR4 activation, in turn, activates NFκB and promotes pro-inflammatory signaling via MyD88/TRIF pathway (Teng et al., 2009).

After brain hemorrhage, heme processing enzymes are upregulated in microglia, including heme oxygenase-1 (HO-1), which is an inducible rate-limiting enzyme that converts heme/hemin to carbon monoxide, biliverdin and ferrous iron (Matz et al., 1996; Wang & Dore, 2007). Since HO-1 exerts its effect through these various metabolites, its exact role after ICH is not clear. Carbon monoxide and biliverdin mainly mediate antioxidant and neuroprotective effects, while ferrous iron is largely associated with tissue damage (Li et al., 2018). Like heme, iron can induce microglia activation through the TLR4/Myd88/TRIF pathway (Lin et al., 2012). After ICH injury, HO-1 is induced in both microglia and astrocytes, and its expression changes during disease progression (Nakaso et al., 2000). Recent studies showed that HO-1exerts its neurotoxic effects in the early stages of injury, at which time its expression is higher in microglia, while it primarily mediates its neuroprotective functions during the recovery stage when it is predominantly expressed in astrocytes (Chen-Roetling et al., 2015; Nakaso et al., 2000; Zhang et al., 2017). These findings implicate microglial HO-1 as a neurotoxic mediator in the early phase of cerebral hemorrhage. Upregulation of HO-1 in microglia can lead to iron overload and exacerbate hemorrhagic brain injury by contributing to further activation of microglia, oxidative stress, brain edema, and neuronal death (Li et al., 2018). In support of this, several studies have shown that selective ablation of HO-1 or the use of iron chelating agents improves functional recovery after ICH, and their protective effects are partly mediated in part by regulation of microglial activity (Wang & Dore, 2007; Wu et al., 2011; Zhao et al., 2011). Overall, the evidence presented in this

section suggests that hematoma-induced activation of microglia and subsequent induction of HO-1 accelerate hemorrhagic brain injury by promoting neuroinflammation, oxidative stress, and iron toxicity.

Microglia activation by thrombin

Microglia are also activated following ICH by the serine protease thrombin, which acts as a blood coagulation factor. Thrombin, normally present in blood plasma, is introduced into the brain immediately after brain hemorrhage or after BBB disruption (Babu et al., 2012). Thrombin accumulation in the brain exacerbates edema formation, inflammation, and neurodegeneration, partly due to its role in inducing microglial activation (Cheng et al., 2014; Kasuya et al., 1998; Li et al., 2019). Several in vivo and in vitro reports have shown that thrombin-mediated microglia activation results in upregulation of M1-associated inflammatory mediators such as iNOS, NO, COX-2, MHCII and pro-inflammatory cytokines, including IL-1β, IL-6, and TNFα (Carreno-Muller et al., 2003; Choi et al., 2003; Huang et al., 2008; Ryu et al., 2000; Suo et al., 2002).

The effect of thrombin on microglia activation and the pro-inflammatory response is primarily attributed to downstream signaling mediated by PAR activation, which are G protein-coupled receptors expressed in various cells, including microglia. In particular, thrombin activates microglia by modulating several intracellular signaling mediators such as PKC (Ryu et al., 2000), NFκB (Ryu et al., 2000), p38 and p44/42 (ERK1 / 2) (Suo et al., 2002; Choi et al., 2003; Ohnishi et al., 2012), and JAK2-STAT3 (Choi et al., 2003; Huang et al., 2008; Ryu et al., 2000; Suo et al., 2002). Prominently, MAPK signaling pathways have been suggested to be an important mechanism underlying thrombin-induced microglial activation and ICH injury (Fujimoto et al., 2007; Ohnishi et al., 2007).

The member of the prototypical protease-activated receptor (PAR) family, PAR1, is strongly expressed on the surface of microglia/macrophages after CNS injury and is highly sensitive to thrombin stimulation (Coughlin, 2000). PAR-1 activation contributes to ICH-induced brain injury by enhancing neuroinflammation, brain edema, DNA damage, and neurotoxicity (Cheng et al., 2014). PAR-1 activity also modulates microglia proliferation, activation, and polarization responses (Carreno-Muller et al., 2003; Nakano et al., 2020; Suo et al., 2002; Wan et al., 2016). In the experimental ICH model, PAR-1 is activated after ICH injury and its activation coincides with the timing of microglia/macrophage activation and polarization, and its deficiency suppressed the activation of M1 phenotype and production of pro-inflammatory cytokines (Wan et al., 2016). These findings implicate PAR-1 as a central player in thrombin-induced microglial activation and polarization in HS.

Thrombin can also modulate microglia activation independently of PAR-1. In cultured rodent microglia cells, thrombin induces transient Ca^{2+} release from intracellular stores and promotes the production of NO and pro-inflammatory cytokines (Moller et al., 2000). This effect of thrombin was shown to be mediated by its enzymatic activity rather than its effect on PAR activation. A potential receptor-independent mechanism for thrombin-induced ICH injury is the cleavage of complement proteins leading to complement activation, which plays an essential role in microglia activation and neuroinflammation (Ducruet et al., 2009; Zhang et al., 2020). In support of this, the complement proteins C3a and C5a have been linked to microglia activation after ICH (Lan et al., 2017). Perihematomal microglia activation and subsequent ICH damage are significantly reduced in complement C3-deficient mice (Yang et al., 2006). In the absence of complement C3, complement activation can be triggered by complement C5a (Huber-Lang et al., 2006). The C5a

receptor is upregulated in microglia after ICH, and its inhibition suppresses the expression of pro-inflammatory M1 markers such as iNOS, TNFα, IL-1β, and IL-6 (Li et al., 2014). In general, these studies highlight the diverse role of thrombin in modulating the response of microglia in HS. Additional studies should characterize the PAR-1 dependent and independent mechanisms underlying thrombin-induced microglial activation response, which will help to specifically identify detrimental targets in HS.

M1 and M2 microglia in HS

Although microglia activation is triggered by thrombin and hematoma component, the nature of the activation state changes throughout the course of the disease, and microglia assume distinct phenotypic states. A few studies have explored the role of different microglia phenotypes in the context of HS, and collective evidence suggests that M1-like microglia primarily mediate neurotoxic effects by enhancing neuronal apoptosis, brain edema, and blood-brain barrier permeability (Lan et al., 2017; V. & C., 2019). Receptors that trigger M1 polarization, such as TLR4, have been shown to be upregulated in hemorrhagic patients and are associated with neuroinflammation, oxidative stress, and poor functional outcomes (Lin et al., 2012; Ma et al., 2015; Murakami et al., 2011; Rodriguez-Yanez et al., 2012; Sansing et al., 2011).

Very little is known about the function of the anti-inflammatory M2 microglia in HS. However, findings from a few studies suggest that alternatively activated M2 microglia exhibit neuroprotective functions. Specifically, various molecular mediators that trigger M2 polarization, including TGF-β, peroxisome proliferator-activated receptor gamma (PPARγ), and anti-inflammatory cytokines (IL-4 and IL-10), have protective functions after ICH and SAH injury due to their role in wound healing and resolution of inflammation (Chang et al., 2017; Taylor et al.,

2017; Yang et al., 2016; Zhao et al., 2007). The M2 activation state is also associated with an enhanced phagocytosis response due to higher expression levels of scavenger receptors, including CD36, CD206, and the hemoglobin-scavenger CD163 (hemoglobin and CD206) (Chang et al., 2017; Fang et al., 2014; Leclerc et al., 2018).Therefore, M2 microglia serve a protective function in HS by phagocytosing hematoma products and removing cellular debris.

Overall, the presented findings suggest that immunotherapies that modulate the phenotypic switch from neurotoxic (M1) to neuroprotective (M2) state are promising candidates for the treatment of HS. Since the stage-specific transition of microglia phenotypes impacts the overall function of microglia, a thorough characterization of time-dependent microglia activation response is needed to identify an optimal therapeutic time window for targeting microglia.

Temporal microglia polarization in HS

Existing evidence suggests a predominant M1-like microglia response in the early phase of hemorrhagic injury followed by a switch to the M2 phenotype in the subacute stage (Kanazawa et al., 2017; Taylor & Sansing, 2013). This M1 to M2 trajectory is supported by microscopy-based preclinical studies in ICH and SAH models (ICH and SAH models) (Lan et al., 2017; Li et al., 2018; Lin et al., 2017; Wan et al., 2016; Yang et al., 2016). In both autologous blood-injection and collagenase-injection models of ICH, M1-specific phenotypic markers are upregulated immediately after injury. A peak in M1 marker expression is evident within the first few hours of injury and remained high after 72 hours, gradually returning to baseline on day 7. Specifically, known pro-inflammatory cytokines such as IL-1β, IL-6, and TNFα are elevated in perihematomal tissue as early as 6 h after ICH, and expression levels of these markers increase within the first 3 days (Lan et al., 2017). In addition to cytokines, transcript levels of prominent M1 surface markers,

such as CD32, CD68, and CD86, are acutely upregulated and remained elevated after 3 days (Lin et al., 2017). A notable increase in CD16/CD32-expressing microglia is also evident in the perihematomal region within the first few days (Lan et al., 2017), and acutely upregulated pro-inflammatory proteins such as CD16 and iNOS decline in expression a week after injury (Wan et al., 2016). Data in SAH experimental models also demonstrated a similar trend of early-phase M1 polarization response post-injury (Li et al., 2018; V. & C., 2019). Overall, these results implicate a detrimental role for M1 microglia in the early stage of hemorrhagic injury.

Unlike rapidly induced M1 markers, M2 phenotype markers gradually increase during HS progression (Lan et al., 2017; Li et al., 2018; Lin et al., 2017; V. & C., 2019; Wan et al., 2016; Yang et al., 2016). However, upregulation of M1 markers does not always precede M2 phenotypic markers, as evidence has shown mixed expression of M1-like and M2-like phenotypic markers in the acute stage of injury (days 1-3) (Li et al., 2018). Nonetheless, in both subtypes of HS, the peak in the expression of M2 markers appears to be delayed compared to M1 markers (Lan et al., 2017; Lan et al., 2017; V. & C., 2019) (Li et al., 2018; Wan et al., 2016;). For example, Lan et al. (2017) demonstrated that, while there are microglia populations expressing both CD16/CD32 and YM-1 in the perihematomal region at days 1 and 3 post-ICH, the proportion of $YM1^{+}$-M2-like microglia was higher at 72 hours compared to CD16/CD32 positive cells (Lan et al., 2017). Studies in the SAH model also showed that anti-inflammatory cytokines expressed by M2-like microglia cells, such as IL-4 and IL-10, show a relatively gradual increase following the acute pro-inflammatory response (Li et al., 2018).

Accurate characterization of the dynamic microglial activation and polarization response has not been possible since interpretations in different studies are based on a few molecular markers.

For example, Yang et al. (2016) showed steady expression of the M1 markers CD68 and IL-1β in activated CD11b+ microglia/macrophage cells in different stages of the disease, ranging from 1 to 28 days after collagenase-induced ICH injury (Yang et al., 2016). This expression pattern is not consistent with other studies and does not support the notion that microglial M1 response declines over time. To comprehensively examine the temporal activation of microglial phenotypes, recent studies have employed bioinformatics approaches that capture a wide variety of signature markers. Taylor and colleagues (2017) incorporated flow cytometry and transcriptome analysis to characterize the M1/M2 microglial response in the acute and resolution phase of injury in a blood-injection ICH model (Taylor et al., 2017). Their findings showed that microglia in perihematomal tissue exhibit a transient pro-inflammatory phenotype in the acute phase (day 1) that was suppressed on day 7, at which point the microglia transitioned to a type of alternative activation state. Multiplexed ELISA analysis of perihematomal tissue samples also revealed a phenotypic transition from M1 to M2 microglia within the first 2 weeks after ICH, further suggesting that the balance of M1/M2 decreases throughout the course of disease. Interestingly, their findings demonstrated that the phenotypic switch during the resolution phase of ICH does not reflect changes in anti-inflammatory signature cytokines such as IL-4 and IL-13, and instead involved upregulation of alternative activation phenotype genes associated with wound healing and brain recovery functions, such as TGFβ-1 signaling pathway (Taylor et al., 2017). These findings shed light on the complex nature of microglial polarization response, such as the presence of a specific subtype of M2 microglia.

The dynamic expression pattern of inflammatory cytokines and surface proteins varies in different experimental models of ICH. For example, the switch from M1 to M2-like phenotype is

reported to be delayed (day 7) in a blood-induced ICH model (Taylor et al., 2017), compared to collagenase injection models (day 1-3) (Lan et al., 2017). This difference has been attributed to the greater disruption of the BBB that occurs in collagenase-induced ICH injury, which enhances the infiltration of peripheral immune cells (Manaenko et al., 2011). Therefore, the increased infiltration of M2-like peripheral macrophages through the leaky BBB may explain the accelerated accumulation of M2 phenotypes in the collagenase model of ICH.

Limited studies have analyzed polarization markers in clinical samples from HS patients. Consistent with findings in experimental models, the expression level of TLR4, which is associated with the M1-like pro-inflammatory response, is upregulated in the early phase of injury in peripheral macrophages isolated from SAH patients, and the expression level declined in the subacute phase, reaching normal levels on day 7 (Ma et al., 2015). On the contrary, the phenotypic marker TGF-β1 is suppressed in the acute stages of injury in plasma samples obtained from ICH patients, and a lower TGF-β1 level in the early phase of injury correlates with poor functional recovery (Taylor et al., 2017). Thus, while there are mixed M1/M2 phenotypes after brain hemorrhage, a balance of evidence suggests a neurotoxic role for M1 microglia in the early phase of hemorrhagic injury and a protective role for M2 microglia in the late phase recovery process. Given the limitations of existing animal models and experimental approaches, further clinical investigations are needed to better characterize the dynamic response of microglia phenotypes in HS.

1.4.2. Microglia in Alzheimer's Disease

Alzheimer's disease (AD) is the most prevalent age-related neurodegenerative disease characterized by a progressive loss of neurons in the cerebral cortex, resulting in cognitive

impairment, executive dysfunction, behavioral deficits, and dementia (Burns & Iliffe, 2009). Although age is the main risk factor, various mechanisms contribute to the onset and progression of AD, making it one of the most complex NDs. AD has two major subtypes, which differ based on genetic predisposition and age of onset (Dorszewska et al., 2016). Familial AD (fAD) is a less common form of AD that commonly manifests its symptoms before the age of 65 years and has a mendelian inheritance pattern with minimal influence from the environment. Sporadic AD (sAD) is the most prevalent form of AD after the age of 65, and its etiology involves a combination of genetic, environmental, and lifestyle factors that contribute to age-associated neuropathological changes (Dorszewska et al., 2016). Neuropathological hallmarks of AD include loss of neurons and synapses in the cortical and subcortical brain regions, accompanied by extracellular accumulation of amyloid-β (Aβ) plaques and intraneuronal aggregation of hyperphosphorylated tau protein (pTau) known as neurofibrillary tangles (NFTs) (Crews & Masliah, 2010).

Aβ is a 37-49 amino acid residue peptide that is produced through proteolytic processing of amyloid-β precursor protein (APP) by sequential cleavage involving β-secretase and γ-secretase enzymes (Olsson et al., 2014; Wilquet & De Strooper, 2004). Aβ peptides are capable of self-assembling and transforming to soluble oligomeric or insoluble heavy aggregate with varying neurotoxic potential (Chen et al., 2017). Various genetic risk factors of AD are linked to Aβ accumulation in the CNS, which is often associated with a defect in Aβ clearance mechanisms (Bertram, 2009). Prominent examples include mutations in genes encoding APP or presenilin 1/2, which are catalytic proteins involved in the breakdown of APP and the release of Aβ (Lanoiselee et al., 2017). Furthermore, the presence of the apolipoprotein ε4 allele (APOE4) is one of the main

genetic risk factors for AD (Corder et al., 1993), and this protein plays a central role in the regulation of lipid homeostasis and Aβ accumulation in the brain (Safieh et al., 2019).

Aβ accumulation in the brain has been proposed as a potential trigger for AD and has formed the traditional 'amyloid hypothesis,' which suggests that a defect in Aβ metabolism in the aged brain leads to a linear sequence of events involving the accumulation of toxic Aβ and the formation of amyloid fibrils that subsequently develop into senile plaques and trigger tau pathology and neurotoxicity (Makin, 2018). This hypothesis led to the development of several Aβ-modifying therapeutic strategies that target the production or aggregation of Aβ or promote its degradation. In June 2021, the FDA approved aducanumab antibody, which degrades toxic Aβ forms for the treatment of AD (Dunn et al., 2021). However, its approval has been controversial, as clinical trials showed little or no functional improvement in AD patients, and the use of aducanumab is now only recommended for patients with mild cognitive impairment (MCI) or mild dementia due to AD (Tampi et al., 2021). Therefore, despite decades of drug discovery efforts, there is currently no effective treatment to cure AD, and several other clinically tested disease-modifying agents have failed to mitigate its progressive symptoms. Therefore, there is a growing need to identify preventive approaches that mitigate the onset of AD. This requires a better understanding of the underlying mechanism of AD pathology.

Microglia activation in AD

Genome-wide association studies (GWAS) have implicated a significant role for microglia in AD pathogenesis (Lambert et al., 2013). Variants of highly expressed microglial transcripts are identified as risk factors for AD, and these AD-associated susceptibility genes strongly affect microglial function. For example, one of the major risk factors associated with AD is mutations in

TREM2, a prominent microglial receptor involved in modulating microglial activation and phagocytosis response (Gratuze et al., 2018). Furthermore, several other risk factors for AD have been identified, such as alterations in the microglial genes CD33, MS4A6, and ABCA7 (Lambert et al., 2013), which mediate important functions of microglia, further suggesting an important role for microglia in AD pathogenesis.

In vivo PET imaging studies have shown that microglia activation occurs early in the pathogenesis of AD before the onset of AD and activated microglia at the prodromal / preclinical stages exhibit a protective phenotype (Hamelin et al., 2016). In the early disease stage prior to plaque formation, microglia engage in protective functions such as clearance of Aβ, suppression of tau hyperphosphorylation, and release of neurotrophic factors that prevent symptoms of AD (Condello et al., 2015; Feng et al., 2020; Gratuze et al., 2018; Merlo et al., 2018; Wang et al., 2016). However, as disease progresses, microglial responses are altered and sustained microglia activation contributing to neurodegeneration (Fan et al., 2017). This suggests a bimodal microglia activation response throughout the progression of AD, where moderate activation leads to a protective phenotype that is prominent in the preclinical stages, while excessive activation leads to a neurotoxic phenotype that emerges in the clinical phase (Fan et al., 2017; Hamelin et al., 2016). By the time symptoms manifest, protective microglia have already transitioned towards a dysfunctional phenotype (Fan et al., 2017), signifying the narrow therapeutic window for microglia-related immunotherapies. Microglia also assume a dysfunctional transition state as they progress from having a protective role to a detrimental one (Hong et al., 2016). The transition to a neurotoxic phenotype is often accompanied by upregulated expression of complement proteins in the CSF and the deposition of complement proteins on synapses (Daborg et al., 2012) These factors

are recognized by microglial phagocytic receptors and are targeted for degradation, which can lead to early synaptic loss and cognitive impairment (Hong et al., 2016).

Clinical studies showed a positive link between microglia activation and AD pathology, which is evident in younger but not older AD patients (Hoozemans et al., 2011). This has been attributed to a decrease in the microglial activation response in older patients (>80 years), suggesting an age-dependent impairment of the immune activation response in the AD trajectory. Microglia-mediated therapeutic approaches are now focusing on targeting the initial biochemical event before disease onset, such as treating patients with mild cognitive impairment who have not yet manifested symptoms of dementia. Therefore, additional large-scale longitudinal research can help identify an appropriate time window to target microglia.

Microglia response to amyloid-β

In the brain, the balance between Aβ production and clearance controls amyloid burden, and mechanisms that regulate Aβ metabolism have been linked to the etiology of AD (Mawuenyega et al., 2010). Microglia play a key role in Aβ metabolism and clearance, and the cholesterol metabolism pathways involved in phagocytosis or enzymatic breakdown of Aβ are enriched in microglia (Loving & Bruce, 2020). In fact, one of the well-known beneficial functions of microglia in the context of AD is their ability to limit plaque formation by clearing pathological Aβ (Condello et al., 2015).

Aβ modulates various microglial responses, such as chemoattraction, activation, and proliferation, and these cellular responses serve as a protective mechanism to facilitate the first-line defense response and limit further Aβ deposition (Lee & Landreth, 2010). Aβ phagocytosis/endocytosis in microglia is mediated by the interaction of Aβ with various microglial

receptors, including TREM2, TLRs, CD36, class A1 scavenger receptors (SR-A1) and receptor for advanced glycation end products (RAGE) (Yu & Ye, 2015). The overall response of microglia depends on the specific type of receptor activated and the structural form of Aβ (Lee & Landreth, 2010).

Various inflammatory pathways are triggered by Aβ and lead to the production of pro-inflammatory cytokines and reactive oxygen and nitrogen species (ROS/RNS). Aβ-mediated activation of the CD36/TLR4/TLR6 complex is largely involved in amplifying pro-inflammatory microglial responses (Stewart et al., 2010), and activation of RAGE also mediates inflammatory responses in microglia and promotes oxidative stress in neurons (Deane et al., 2012). Aβ also activates the NLRP3 inflammasome, an intracellular tricomplex containing a sensor protein (NLRP3), an adaptor protein (ASC) and an effector protein (caspase-1), which promotes the production of IL-1β and induces neurotoxicity (Hanslik & Ulland, 2020). NLRP3 inflammasome activation can alter the microglial phagocytosis response and promote Aβ deposition (Heneka et al., 2013), and the release of ASC from activated microglia also facilitates plaque formation by inducing the Aβ oligomerization and aggregation (Venegas et al., 2017). Transient receptor potential melastatin 2 (TRPM2), a Ca^{2+}-permeable non-selective cation channel, has recently been implicated in Aβ-induced AD pathologies (Alawieyah Syed Mortadza et al., 2018; Ostapchenko et al., 2015). In a transgenic AD model, loss of this channel restores Aβ-induced synaptic loss, memory impairment, and microglial activation (Alawieyah Syed Mortadza et al., 2018). Supporting in vitro studies also demonstrated that the TRPM2 channel mediates Aβ-induced microglia activation and TNFα production. This receptor is upregulated by a high level of ROS, and Ca^{2+} influx through this channel was shown to mediate ROS-induced activation of NLRP3 in

Aβ-activated microglia (Aminzadeh et al., 2018). Overall, Aβ can activate various inflammatory and neurotoxic pathways in microglia that can mediate AD pathology.

Microglial senescence upon aging can sensitize microglia to inflammatory signals and exacerbates Aβ-pathology (Hu et al., 2021). While Aβ can trigger chronic activation of microglia, inflammation in the brain microenvironment can, in turn, weaken clearance mechanisms and promote Aβ deposition, suggesting a positive feedback loop for AD pathology. For example, pro-inflammatory cytokines produced by microglia such as TNFα and IFNγ can diminish the ability of microglia to degrade Aβ and suppress the expression of Aβ-degrading proteases, contributing to plaque formation (Michelucci et al., 2009; Yamamoto et al., 2008). Pro-inflammatory cytokines also upregulate microglial iNOS in the AD brain, leading to toxic NO production (Goodwin et al., 1995; Vodovotz et al., 1996). High concentrations of NO in the brain can alter mitochondrial function, induce neurotoxicity, and trigger the nitration of Aβ particles, which promotes plaque aggregation (Kummer et al., 2011). Furthermore, other microglial activation DAMPs, such as chromogranin A and myeloid-related protein 14 (MRP14), can trigger chronic neuroinflammation in the AD brain and further compromise the microglial phagocytosis response, thus contributing to plaque build-up (Kummer et al., 2012; Taupenot et al., 1996).

Evidence suggests that Aβ accumulation in the early phase of AD is, in part, caused by impaired microglial clearance mechanisms. For example, a dysfunctional autophagic response is evident in the AD brain and has been attributed to reduced expression of microglial beclin-1 (Pickford et al., 2008), a protein that plays an important role in Aβ phagocytosis by promoting the recycling of scavenger receptors such as CD36 and TREM2 (Lucin et al., 2013). Aβ deposition and buildup of senile plaques increase with age and may be related to age-associated microglial

senescence, which impairs the ability of microglia to detect phagocytic targets (Hu et al., 2021). In support of this, various microglial Aβ-binding cognate receptors involved in the uptake of Aβ, such as CD36, SR-A, and RAGE, are reduced in aged mice and AD brain (Hickman et al., 2008), suggesting an impaired phagocytosis response with age. In addition, aging studies comparing isolated microglia cultured for 2 or 16 days showed that older microglia have lower phagocytosis and autophagic response after Aβ treatment, accompanied by reduced expression of TREM2 and increased expression of the senescence-associated β-galactosidase (SA-B-gal) (Caldeira et al., 2017). Furthermore, a study using an ex vivo organotypic coculture model demonstrated that young microglia could restore the amyloid plaque clearance capacity of aged microglia (Daria et al., 2017). These findings indicate that dysfunctional microglial Aβ clearance contributes to plaque buildup upon aging, thus targeting age-associated microglial senescence has a therapeutic potential to prevent the onset and progression of AD.

Microglia response to tau

Tau is a microtubule-associated protein that is abundantly expressed in neurons and is normally involved in axonal microtube assembly and stabilization (Barbier et al., 2019). Post-translational modifications play an important role in modulating tau functions; in particular, hyperphosphorylation of tau impairs the interaction of tau with microtubules and induces abnormal folding that promote aggregation and the formation of neurofibrillary tangles (NFTs) (Barbier et al., 2019). Activated microglia are observed in close proximity to NFTs in AD patients (Sheffield et al., 2000), and compelling experimental evidence demonstrated both a beneficial and detrimental role of microglia in tau pathology. Microglia can engulf and degrade pathological tau

particles, but they can also propagate the spread of tau pathology (Asai et al., 2015; Bolos et al., 2016).

In experimental AD models, activated microglia populations are evident prior to tau deposition (Hopp et al., 2018; Yoshiyama et al., 2007), thereby implicating the role of microglial inflammation in exacerbating tau aggregation and spreading. In support of this, known immunosuppressants that modulate microglia activity have been used to treat AD and have shown attenuation of tau pathology (Garwood et al., 2010; Howard et al., 2020) Microglia can contribute to the spread of tau pathology through various mechanisms. Studies have shown the presence of hyperphosphorylated tau in aged dystrophic microglia (Bussian et al., 2018), suggesting that impairment of clearance mechanisms upon aging can lead to intracellular accumulation of pathological tau particles that promote microglia dystrophy. Impaired processing of pathological tau in microglia can contribute to tau propagation by releasing tau-containing exosomes/microvesicles (MV) (Asai et al., 2015). High concentrations of MVs containing bioactive molecules are evident in the AD brain, and the release of bioactive mediators from these MVs, including toxic tau seeds, is known to alter the brain microenvironment and promote microgliosis and tau spreading (Ramirez et al., 2017; Ruan et al., 2021).

Studies have shown that NFT formation is accelerated by microglial inflammation (Asai et al., 2015; Bhaskar et al., 2010). Microglial uptake of tau can also trigger activation of the NLRP3 inflammasome complex, which promotes tau seeding (Hanslik & Ulland, 2020). Activated microglia can also modulate tau function through post-translational modifications. For example, pro-inflammatory cytokines released by activated microglia, such as IL-1 and IL-6, induce tau phosphorylation, thus promoting NFT formation (Wang et al., 2015). Microglia also promote tau

ubiquitination, and ubiquitinated forms of tau are better incorporated into exosomes that can facilitate extracellular release of tau seeds (Asai et al., 2015). Pro-inflammatory responses in microglia can also disrupt regulatory CX3CR1-CX3CL1 signaling (Inoue et al., 2021), which can further lead to sustained microglial activation and promote NFT formation (Pawelec et al., 2020).

Proteasomal and autophagic mechanisms are involved in tau degradation, and there is evidence that these clearance mechanisms are impaired in AD (Tang et al., 2019). The receptors involved in tau interaction are not well characterized. However, Bolos et al. (2017) demonstrated that the microglial CX3CR1 receptor interacts with tau and promotes its phagocytosis and internalization, and S396 tau mutant with impaired binding to CX3CR1 is associated with a defect in tau clearance (Bolos et al., 2017). However, in the AD brain, tau competes with CX3CL1, and sustained CX3CR1/Tau signaling can amplify pro-inflammatory and neurotoxic pro-inflammatory responses (Chidambaram et al., 2020). The exact mechanism for the dual role of microglia is not clear; however, microglia probably mediate different effects on tau pathology, depending on the stage of the disease. Overall, microglia-induced tau pathology is facilitated by a combination of factors involving a defect in tau clearance mechanisms and neuroinflammatory mechanisms that promote tau aggregation and propagation. More studies are needed to characterize the role and mechanism of the reciprocal microglia-tau interaction at different stages of AD progression.

Microglia morphologies and phenotypes in AD

Various immunohistology studies in transgenic AD models and human clinical samples demonstrated the presence of various morphologically distinct populations of microglia in AD brain, including traditional ramified resting microglia and amoeboid-shaped activated microglia (Davies et al., 2017). Amoeboid-shaped microglia are predominantly localized in the hippocampus

and cerebral cortex region where amyloid plaques and NFTs are commonly found, while ramified microglia are dispersed away from these pathogenic regions (Davies et al., 2017; Franco-Bocanegra et al., 2021; Plescher et al., 2018). A dystrophic/degenerating microglia phenotype, exhibiting thin fragmented processes, is also reported in the hippocampus of human AD autopsy brains (Bachstetter et al., 2015).

Some of the activated microglia population located near senile plaques assume an elongated and polarized morphology, commonly referred to as bipolar/rod-shaped microglia, and these microglia phenotypes are mostly aligned end-to-end in the CA1 and CA2/3 region of the hippocampus (Bachstetter et al., 2015; Wierzba-Bobrowicz et al., 2002). Bipolar/rod-shaped microglia are evident in the affected brain region in the early phase of AD, and as disease progresses, amoeboid microglia predominate, while bipolar microglia appear in less affected brain regions in the later stage of AD (Au & Ma, 2017; Bachstetter et al., 2017; Bachstetter et al., 2015). Compared to amoeboid microglia, in vitro studies demonstrated that bipolar/rod-shaped microglia highly express low levels of pro-inflammatory markers and can transform into an amoeboid phenotype by LPS treatment (Suzumura et al., 1991; Tam & Ma, 2014). Transformation towards an amoeboid phenotype enhanced the production of proteolytic extracellular matrix-degrading molecules, suggesting a neurotoxic role of amoeboid microglia (Tam et al., 2016). Although these observations implicated a potential neuroprotective effect of bipolar/rod-shaped microglia in AD pathology, more studies are needed to understand the exact role and regulation of this microglia phenotype.

A recent ultrastructural analysis using a high-resolution transmission electron microscopy (TEM) revealed a unique phenotype of microglia known as ‘dark microglia’ (DM), which is named

for its characteristic dark appearance under TEM (Bisht et al., 2016; Bisht et al., 2016). This phenotype, which was nearly absent in normal adult brains, was abundant under conditions of chronic stress, aging, and in a transgenic AD model. DM exhibited a distinct ultrastructural morphology and showed signs of severe oxidative stress, such as condensed cytoplasm and nucleoplasm, abnormal nuclear chromatin, dilated ER and Golgi body, and mitochondrial alterations. Furthermore, this microglia phenotype is highly reactive and rich in endosomes, implicating a strong phagocytic function. Unlike normal microglia with shorter and thicker processes, DM have thin and highly branched ramifications that enable them to extensively circle and engulf axon terminals, dendrites, and entire synapses (Bisht et al., 2016; Bisht et al., 2016).

DM strongly express the CD11b microglia receptor while encircling synaptic elements and have high expression of TREM2 when associated with amyloid plaques; these receptors have important synaptic pruning and phagocytosis functions, suggesting an important function of DM in pathological remodeling of synapses (Bisht et al., 2016; Bisht et al., 2016). The significance of DM is yet to be elucidated, but their distinct structural properties, specific occurrence in aging and chronic stress environment, and their implicated role in pathological synapse remodeling suggest an important function of DM in AD pathology. DM has recently been identified in humans and other species (Elgayar et al., 2018; Uranova et al., 2018), suggesting that this microglia morphology is highly conserved across species and may modulate disease progression. Overall, the presence of various microglia morphologies demonstrates a complex role of microglia in AD pathology.

M1 and M2 microglia in AD

The dichotomous paradigm of M1 and M2 is less commonly applied in the context of AD; however, it is sometimes used as a general reference to describe either pro-inflammatory microglia or a phagocytic phenotype, which is distinguished based on molecular markers and the overall functional response. It is believed that M2 microglia are efficient phagocytes and mediate protective functions, while M1-like pro-inflammatory microglia have a poor ability to clear Aβ and toxic tau, thus exacerbating AD pathology (Yao & Zu, 2020). Inhibition of pro-inflammatory responses, such as the activation of the NLRP3 inflammasome, has a protective effect in reducing amyloid burden and associated toxicity (Kuwar et al., 2021). Pro-inflammatory cytokines released by M1 microglia, such as IFNγ and TNFα, are implicated in AD pathology as they can inhibit the uptake of Aβ or the degradation of internalized Aβ (Michelucci et al., 2009; Yamamoto et al., 2008). In addition to their role in Aβ pathology, pro-inflammatory microglia can also mediate tau neurotoxicity by triggering tau hyperphosphorylation (Bhaskar et al., 2010). In fact, the presence of pro-inflammatory microglia has been reported in vivo in transgenic AD models before the manifestation of tau neurotoxicity (Yoshiyama et al., 2007), suggesting a detrimental role of M1 microglia in tau pathology.

Studies have shown that microglia surrounding amyloid plaque exhibit an activation profile of M2 microglia, and this microglia phenotype is largely associated with protective functions (Fan et al., 2017; Hamelin et al., 2016; Jimenez et al., 2008). Both in vitro and in vivo findings demonstrated that microglia polarization toward an M2 phenotype alleviates neuroinflammation, M1-mediated neurotoxicity, and AD pathogenesis (Wang et al., 2021) M2 polarization reduces microglial reactivity toward pathogenic forms of Aβ, which helps limit Aβ-toxicity (Tang & Le,

2016). Unlike the pro-inflammatory M1phenotype with impaired phagocytosis function, M2 microglia exhibited enhanced Aβ phagocytosis and clearance (Yao & Zu, 2020), which implies a beneficial role of M2 phenotype in AD pathology. M2 microglial responses can be diverse, depending on the specific M2 subtype. For example, the M2a phenotype, which is induced by IL-4, has enhanced phagosome/lysosome function and increased scavenging capacity, which facilitates Aβ degradation (Balce et al., 2011; Majumdar et al., 2007), while the M2c phenotype is involved in tissue repair and wound healing functions (Yao & Zu, 2020). In general, chronic induction of the M1-like pro-inflammatory phenotype or defect in M2-like phagocytic and wound-healing microglia can exacerbate AD pathogenesis.

Studies exploring the role of cytokines in AD pathology have yielded conflicting findings. Intracerebral administration of IL-4 and IL-13 has shown neuroprotective effects in limiting plaque buildup and improving cognitive functions in APP transgenic mice (Kawahara et al., 2012). However, in a different mouse model with preexisting amyloid plaques, adenovirus-based overexpression of recombinant IL-4, while inducing M2 polarization, exacerbated amyloid deposition after 6 weeks (Chakrabarty et al., 2012), suggesting that IL-4 impairs microglial phagocytosis response. A paradoxical beneficial role of pro-inflammatory cytokines (IL-6, IFNγ, and TNFα) has also been reported, such as enhancing complement-mediated Aβ phagocytosis and clearance (Chakrabarty et al., 2010; Chakrabarty et al., 2011; Chakrabarty et al., 2010). These findings suggest diverse roles of cytokines and microglia phenotypes in AD pathology, which can vary depending on the specific disease stage. For example, it is suggested that Aβ clearance in AD may be primed by the M1 microglia response and maintained by M2 microglia (Tang & Le, 2016; Wang et al., 2015). Although M1 microglia have a potential role in Aβ uptake, sustained M1

polarization and chronic inflammation in the AD brain can overwhelm the functional response of M2 microglia and lead to impaired Aβ clearance and M1-neurotoxicity.

Timeline of Microglia Phenotypes in AD

Studies have explored age-associated changes of microglia phenotypes in the context of AD. Jimenez et al. (2008) characterized the age-dependent change of microglia phenotypes in the hippocampus of double PS1xAPP transgenic AD mice (Jimenez et al., 2008). They observed that YM1-positive M2 microglia with low expression of pro-inflammatory markers predominated at 6 months, and later switched to M1-like microglia at 18 months. The M2-phenotype microglia in 6-month-old mice were located exclusively located surrounding Aβ plaque and exhibited phagocytic abilities, while the M1 activation response in the older age group was more widespread and included plaque-free brain regions. This M2-to-M1 switch also coincided with significant neurodegeneration and accumulation of Aβ oligomers, further suggesting the loss of microglial phagocytosis response. This age-dependent impairment of Aβ clearance has also been demonstrated in vitro in aging microglia (Caldeira et al., 2017). Overall, these findings imply that microglia transition from a phagocytic and protective alternative activated phenotype, in the early stage of Aβ pathology, to a pro-inflammatory and neurotoxic phenotype in advanced stages.

Longitudinal PET imaging studies in patients with MCI and AD have also revealed a similar microglia activation profile in human subjects where a protective phenotype is believed to be present in the early stage of AD, while a pro-inflammatory phenotype is prominent as the disease progresses and Aβ clearance fails (Fan et al., 2017; Hamelin et al., 2016; Shen et al., 2018). M2-like microglia peak in the MCI stage of disease while the M1 phenotype is more apparent in symptomatic AD patients (Shen et al., 2018). The transition from M2-to-M1 phenotype is

attributed to a change in the brain microenvironment. In the early presymptomatic phase of AD, there is moderate activation of microglia and protective functions of microglia dominate, such as clearance of Aβ/tau. On the contrary, a sustained inflammatory environment during AD progression can alter microglial housekeeping and sensing functions, as well as the host defense mechanism, thereby promoting neuroinflammation and neurotoxicity (Hickman et al., 2018) For example, there is evident dysregulation of endogenous microglia regulatory molecules such as loss of CX3CR1 and TREM2 that can cause microgliosis and exacerbate AD pathology (Bhaskar et al., 2010; Parhizkar et al., 2019) While these findings implicate a dynamic microglia activation profile, the overall response of microglia in AD is more complicated than what is described by the two distinct activation phenotypes.

Colton and colleagues (2006) described a complex pattern of microglial gene expression in AD patients and two different transgenic mouse models: the APPsw model for amyloid deposition and the Tg-SwDI model for cerebral amyloid angiopathy (Colton et al., 2006). They observed an M2-like activation profile in both the experimental models and clinical samples, but the assessment of different phenotypic markers showed a heterogeneous gene expression profile in the AD brain representing a mixture of classical and alternative activated states. Various factors can contribute to a complex microglia response in AD. For example, microglia can have a diverse response in AD brain depending on the specific activation trigger, eg. Aβ vs tau. Amyloid plaques and NFTs also have regional distributions that can lead to a heterogeneous activation response of microglia in the diseased brain (Pereira et al., 2019). Furthermore, extracellularly deposited mediators such as Aβ can activate the peripheral immune response and elicit infiltration of other immune cells into the brain, which can modulate microglia phenotypes (Dionisio-Santos et al., 2019). While

these findings highlight the complex activation response of microglia, a specific phenotype of microglia may dominate at different stages of AD. Therefore, longitudinal studies characterizing stage-specific responses of microglia in different brain regions can help identify an optimal therapeutic time window to specifically target detrimental phenotypes of microglia.

Diversity of microglia in AD inferred from transcriptome studies: DAM and HAM

Transcriptome studies that examine microglial signatures in AD models have highlighted the complex nature of the microglial response in AD pathology (Orre et al., 2014; Srinivasan et al., 2016; Wang et al., 2015). Orre et al. (2014) reported transcriptome alterations observed in late-stage (15-18 months) APP/PS1 transgenic mouse model and revealed that microglia in AD brain exhibit lower expression of genes important for phagocytosis and endocytosis functions, while showing upregulation of innate activation genes such as those involved in antigen processing and presentation responses (Orre et al., 2014). Wang et al. (2015) identified similar remodeling of the microglial transcriptome in 8.5-month-old plaque depositing AD model (5XFAD, harboring five AD-linked mutations) that represented a late stage of AD progression (Wang et al., 2015). Using coexpression network analysis, Holtman et al. (2015) compared the microglial transcriptome in mouse models of aging, AD, and ALS and identified shared transcriptional profiles such as dysregulation of genes involved in antigen presentation, AD signaling, and phagocytosis (Holtman et al., 2015). However, they observed a highly heterogeneous microglia transcriptome profile, which varied by age and brain region. Recently, Lopes et al. (2022) identified similar regional and age-related differences in the microglia transcriptome of human AD brain tissue, including alteration in a wide range of inflammatory responses such as the IFN, glucocorticoid, STAT3, and IL-6 signaling pathways (Lopes et al., 2022).

Transcriptome analyses have also revealed a novel disease-associated microglia (DAM) phenotype found near Aβ plaques (Keren-Shaul et al., 2017; Krasemann et al., 2017). Krasemann et al. (2017) identified a novel molecular signature associated with the induction of DAM phenotype; the switch towards DAM was triggered by phagocytosis of apoptotic neurons and depended on the activation of TREM2-APOE signaling and subsequent suppression of homeostatic microglia signatures (Krasemann et al., 2017). In a plaque-deposited mouse 5XFAD model, Keren-Shaul et al. (2017) also identified a subset of protective DAM population enriched near senile plaques that exhibited a distinct molecular signature compared to microglia in the normal brain (Keren-Shaul et al., 2017). In the same disease model, Grubman et al. (2021) transcriptionally profiled amyloid plaque containing microglia (labeled with methoxy-XO4, XO4+) and plaque-free microglia (XO4-) during disease progression and showed that XO4+ microglia were functionally distinct, as defined by active fibrillar Aβ phagocytosis (Grubman et al., 2021). Their study also identified distinct processes such as accelerated aging and direct response to plaque phagocytosis that were associated with microglial changes in AD.

DAM activation occurs through two sequential steps: The first activation step is considered an intermediate state and involvesTREM2-independent downregulation of homeostatic markers such as P2RY12, while the second activation state is TREM2-dependent and is associated with overexpression of genes involved in lipid metabolism and phagocytosis functions (Keren-Shaul et al., 2017). DAM-like phenotype was also identified in AD patients and in other diseases such as ALS (Deczkowska et al., 2018). So, DAMs may exist in various NDs that exhibit a characteristic defect in clearance of pathogenic proteins, and this microglia phenotype may mitigate disease progression through phagocytosis of misfolded and aggregated proteins.

Using single-cell RNA sequencing (scRNA-seq) technology, Mathys et al. (2019) profiled ~80,000 single-nucleus cortical transcriptome samples from 48 patients with varying degrees of AD pathology and identified transcriptional profiles linked to AD pathogenesis, such as altered expression of genes involved in inflammation and Aβ clearance pathways including APOE, TREM2, MHCII, and C1qb (Mathys et al., 2019). Age-related dysfunction of the microglial endolysosomal system has also been evident in human bulk RNA-seq samples from AD patients, such as alteration of the GTPase-activating protein USP6NL and the phosphatidylinositol-binding clathrin assembly protein (PICALM), which function to regulate Aβ endocytosis and processing (Lopes et al., 2022).

While the aforementioned transcriptome studies were performed in RNA samples isolated from postmortem brain tissue, Olah et al. (2020) recently performed scRNA-seq experiments in live microglia cells purified from human cerebral cortex and identified 9 diverse clusters of human microglia subpopulations enriched for disease-related genes (Olah et al., 2020). A specific antigen-presenting cluster was histologically verified and appeared to be prominently enriched for AD genes whose expression was suppressed in AD patients. A significant portion of the genes identified in the different clusters of human microglia appeared to overlap with signature genes previously reported in murine DAM phenotypes (Keren-Shaul et al., 2017). A recent study by Srinivasan et al. (2020) also characterized a human Alzheimer's microglia (HAM) profile from frozen postmortem brain tissue using bulk RNA-seq and identified similar profiles between DAM and HAM genes, particularly in AD risk factor genes involved in lipid transport and lysosome biology such as APOE, CLU, PLCG2 (Srinivasan et al., 2020). However, a detailed comparison of their data with a recently published human microglia scRNA-seq and snRNA-seq datasets

(Hasselmann et al., 2019; Masuda et al., 2019; Mathys et al., 2019), revealed a distinct profile of HAM microglia. The DAM phenotype is evident in other NDs, such as multiple sclerosis, and is mainly characterized in rodent AD models with implicated protective roles in Aβ pathology (Keren-Shaul et al., 2017). However, HAM showed an enhanced human aging phenotype and a unique transcriptome profile specific to human AD and exhibit defective activation and functional responses (Hansen et al., 2018). Aside from species-specific intrinsic differences, the distinction between DAM and HAM profile can be attributed to experimental factors; many transgenic AD models harboring Aβ-related mutations mimic Aβ pathology, which is an early stage of AD before the manifestation of neurodegenerative symptoms (Vitek et al., 2020). Therefore, microglia, responses in rodent models may not represent features of clinical AD. While advanced genome-wide analyses have revealed the complex and heterogeneous nature of microglia, additional longitudinal transcriptome and functional studies in various age groups are necessary to better understand the stage-specific response of microglia in human AD.

1.4.3. Microglia in Parkinson's Disease

Parkinson's Disease (PD) is the second most prevalent neurodegenerative disease and is characterized by a progressive and selective loss of midbrain dopaminergic (DA) neurons in the substantia nigra pars compacta (SNpc) and nerve terminals in the striatum (Poewe et al., 2017). This leads to a gradual impairment of DA transmission in the motor regions of the striatum that causes dysfunctional motor functions such as bradykinesia, tremor, and rigidity (Poewe et al., 2017). Although PD is mainly considered a movement disorder, motor deficit usually occurs at an advanced stage after approximately 50% of DA neurons are lost (Dijkstra et al., 2014), and patients experience many nonmotor symptoms in the early phases, such as cognitive impairment,

autonomic dysfunction, and psychiatric changes (Poewe et al., 2017). The main pathological hallmark of PD is the formation of Lewy bodies (LBs), which are abnormal intracellular inclusions containing aggregated proteins largely made up of α-synuclein (α-syn) (Iacono et al., 2015).

Aging is the major risk factor for PD, but the exact mechanism for the onset of PD is unknown and likely involves a combination of factors such as genetic and environmental predisposition (Kouli et al., 2018). PD can either be familial (fPD), which is a less common form primary caused by genetic factors, or sporadic (sPD) which has a multifactorial origin and is a more prevalent form. More than 30 loci are identified as risk factors for PD, some of which are extensively studied, such as mutations in genes encoding synuclein (SNCA), leucine-rich repeat kinase 2 (LRRK2), parkin (PRKN), and Parkinson disease protein 7 (PARK7) (Maiti et al., 2017). In addition to genetic susceptibility, sedentary lifestyle, poor diet, and exposure to environmental toxins (eg herbicide/pesticides) also contribute to a lifetime risk of developing PD (Kouli et al., 2018).

Various pathogenetic mechanisms contribute to PD-mediated neurotoxicity, including impairment in α-syn proteostasis, mitochondrial dysfunction, oxidative stress, glutamate excitotoxicity, and neuroinflammation (Kouli et al., 2018; Maiti et al., 2017). Developing effective therapies for PD has been a challenge due to the complex etiology and mechanism of PD, and the diverse neuropathological changes and symptoms among patients. Therapeutic options for PD are mainly limited to symptomatic interventions focused on dopaminergic pharmacological targets, such as the FDA-approved dopamine replacement agent levodopa (L-DOPA), a dopamine precursor used to restore decreased dopamine levels in patients (Poewe et al., 2017). Although this treatment option relieves motor symptoms, it does not target the underlying mechanism of neurodegeneration and is not effective in slowing the progression of PD (Gandhi & Saadabadi,

2022). A better understanding of the underlying mechanism of PD pathogenesis and the identification of early biomarkers is crucial to develop preventative and neurorestorative therapies.

One of the most prevalent pathogenic players in PD is α-syn. This 140-amino acid protein is highly expressed in the brain and its aggregated toxic form constitutes the core of LBs (Iwai et al., 1995; Zhang et al., 2019). Monomeric and aggregated forms of α-syn are commonly found in the brain, CSF, and blood of PD patients (Borghi et al., 2000; El-Agnaf et al., 2003). Aggregation of α-syn in the brain is a characteristic feature of both sPD and fPD, and various pathogenic mechanisms contribute to aggregation, including changes in the SNCA gene (point mutations, duplications, and triplication) and various post-translational modifications of the protein (e.g. phosphorylation, oxidation, nitration, ubiquitination) (Zhang et al., 2019). Therefore, preclinical studies in PD commonly utilize rodent models with treatment or overexpression of human α-syn, or transgenic models harboring α-syn mutations. α-syn homeostasis in the CNS is regulated by the proteasomal and autophagic degradation systems (Webb et al., 2003), and age-related progressive decline in these α-syn clearance mechanisms contributes to α-syn accumulation in the aged brain (Kiffin et al., 2007; Wong & Krainc, 2017). In addition to age-associated changes, various genetic mutations linked with fPD, such as the G2019S mutation in LRRK2, are associated with decreased a-syn homeostasis (O'Hara et al., 2020). Furthermore, alterations in the brain microenvironment, including oxidative stress and inflammation, also play an important role in the pathogenic mechanism of α-syn (He et al., 2020).

Microglia activation in PD

Collective evidence from human postmortem analysis, in vivo PET imaging, and gene-wide association studies (GWAS) has revealed genetic and neuropathological evidence for the contribution of microglia in PD pathology (Subramaniam & Federoff, 2017). The nigrostriatal system, in particular the SN region, has a high abundance of microglia, and neurons within this region are very sensitive to inflammatory and oxidative damage (Kim et al., 2000). An early study by McGeer et al. (1988) provided the first indication of microgliosis in the SN of postmortem PD tissue (McGeer et al., 1988). Langston et al. (1999) further revealed the presence of chronic microgliosis in the postmortem human brain exposed to MPTP (Langston et al., 1999), a neurotoxin that triggers acute and irreversible human parkinsonism (Nonnekes et al., 2018). Interestingly, activated microglia were present even up to 16 years after intoxication, suggesting a sustained inflammatory response. Further, in vivo imaging employing inflammatory and microglia activation markers revealed that activated microglia are present in early-stage PD, and sustained activation and inflammatory response in the brain are positively correlated with disease progression (Gerhard et al., 2006; Ouchi et al., 2009; Pradhan & Andreasson, 2013; Terada et al., 2016). Activation of microglia was also observed in the midbrain region of patients with REM sleep disorder, which is considered the prodromal phase of PD (Stokholm et al., 2017). Unlike the region-specific activation response shown in the early stage, a more widespread microglial activation response was evident in additional brain regions, including the hippocampus and cortex of diagnosed PD patients (Doorn et al., 2014; Imamura et al., 2003). GWAS further showed that key PD-susceptibility genes encode microglial proteins that play important roles in immune regulation and microglial phagocytosis, such as LRRK2 (Ma et al., 2016)). Overall, these pieces

of evidence suggest that microglia play an essential role in the pathogenesis of PD and that their activation response is highly dynamic, exhibiting regional and stage-specific heterogeneity.

Microglia response to α-synuclein

A key neurotoxic mechanism of α-syn in PD is the activation of microglia to promote neuroinflammation (Zhang et al., 2017). In the PD brain, activated microglia are commonly associated with α-syn-containing LBs (Croisier et al., 2005), and α-syn released from degenerating DA neurons is an endogenous DAMP that activates microglia (Zhang et al., 2017)). In vivo studies in transgenic and neurotoxin-based PD model demonstrated that activated microglia and inflammatory responses are evident and precede neurotoxicity (Chung et al., 2009; Marinova-Mutafchieva et al., 2009). This suggests that neuronal death is not a necessary event for microglial activation and that microglial inflammatory responses likely mediate α-syn neurotoxicity.

Reciprocally, a key neurotoxic mechanism of activated microglia is their ability to facilitate α-syn misfolding and propagation, which can subsequently cause microgliosis and exacerbate disease progression (Gao et al., 2011). For example, α-syn can activate NADPH oxidase (Phox) and trigger the release of ROS from microglia, creating an environment of oxidative stress (Zhang et al., 2005). This response can further induce α-syn oxidation in neighboring neurons and promote α-syn aggregation, propagation, and disease progression (Shavali et al., 2006). In turn, modified α-syn (eg. mutated, fibrillar, and oligomeric forms) has a stronger propensity to activate microglia and lead to further microgliosis and neurodegeneration (Ferreira & Romero-Ramos, 2018). Specifically, misfolded α-syn can trigger a reactive M1-like pro-inflammatory phenotype. For example, a specific mutant form of α-syn (A53T), which is linked to fPD, induces a stronger activation of the NFκB/AP-1/Nrf2 pathway that leads to the production of pro-inflammatory

cytokines and ROS, compared to wild-type α-syn (Hoenen et al., 2016). Furthermore, oligomeric/fibrillar α-syn activates microglial NLRP3 inflammasome, which can lead to the release of IL-1β and ASC in the extracellular space, promoting a pro-inflammatory response (Trudler et al., 2021). In general, these findings suggest a positive feedback loop in which α-syn disorder and microglial neuroinflammatory processes propagate one another and drive chronic neurodegeneration.

Microglia activation in response to α-syn also mediates protective effects; it triggers a defense response that limits disease progression by modulating α-syn clearance and toxicity (Ferreira & Romero-Ramos, 2018). Microglia are capable of internalizing and degrading α-syn, and studies have shown that ingested α-syn is sequestered by the microglial autophagosome complex for degradation (Choi et al., 2020). Microglia-mediated clearance of α-syn is regulated by LRRK2, and a pathogenic variant of LRRK2, which is evident in patients with PD, affects the ability of microglia to internalize and degrade α-syn thereby contributing to PD (Ma et al., 2016). However, the protective function of microglia in α-syn clearance is weakened during aging and upon sustained activation of microglia, and defect in microglial phagocytosis mechanisms can contribute to α-syn accumulation, microgliosis, and neurotoxic response (Kawabori et al., 2015; Wong & Krainc, 2017). Bido et al. (2021) recently used a novel mouse model with selective overexpression of α-syn in microglia and demonstrated that these mice, albeit lacking endogenous aggregated α-syn, develop progressive DA neurodegeneration by phagocytic exhaustion and oxidative stress (Bido et al., 2021), further supporting the notion that α-syn responses in microglia can drive neurotoxicity. The vicious cycle of phagocytic defect and oxidative/pro-inflammatory toxicity in α-syn-accumulating microglia leads to progressive DA damage. However, microglial

α-syn also plays an important for homeostatic lipid signaling (Ferreira & Romero-Ramos, 2018), and its loss has been shown to impair phagocytosis and promote excess COX-2 activation in response to inflammation (Austin et al., 2006). Therefore, microglial response to α-syn is complex and varies depending on the α-syn forms, and the solubility and aggregation properties of α-syn change during disease progression, which affects the overall response of microglia (Melki, 2015).

Microglial uptake of α-syn and subsequent activation are mediated by mechanisms and receptors similar to those involved in Aβ-signaling, prominently TLR2, TLR4, and the scavenger receptor CD36 (Hickman et al., 2018). Activated microglia expressing TLR2 are present at the site of neurodegeneration in patients with PD (Doorn et al., 2014), and α-syn interaction with this receptor mediates pro-inflammatory and neurotoxic responses (Zhang et al., 2017). The expression of TLR2 in SN is higher in PD patients, predominantly in the prodromal stage, suggesting a detrimental role of this receptor in early disease processes (Doorn et al., 2014). The activation of CD36 facilitates the uptake of α-syn and microglial activation, and by forming a complex with TLRs, it induces the pro-inflammatory responses (Stewart et al., 2010; Zhang et al., 2017). CD36 and TLR2 are primarily involved in the uptake of oligomeric or fibrillar α-syn (Ferreira & Romero-Ramos, 2018; Kim et al., 2021), and their harmful role in PD may be attributed to their sensitivity to toxic forms of α-syn.

TLR4-mediated α-syn uptake in microglia is not limited to aggregated forms of α-syn, and activation of this receptor has been linked to protective functions such as enhanced endocytosis response and autophagosome function (Ferreira & Romero-Ramos, 2018). In vitro and in vivo studies by Choi et al. (2020) demonstrated that α-syn interaction with TLR4 and the subsequent activation of NFκB induces transcriptional upregulation of the autophagy receptor SQSTM1/p62,

which is involved in autophagic clearance of α-syn inclusions (Choi et al., 2020). However, the activation of TLR4/NFκB pathway can also promote pro-inflammatory responses and ROS release, which contributes to neurodegeneration. Given that TLRs have temporal and regional activation in PD model (Watson et al., 2012), the precise role of TLR4 in PD pathology may depend on the timing of activation and the severity of the disease.

In addition to direct interaction and activation of microglia receptors, α-syn can also activate microglia through other indirect mechanisms involving the release of microglial mediators. For example, α-syn induces the release of MMPs that subsequently activate microglial PAR-1 receptors (Lee et al., 2010). Furthermore, while the microglial response to PD is extensively studied in the context of α-syn toxicity, microglia can also be activated by other mediators to promote pro-inflammatory responses. In fact, microgliosis occurs in various experimental PD models that utilize neurotoxins such as MPTP, 6-OHDA, and the organic insecticide rotenone. Some of the mediators that activate microglia in PD include dopamine-derived neuromelanin and mitochondrial DAMPs such as mitochondrial DNA (mtDNA), cytochrome c, and ROS (Au & Ma, 2017; Dela Cruz & Kang, 2018). Overall, the progression of PD is exacerbated by a self-propagating cycle of microglial activation and neurotoxicity, driven by a combination of factors that include neuroinflammation, α-syn aggregation, oxidative stress, and mitochondrial and autophagy dysfunction.

Microglia phenotypes in PD

Collective evidence from postmortem human brain analysis and in vivo studies suggests that the M1 phenotype of microglia is prominent in PD. Specifically, M1 microglia markers are elevated in PD clinical samples and largely cluster near α-syn deposits in the SN of patients (Boka

et al., 1994; Imamura et al., 2003). Furthermore, most of the activated microglia observed in various experimental PD models, utilizing either α-syn, environmental toxins and inflammatory agents, exhibit a characteristic M1-like activation response (Tang & Le, 2016). Some of the key PD genetic variants identified in GWAS studies, such as LRRK2, parkin, and DJ-1, are also involved an M1-like pro-inflammatory responses (Subramaniam & Federoff, 2017; Tang & Le, 2016). Studies have also demonstrated a positive correlation between pro-inflammatory microglial responses and aging, as well as DA neuronal loss (L'Episcopo et al., 2018; L'Episcopo et al., 2011), suggesting that therapeutic targeting of the M1 microglia phenotype can help protect vulnerable midbrain DA neurons from inflammation-induced neurodegeneration. In support of this, strong microglial COX-2 and iNOS reactivity is observed in PD patients (Hunot et al., 1996; Knott et al., 2000), and COX-2 activity in neurotoxin PD model suppresses microglial activation and secondary DA neurodegeneration (Vijitruth et al., 2006). Furthermore, studies in a transgenic PD model demonstrated that microglial activation and the production of pro-inflammatory cytokines such as TNFα, IFNγ, and IL-1β precedes neurotoxicity (Chung et al., 2009; Marinova-Mutafchieva et al., 2009), and inhibition of these cytokines suppresses microglia-mediated neurodegeneration (Subramaniam & Federoff, 2017). Overall, these findings strongly suggest that M1 microglial responses contribute to neurodegeneration in PD.

The role of M2 microglia in PD pathology is not well understood, and limited studies have implicated the role of M2 microglia in α-syn toxicity and PD. Glatiramer acetate (GA) is an FDA-approved drug for multiple sclerosis and promotes anti-inflammatory M2 activation (English & Aloi, 2015). In experimental PD model, GA treatment reversed MPTP-induced motor dysfunction and restored striatal dopamine levels (Benner et al., 2004), implicating a potential neuroprotective

role of M2 activation in PD pathology. In both LPS-inflammation and MPTP-model of PD, human IL-10 infusion limited microglial activation and protected against DA neuronal loss in the SN (Arimoto et al., 2007; Joniec-Maciejak et al., 2014). Although these results suggest a potential anti-inflammatory and neuroprotective role for this cytokine, a detrimental effect of IL-10 has also been reported. In a recent study, Cockey et al. (2021) used AAV to express recombinant IL-10 and its immunosuppressive variant I87A (vIL-10) in a mouse model of synucleinopathy and showed that sustained intraspinal expression of both IL-10 forms resulted in a shorter lifespan, associated with increased microgliosis, neuronal autophagy dysfunction, accelerated α-syn pathology, and enhanced apoptosis (Cockey et al., 2021). Various contradictory studies have also assessed IL-10 expression in human PD brains. A high circulating level of IL-10 is detected in patients with PD patients and was shown to correlate with various nonmotor symptoms of PD, such as anxiety, depression, and gastrointestinal dysfunction (Karpenko et al., 2018; Shu et al., 2018), suggesting that this anti-inflammatory cytokine is involved in the pathogenic mechanism of PD. However, there is no conclusive consensus on the correlation between IL-10 and PD, as other reports have negative correlation between IL-10 and PD-related pain (Li et al., 2018).

The anti-inflammatory cytokine IL-4 is also implicated in PD pathology. In mixed neuron-glia culture, inhibition of endogenous microglia-derived IL-4 enhanced MPTP-induced neurotoxicity, and exogenous administration of IL-4 in the mouse MPTP model protects against neurotoxicity, indicating a potential protective role of IL-4 in PD (Huhner et al., 2017). In addition to IL-4 and IL-10, the pleiotropic M2 cytokine TGF-β mediates neuroprotective functions in inflammation and neurotoxin PD models; it limits M1 microglial activation and dopaminergic neurodegeneration (Tesseur et al., 2017; Zhou et al., 2015). Specifically, microglia-derived TGF-β2 is beneficial in

PD pathology; addition of exogenous TGF-β2 peptide in TGF-β-depleted microglial conditioned media has been shown to counteract 6-OHDA-induced neurotoxicity of cerebellar granule neurons (Polazzi et al., 2009). Despite its implicated neuroprotective effect, the concentration of TGF-β is elevated in the CSF of PD patients (Vawter et al., 1996), and its role in PD is not clear. Overall, the contradictory results of studies on the role of M2 cytokines highlight the complex function of anti-inflammatory cytokines in PD pathology.

There is a lack of knowledge on the overall activation trajectory of the M1 and M2 phenotypes during the progression of PD. A study utilizing human α-syn overexpression model demonstrated a progressive increase in pro-inflammatory M1 markers after 2 and 4 weeks of α-syn induction, while expression levels of M2 markers were not significantly altered (Theodore et al., 2008). However, this study did not examine the activation profile in an advanced stage with apparent neurodegeneration. Therefore, additional longitudinal studies are needed to understand the dynamic M1/M2 activation profile in PD. Overall, microglial response in PD is heterogeneous and cannot be simplified by the distinction of M1 or M2 markers. There are also morphologically diverse microglia phenotypes in PD, including the bipolar/rod-shaped microglia that is also prominent in AD. Bipolar/rod-shaped microglia are present in the SN of PD patients surrounding degenerating DA neurons (McGeer et al., 1988), and in an experimental PD model, this phenotype emerged in the early stage before transitioning to a neurotoxic amoeboid phenotype, suggesting a potentially protective role for bipolar/rod-shaped microglia (Gao et al., 2002).

Microglia diversity in PD inferred from transcriptome studies

Recent advances in single-cell isolation techniques have enabled the transcriptional profiling of microglia in the PD brain, which has revealed the complex response of microglia. Mastroeni

and colleagues (2018) used single-cell laser microscopy technology in conjunction with RNA sequencing to specifically assess microglia-specific transcriptome changes between normal elderly control brains and in AD and PD-diseased brains in two pathologically affected brain regions: the SN (a PD-susceptible region) and the hippocampus region (prominent in AD pathology) (Mastroeni et al., 2018) Their findings identified regional and disease-specific heterogeneity in microglial response. Interestingly, despite the prominent role of microglia in inflammatory responses, inflammation-related transcripts did not appear to be the most significantly altered changes in the diseased brain. Aldosterone synthesis, ROS pathways, and biological processes related to behavior were enriched in PD samples, whereas neuronal repair and viral response functions significant enriched in AD samples. Only 2% of differentially expressed transcripts, mostly enriched in synaptic transmission functions, were shared between the vulnerable AD and PD regions, implying a complex and disease-specific microglial response.

Uriarte Huarte et al. (2021) recently examined microglial heterogeneity in the PD-susceptible SN region of non-diseased 6-month-old mice using a combination of in situ morphological analysis and single-cell transcriptomics (Uriarte Huarte et al., 2021). In comparison to microglia in the cortex and striatum, microglia in the midbrain region exhibited a distinct morphology with reduced ramification and branching, indicative of an activated state. A subset of microglia in the midbrain displayed a unique 'immune-alerted' transcriptional profile. The identified microglia cluster shares ~50% transcriptional similarity to reactive microglia under inflammatory conditions, including enrichment in processes associated with antigen presentation, cytokine signaling, and inflammatory responses, as well as inflammation-related biological pathways such as the TLR, TNF, and NFκB pathways. In addition to immune-related profiles, this 'immune-alerted' microglia

population also exhibited altered expression of genes essential for autophagy and ROS-related neurotoxicity. While this study did not examine microglia in a PD model, its findings highlighted the region-specific complexity of microglia, which may aid in elucidating potential mechanisms for the onset of PD.

More recently, Smajic et al. (2021) employed immunolabeling and single nuclei RNA-seq approaches to characterize the cell-specific response of cells in the midbrain of postmortem human PD tissue (Smajic et al., 2021). An increase in the number of microglia and a morphological change toward the amoeboid phenotype were evident in the SN of PD samples. Additionally, microglia in the PD brain exhibited a pro-inflammatory phenotype characterized by upregulation of Glycoprotein Nmb (GPNMB), Heat Shock Protein 90α (HSP90AA1) and IL-1β. Of the seven identified microglia clusters, three major microglia subpopulations were highlighted, representing various microglial activation responses. $P2RY12^{high}$ microglia cells were identified as resting subpopulations, whereas two activation branches were evident: one comprising $GPNMB^{high}$ cells and another subpopulation containing cells with upregulated expression of HSP90AA1 or IL-1B expression. Further characterization of the molecular phenotypes in PD revealed that the two activated subpopulations are enriched in cytokine signaling and unfolded protein response (UPR) pathways, and various PD risk factor genes linked with microglia activation profile are also present in these clusters, such as LRRK2 (Smajic et al., 2021). Also evident in the disease trajectory was the upregulation of genes encoding heat shock proteins, which facilitate neuroinflammatory responses by acting as DAMPs. Despite the limited knowledge of microglia phenotypes in PD, the highlighted transcriptome studies using scRNA-seq technology demonstrated that microglial responses in PD are heterogeneous and cannot be represented by the traditional M1/M2 paradigm.

Additional studies of human microglia with a large sample size are needed to better characterize the temporal and regional responses of microglia at various stages of PD.

1.5. Modulators of Microglia Phenotypes in NDs

As previously described, microglia in aging and NDs are highly plastic and can adopt a variety of activation phenotypes, which are often accompanied by an augmented inflammatory response and impaired homeostatic functions. There is considerable interest in identifying therapeutic targets that modulate microglia activity and promote protective anti-inflammatory/phagocytic phenotype while suppressing pro-inflammatory and neurotoxic responses. This section will summarize a few therapeutically relevant receptors, signaling molecules, and pathways that have been implicated in modulating microglial phenotypes in a variety of pathological contexts. Apart from the targets discussed here, additional microglia modulators have been reviewed elsewhere (Lan et al., 2017; Song & Suk, 2017), including many surface receptors (CD200R, CD36, prostaglandin E2 receptors) and key signaling molecules (PI3K/AKT, AMP-associated protein kinases (AMPKs), glycogen synthase kinase-3β (GSK3β), Rho-associated protein kinase (ROCK), and high-mobility group box-1 (HMGB1)).

1.5.1. TLR signaling pathway

Toll-like receptors (TLRs) are transmembrane pattern recognition receptors expressed on a wide variety of cells. TLRs are particularly abundant in microglia and their activity is dynamically regulated by different signals, including secreted endogenous DAMPs or exogenous PAMPs, such as bacterial endotoxin LPS (El-Zayat et al., 2019; Fiebich et al., 2018). Signaling mediated by these receptors, particularly TLR2 and TLR4, is one of the most extensively studied mechanism for inducing classical microglia activation and neuroinflammation (V. & C., 2019). Both TLR2

and TLR4 signal via receptor dimerization and subsequent recruitment of the adapter protein Myd88 to activate the pro-inflammatory NFκB pathway; TLR4 can alternatively signal via a Myd88-independent mechanism involving the TRIF adaptor (El-Zayat et al., 2019; Fiebich et al., 2018).

Activation of the TLR/Myd88/NFκB pathway results in the production of pro-inflammatory cytokines, chemokines, and ROS/RNS species, thereby enhancing neuroinflammation and neurotoxicity (V. & C., 2019). TLR4 activation also triggers other pro-inflammatory cascades such as mitogen-associated protein kinases (MAPKs) pathways (Wang et al., 2008). TLR4 activation is observed in many NDs, including AD, PD, and both hemorrhagic stroke subtypes (ICH and SAH), and its upregulation is associated with a pro-inflammatory response and adverse outcomes (Hickman et al., 2018; Lan et al., 2017; Lan et al., 2017; V. & C., 2019). High TLR4 expression correlates with cerebral vasospasm, ischemia, and neuronal injury in patients with SAH (Ma et al., 2015), and its expression in ICH impairs hematoma clearance and aggravates neurological deficit (Lan et al., 2017; Rodriguez-Yanez et al., 2012). TLRs serve as receptors for Aβ and α-syn in AD and PD, respectively, and their activation can promote pro-inflammatory and neurotoxic responses (Hickman et al., 2018).

Significant evidence in experimental disease models suggests that TLR4 or Myd88 deficiency provides neuroprotective effects by promoting the switch of microglia from the M1 to M2 phenotype and limiting microgliosis (Liu et al., 2018; Yao et al., 2017). Similarly, NFκB activation plays a role in a variety of NDs, and inhibition of this pathway limits pro-inflammatory responses and promotes a protective M2 phenotype (Ganbold et al., 2020; Lan et al., 2017). Therefore, therapeutic strategies that block the TLR4 pathway, such as astaxanthin and peroxiredoxin 2, have

been explored in various experimental models. In an ICH model, TLR4 antagonism or genetic deletion showed neuroprotection by limiting microglial activation in perihematomal tissue (Wang et al., 2013; Yang et al., 2015). Similarly, inhibition of TLR4 induces M2 polarization and provides neuroprotection in AD model (Cui et al., 2020).

Conflicting evidence suggests that TLR4 plays a protective role in various NDs models, due to its role in enhancing microglial phagocytosis of pathogenic proteins (Zhou et al., 2020). TLR4-mediated activation of microglia in the early stage of AD protects neurons by limiting Aβ deposition (Song et al., 2011); however, sustained Aβ exposure and TLR4 activation during disease progression alters microglial response by promoting a switch from the phagocytic phenotype to a neurotoxic phenotype (Go et al., 2016; Zhou et al., 2020). In addition to TLR4, TLR2 is also implicated in NDs, and activation of this receptor has been shown to induce microglial response and exacerbate neuronal injury in models of cerebral stroke, AD, and PD (Fiebich et al., 2018). However, its activation in a spinal injury model was shown to be protective by promoting a switch of microglia phenotype from M1 to an alternative M1:M2 phenotype (Stirling et al., 2014). Therefore, the precise role of TLRs in modulating microglial polarization or injury outcome is unclear and varies according to the specific pathological condition, activating signals, and the disease stage.

1.5.2. JAK/STAT pathway

Another critical pathway involved in pathogenic inflammatory responses is the Janus kinase (JAK)-STAT signaling cascade. JAK-STAT signaling is important in modulating both innate and adaptive immune responses, and abnormal activation of this pathway is observed in multiple NDs (Jain et al., 2022). JAK/STAT signaling is activated upon binding of cytokines and interferons to

their cognate receptors. Receptor-associated activation of JAKs induces the phosphorylation and subsequent nuclear translocation of STAT transcription factors, which promote the expression of inflammatory genes (Jain et al., 2022). JAK/STAT signaling has been shown to modulate microglia phenotypes in vitro and in vivo. STAT1 promotes M1 polarization in response to hypoxic stimuli by upregulating CD86, COX-2, and iNOS (Butturini et al., 2019). In vivo, inhibition of JAK/STAT reduces M1 polarization while increasing M2 polarization (Ding et al., 2019; Meng et al., 2016; Qin et al., 2017). JAK/STAT signaling is also involved in the regulation of microglial responses in pathological conditions. For example, SAH can trigger immediate phosphorylation and nuclear translocation of STAT3 and JAK/STAT3 inhibitors such as erythropoietin and AG490 limit M1 pro-inflammatory responses and improve brain injury (An et al., 2018; Wei et al., 2017). Similarly, inhibiting the JAK/STAT pathway in PD prevented neuroinflammation and neurotoxicity by limiting a-syn-induced microglial pro-inflammatory mediators (Qin et al., 2016). These findings suggest that inhibiting microglial JAK/STAT signaling may have therapeutic potential for NDs.

1.5.3. CX3CR1-CX3CL1 signaling

The CX3C chemokine receptor 1 (CX3CR1) and the fractalkine ligand (CX3CL1) form another important signaling axis that regulates microglial activation and function. CX3CR1 is expressed primarily by microglia and interacts with its neuron-secreted CX3CL1 ligand to mediate reciprocal microglia-neuron crosstalk, which serves as an important immune checkpoint (Pawelec et al., 2020). For example, the interaction of CX3CR1 and CX3CL1 suppresses microglial M1 pro-inflammatory responses such as the expression of IL-1β, IL-6, TNFα, and iNOS (Cardona et al., 2006; Mizuno et al., 2003; Zujovic et al., 2001), and downregulation of either CX3CR1 or

CX3CL1 is associated with enhanced microglial activation and neuroinflammation (Rogers et al., 2011). CX3CR1-CX3CL1 signaling has been shown to be neuroprotective in a variety of neurodegenerative models (Pawelec et al., 2020). For example, dysregulated CX3CR1-CX3CL1 signaling enhances microglial activation and promotes DA neuronal degeneration in PD (Cardona et al., 2006; Castro-Sanchez et al., 2018; Morganti et al., 2012). In both neurotoxic and α-syn PD models, overexpression of CX3CR1 or exogeneous CX3CL1 administration protected against microglia-mediated neurotoxicity (Nash et al., 2015; Pabon et al., 2011). A recent study showed that CX3CR1 knockout young microglia exhibit a premature aging transcriptome, accompanied by an age-associated alteration in microglial morphology and upregulation of inflammatory of inflammatory pathways (Gyoneva et al., 2019). These findings implicate a protective role of CX3CR1-CX3CL1 in suppressing neurotoxic microglial activation during aging. Interestingly, CX3CR1 has been associated with both neurotoxic and neuroprotective functions in AD model, and its diverse role in the AD has been attributed in part to competitive interaction of CX3CR1 with its endogenous ligand CX3CL1 or its pathological ligand tau, which can differentially affect microglial phagocytosis or activation response (Bolos et al., 2017; Pawelec et al., 2020). Overall, the CX3CR1-CXCL1 signaling modulates microglial inflammatory responses, and therapeutic modulation of these molecules should take into account the specific pathological insult and the disease stage.

1.5.4. Triggering receptors expressed on myeloid cells 2 (TREM2)

Triggering receptors expressed on myeloid cells 2 (TREM2) is a cell surface receptor that is expressed in myeloid cells and participates in various innate immune responses (Gratuze et al., 2018). In the CNS, TREM2 and its adaptor protein DNAX-activation protein 12 (DAP12) are

enriched in microglia, and activation of this complex regulates pro-inflammatory and phagocytosis responses (Gratuze et al., 2018; Zhong et al., 2017) TREM2 also mediates various protective functions, including sensing, housekeeping, and host defense responses (Hickman et al., 2018). TREM2 recognizes damage-associated lipid substrates such as phosphatidylserine expressed on the surface of apoptotic neurons, and it also binds ligands such as apoprotein E (apoE) and Aβ, subsequently eliciting chemotactic and phagocytic responses that ultimately mediates the clearance of apoptotic neurons and pathogenic proteins (Gratuze et al., 2018; Yeh et al., 2016; Zhao et al., 2018).

TREM2 was recently identified as an important receptor that regulates the microglial phenotypic switch from the inflammatory M1 microglia to the immunosuppressive M2 phenotype (Zhang et al., 2018). TREM2 knockdown in BV2 cells upregulates M1 microglial inflammatory responses and inhibits M2 polarization, while overexpression reverses this phenotype. In the absence of TREM2, the M2 polarizing cytokines, IL-4 and IL-13, cannot induce the expression of the M2 marker, indicating that TREM2 is required for adequate M2 polarization (Zhang et al., 2018). The expression of TREM2 is also downregulated by pro-inflammatory signals (Liu et al., 2020), which can further promote chronic neuroinflammation.

TREM2 also modulates microglial function in disease states, and several studies demonstrated that TREM2 deficiency impairs the clearance of apoptotic neurons and pathological substrates, thus attenuating disease progression (Gratuze et al., 2018; Kawabori et al., 2015; Zhao et al., 2018). TREM2 inhibition promotes pro-inflammatory microglial response and neurological deficit in a HS model (Hu et al., 2021). Microglial TREM2 is also strongly implicated in AD pathology, and loss of its expression alters microglial phagocytosis responses, which contribute to the formation

of dispersed Aβ plaques associated with enhanced neurotic damage (Wang et al., 2016). However, contradictory findings indicate that TREM2 may also play a detrimental role in AD pathology, suggesting that TREM2 functions differently depending on the stage of disease progression. For example, Sheng et al. (2019) demonstrated a dual role of TREM2 in different stages of APP/PS1 mice (Sheng et al., 2019). The phagocytic function of microglial TREM2 in the early-middle pathological stage (2-6 months old mice) exacerbated AD pathology by inducing synaptic loss, while its expression in advanced stages (6-10 months) prevented amyloidosis by limiting amyloid deposition. Therefore, the multifaceted function of TREM2 and its contradictory role in disease models warrant additional longitudinal research to determine its therapeutic potential.

1.5.5. P2Y receptors

Purinergic P2Y receptors are G-protein-coupled receptors that are activated by endogenous DAMPs such as nucleotides and play an essential role in modulating microglial response to stress and injury (Lovaszi et al., 2021). Recent research in animal models and human tissues has implicated the P2Y6 receptor (P2Y6R) and the P2Y12 receptor (P2Y12R) in the pathogenesis of multiple NDs. P2Y6R is essential for microglial phagocytosis of neurons and is primarily activated by UDP released by stressed/injured neurons (Koizumi et al., 2007) . P2Y6R also facilitates microglial clearance of amyloid plaques and improves cognitive defects in AD (Anwar et al., 2020). Additionally, P2Y6R-mediated phagocytosis mediates the removal of neuronal debris in a cerebral stroke model (Wen et al., 2020). Although these findings demonstrate the protective role of P2Y6R, microglial phagocytosis response induced by this receptor has been shown to exacerbate AD pathology by promoting microglial phagocytosis of stressed but viable neurons, which are capable of releasing UDP (Puigdellivol et al., 2021). In mixed neuron/glia culture, the

use of P2Y6R antagonist MRS2578 delayed neuronal loss induced by Aβ, and this effect was mediated by inhibiting microglial phagocytosis response. Similarly, mice lacking P2Y6R were protected from neuronal loss and cognitive deficit caused by aging and Aβ/tau pathology (Anwar & Rivest, 2020; Puigdellivol et al., 2021). P2Y6R is also implicated in PD pathology and has been considered a potential PD biomarker due to its high expression in patients (Yang et al., 2017). The role of P2Y6R in PD is unclear but has been implicated in enhancing neuroinflammatory responses (Yang et al., 2017). These studies highlighted the multifaceted role of UDP/P2Y6R signaling in mediating microglia-induced neurodegeneration.

The P2Y12 receptor is expressed exclusively in microglia in the CNS and is primarily activated by ADP, which is derived from the breakdown of ATP released from neurons and glia cells (Lovaszi et al., 2021). P2Y12R regulates microglial activation and migration and is strongly involved in the early-stage response of microglia in NDs (Haynes et al., 2006; Keren-Shaul et al., 2017; Maeda et al., 2021; Zrzavy et al., 2017). Recent scRNA-seq studies in various ND models identified P2Y12R-expressing microglia as a resting microglia subpopulation with crucial housekeeping and defense functions (Keren-Shaul et al., 2017). Downregulation of P2Y12R was shown to be one of the key alterations in signature transcripts as microglia transition from a homeostatic state to a neurotoxic phenotype (Keren-Shaul et al., 2017; Zrzavy et al., 2017). Diminished expression of P2Y12R has been evident in models of AD and other tauopathies, and P2Y12R-deficient microglia are closely found in brain regions with dense tau aggregates and significant neurodegeneration (Maeda et al., 2021). The expression level of P2Y12 also declines with age, which may contribute to age-associated changes in the microglial activation response (Lopes et al., 2022). Overall, these findings suggest that rescuing the loss of P2Y12R during aging

may have a potential therapeutic effect for NDs. However, additional research is necessary to investigate the mechanism and functions of P2Y6R and P2Y12R in different pathological conditions and disease stages.

1.5.6. Peroxisome proliferator-activated receptor γ (PPARγ)

The peroxisome proliferator-activated receptor γ (PPARγ), a highly expressed nuclear receptor in microglia, is a ligand-activated transcription factor that plays an important role in immune responses (Tyagi et al., 2011). Preclinical evidence suggests that PPARγ activation exerts neuroprotective effects in response to harmful stimuli and induces a phenotypic switch from M1 to M2 microglia (Mandrekar-Colucci et al., 2012; Pan et al., 2015; Wen et al., 2018; Zhao et al., 2017). Given the anti-inflammatory and neuroprotective roles of PPARγ, the FDA-approved antidiabetic drugs rosiglitazone and pioglitazone, which function as agonists for PPARγ, have been considered for the treatment of NDs (Saunders et al., 2021). Experimental studies in stroke models demonstrated that agonist-induced PPARγ activation promotes the expression of M2 markers (CD206, YM-1, IL-10, and TGF-β) while inhibiting classic M1 markers (iNOS, CD16, CD32, CD86, MMP-9) (Pan et al., 2015; Wen et al., 2018; Zhao et al., 2017).

PPARγ also plays a protective role in AD and PD. In a PD model, administration of PPARγ agonists reduced MPTP-induced pro-inflammatory cytokine production and prevents DA neuronal loss in the SN (Carta et al., 2011; Pisanu et al., 2014). Similarly, PPARγ agonists promote a phenotypic switch from the the M1 to M2 phenotype in AD mice and enhance microglial amyloid clearance by upregulating microglial scavenger receptors such as CD36 (Mandrekar-Colucci et al., 2012; Subramaniam & Federoff, 2017; Yamanaka et al., 2012). PPARγ agonist improves the uptake of misfolded protein deposits in AD mice, thereby suppressing Aβ levels and rescuing

cognitive function (Yamanaka et al., 2012). In a preclinical ICH model, PPARγ agonist improved hematoma clearance, neuronal injury, and functional recovery (Wang et al., 2018), and in vitro, PPARγ activation induces upregulation of CD36 and facilitates microglial phagocytosis of red blood cells (Zhao et al., 2009). Due to the beneficial role of PPARγ in modulating microglial function, several clinical trials have been initiated to evaluate the therapeutic potential of pioglitazone in NDs.

1.6. Challenges in Microglia Research

1.6.1. Specific microglia markers

Neuroscience research on microglia commonly employs a variety of techniques, including immunohistochemistry, microglia depletion method, in vivo imaging, and cre-lox systems (Miron & Priller, 2020). These technologies rely on markers to detect and/or target microglia, such as CX3CR1, CSF1R, Cd11b, and Iba1. However, commonly used microglia markers, particularly those that identify an activated state, do not differentiate resident microglia from infiltrating monocytes that enter the brain under pathological conditions characterized by a compromised blood-brain barrier (Amici et al., 2017). This lack of specificity is a significant impediment to microglia research, as most studies are limited to examining a mixed microglia/macrophage population. Flow cytometry enables a more selective separation of microglia cells that exhibit CD11b expression and low-to-intermediate levels of CD45 ($CD11b^{+}$, $CD45^{low\text{-}to\text{-}intermediate)}$, from a macrophage population with high expression of CD45 ($CD11b^{+}$, $CD45^{high}$) (Martin et al., 2017). However, this approach has been ineffective in pathological models, as microglial CD45 expression is upregulated in response to inflammation (Honarpisheh et al., 2020). Recently, unique microglial markers such as P2Y12R and Tmem119 have been identified (Bennett et al., 2016;

Butovsky et al., 2014). However, the utility of these putative markers in disease models has not been thoroughly investigated, and there are reports of decreased expression of these receptors under pathological conditions (van Wageningen et al., 2019), which may present a hurdle to targeting microglia in disease models.

1.6.2. Sex-specific heterogeneity of microglia

Another major hurdle in microglia research is the sex-associated differences in microglial responses. Microglia from male and female brains exhibit different characteristics, including differences in cell morphology, density, transcriptional profile, and cellular functions (Yanguas-Casás, 2020). Male microglia are characterized by a larger soma size, a higher migration capacity, increased pro-inflammatory gene expressions, and shorter lifespan, while female microglia have enhanced phagocytic capacity accompanied by increased expression of scavenger receptors, and have higher expression of protective genes involved in immune regulation and cellular repair. Given the central role of microglial phagocytosis and inflammation in NDs, gender-specific differences in microglial response should be carefully examined to elucidate disease mechanisms that contribute to sex bias in susceptibility to aging and NDs (Refer to Yanguas-Casas, 2020 for a detailed review (Yanguas-Casás, 2020)).

1.6.3. Limitation and heterogeneity of human microglia

Another complication in aging studies arises from species-specific heterogeneity of microglia. Despite the significant utility of animal models, there are inherent differences between human and rodent microglia, most notably in the aged brain, that can influence how microglia respond in NDs. Recently, a major distinction between human and mouse microglia was reported, demonstrating that human microglia have a unique transcriptional signature, including exclusive expression of

cell cycle and proliferation genes, as well as signature genes involved in the complement system and neurodegeneration (Geirsdottir et al., 2019). Human microglia exhibited age-dependent upregulation of genes associated with immune functions and pro-inflammatory responses, suggesting a "preactivated" state. In the presence of a disease-specific environment, already primed human microglia can foster a sustained inflammatory response. Furthermore, human microglia have been shown to exhibit greater transcriptome heterogeneity than microglia from animal models (Geirsdottir et al., 2019).

Since microglial activation and function are influenced by the natural aging process, commonly used preclinical models, such as transgenic animals that harbor risk factor alleles or genetic mutations, may not accurately mimic the response of microglia to human NDs. These factors, in addition to age-associated interspecies microglial differences, strongly support the need for human microglia research, which unfortunately has its own limitations. Obtaining primary human microglia for in vitro research is highly invasive, and the 'preactivated' nature of human microglia and its dynamic plasticity may preclude their use in vitro cultures, as changes in the microenvironment can significantly alter microglial transcriptome signatures and function (Gosselin et al., 2017).

Given these limitations, recent tools for large-scale studies of human microglia have been explored (**Figure 1.4**). Single-cell sequencing has become a powerful method to effectively capture the cellular heterogeneity of the brain and has helped characterize heterogeneous microglia subpopulations in the human brain using limited starting material. Additionally, the generation of microglia-like cells from human-induced pluripotent stem cells (hiPSCs) enables researchers to conduct mechanistic studies that require a large supply of human cells (Abud et al., 2017). hiPSC-

derived microglia also have the advantage in that they can be derived from neurodegenerative patients or genetically modified to mimic specific pathological conditions, allowing researchers to study the heterogeneous microglial responses in the context of human disease.

Incorporation of iPSC-derived microglia into a 3D cerebral organoid model also provides a great opportunity to study the complex interaction of microglia with neurons and other glial cells (Ormel et al., 2018). One major technical challenge in using organoid models is the fact that cell culture conditions may not permit simultaneous growth of different cell types, making it difficult to maintain the physiological ratio and distribution of cells in the brain. Recently, a cell-based microfluidics system was engineered, such as Brain-on-a-Chip technology, allowing researchers to incorporate organoid models in a continuous flow of microscopic fluid (Bang et al., 2019). This approach can help mimic the complex structural and functional properties of brain tissue by integrating components of the extracellular matrix. In addition, pathological stimuli, such as amyloid-β or α-synuclein, can be added to the microfluidic system to emulate disease-specific brain microenvironments. Finally, humanized microglia models have been developed by xenotransplanting human iPSC-derived microglia into immunodeficient mice expressing human microglia growth factors such as human CSF1 to maintain survival (Hasselmann et al., 2019; Mancuso et al., 2019; Svoboda et al., 2019). Interestingly, compared to microglia derived from human iPSC, the transcriptional profile of microglia from a humanized model more closely resembled human microglia (Mancuso et al., 2019; Svoboda et al., 2019). Overall, the use of multiomics technologies and innovative experimental models, such as organoid cultures and humanized chimeric mice, can provide powerful systems for studying the complex response of human microglia during aging and in NDs (**Figure 1.4**).

1.7. Conclusion & Outlook

This paper reviewed existing knowledge on the diverse functions and phenotypes of microglia in health, aging, and neurodegenerative diseases (NDs), highlighting the crucial role of microglia in the onset and progression of hemorrhagic stroke (HS), Alzheimer's disease (AD), and Parkinson's disease (PD). HS is an acute vascular disorder that causes neurodegeneration, while AD and PD are progressive chronic NDs with complex etiologies. PD selectively affects midbrain dopaminergic motor neurons in the substantia nigra and is commonly associated with motor deficit, while AD has a more widespread effect on hippocampal and cortical neurons and primarily affects cognitive functions. These three neurodegenerative conditions share pathogenic mechanisms associated with age, such as inflammation and oxidative stress, in which activated microglia play an important role.

Microglia can be activated by blood-derived components such as heme/thrombin in the case of HS, by misfolded α-synuclein aggregates in PD, and by extracellular amyloid-β and/or intraneuronal phosphorylated tau in AD. Microglial phagocytosis and activation in response to these mediators are facilitated through the activation of shared receptors, such as TLRs and scavenger receptors, which can lead to activation of various inflammatory pathways, including the NF_kB, JAK-STAT, and NLRP3 inflammasome (**Figure 1.3**). Microglia-mediated uptake of heme, α-syn, and Aβ/tau can also have protective effects by removing these pathogenic mediators from the extracellular space. However, as disease progresses, a chronic inflammatory and oxidative environment can promote sustained microglial activation that can cause neuroinflammation, oxidative stress, iron overload, and neurotoxicity. Microglia can also be activated by secondary mediators such as nucleotides, complement proteins, cytokines, and matrix metalloproteinases.

The general response of microglia has traditionally been simplified into two phenotypic states: an M1 pro-inflammatory phenotype associated with neurotoxicity, and an M2 anti-inflammatory and/or phagocytic phenotype involved in the clearance of hematoma/misfolded proteins, the resolution of inflammation, and tissue recovery. However, microglial response in NDs is highly dynamic and have diverse activation profiles. As disease progresses, the balance between protective and neurotoxic responses changes, and a dominant microglia phenotype can exist at a specific disease stage. Thus, targeting microglial M1/M2 balance and promoting a phenotypic switch from a pro-inflammatory phenotype to a protective phenotype have great therapeutic potential, and this can be achieved using immunomodulators that activate TREM2, PPARγ, and CX3CR1-CX3CL1 signaling, or by inhibiting TLR/NF_kB and JAK/STAT pathways (**Figure 1.3**).

Microglial response is complex and is shaped by the underlying pathology, which depends on the nature of the disease, as well as the severity, and clinical stage. For instance, in HS, rapid hematoma formation induces acute M1 polarization, and the M1/M2 balance declines with time, with the M2 phenotype serving a protective role in the recovery phase. This polarization trajectory appears to be reversed in AD, with a protective M2 phenotype predominating in the early stages of AD and a pro-inflammatory phenotype emerging as the disease progresses and Aβ clearance fails. Therefore, therapeutic interventions should consider the stage-specific microglial response. In HS, inhibiting the M1 microglia response at the acute stage and promoting an early transition towards the protective M2 phenotype may be beneficial, while in AD, immunomodulators that stabilize the protective microglia phenotype in the early/presymptomatic phase, prior to their transition to a neurotoxic phenotype, may be beneficial.

Since age is a shared risk factor for all three diseases, it may be beneficial to define and target preventive mechanisms that predispose people to NDs, such as age-dependent microglial alterations (**Figure 1.2**). Microglial priming and/or dysfunction are triggered by aging and are characterized by increased M1/M2 balance, impaired calcium homeostasis, and loss of sensing and phagocytosis responses. Defect in microglial phagocytosis limits the clearance of cellular debris, misfolded proteins (AD and PD), and hematoma elements (HS), which can trigger the onset and progression of NDs. Therefore, immunomodulators capable of restoring age-related loss of immunoregulatory proteins, such as TGF-β and CX3CL1, or those that block upregulated pro-inflammatory receptors, such as TLR4 and MHCII, have potential preventative roles. Furthermore, complement-mediated clearance mechanisms that are reactivated in the aged brain could be targeted to prevent age-related synaptic loss. Therefore, rescuing age-dependent microglia alterations may be beneficial to prevent the onset of NDs.

In conclusion, a detailed and longitudinal characterization of microglial phenotypes during aging, and in presymptomatic and symptomatic individuals, is necessary to identify an optimal disease-specific therapeutic window. Tremendous developments such as single-cell transcriptomics, innovative in vivo imaging technologies, humanized microglia models, and 3D organoid and Brain-on-a-Chip models are advancing mechanistic and translational microglia research, which will help elucidate the dynamic activation and functional changes of microglia in NDs.

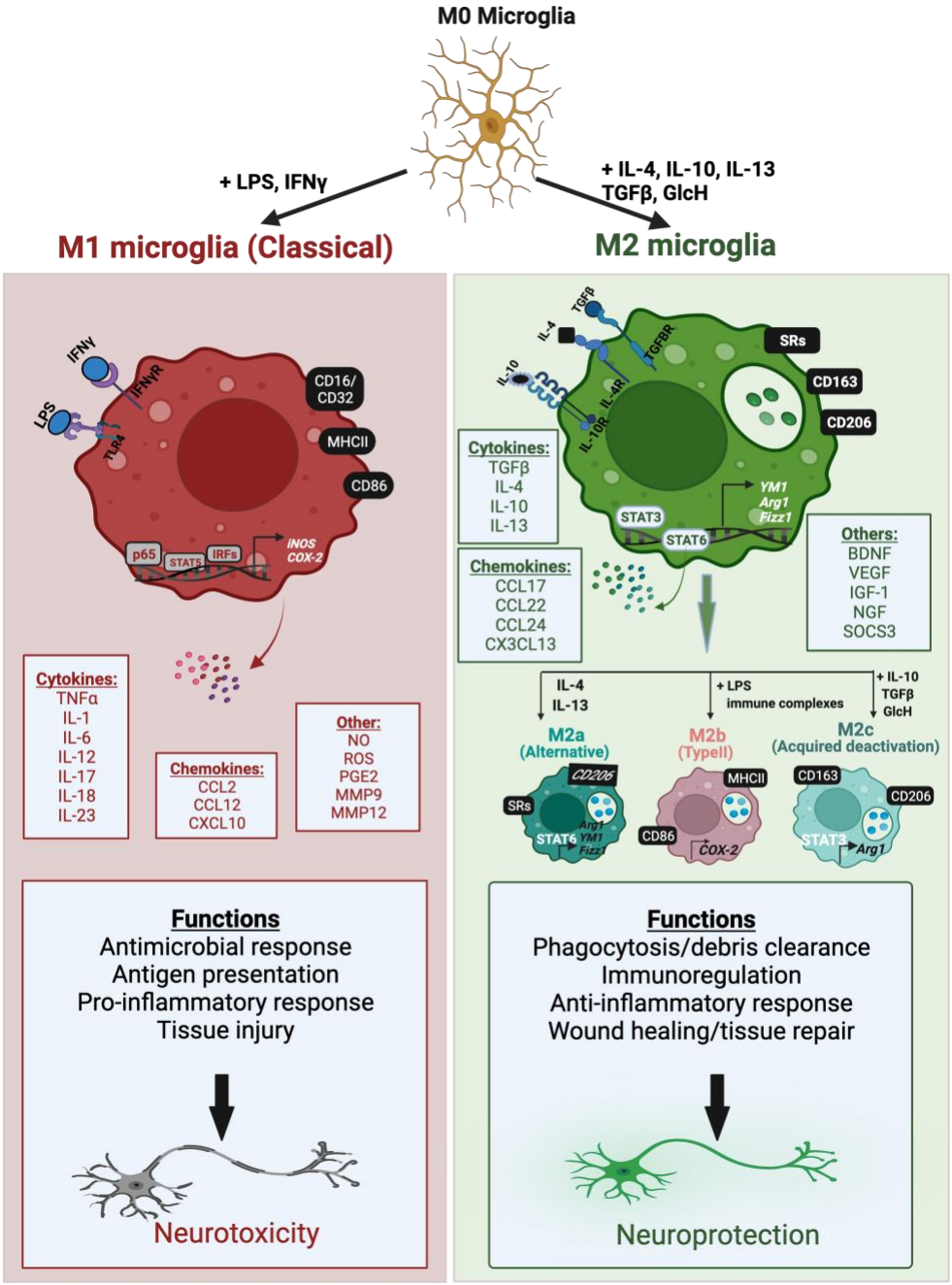

Figure 1.1. Microglial activation phenotypes and functions. Microglia can be polarized from a resting state (M0 microglia) to two main activation phenotypes, classically activated M1 microglia and alternatively activated M2 microglia, which are induced by interaction of inflammatory molecules with their respective cognate receptors. These microglia phenotypes exhibit a variety of phenotypic markers that are expressed intracellularly or on the cell surface, as well as molecules that are secreted from the cell, such as chemokines, cytokines, and other effector molecules. The M2 phenotype is further subdivided into three subtypes: M2a (alternatively activated state), M2b (type II activation phenotype), and M2c (acquired deactivation state). The M2b subtype shares similar features as M1 microglia and is induced by inflammatory molecules. The phenotypes of M1 and M2 microglia perform distinct functions that can be neurotoxic or neuroprotective, respectively. Figure created using BioRender.com.

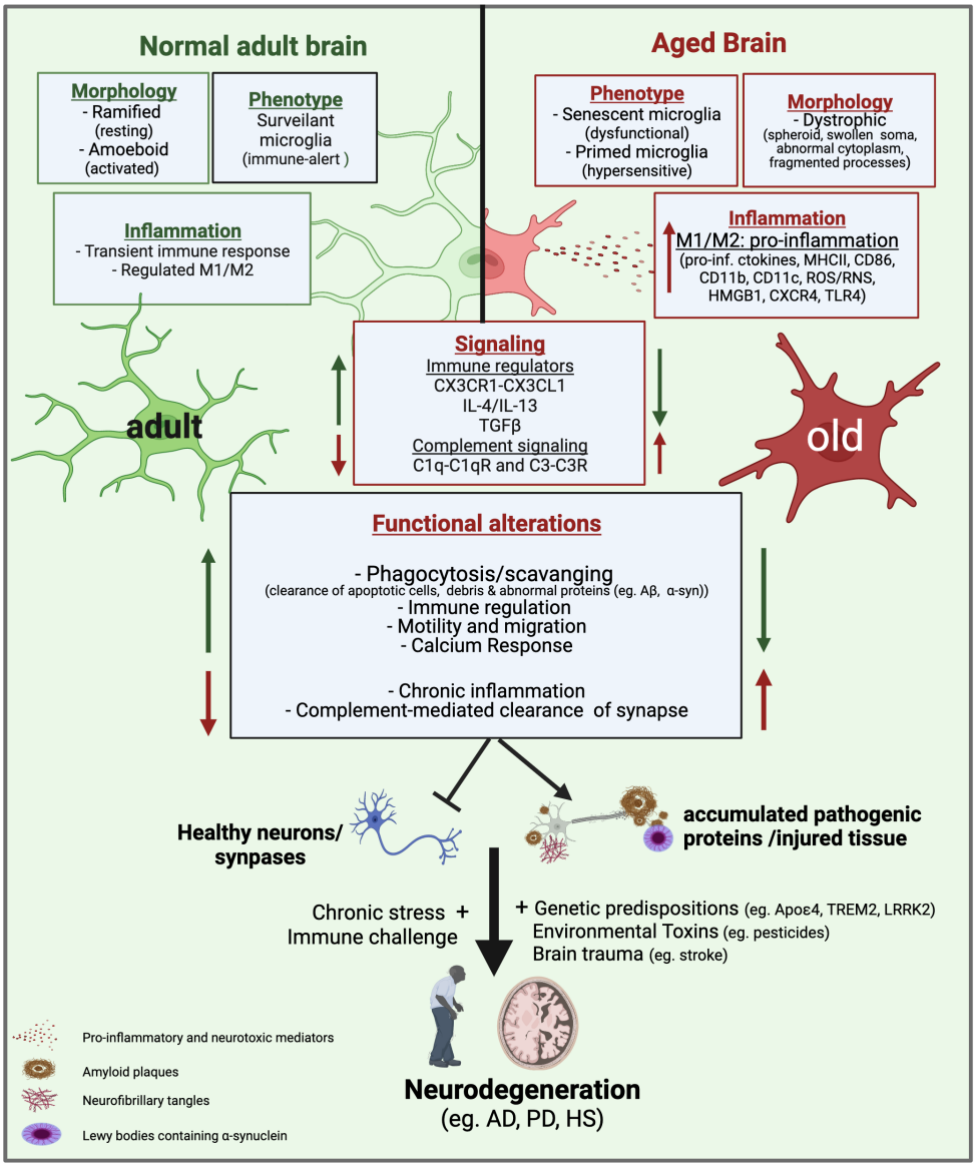

Figure 1.2. Age-dependent microglial changes implicated in neurodegenerative diseases. During aging, microglia exhibit alterations in their morphology, phenotypes, inflammatory response, and overall functional response. Healthy adult microglia with normal branched processes can effectively survey the brain microenvironment, and upon encountering infections, injury, and inflammatory agents, they change morphology and execute effector functions by becoming transiently activated. In comparison, old microglia have a dystrophic morphology associated with cellular senescence and exhibit a primed phenotype in which they are hypersensitive to environmental changes and produce large amounts of M1-like pro-inflammatory and neurotoxic mediators which contribute to chronic neuroinflammation. Age-associated loss of endogenous microglial regulatory pathways, such as CX3CR1-CX3CL1 signaling and TGF-β signaling, impairs microglial ability to regulate inflammatory responses. Aging is also associated with a decline in calcium response, motility, and phagocytosis functions, all of which impair microglial clearance of injured cells, tissue debris, and pathogenic proteins. However, complement-mediated phagocytosis mechanisms are upregulated in aged microglia and contribute to the loss of healthy neurons. These age-related microglial dysfunctions, in combination with either a chronic stress environment, brain trauma, or genetic predisposing factors, can contribute to the progressive onset of neurodegenerative diseases. AD: Alzheimer's disease; PD: Parkinson's disease; HS: Hemorrhagic stroke. Figure created using BioRender.com.

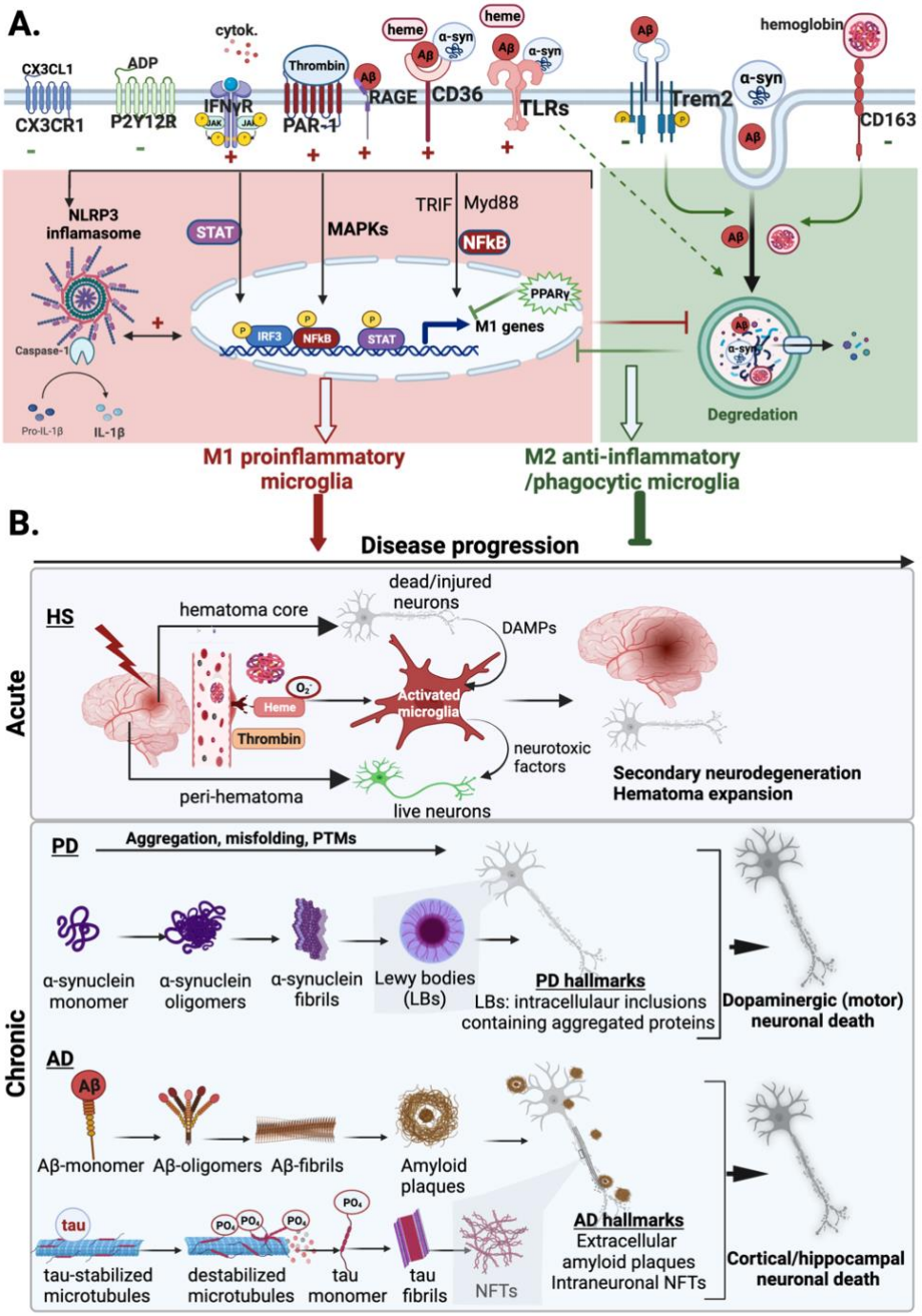

Figure 1.3. Microglial functions and diverse activation responses in neurodegenerative diseases. A) Summary of the major activation mediators and receptors involved in microglial responses to Alzheimer's disease (AD), Parkinson's disease (PD), and hemorrhagic stroke (HS). Microglia can be activated directly by disease-specific triggers such as amyloid-β (Aβ) in AD, α-synuclein (α-syn) in PD, or hematoma products such as heme/hemoglobin and thrombin in HS. Various shared microglial receptors interact with these pathogenic molecules, and their overall response depends on the nature of the disease, the stage of the disease, and the specific molecular trigger. Microglial response is also modulated by other mediators such as cytokines present in the

cerebrospinal fluid, damage-associated molecules (DAMPs), such as ADP, released from injured neurons, and neuron-derived endogenous signals such as CX3CL1. In general, microglial response can be pro-inflammatory/neurotoxic (+) or anti-inflammatory/neuroprotective (-). Activation of PAR-1, RAGE, CD36, and TLR receptors generally promotes pro-inflammatory responses by activating a range of pro-inflammatory pathways, such as JAK/STAT, MAPK, or NFκB, as well as the NLRP3 inflammasome. These diverse pro-inflammatory pathways can also interact synergistically, promoting chronic neuroinflammation. On the contrary, activation of P2YR12 and CX3CR1 negatively regulates microglial activation and pro-inflammatory responses and generally mediates protective functions. Similarly, activation of TREM2 and other scavenger receptors induces microglial phagocytosis of Aβ and other pathogenic proteins, aiding in their clearance. These two generally distinct microglial responses also antagonize one another; degradation of abnormal proteins and pathogenic mediators helps limit chronic neuroinflammation, while pro-inflammatory responses can compromise the microglial phagocytosis response. **B)** Summary of the role of microglia phenotypes in neurodegenerative disease progression. In HS, microglia can be activated by thrombin or heme or indirectly by DAMPs from injured neurons, and a sustained microglial pro-inflammatory response contributes to secondary neurodegeneration in areas outside the initial injury zone. Pro-inflammatory microglial responses in PD and AD trigger post-translational modifications (PTMs) and the misfolding and aggregation of α-syn and Aβ, that can contribute to the formation of amyloid plaques and Lewy bodies, thereby contributing to disease progression. Pro-inflammatory microglia also induce tau phosphorylation and subsequent aggregation, which promotes neurofibrillary tangle formation (NFT) and overall disease progression. Furthermore, pro-inflammatory microglia exhibit a dysregulated phagocytosis response, limiting the clearance of hematoma products and misfolded proteins that contribute to disease progression. On the contrary, anti-inflammatory/phagocytic microglia phenotypes mediate protective roles and limit disease progression by promoting tissue recovery. Figure created using BioRender.com.

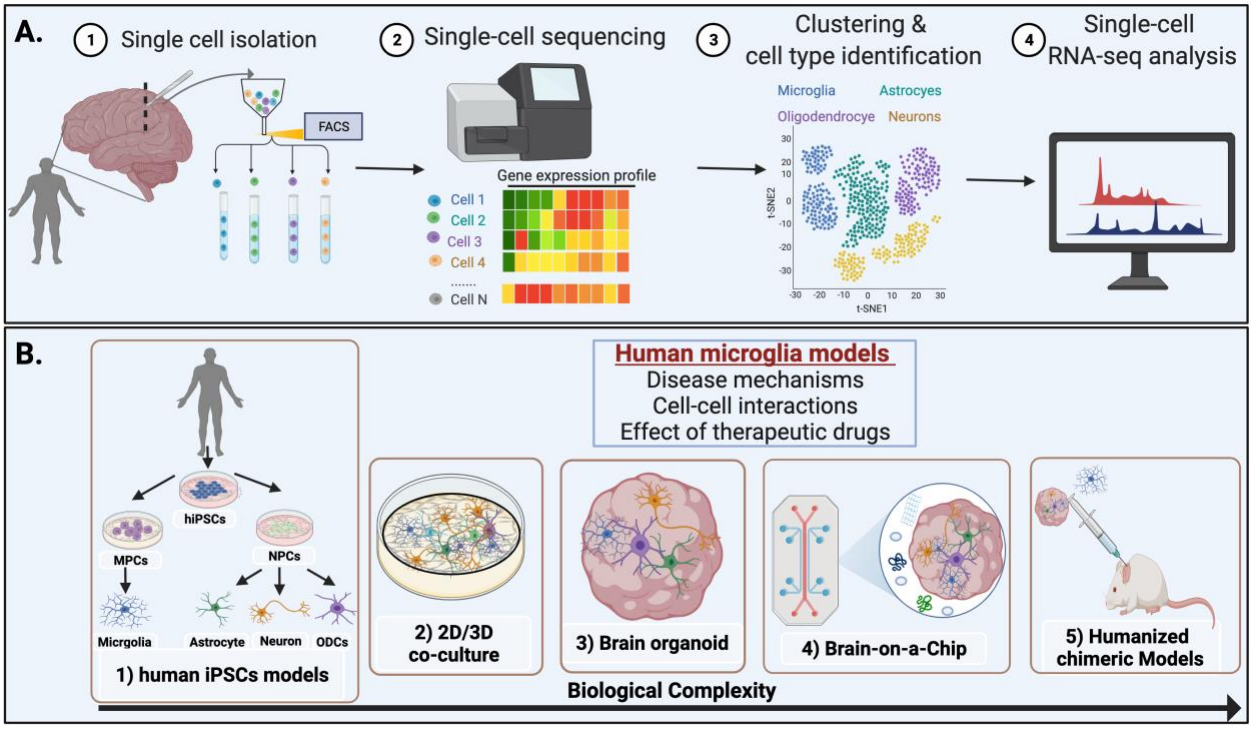

Figure 1.4. Innovative tools to study human microglia in neurodegenerative diseases. A) Single-cell sequencing can be performed by isolating single cells from live or postmortem brains. This tool assists in characterizing the gene expression profiles of various cell types, which helps to understand the heterogeneous phenotypes of microglia in human diseases. **B)** The generation of microglia-like cells from human-induced pluripotent stem cells (hiPSCs) has advanced mechanistic studies. iPSC can be derived from patients with neurodegenerative diseases or can be genetically modified to study human microglia responses in a specific disease environment. iPSC-derived microglia can also be co-cultured in two/three-dimensional systems or incorporated into brain organoids to study complex interactions of microglia with neurons and other cells. Brain-on-a-Chip technology employs a continuous flow of microscopic fluid in organoid systems, which enables the addition of extracellular matrix components to mimic the complex properties of the brain or incorporates pathogenic stimuli to emulate disease-specific brain microenvironment. Humanized microglia models, created through xenotransplantation of human iPSC-derived microglia models, help to study human microglia in intact models, and this technology is beneficial for translational research, such as therapeutic drug testing. Figure created using BioRender.com.

CHAPTER 2

RGS10 INTRODUCTION AND LITERATURE REVIEW

2.1. G protein signaling

2.1.1. G protein coupled receptors

G protein coupled receptors (GPCRs) constitute the largest and most diverse family of transmembrane receptors in eukaryotes (Hauser et al., 2017). GPCRs are involved in various physiological and pathological functions and dysregulated activity of these receptors are implicated in various neurodegenerative disorders (Azam et al., 2020). GPCRs are targets for 34% of all approved drugs from the Food and Drug Administration (FDA), making them the most frequently targeted receptors (Azam et al., 2020; Hauser et al., 2017).

GPCRs consist of seven transmembrane-spanning domains, and they bind to and propagate extracellular signals into cells by coupling with heterotrimeric G proteins (Wootten et al., 2018). GPCRs can mediate both sensory and nonsensory functions. Approximately 90% of the 370 nonsensory GPCRs are expressed in the central nervous system (CNS) and play an essential role in the regulation of the immune response, pain, cognition, mood, and synaptic transmission (Huang et al., 2017). GPCRs are widely expressed in microglia and modulate microglial activation response. Microglial GPCRs can transmit signals from chemokines, pathogenic peptides, hormones, and damage-associated molecular patterns (DAMPs) (Haque et al., 2018).

2.1.2. G proteins

G proteins are intracellular molecular switches that initiate various signaling pathways. There are two main classes of G proteins: small monomeric G proteins and heterotrimeric G proteins. The heterotrimeric G proteins consist of three subunits: α, β and γ subunits (Wootten et al., 2018). Gα binds to two guanine nucleotides (GDP and GTP) and dynamically transitions between inactive and active conformations. In resting state, Gα is bound to GDP and interacts with Gβγ dimers. Agonist-mediated activation of GPCR induces a conformational change that allows GPCR to interact with Gα subunit and function as a guanine nucleotide exchange factor (GEF), facilitating the exchange of GDP for GTP and the subsequent dissociation of the heterotrimeric complex (Syrovatkina et al., 2016; Wootten et al., 2018). The GTP-bound active Gα and the Gβγ dimmer interact with and regulate intracellular effectors, thereby initiating downstream G protein signaling cascades. Based on function and sequence, Gα subunits are categorized into four main families; Gαs (s: stimulatory) activates adenylyl cyclase, Gαi (i: inhibitory) inhibits adenylyl cyclase, Gαq/11 activates phospholipase Cβ (PLCβ), and the Gα12/13 family regulates small monomeric GTPase. The β and γ subunits form stable dimer and interacts with G proteins, as well as ion channels and downstream targets, and coordinate multiple GPCR functions (Syrovatkina et al., 2016; Wootten et al., 2018).

2.1.3. Gαs, Gαi, Gαq signaling

Due to the expression of diverse GPCRs and Gα subunits and specific coupling of GPCR-Gα, distinct intracellular signaling events can be activate that help regulate a broad range of cellular processes. The Gαs family of proteins activates adenylyl cyclase (AC) and leads to cyclic adenosine monophosphate (cAMP) production (Wettschureck & Offermanns, 2005). This

response is inhibited by Gαi/o family which functions to inactivate AC. AC catalyzes the synthesis of cAMP from ATP and triggers activation of cAMP-sensitive target effectors, including protein kinase A (PKA) and exchange proteins activated by cAMP (EPAC) (Rhee & Bae, 1997). PKA activation subsequently leads to phosphorylation of downstream effectors and activates several signaling responses (Sassone-Corsi, 2012). Therefore, these signaling events are amplified by Gαs and inhibited by Gαi.

Gαq activates the membrane enzyme phospholipase C β (PLCβ) which catalyzes the hydrolysis of plasma membrane (PM)-localized phospholipid, phosphatidylinositol 4,5-bisphosphate (PIP2) (Harden et al., 2011). Subsequently, this triggers the production of two important secondary messengers: diacyl glycerol (DAG) and inositol triphosphate (IP3). DAGs remain attached to the plasma membrane while soluble IP3 diffuses into the cytosol and activates the IP3 receptor (IP3R), a specific calcium channel in the endoplasmic reticulum, which allows calcium release from the ER to the cytosol (Harden et al., 2011). Membrane-bound DAG, in cooperation with cytoplasmic calcium, activates protein kinase C (PKC) and downstream PKC signaling (Harden et al., 2011; Huang, 1989). Therefore Gq-mediated signaling pathway plays an important role in regulating a wide range of calcium signaling events and calcium-sensitive cellular responses.

2.2. Regulator of G protein signaling

The signal and duration of G protein signaling pathways are regulated by various mechanisms. Gα subunits of proteins have intrinsic GTPase activity, which catalyzes the hydrolysis of GTP to GDP (Sprang, 2016). However, the intrinsic GTPase activity of Gα is slow and, for most Gα proteins, this process is accelerated by GTPase activating protein (GAPs)

(Sprang, 2016). Early genetic studies in yeast and nematodes has led to the discovery of a specific class of GAPs known as Regulator of G protein signaling (RGS), which has been shown to improve the rate of Gα-catalyzed GTP hydrolysis by > 1000-fold in vitro (Dohlman, 2009; Mukhopadhyay & Ross, 1999).

The RGS domain (~120 aa), found in over 20 proteins, consists of nine α helices and canonically functions to allosterically bind to activated Gα in the transition state and stabilizes the transition intermediate of the GTP binding pocket (Soundararajan et al., 2008; Tesmer et al., 1997). This enhances the intrinsic GTPase activity of Gα subunit leading to the hydrolysis of GTP to GDP and the reassembly of the heterotrimeric complex, thereby terminating downstream G protein signaling (**Figure 2.1**).

Ever since their discovery in the mid-1990s (Dohlman, 2009), much has been learned about the basis for Gα class specificity exhibited by members of the RGS family and their important role in regulating cellular signaling processes. To date, 39 human RGS-like proteins have been identified, containing at least one region of homology to the canonical RGS domain, and have been broadly classified into eight subfamilies based on structural and functional similarities (Almutairi et al., 2020). Among them, four subfamilies represent canonical RGS proteins: RZ, R4, R7, and R12. The RGS domain mainly mediates GAP activity for the Gαi/o and Gαq families and thus functions to regulate various Gi- and Gq-signaling pathways (Masuho et al., 2020).

Although the RGS domain is highly conserved, minor structural differences between the different RGS proteins determine Gα selectivity. The transition state for RGS-Gα interaction is mimicked in vitro using GDP+AlF_4^- that has allowed researchers to characterize the structural determinant for RGS-Gα interaction (Tesmer et al., 1997). The selectivity of the RGS domain for

a specific Gα class is dictated by the α5-6 loop of RGS which is a crucial Gα interacting surface on the RGS domain (Natochin & Artemyev, 1998). This region interacts mainly with the switch I, II and III interface on Gα subunit. Minor structural differences on the crucial Gα interacting surface of RGS or the switch I/II of Gα determine which RGS protein acts as a GAP for a specific subclass or member of Gα (Natochin & Artemyev, 1998; Tesmer et al., 1997). For example, Gαs is not a substrate for any known RGS protein due to a steric hindrance caused by a single residue difference between members of the Gαs and Gαi/Gαq class. A small conserved serine residue in switch II of Gαi and Gαq members is replaced by a larger aspartate residue in Gαs that impairs the interaction of Gαs with the RGS domain (Natochin & Artemyev, 1998).

The R4 subfamily RGS proteins are GAPs for both Gαi and Gαq, except for RGS2, which is selective for Gαq (Nance et al., 2013). Members of the R12 family have a selective preference for Gαi and primarily regulate Gi-signaling pathways, although weak Gαq GAP activity has been detected in vitro (Masuho et al., 2020; Taylor et al., 2016). Therefore, the expression of different types of RGS proteins and distinct selectivity towards a Gα class allow cells to modulate various signaling pathways and cellular processes.

2.2.1. Non-RGS domain of RGS proteins

In addition to structural requirements for RGS-Gα selectivity, the GAP functions of RGS proteins are influenced by other factors including tissue expression, subcellular localization, and protein-protein interactions with other effectors. For example, RGS proteins can mediate both G protein-dependent and G protein-independent functions through non-canonical mechanisms. However, most of these influencing factors have been reported to be determined by regions outside the conserved RGS domain.

The RZ (RGS17, -19, -20) and the R4 family (RGS1, -2, -3, -4, -5, -8, -13, -16, -18, -21) mainly contain the conserved RGS domain and a small N-terminal region involved in membrane targeting and receptor-selectivity, with the exception of RGS3, which also contains a multiprotein interaction PDZ domain (Almutairi et al., 2020; Hollinger & Hepler, 2002). Members of the R7 subfamily (RGS6, -7, -9 and 11) contain Gγ-like domain upstream of the RGS domain that mediates interaction with Gβ5 that indirectly regulates the GAP activity (Siderovski & Willard, 2005). They also contain a DEP domain that mediates interactions with some GPCRs, as well as the R7H domain postulated to play a role in membrane targeting (Hollinger & Hepler, 2002).

The R12 subfamily (RGS10, RGS12 and RGS14), although grouped based on high homology in the RGS domain, have distinct structural elements. While RGS10 is small and contains only the functional RGS domain, RGS12 &14 share two additional scaffolding domains: the Ras-binding domains (RBDs) binds to Ras and inhibit downstream Ras-signaling (Shu et al., 2010), while the C-terminal GoLoco motif functions as GDP-disassociation inhibitors for Gαi (Kimple et al., 2001). In addition to shared scaffolding domains, RGS12 also contains a phosphotyrosine-binding (PTB) domain and a PDZ domain and is the longest member of the RGS family. The PTB and PDZ domains mediate diverse interactions with GPCRs and other proteins (Xie & Palmer, 2007). These additional protein domains enable some RGS proteins to serve as scaffolding proteins and bring signaling components together to activate downstream pathways.

2.2.2. Non-canonical interactions and mechanisms of RGS proteins

In addition to regulating G protein signaling pathways, RGS proteins can modulate intracellular signaling responses downstream of different receptors and mediate noncanonical functions. For example, RGS3 regulates transforming growth factor β (TGFβ) signaling, activated

through the transmembrane serine-threonine kinase receptor. RGS3 binds to Smad2/3/4 transcription factors through a region outside its conserved RGS domain and inhibits TGFβ signaling by preventing Smad heterodimerization and gene transcription (Yau et al., 2008). RGS2 also uses a GAP-independent mechanism to regulate de novo protein synthesis by interacting with the eukaryotic initiation factors eIF2B, which is a heterotrimeric GTPases that controls mRNA translation (Nguyen et al., 2009). RGS2 uses its N-terminus region to interact with eIF2B which inhibits the GEF activity of eIF2B. This novel function of RGS2 has recently been shown to play a key role in stress response signaling by reducing global protein synthesis (Wang & Chidiac, 2019). RGS2 also uses its RGS domain to interact with the leucine-rich-repeat-kinase 2 (LRRK2), which is a multifunctional protein comprising of GTPase, kinase, and a scaffolding domain (Dusonchet et al., 2014). Aberrant activity of LRRK2 is a strong risk factor for Parkinson's disease (PD), and RGS2 interaction with LRRK2 inhibits both the GTPase and kinase activity of LRRK2, thus reducing LRRK2-induced neurotoxicity (Dusonchet et al., 2014).

RGS proteins can also use different mechanisms to interact with the same protein and regulate diverse functions. Prominent examples are RGS13 and RGS16 which interact with the regulatory subunit of PI3K (p85) (Bansal et al., 2008; Liang et al., 2009). RGS13 and RGS16 are members of the small R4 family that only have RGS functional domain but they regulate p85 through different mechanisms; while RGS13 interacts with p85 via its N-terminus region and regulates allergic responses in mast cells (Bansal et al., 2008), RGS16 interacts with p85 through its RGS domain and inhibits the downstream PI3K/Akt pathway, thereby regulating cancer proliferation (Liang et al., 2009).

An increasing number of studies reveal that, instead of localizing near the cell surface, RGS proteins can shuttle across different subcellular compartments, such as the nucleus, where G proteins and their effectors are not believed to exist (Branch & Hepler, 2017; Chatterjee & Fisher, 2000). These diverse localization patterns are suggestive of non-canonical roles of RGS proteins. Most of the previously reported GAP-independent functions of RGS proteins mediated by noncanonical interactions which occurs through regions outside the conserved RGS domain.

The dynamic localization and interaction of RGS proteins can also be modulated by intracellular signals. For example, cAMP or Ca^{2+}-signaling induces nuclear accumulation of RGS13, where it forms a location-specific interaction with phosphorylated CREB and disrupts the binding of CREB to DNA and the CREB binding protein (CBP)/300 (Xie et al., 2008). RGS13 does not utilize its GAP activity to inhibit CREB-mediated transcription. However, this interaction occurs upstream of the RGS domain, in the diverged N-terminus region. In addition to the nucleus, RGS proteins can also be targeted to a specific subcellular location where they mediate diverse G protein-independent functions via non-canonical interaction partners. For example, microtubule-localized RGS14 interacts with tubulin and promotes tubulin polymerization (Martin-McCaffrey et al., 2005), and similarly RGS2 interacts with Nek7 in the mitotic spindle and mediates noncanonical function in promoting mitotic spindle organization (de Souza et al., 2015).

G proteins play an important role in activating G protein-gated ion channels via direct interactions with ion channels or through indirect mechanisms (Breitwieser, 1991). Similarly, the GAP function of RGS enables RGS proteins to modulate intracellular calcium signals (Wang et al., 2004). For example, RGS proteins that have Gαq selectivity alter calcium signaling by regulating the GPCR/PLC/IP3 pathway (Kimple et al., 2011; Wang et al., 2004). The RGS domain

of some small RGS proteins, including RGS10, has been shown to form a direct interaction with calcium-sensitive proteins such as calmodulin in a calcium-dependent manner, and competitive and dynamic interaction between calmodulin and PIP3 induces Ca^{2+} oscillation (Yang & Li, 2007). These findings suggest that RGS proteins can use various mechanisms to regulate intracellular calcium response. Interestingly, GAP-independent mechanisms have also been attributed to RGS-dependent regulation of calcium responses. The N-terminus region of the small RGS2 protein has been shown to directly associate with and inhibit the calcium channel TRPV6, thus altering the gating properties of this ion channel in a G protein-independent mechanism (Schoeber et al., 2006). In general, these findings suggest that RGS proteins can control calcium signaling through both GAP-dependent and independent mechanisms.

In conclusion, while RGS proteins play an essential role as GTPase-activating proteins through their conserved RGS domain, their dynamic subcellular localization and and context-dependent interactions with noncanonical proteins provide an additional layer of regulation of cellular signaling. Given the high homology among various RGS proteins, characterizing non-canonical interactions and functions of RGS is advantageous to identify specific regulatory mechanisms of RGS that do not interfere with the physiologically relevant GAP function or affect the activity of other RGS proteins.

2.3. Regulator of G protein signaling 10

RGS10 is the smallest RGS protein (~20kDa), which makes it a unique member of the R12 subfamily. Although classified into the R12 family based on the homology of RGS domain, RGS10 resembles the R4 family members in that it only contains the conserved RGS domain (Hollinger & Hepler, 2002). Other than its conserved 120 aa core RGS domain, RGS10 only

contains small N-terminus and C-terminus extensions that harbor regulatory modification residues (Almutairi et al., 2020). RGS10 is conserved between different species, and the *Rgs10* gene is located on the human chromosome 10q26.11 and the mouse chromosome 7 F3. According to the latest NCBI annotation, there are two isoforms of the human and mouse RGS10 protein, a 181aa long variant (RGS10-1) and a 167aa short variant (RGS10-2). The two isoforms differ only in the first few residues at the N-terminus region and have identical RGS domain. These isoforms are produced by alternative splicing of the first exon of the *Rgs10* gene (Sierra et al., 2002). Interestingly, RGS10-2 has been shown to have impaired GAP function (Ajit & Young, 2005), implying that the N-terminus region has a functional role for effective GAP activity of RGS10. In humans, a third isoform containing a 173a.a has been reported that is translated from an upstream alternative start site (Almutairi et al., 2020). These isoforms have tissue-specific expression, and a dominant isoform exists in most tissues. RGS10-1 is thought to be the most dominant isoform in immune cells.

2.3.1. Canonical GAP function of RGS10

RGS10 has GAP selectivity for Gi family Gα subunits, including Gαi, Gαo, and Gαz (Masuho et al., 2020). Through its canonical GAP function, RGS10 regulate the activity of various Gαi-coupled GPCRs. The determinants of RGS10 selectivity have previously been characterized through structural studies of unbound and Gα-bound RGS10 (Soundararajan et al., 2008; Taylor et al., 2016). Unlike the R4 subfamily members that bind to both Gαi and Gαq, RGS10 has specific preference for Gαi that is dictated by minor structural differences. For example, the α6 helix region is different between RGS10 and other R4 subfamilies that determines its Gαi/Gαq selectivity. Due to a disordered and a smaller α6 helical region in RGS10, the α7 helix of RGS10 starts earlier than

other R4 families. Therefore, a conserved Glu-Lys dyad that is present in R4 family RGS domain is absent in RGS10. Instead, this region of RGS10 has a Lys-Tyr dyad, and the presence of a charged lysine at position 1 and a bulkier tyrosine side chain position 2 creates a steric clash with Gα interacting surface of Gαq, making RGS10 an ineffective GAP for Gαq (Soundararajan et al., 2008; Taylor et al., 2016; Tesmer et al., 1997).

Due to its selective preference for Gαi, the GAP activity of RGS10 primarily regulates the activity of Gαi-coupled GPCRs. By inhibiting Gαi activity, RGS10 functions to enhance adenylyl cyclase activity and the subsequent production of cAMP, which activates downstream PKA signaling. In CHOK1 cells stably overexpressing human serotonin 5-HT1A (Gi-coupled GPCR), overexpression of RGS10 attenuates Gαi-mediated inhibition of AC (Ghavami et al., 2004). Similarly, RGS10 expression in HEK293 cells was shown to attenuate μ-opioid receptor (μ-OR)-mediated inhibition of AC activity (Xie & Palmer, 2007). Furthermore, RGS10 regulates M2 muscarinic receptor-mediated activation of GIRK channels, which are activated by Gβγ subunits released from G proteins of the Gαi family (Burgon et al., 2001). Most chemokine receptors utilize pertussis toxin (PTX)-sensitive Gαi for signaling; therefore, RGS10 GAP functions can regulate chemokine signaling pathways. Stimulation of T cells with the chemokine CXCL12 was shown to induce a rapid association of RGS10 with Gαi (Thelen & Stein, 2008), and RGS10 attenuates both CXCL12 and CCL21-induced signaling that is necessary for T cell adhesion. This effect of RGS10 was abrogated with PTX, suggesting that RGS10 is an important regulator of Gi-dependent function (Garcia-Bernal et al., 2011).

2.3.2. Subcellular localization and post-translational regulation of RGS10

Unlike other small RGS proteins, RGS10 lacks the amphipathic helix and cysteine string found in the N-terminus region of the R4 family that target some RGS proteins to the plasma membrane (PM) (Almutairi et al., 2020). However, it harbors a conserved cysteine 66 (Cys66) residue within the RGS domain, that is thought to be a site for palmitoylation and targets RGS proteins to the PM, as evident in in vitro palmitoylation assay and in Sf9 insect cells (Tu et al., 1999). Palmitoylation of Cys66 increases the steady-state GAP activity of RGS10 BY >20 fold in receptor-G protein reconstituted proteoliposomes (Tu et al., 1999).

In addition to regulation of GAP activity through membrane-targeting mechanism, the GAP activity of RGS10 can be influenced by other mechanisms that affect the subcellular translocation of RGS10. Strong evidence suggests that RGS10 is localized in both the nucleus and the cytoplasm and that its subcellular expression is dynamically regulated (Burgon et al., 2001; Lee et al., 2008). However, an early study by Chatterjee et al. (2000) demonstrated that ectopically expressed RGS2 and RGS10 predominantly localize in the nucleus in COS-7 cells, while other small RGS proteins such as RGS4 and RGS16, are nucleocytoplasmic shuttling proteins (Chatterjee & Fisher, 2000). Furthermore, this localization pattern of RGS10 was shown to be similar in H4 human neuroglioma cells that endogenously express RGS10 (Chatterjee & Fisher, 2000). In this study, they also characterized the molecular determinant for RGS localization and identified nuclear localization signal (NLS) within the conserved RGS domain, and a nuclear export signal (NES) that exists in some RGS proteins in the variable N-terminus region. However, other studies that characterized RGS10 expression in human HEK293 cells and in microglia

demonstrate that RGS10 can be localized in both the cytosol and the nucleus (Burgon et al., 2001; Lee et al., 2008).

The C-terminus region of RGS10 contains a proline-glutamate-serine-threonine (PEST) sequence, which is believed to serve as a proteolytic signal for proteasome degradation (Rechsteiner & Rogers, 1996). RGS10 also contains a conserved lysine residue (Lys148), which is thought to be a putative ubiquitination site. A recent quantitative proteomics study identified RGS10 as a substrate for the E3 ubiquitin ligase TRIM32, and endogenous binding between RGS10 and TRIM32 was validated in Hela cells and embryonic brains (Zhu et al., 2020). TRIM2 enhanced RGS10 ubiquitination and subsequent proteasomal degradation in lateral/medial ganglionic eminence (L/MGE) progenitors. Accumulation of RGS10 in TREM2 knockout mice or in the presence of MG-132 proteasome inhibitor suppressed downstream mTOR signaling, which resulted in impaired L/MGE proliferation, GABAergic interneuron generation, autism-like behaviors (Zhu et al., 2020). This is the first evidence implicating post-translational mechanism in the regulation of RGS10 stability. Therefore, the expression and function of RGS10 can be dynamically regulated by various post-translational modifications.

2.4. RGS10 in neuroinflammation

Neurodegenerative diseases (NDs), which affect around 30 million people worldwide, are prevalent in elderly people and cause progressive neurodegeneration and neuronal dysfunction (detailed in Chapter 1). Extensive research is ongoing to understand the underlying mechanism of neurodegeneration. Several pieces of evidence suggest that chronic activation of microglia are involved in the onset and progression of several NDs. Activated microglia release soluble factors that are neuroprotective or neurotoxic depending on their activation state. Pro-inflammatory

microglia release various neurotoxic mediators, including pro-inflammatory cytokines, prostaglandins, and reactive oxygen species that induce neurotoxicity. Injured neurons in turn release danger signals known as damage-associated molecular pattern molecules (DAMPs), which directly activate microglia. The importance of this bidirectional crosstalk between microglia and neurons is gaining attention in neurodegenerative diseases. Growing evidence suggests that M1 microglia are a chronic source of several neurotoxic factors, including reactive oxygen species (ROS), complement elements, and pro-inflammatory cytokines. In contrast, M2 microglia release anti-inflammatory and neuroprotective factors. Therefore, current therapeutic strategies focus on identifying mechanisms to regulate the activity of M1 microglia and enhance M2 phenotypic state and limiting the neurotoxic interplay between microglia and neurons (detailed in Chapter 1).

2.4.1. RGS10 regulates microglial activation and protects against inflammation induced neurotoxicity.

RGS10 is abundantly expressed in the brain, prominently in microglia (Butovsky et al., 2014). Previous studies have identified RGS10 as an important regulator of microglial activation. Loss of RGS10 expression in microglia is associated with dysregulation of inflammatory milieu in the brain and a risk for age-related neurodegeneration (Kannarkat et al., 2015; Lee et al., 2012; Lee et al., 2011; Lee et al., 2008). A significant understanding of RGS10 function in CNS pathology came from previous studies by Lee et al. that identified neuroprotective effects of microglial RGS10 in the lipopolysaccharide (LPS) inflammation model of Parkinson's disease (PD) (Lee et al., 2012; Lee et al., 2008). The bacterial endotoxin LPS is a pathologically relevant stimulus that activates microglial Toll-like receptor 4 (TLR4) (Goulopoulou et al., 2016). Microglial TLR4 is also activated by various pathological triggers, and enhanced upregulation and

activation of TLR4 is implicated in diverse neurodegenerative diseases (detailed in Chapter 1). Therefore, LPS-mediated activation of TLR4 is commonly used to mimic neuroinflammatory processes associated with neurodegeneration, and mediators that regulate LPS/TLR4 signaling, such as RGS10, are potential therapeutic targets.

Key findings from Lee et al. demonstrates that compared to wild-type (WT) mice, RGS10-deficient ($RGS10^{-/-}$) mice exhibit significant loss of dopaminergic neurons in the substantia nigra pars compacta (SNpc) in response to a chronic low-dose injection of LPS compared to wild-type mice (Lee et al., 2008). Additional key findings from their study indicate that $RGS10^{-/-}$ mice also exhibit increased microglia burden and activation, and primary microglia isolated from these mice have dysregulated inflammatory signals such as enhanced production of pro-inflammatory cytokines, including tumor-necrosis factor α (TNFα) and pro-inflammatory interleukins (IL-1β, IL-6, IL-12) (Lee et al., 2013; Lee et al., 2008). In a follow-up target-effector experiment, Lee et al. further characterized the mechanism for neurodegeneration. They exposed differentiated MN9D dopaminergic neurons to conditioned media collected from wild type (WT) and $RGS10^{-/-}$ primary microglia and observed that LPS-activated conditioned media from $RGS10^{-/-}$ are significantly more toxic compared to activated WT microglia. This result demonstrates that RGS10's ability to downregulate microglial inflammatory response is neuroprotective for dopaminergic neurons.

In addition to LPS inflammation model, the neuroprotective effect of RGS10 is also evident in the 6-OHDA neurotoxin model of Parkinson's disease (Lee et al., 2011). Adenovirus-mediated expression of RGS10 into the SNpc of rats attenuated microgliosis and protected against 6-OHDA-induced degeneration of dopaminergic neurons. The anti-inflammatory effect of RGS10 is also

observed and consistently modeled in immortalized BV2 microglia cell lines (Almutairi et al., 2021; Alqinyah et al., 2018; Wendimu et al., 2021). Collectively, these results demonstrate that RGS10 plays a neuroprotective role by suppressing pro-inflammatory and neurotoxic mediators released from microglia.

Mechanistically, Lee et al. demonstrated that loss of RGS10 in microglia enhances NFκB signaling (Lee et al., 2011), a pro-inflammatory pathway activated downstream of TLR4 activation, and is also implicated in the pathophysiology of various neurodegenerative diseases (see Chapter 1). However, the anti-inflammatory mechanism of RGS10 in the regulation of NFκB is not yet defined. It was also shown that RGS10 is evenly localizes throughout both the cytoplasm and nuclear compartments in resting microglia; but LPS-mediated-activation induces increased nuclear translocation (Lee et al., 2008). The dynamic localization pattern of RGS10 in response to microglia activation is unexpected, since the canonical GAP function of RGS proteins occurs in the cytoplasm near the plasma surface surface. Therefore, this finding suggests a potential noncanonical mechanism of RGS10 in activated microglia.

Previous evidence showed that specific and inducible phosphorylation of RGS10 on serine 168 by the cAMP-dependent kinase (PKA) induces RGS10 localization from the cytoplasm to the nucleus, thus impairing its canonical activity near the PM which is necessary to regulate G protein-dependent activation of GIRK (Burgon et al., 2001). Interestingly this phosphorylation residue is located downstream of the RGS domain, which is thought to harbor the NLS (Chatterjee & Fisher, 2000). Thus, the molecular determinant dictating PKA-mediated RGS10 nuclear translocation is not known. Overall, while these findings implicate a protective role of RGS10 in TLR4/NFκB regulation, its anti-inflammatory mechanism has not been defined.

2.4.2. RGS10 exerts neuroprotective effects by regulating Tumor necrosis factor α

Tumor necrosis factor α (TNFα) is one of the critical pro-inflammatory and neurotoxic cytokines synthesized by activated microglia (Raffaele et al., 2020). TNFα is a potent activator of inflammatory responses and can induce activation of additional resting microglia cells and other glial cells in the adjacent brain region by binding to and activating TNFR1 (p55) and TNFR2 (P75), further amplifying neuroinflammatory responses (Raffaele et al., 2020). Furthermore, dopaminergic neurons in the SNpc have high expression of TNF receptor 1, which is a canonical death receptor that elicits a pro-apoptotic response and sensitizes cells to TNF-mediated neurotoxicity (Probert, 2015). Etanercept is an FDA-approved biologic TNF inhibitor that acts as a soluble TNF receptor and binds TNF, thereby preventing TNF interaction with its natural receptors (Gencoglan et al., 2009). Etanercept exhibits neuroprotective effects in various neurodegenerative diseases. Given the pro-inflammatory and neurotoxic role of TNFα, endogenous mechanisms that regulate TNFα synthesis in microglia are important therapeutic targets. RGS10 strongly suppresses the release of TNFα from microglia (Lee et al., 2012; Lee et al., 2011; Lee et al., 2008). Furthermore, the neurotoxic effect of microglial RGS10 was shown to be blocked by the addition of etanercept, suggesting that RGS10 limits microglial-derived TNF secretion (Lee et al., 2008).

In addition to microglia, RGS10 is also expressed in dopaminergic neurons, albeit to a lesser extent (Lee & Tansey, 2015). Interestingly, neuronal RGS10 is also shown to be protective, as stable overexpression of RGS10 in differentiated MN9D dopaminergic cells attenuated TNF-induced cytotoxicity. The protective effect of RGS10 was shown to be mediated by inhibition apoptotic effectors such as PARP-1 and caspase 3, and enhanced activation of PKA/CREB pro-

survival pathway (Lee et al., 2012). This neuroprotective effect of RGS10 required PKA-mediated phosphorylation of RGS10 at Ser168. These results suggest that RGS10 expressed in microglia and neurons exerts a synergistic role in limiting microglia-derived TNF secretion and subsequent TNF-mediated cytotoxicity. It is not known whether RGS10 also regulates apoptotic and survival pathways in microglia. Therefore, RGS10 may have diverse neuroprotective mechanisms in different cell types.

2.4.3. RGS10 suppresses the induction of cyclooxygenase-2 in microglia

Cyclooxygenase isoforms (COX-1 and COX-2) are direct targets for many nonsteroidal anti-inflammatory drugs, and their regulation is crucial for therapeutic management of inflammation. COX catalyzes the initial rate-limiting step in prostaglandin (PG) biosynthesis, which is the conversion of arachidonic acid to an intermediate PGH2 (Ricciotti & FitzGerald, 2011). PGH2 is further metabolized by downstream enzymes, producing various PGs. COX-2, predominantly present in neurons, is induced in immune cells such as microglia and is strongly involved in neuroinflammation and neurodegeneration (Ricciotti & FitzGerald, 2011; Vijitruth et al., 2006). COX-2 has emerged as the primary isoform responsible for the production of prostanoid in acute and chronic neurodegenerative diseases. In a PD model, it has been shown that PGE2 produced by the enzymatic action of COX-2 activates prostaglandin E2 receptor 2 (EP2) in microglia in an autocrine manner, thereby resulting in sustained microglial activation during chronic stress that contributes to neurotoxicity (Vijitruth et al., 2006). PGE2 also interacts with EP receptors on neurons, resulting in enhanced neurodegeneration (Kang et al., 2017). COX-2 also plays a detrimental role by oxidizing a variety of targets that contributes to oxidative stress (Madrigal et al., 2003). Various neuroinflammatory processes are involved in the induction of

COX-2; therefore, mechanisms that regulate COX-2 induction and the subsequent production of PGE2 have emerged as an important therapeutic target for neurological diseases, including PD and stroke (Kang et al., 2017; Vijitruth et al., 2006) .

To further expand the neuroprotective roles of RGS10, our group recently explored the role of RGS10 in the regulation of COX-2. In addition to its role in the regulation of pro-inflammatory cytokines, our recent findings showed that both siRNA-mediated loss of RGS10 and CRISPR/Cas9 mediated deletion of RGS10 significantly amplified LPS-induced COX-2 production and the subsequent PGE2 production (Alqinyah et al., 2018). Therefore, the ability of RGS10 to downregulate COX-2/PGE2, along with its previously implicated anti-inflammatory and neuroprotective roles, further position RGS10 as an important therapeutic target.

2.4.4. RGS10 exerts protective roles in various inflammatory and pathological models.

RGS10 exerts protective roles in multiple models, and loss of its expression is implicated in the pathophysiology of various diseases including Parkinson's disease (PD) (Lee et al., 2011), influenza (Almutairi et al., 2021), osteoporosis (Yang & Li, 2007), vascular injury (Hensch et al., 2016; Miao et al., 2016), rheumatoid arthritis (Ren et al., 2021), and periodontitis (Chan et al., 2022). Essential to the pathophysiology of neurodegenerative disease is the contribution of the vasculature and circulating immune cells that infiltrate the CNS following blood-brain barrier (BBB) dysfunction and induce systemic inflammation (Lopes Pinheiro et al., 2016).

Considering the detrimental effects of systemic inflammation in neurodegenerative diseases, it is apparent that the role of RGS10 in peripheral immune cells may also be implicated in neuroinflammatory processes. For example, RGS10 is expressed in peripheral macrophages, where it has been shown to play an important role in suppressing TLR4-induced M1-like pro-

inflammatory response while enhancing M2-like anti-inflammatory response (Lee et al., 2013). Peripheral macrophages have essential role in communication between the brain and systemic inflammation (Yang et al., 2020). The loss of RGS10 has recently been shown to exacerbate periodontitis and rheumatoid arthritis by promoting NFKB signaling pathways and contributing to increased inflammatory factors (Chan et al., 2022). Furthermore, recent evidence implicates a protective role of RGS10 in influenza-induced inflammatory lung injury (Almutairi et al., 2020). Platelet aggregation and persistent activation are strongly linked to the pathogenesis of cerebral stroke (Fateh-Moghadam et al., 2007); RGS10 is expressed in platelets and suppresses activation and thrombogenesis, thereby playing a protective role during vascular injury (Hensch et al., 2016). These stated protective functions of RGS10 in different cell types suggest that RGS10 dysregulation has a substantial effect in the pathophysiology of CNS and peripheral inflammation. Therefore, investigating tissue-specific or shared molecular mechanisms involved in RGS10 function is advantageous for identifying specific therapeutic targets that mitigate RGS10 loss induced abnormalities.

2.4.5. RGS10 expression is suppressed during inflammation and in pathological models

Growing evidence suggests that age-associated changes in microglia activation, such as hypersensitive response and production of pro-inflammatory and neurotoxic mediators, contribute to progressive neurodegeneration (Chapter 1). Age-associated loss of microglial RGS10 has been reported and implicated as a potential risk factor for neurodegenerative maculopathy (Jakobsdottir et al., 2005; Kannarkat et al., 2015). Furthermore, polymorphism in the RGS10 gene has been associated with human schizophrenia (Hishimoto et al., 2004).

Despite its protective functions in the CNS, microglial RGS10 is silenced by chronic treatment of LPS and TNFα, stimuli used as potent activators of immune cells (Almutairi et al., 2021; Lee et al., 2008). RGS10 suppression is also reported in an *in vivo* model of inflammatory neuropathic pain (Alqinyah et al., 2017), further indicating that RGS10 levels are regulated by inflammation. In addition to the CNS, suppression of RGS10 is evident in other pathologies, including cancer chemoresistance (Hooks & Murph, 2015) and human heart failure (Miao et al., 2016).

The expression of RGS10 in various cellular models is believed to be regulated at the transcriptional level through epigenetic mechanisms. DNA methylation by DNA methyltransferases (DNMTs) and histone-deacetylation by histone acetyltransferases (HATs) have been implicated as mechanisms for RGS10 suppression, and the specific epigenetic mechanism is shown to vary based on cell types and the triggering stimuli (Almutairi et al., 2021; Alqinyah et al., 2017; Hooks & Murph, 2015; Tuggle et al., 2014). In microglia, RGS10 is transcriptionally suppressed in response to chronic stimulation of LPS and TNFα, and LPS-induced suppression is mediated by histone deacetylation rather than DNA methylation and involves HDAC1 recruitment to the promoter region of RGS10 and subsequent hypermethylation of H3 histones (Almutairi et al., 2021; Alqinyah et al., 2017). The HDAC inhibitor Tichostatin A (TSA) rescues LPS-mediated suppression of RGS10 transcript. Interestingly, RGS10 transcript is elevated in response to spingosphine-1 (SP-1) treatment, which is an endogenous microglial signaling mediator that inhibits HDAC activity (Alqinyah et al., 2017). Consistent with this finding, Almutairi et al. (2021) recently showed that pharmacological inhibition of HDACs (1-3) and PI3K/NFκB/TNFα signaling cascade rescues LPS-induced suppression of RGS10 in various macrophages and microglia cell

models (Almutairi et al., 2021). Taken together, these findings suggest that RGS10 expression is suppressed during inflammatory stress, and mechanisms that stabilize RGS10 expression during inflammation may have a therapeutic effect. Given that epigenetic alterations such as HDAC dysregulations have broad targets, it may be beneficial to stabilize RGS10 or modulate specific RGS10-regulated pathways. Therefore, understanding the anti-inflammatory and neuroprotective mechanisms of RGS10 can facilitate the development of therapeutic strategies to compensate for the functional loss of RGS10 during inflammation.

2.4.6. RGS10 regulates inflammatory response via an unknown non-canonical mechanism

As described in previous sections, RGS10 is a canonical GTPase-activating protein (GAP) for Gαi/o family of G proteins. Through its GAP function, RGS10 can moderately regulate downstream Gi signaling pathways. Although RGS10 is selective for Gαi, week interactions with Gαq have previously been reported in other models (Masuho et al., 2020; Soundararajan et al., 2008). In our previous study, we confirmed that RGS10 acts as a canonic GAP protein and selectively associates with activated Gαi but not Gαq. Furthermore, RGS10 can modestly regulate a canonical Gi-coupled signaling event in microglia; loss of RGS10 in BV2 microglia enhances CXCL12-mediated activation of ERK Map kinase (Alqinyah et al., 2018). However, most of the previously characterized role of RGS10 in microglia is in the regulation of pro-inflammatory cytokines in response to LPS/TLR4 activation. Conversely, the toll-like receptor 4 (TLR4) pathway is not initiated by GPCR and thus is not a canonical GAP target. Therefore, the molecular mechanism by which a small GAP protein regulates inflammatory responses downstream of a non-GPCR receptor is not known.

RGS10 may regulate TLR4 signaling indirectly through a G protein-dependent mechanism, and TLR4 activation may also influence RGS10 GAP activity. Therefore, we examined whether LPS regulates RGS10-Gαi interaction or facilitates RGS10-Gαq interaction (**Figure A.1A**) (Alqinyah et al., 2018). Our results showed that RGS10-Gαi interaction occurs in LPS-activated microglia, with no interaction observed between RGS10 and Gαq. Since LPS enhances the interaction of RGS10 with Gαi, we determined if Gi-signaling is involved in RGS10-mediated regulation of TLR4 signaling. Although RGS10 associated with Gαi in response to LPS activation, we found that inhibition of Gαi using pertussis toxin (PTX) has no effect on RGS10-mediated regulation of LPS-induced COX-2, implying a potential G protein-independent mechanism (**Figure A.1B**) (Alqinyah et al., 2018).

To directly assess the GAP-independent effect of RGS10 on LPS-induced inflammatory responses, we transiently expressed wild-type (WT) and GAP-deficient RGS10 (E52K) mutant. Since BV2 cells have high endogenous RGS10 expression, we tested this effect in HEK293-hTL4 cells, which express TLR4 and its co-receptors but have low endogenous RGS10 (Alqinyah et al., 2018). The findings confirmed that LPS-induced expression of TNFα is equally suppressed by WT and E52K mutant RGS10, confirming that RGS10 suppresses TLR4-mediated expression of pro-inflammatory genes independently of its known Gi-dependent mechanism. Although the overexpression study suggested a potential G protein-independent role for RGS10, it had several limitations: 1) it was conducted in the HEK293 cell line, which does not fully mimic microglial immune response such as the induction of COX-2; 2) it utilized a transient expression system; and 3) it overexpressed a less dominant variant of human RGS10 (hRGS10-2). As a result, these

findings should be replicated in a microglia model, to further validate the Gαi-independent mechanism of RGS10 in microglia.

The finding so far suggests that RGS10 regulates TLR-4 mediated pro-inflammatory signals in a G protein-independent mechanism. Although this result is surprising considering the small size of RGS10 and the presence of only the conserved GAP domain, other small RGS proteins have been shown to perform various noncanonical functions in different cellular models (discussed above). Although most of these effects are mediated by non-canonical protein interactions in regions outside the GAP domain, there is some evidence that suggest that the RGS domain can also mediate noncanonical functions. A prominent example is the small RGS2 protein, which utilizes its RGS domain to interact with LRRK2, a multifunctional protein consisting of a GTPase, a kinase, and a scaffolding domain (Dusonchet et al., 2014). LRRK2 dysregulation is a major risk factor for PD, and RGS2 interaction with LRRK2 suppresses both the GTPase and kinase activity of LRRK2, thus reducing LRRK2-induced neurotoxicity (Dusonchet et al., 2014). While RGS proteins do not regulate Gs-coupled GPCR, it has been shown that RGS10 suppresses forskolin-stimulated cAMP production (Ghavami et al., 2004). Since this response is response is initiated downstream of Gs-mediated activation of AC, the mechanism by which RGS10 regulates this pathway is not known. RGS2 has also been shown to modulate the same signaling response in another model, but its effect has been shown to be mediated by direct binding to AC. Its inhibitory effect on AC only required three residues in the N-terminus region (Salim et al., 2003). Therefore, RGS10 may also utilize its RGS domain or its short N- and C-terminus extensions to mediate GAP-independent functions downstream of either TLR4 or GPCR activation.

2.5. Conclusion, Hypothesis and Specific Aims

RGS10 has been identified as a potential anti-inflammatory and neuroprotective therapeutic target (Lee & Tansey, 2015); it regulates microglial proliferation and activation in response to TLR4-activation; it suppresses the production of microglial proinflammatory factors; and it protects neurons from inflammation-associated neurotoxicity (**Figure 2.2**). Additionally, in response to TLR4 activation, RGS10 enhances M2 anti-inflammatory activation state and suppresses M1 pro-inflammatory responses in peripheral macrophages (Lee et al., 2013). However, RGS10 regulates inflammatory gene expression mediated by TLR4, through an unknown mechanism that is distinct from its canonical G protein regulatory role (Alqinyah et al., 2018).

Although RGS10 has anti-inflammatory and neuroprotective roles, its expression in microglia is downregulated during aging and inflammation (Alqinyah et al., 2017; Kannarkat et al., 2015) (Almutairi et al., 2021; Alqinyah et al., 2017) (Lee et al., 2008). Therefore, while RGS10 is a potential therapeutic target for neurodegenerative diseases, the lack of information on its molecular mechanism hinders drug discovery efforts to rescue its functional loss during neuroinflammation. Therefore, it is important to characterize the molecular mechanism by which a small GAP regulates G protein-independent inflammatory responses, which is the focus of this study.

The discovery of a G protein-independent effect of RGS10 in microglia, combined with previously implicated non-canonical roles for other small RGS proteins, led to the **hypothesis** that novel binding partners link RGS10 to the TLR4-inflammatory signaling pathway, thereby mediating the non-canonical anti-inflammatory effects of RGS10. In this study, we will test this

hypothesis by unbiased proteomics analysis to first identify non-canonical protein-protein interaction partners in BV2 microglia, and then examine whether novel interaction partners mediate the anti-inflammatory effects of RGS10 downstream of both TLR4 and non-TLR4 pro-inflammatory pathways (**Figure 2.3: Aim 1**). Furthermore, given that protective functions of RGS10 are implicated in various immune and non-immune cells, we further hypothesize that RGS10 can affect various cellular responses in resting and activated microglia. Therefore, we will conduct unbiased transcriptomics to investigate the global effect of RGS10 in regulating gene expression in resting and LPS activated microglia (**Figure 2.3: Aim 2**). Specifically, we will first generate stable BV2 microglia cell lines overexpressing wild-type human RGS10-1 and a GAP-dead E52K variant in CRISPR/Cas9 RGS10 knockout background and then validate if mutant RGS10 regulates TLR-4 induced expression of pro-inflammatory genes without interacting with Gαi. We will then perform RNA sequencing to identify global transcriptome alterations in RGS10 knockout and RGS10 overexpression BV2 cell lines in resting and activated microglia, and determine biological processes and pathways regulated by RGS10.

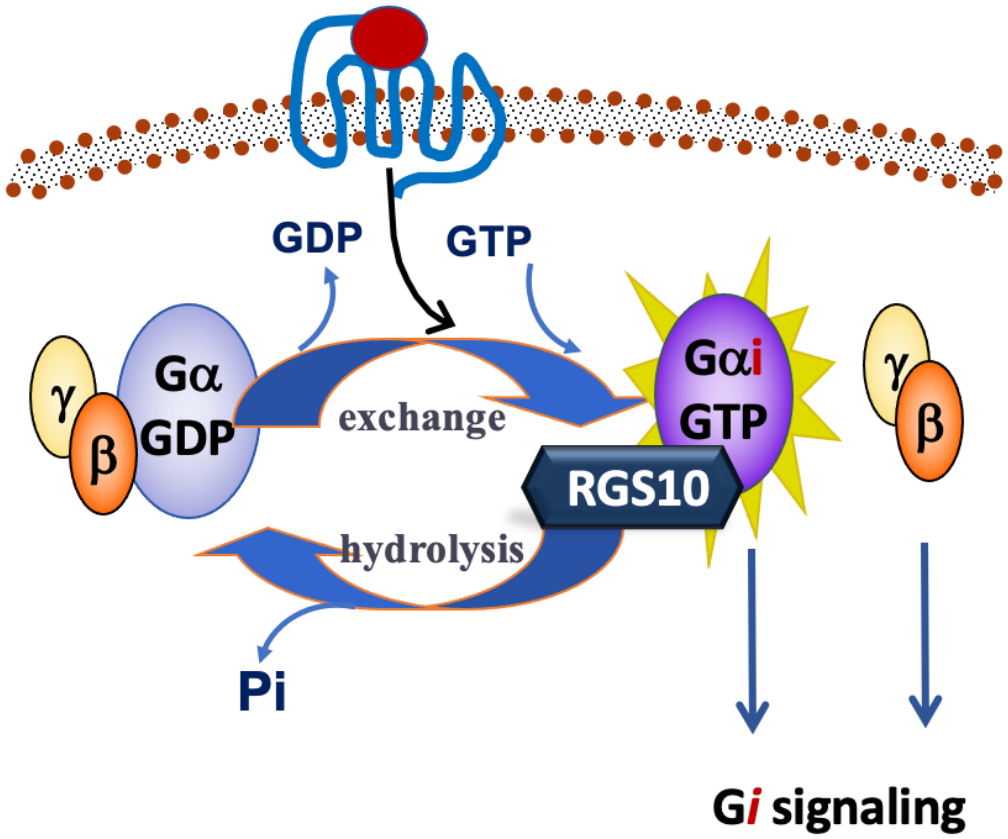

Figure 2.1: Heterotrimeric G protein activation and GTPase-activating protein. Heterotrimeric G proteins are activated in response to ligand binding to G protein-coupled receptors (GPCRs). In resting state, G proteins exist as a heterotrimer where Gα subunit binds to GDP. Upon ligand binding to GPCR, there is an exchange of GDP with GTP which activates Gα subunit and promotes the dissociation of the complex. Activated GTP-bound Gα subunit and Gβγ dimer act on various effectors and initiate downstream G protein signaling. Gα subunit has a slow intrinsic GTPase activity, which is significantly accelerated by Regulator of G protein Signaling (RGS) proteins, which are GTPase-activating proteins (GAP). The GAP activity of the RGS domain promotes GTP hydrolysis and reassembly of the heterotrimeric complex, thereby regulating downstream G protein signaling. RGS proteins have selective preference for a specific Gα class. This schematic figure shows the GAP activity of RGS10, which selectively associates with Gαi subfamily and terminates downstream Gi-signaling pathways. Through its GAP activity, RGS10 suppresses Gi-coupled GPCR signaling, which is an inhibitory pathway that suppresses Adenylyl cyclase and limits cAMP production.

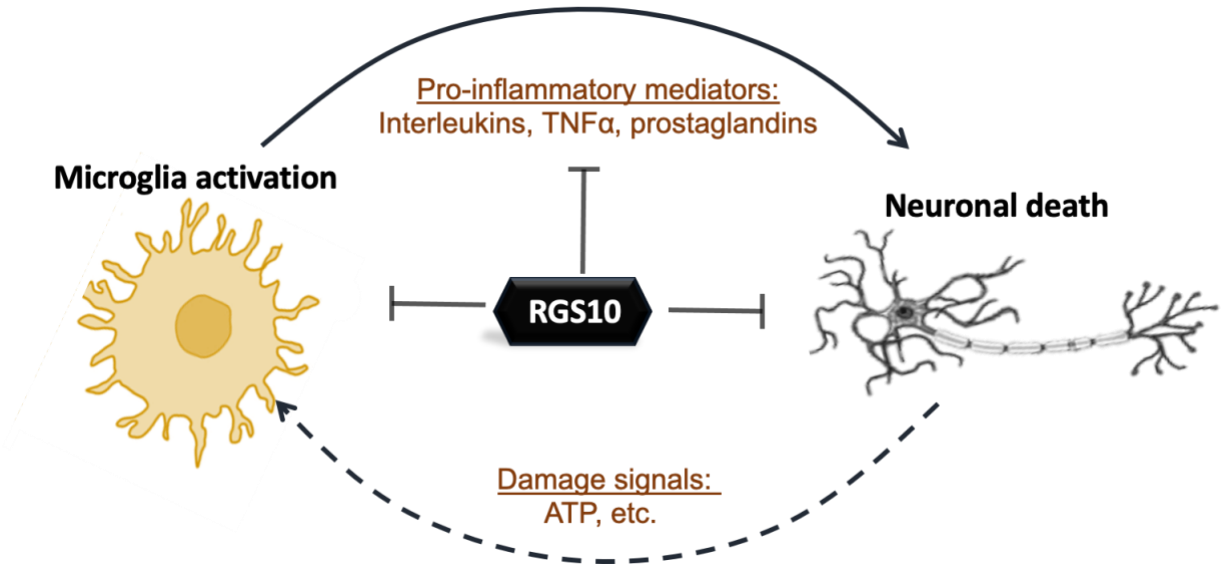

Figure 2.2. Protective roles of RGS10 in neuroinflammation. In the central nervous system, various signals activate microglia, such as pathogens, inflammatory stimuli, and brain injury. Activated microglia release pro-inflammatory and neurotoxic mediators that can lead to neuronal death. Dying neurons in turn release damage signals, such as nucleotides, that can interact with and activate microglia. This two-way cycle results in neuroinflammation and neurotoxicity. Microglial RGS10 is a potential anti-inflammatory therapeutic target; it regulates microglia activation, suppresses the release of pro-inflammatory and neurotoxic mediators, and its expression in both microglia and neurons exerts neuroprotective roles in limiting inflammation-associated neurodegeneration.

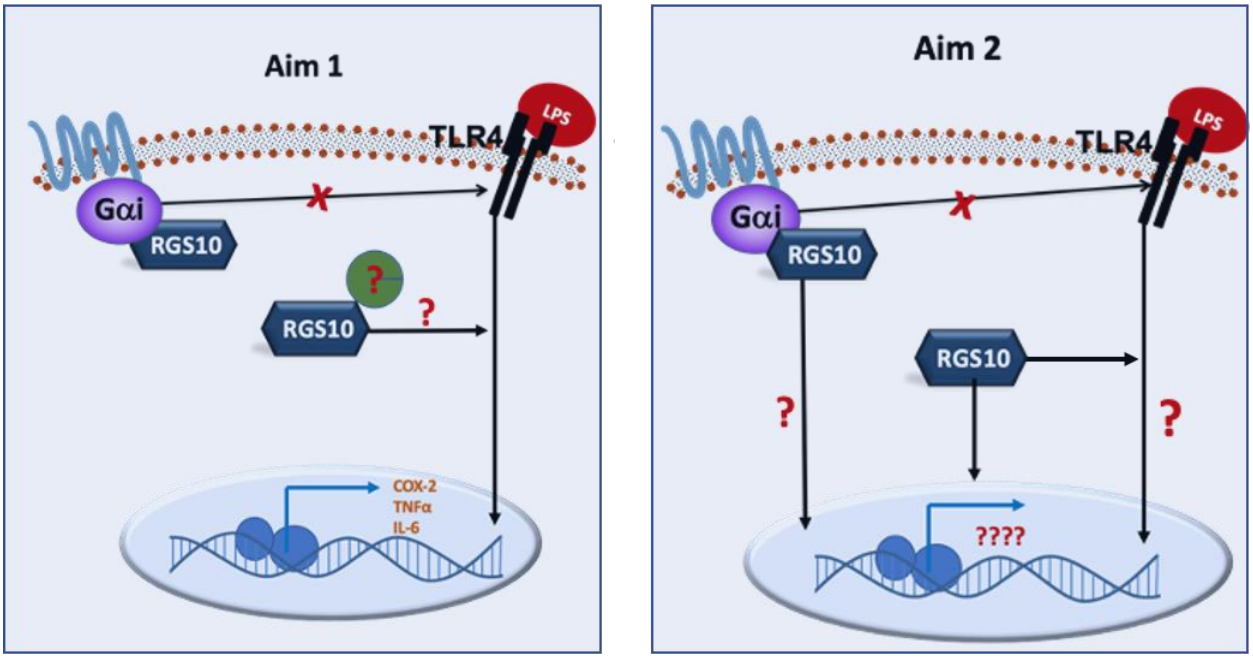

Figure 2.3. Hypothesis and study objectives. RGS10 regulates pro-inflammatory gene expression downstream of TLR4 activation through an unknown mechanism, independent of its canonical GAP function. Other RGS proteins have non-canonical roles, most of which are mediated through non-canonical interactions. Therefore, we hypothesize that novel binding partners link RGS10 to the TLR4 inflammatory signaling pathway, which may mediate the anti-inflammatory effects of RGS10. We also hypothesize that RGS10 regulates various processes in both resting and activated microglia, which may be mediated through its GAP function or through other mechanisms. To test these hypotheses, we will use unbiased proteomics to identify non-canonical RGS10 interaction partners (Aim 1) and determine if the interacting partners affect the anti-inflammatory effects of RGS10 in suppressing COX-2 and other pro-inflammatory genes. In Aim 2, we will conduct an unbiased transcriptomic analysis to investigate the global role of RGS10 in regulating both basal and LPS/TLR4-stimulated gene expression in microglia.

CHAPTER 3

RGS10 PHYSICALLY AND FUNCTIONALLY INTERACTS WITH STIM2 AND REQUIRES STORE-OPERATED CALCIUM ENTRY TO REGULATE PRO-INFLAMMATORY GENE EXPRESSION IN MICROGLIA[2]

[2] **Wendimu, M. Y**., Alqinyah, M., Vella, S., Dean, P., Almutairi, F., Davila-Rivera, R., Rayatpisheh, S., Wohlschlegel, J., Moreno, S., & Hooks, S. B. (2021). *Cellular Signalling, 83,* 109974. https://doi.org/10.1016/j.cellsig.2021.109974

ABSTRACT

Chronic activation of microglia is a driving factor in the progression of neuroinflammatory diseases, and mechanisms that regulate microglial inflammatory signaling are potential targets for novel therapeutics. Regulator of G protein Signaling 10 (RGS10) is the most abundant RGS protein in microglia, where it suppresses inflammatory gene expression and reduces microglia-mediated neurotoxicity. In particular, microglial RGS10 downregulates the expression of pro-inflammatory mediators including cyclooxygenase 2 (COX-2) following stimulation with lipopolysaccharide (LPS). However, the mechanism by which RGS10 affects inflammatory signaling is unknown and is independent of its canonical G protein targeted mechanism. Here, we sought to identify non-canonical RGS10 interacting partners that mediate its anti-inflammatory mechanism. Through RGS10 co-immunoprecipitation coupled with mass spectrometry, we identified STIM2, an endoplasmic reticulum (ER) localized calcium sensor and a component of the store-operated calcium entry (SOCE) machinery, as a novel RGS10 interacting protein in microglia. Direct immunoprecipitation experiments confirmed RGS10-STIM2 interaction in multiple microglia and macrophage cell lines, as well as in primary cells, with no interaction observed with the homologue STIM1. We further determined that STIM2, Orai channels, and the Ca^{2+}-dependent phosphatase calcineurin are essential for LPS-induced COX-2 production in microglia, and this pathway is required for the inhibitory effect of RGS10 on COX-2. Additionally, our data demonstrated that RGS10 suppresses SOCE triggered by ER calcium depletion and that ER calcium depletion, which induces SOCE, amplifies proinflammatory genes. In addition to COX-2, we also show that RGS10 suppresses the expression of proinflammatory cytokines in microglia in response to thrombin and LPS stimulation, and all of these effects require SOCE. Collectively, the physical and functional

links between RGS10 and STIM2 suggest a complex regulatory network connecting RGS10, SOCE, and pro-inflammatory gene expression in microglia, with broad implications in the pathogenesis and treatment of chronic neuroinflammation.

3.1. Introduction

Chronic inflammation is an underlying mechanism for the initiation and progression of multiple diseases (Furman et al., 2019). Chronic activation of microglia cells is a driving factor of neuroinflammation and a hallmark of several neurodegenerative diseases including Parkinson's disease, Alzheimer's disease, and Multiple Sclerosis. Aberrant activation of microglia leads to amplified production of proinflammatory cytokines, prostaglandins, and other neurotoxic molecules, ultimately contributing to neuroinflammation and neurotoxicity (Hickman et al., 2018; Lull & Block, 2010). Therefore, targeting novel molecular mechanisms for the regulation of microglial inflammatory signaling is a promising therapeutic strategy for neurodegenerative diseases.

Regulator of G protein Signaling 10 (RGS10) is the most abundant RGS protein in microglia, where it exerts anti-inflammatory and neuroprotective effects (Alqinyah et al., 2018; Lee et al., 2012; Lee et al., 2011; Lee et al., 2008). A series of studies by Lee et al. demonstrated that RGS10 knockout mice display significantly more activated microglia and higher levels of inflammatory cytokines. Further, loss of RGS10 exacerbates inflammation-induced toxicity of dopaminergic neurons, suggesting a neuroprotective role of RGS10 (Lee et al., 2012; Lee et al., 2011; Lee et al., 2008). This anti-inflammatory role of RGS10 is also observed and consistently modeled in BV2 microglia, a suitable cellular model for neuroinflammation studies (Henn et al., 2009). We and others have shown that loss of RGS10 in BV2 microglia cells enhances the expression of various pro-inflammatory cytokines in response to toll-like receptor 4 (TLR4) activation (Alqinyah et al., 2018; Alqinyah et al., 2017; Lee et al., 2011; Lee et al., 2008). In particular, RGS10 downregulates Lipopolysaccharide (LPS)-stimulated expression of multiple

pro-inflammatory genes, including a profound negative regulation of the inflammatory kingpin cyclooxygenase-2 (COX-2) and its primary metabolic product Prostaglandin E2 (PGE2) (Alqinyah et al., 2018).

RGS proteins canonically act as GTPase accelerating proteins (GAPs) for heterotrimeric G proteins and inhibit signaling initiated by G protein-coupled receptors; this GAP function is mediated through interaction with activated G protein subunit (Popov et al., 1997; Watson et al., 1996). However, the mechanism by which RGS10 affects LPS-induced pro-inflammatory gene expression is independent of its canonical G protein targeted mechanism and does not require G protein interaction (Alqinyah et al., 2018). This suggests that novel RGS10 interacting partners may account for its effect on regulating LPS/TLR4 proinflammatory signaling. The goal of this study was to identify and validate non-canonical microglial RGS10 interacting partners that may mediate the anti-inflammatory functions of RGS10. Here, we describe a novel interaction between RGS10 and stromal interaction molecule 2 (STIM2) and establish STIM2 as an important regulator of LPS-induced inflammatory gene expression in microglia. STIM2 is an endoplasmic reticulum (ER) calcium sensor which detects ER calcium depletion and triggers store-operated calcium entry (SOCE) via activation of plasma membrane Orai channels (Berna-Erro et al., 2017; Hoth & Niemeyer, 2013; Ong et al., 2015). This study characterizes the physical and functional interaction of RGS10 and STIM2 and defines the role of the SOCE pathway on RGS10's anti-inflammatory function.

3.2. Materials and Methods

Cells and Reagents

The murine BV2 microglial cell line was a generous gift from G. Hasko at the University of Medicine and Dentistry of New Jersey (Newark, NJ), and was generated by Blasi et al. . RAW 264.7 macrophage cell line was purchased from ATCC (T1B-71). The N9 microglia cell line was a generous gift from N. Filipov at the University of Georgia (Crittenden & Filipov, 2008). CRISPR/Cas9 control and CRISPR/Cas9 RGS10 knockout BV2 cell lines were established by our group, as previously described (Alqinyah et al., 2018). Wild type and RGS10 knockout breeder mice were gifted to us by J.K Lee at the University of Georgia, and have previously been used for neuroinflammation research (Lee et al., 2012; Lee et al., 2011; Lee et al., 2008). The compounds used in this study are Lipopolysaccharide (Sigma-Aldrich: L2880), Thrombin (Sigma-Aldrich: T4648), Cyclosporin A (FagronLab: 803651), YM-58483 (Tocris Bioscience: 3939), and Thapsigargin (Abcam: ab120286).

Cell Culture

BV2, N9, and RAW264.7 cell lines and isolated mouse peritoneal macrophages were maintained in Dulbecco's modified Eagle's medium (DMEM) (37 ^{o}C, 5% CO_2) supplemented with 10% low-endotoxin fetal bovine serum (FBS) (Thermo Fischer Scientific: 10082147), and 1% penicillin/streptomycin (P/S). Mixed glia and isolated microglia cultures were maintained similarly but using DMEM/Hams F-12 50/50 mix medium (Corning: 10-090-CV).

Primary Cell Isolation

Primary microglia were isolated from mixed cortical cultures using a modified protocol adapted from previous studies (Lian et al., 2016; Yao et al., 2010). Briefly, 1-3 days old wild type

and RGS10 knockout postnatal mouse pups were anesthetized using isoflurane, and whole brains were collected. After removing the cerebellum and meninges, tissues from the two hemispheres were cut into small pieces and digested with 0.25% trypsin for 20 min at 37ºC. Digested tissue was further mechanically dissociated by trituration and filtered through a 40 µm filter. Single-cell suspensions were plated onto a poly-D-lysine (PDL)-coated T75 tissue culture flasks (2-3 brains/flask) and maintained in FBS-containing DMEM/F12 medium. The growth medium was changed on days 3 and 7, and an additional medium was added to the mixed glia culture on day 10 followed by microglia isolation on day 15. Microglia were isolated by shaking the confluent mixed glial culture at 130 RPM (37ºC) for 3-4h, and non-adherent microglia cells were centrifuged for 5 min at 400g (4ºC) and resuspended with growth media. Cells were plated in PDL-coated 12-well plates ($0.25x10^6$ cells/well) and cultured for additional 2 days prior to experimental treatments.

Mouse peritoneal macrophages were elicited by intraperitoneal injection of 3% thioglycolate broth from adult mice (Millipore Sigma: 70157). Macrophages were harvested 4 days post-injection via peritoneal lavage with cold PBS, as previously detailed (Zhang et al., 2017). Harvested cells were cultured for 24h in a 10cm dish with DMEM, supplemented with 10% FBS and 1% P/S. After 24h, cells washed with PBS and continued to grow for an additional 24h prior to immunoprecipitation experiments.

Immunoprecipitation

Immunoprecipitation (IP) experiments for mass spectrometry (MS) analysis were performed using BV2 microglia cells plated in six 15 cm dishes and grown to ~85% confluency. Cells were washed twice with PBS and harvested with 1mL of modified lysis buffer (50 mM Tris

HCl, 150 mM NaCl, 6mM $MgCl_2$, 1% Nonidet P-40, 0.5% sodium deoxycholate), containing protease/phosphatase inhibitor cocktail (Cell Signaling Technology). Cell lysates were incubated on ice for 30 min, and insoluble cellular debris was removed by centrifugation at 27,216 g for 10 min at 4°C. Cleared lysates were incubated overnight at 4°C with 2 µg/mL agarose-conjugated goat polyclonal RGS10 antibody (Santa Cruz Biotechnology: sc-6206AC) or agarose-conjugated goat IgG antibody (Santa Cruz Biotechnology: sc-2346). Samples were centrifuged at 410 g for 5 min, and pellets were washed 3 times with wash buffer (50mM Tris HCl, 150 mM NaCl, 6 mM $MgCl_2$). Immunoprecipitating proteins were eluted from agarose-conjugated beads by incubation with 100 µL elution buffer (0.15 M glycine, pH 2.6) for 10 min at room temperature with gentle shaking. Eluted samples were centrifuged again to remove beads (410g, 5 min, 4°C), and the supernatant was neutralized with an equal volume of 1M Tris HCl, pH 8, and subsequently subjected to overnight acetone precipitation (4x volume) at -20° C. Samples were centrifuged twice (16,000 g, 10 min, 4°C) with an acetone wash in between centrifugation. The final pellet was air-dried for 30 min prior to LC/MS-MS analysis.

Follow up Co-IP validations were performed in cells grown in a 10cm dish. Cells were harvested as indicated above, but lysates were split in half and immunoprecipitated with either 2 µg/mL of goat RGS10 antibody (Santa Cruz Biotechnology: sc-6206) or normal goat IgG (R&D Systems: AB-109-C). Subsequently, lysates were incubated with 20 µL of a 50% slurry of Protein G-conjugated sepharose (GE Healthcare: 17-0618-01) for 2 h at 4°C, and centrifuged at 410 g for 5 minutes. The beads were washed twice with PBS and resuspended with 50 µl of 2X SDS-PAGE sample buffer for western blot analysis. Co-IP experiments in N9 cells, RAW264.7 cells, and primary peritoneal macrophages were conducted following the same protocol. Calcium-containing

co-IP experiments were conducted similarly, but cleared lysates were incubated with either $CaCl_2$ (1mM) or EGTA (0.5 mM) for 1 h at 4ºC prior to immunoprecipitation.

Mass Spectrometry

Acetone precipitated immunoprecipitates were resuspended in digestion buffer (100 mM Tris pH 8.5, 8M urea) and then reduced, alkylated, and digested by the sequential addition of lys-c and trypsin proteases as previously described (Wohlschlegel, 2009). Digested samples were then fractioned online by C18 reversed-phase chromatography and then analyzed by tandem mass spectrometry using a Thermofisher Fusion Lumos Mass Spectrometer as described (Stehling et al., 2012). MS/MS data were analyzed using MSGF+ for peptide identification, Percolator for decoy database-based statistical filtering, Fido for protein interference, and SAINT algorithm for the identification of proteins enriched in RGS10 IPs relative to control Ips (Choi et al., 2012; Granholm et al., 2014; Serang & Noble, 2012).

Quantitative Real-Time Polymerase Chain Reaction

Total RNA was isolated from cells with TRIzol reagent (Invitrogen). cDNA was synthesized using the High-Capacity Reverse Transcriptase cDNA kit (Applied Biosystems). Real-time PCR was performed using SYBR Green PCR Master Mix (Applied Biosystems). The housekeeping β-actin gene was used for data normalization and relative mRNA abundance was calculated using the $2^{-\Delta\Delta CT}$ method. Mouse primers sequences used for RT-PCR are listed as follows: RGS10, 5'-CCCGGAGAATCTTCTGGAAGACC-3' (forward) and 5'-CTGCTTCCTGTCCTCCGTTTTC-3' (reverse); TNFα, 5'-CCTGTAGCCCACGTCGTAG-3' (forward) and GGGAGTAGACAAGGTACAACCC (reverse); COX-2, 5'-TGCAAGATCCACAGCCTACC-3' (forward) and 5'-GCTCAGTTGAACGCCTTTTG-3'

(reverse); IL-6, 5'-CTGCAAGAGACTTCCATCCAG–'3 (forward) and 5'-AGTGGTATAGACAGGTCTGTTGG-3' (reverse); β-actin, 5'-GGCTGTATTCCCCTCCATCG-3′ (forward) and 5'-CCAGTTGGTAACAATGCCATGT-3′ (reverse). Primers for RGS10 and TNFα were purchased from Integrated DNA Technology, and COX-2 and β-actin primers were obtained from Sigma-Aldrich.

Western Blot Analysis

Cell lysates were subject to SDS-PAGE followed by transfer to nitrocellulose membranes using standard protocols, as previously detailed (Alqinyah et al., 2017). Membranes were blocked with 5% milk and incubated overnight with the following primary antibodies: goat anti-RGS10 (Santa Cruz Biotechnology: sc-6206), mouse anti-COX-2 (Santa Cruz Biotechnology: sc-166475), mouse anti-Syntaxin 5 (Santa Cruz Biotechnology: sc-365124), mouse anti-GAPDH (Thermo Fisher Scientific: am4300), mouse anti-Calmodulin (MilliporeSigma: 05-173), rabbit anti-GNAI3 (Proteintech: 11641-1-AP), rabbit anti-STIM1 (Proteintech: 11565-1-AP), rabbit anti-STIM2 (Proteintech: 21192-1-AP), and rabbit anti-PDE4A (Proteintech: 16226-1-AP). Primary antibodies, except for GAPDH (1:6000), were used at 1:500-1:1000 dilutions. Membranes were subsequently incubated for 1h with the following secondary antibodies (1:5000): donkey anti-goat IgG-HRP (Santa Cruz Biotechnology: sc-2020), goat anti-rabbit IgG-HRP (MilliporeSigma: 12-348), and goat anti-mouse IgG HRP (Bethyl Laboratories: A90-116P). Immunoreactivity of HRP was detected using Supersignal West Pico Chemiluminescent Substrate (Pierce). Western Blot images were quantified using FluorChem HD2 software (Proteinsimple), and quantified data were normalized to the endogenous control GAPDH.

Small Interfering RNA Transfection

Mouse STIM2 small interfering RNA (siRNA) (sc-76592) and control siRNA (sc-37007) were purchased from Santa Cruz Biotechnology. Transfection was performed using Lipofectamine-LTX with PLUS reagent (Thermo Fisher Scientific: 15338100) according to the manufacturer's protocol, with a final siRNA concentration of 60 nM in an antibiotic-free culture media. Cells were harvested 48 h after transfection. STIM2 protein western blotting was used to assess knockdown efficiency, and STIM1 protein level was measured to assess target specificity.

Calcium Imaging

CRISPR-control BV2 and CRISPR-RGS10 knockout cells were plated on 35mm MatTek glass-bottom dishes. Prior to loading, cells were washed twice with Ringer Solution (155 mM NaCl, 3 mM KCl, 1.8 mM $CaCl_2$, 1 mM $MgCl_2$, 3 mM NaH_2PO_4, 10 mM Hepes, pH 7.3, and glucose 10 mM). Cells were loaded with 5µM Cal-520, AM (Abcam: ab171868) in Ringer buffer in the presence of 1mM Probenecid (Sigma Aldrich: P8761) in the dark at 37^{o}C for 20 mins. Cells were washed twice and the media was replaced with Ringer Buffer supplemented with 100 µM EGTA to chelate contaminating calcium. Fluorescent imaging was performed at 37^{o}C using an Olympus 1X-71 inverted fluorescence microscope with a Photometrics CoolSnapHQ charge-coupled device (CCD) camera driven by DeltaVision software (Applied Precision). Images were collected every 3 s for a total of 15 min, and traces were transformed in videos using SoftWorx suite 2.0 software (Applied Precision). Images were processed using the FIJI ImageJ software suite (Schindelin et al., 2012), and the fluorescence signal at each time point was normalized to the baseline fluorescence of each cell.

Statistical Analysis

All quantified data were analyzed using GraphPad Prism Software and assessed for normality using D'Agostino & Pearson omnibus normality test. Statistical differences between groups were determined using student's t-test or one-way ANOVA followed by Tukey post hoc analysis. Data are presented as mean ± SEM pooled from a minimum of three independent experiments. The p-value cutoff ranges are indicated by *$p < 0.05$, **$p<0.01$, and ***$p<0.001$.

3.3. Results

3.3.1. RGS10 interaction partners in microglia

We previously demonstrated that RGS10 regulates inflammatory gene expression in microglia through a G protein-independent mechanism (Alqinyah et al., 2018). To identify RGS10 interacting proteins that may mediate this activity, wildtype BV-2 cell total cell lysates were immunoprecipitated with either control IgG or RGS10 antibody, and retained proteins were eluted and analyzed. Robust and selective RGS10 pulldown was observed, with no detectable RGS10 immunoreactivity remaining in the supernatant following immunoprecipitation (IP), and no detectable RGS10 precipitating with control IgG. RGS10 immunoreactivity was fully recovered in a single round of elution (**Figure S3.1A**). The elution fractions were subjected to protease digestion and reversed-phase separation coupled to tandem mass spectrometry. As expected, we identified strong RGS10 enrichment along with the classic RGS interacting proteins guanine nucleotide-binding protein subunits Gαi2 and Gαi3. In addition to the canonical G protein partners, we identified 23 proteins that were specifically enriched in RGS10 co-IP compared to control IgG pulldown with a SAINT score of 0.8 or higher (**Table S3.1**). Consistent with previous reports of RGS10 distribution throughout the cytoplasm and nucleus (Chatterjee & Fisher, 2000), more than

half of the interacting proteins are localized in these two compartments (**Figure S3.1B**). To validate the data obtained from LC-MS/MS analysis, we conducted direct co-IP experiments probing for select individual proteins, including Gαi3, STIM2, Syntaxin 5, and PDE4A (**Figure S3.1C**). These results indicate that endogenous RGS10 physically interacts—directly or indirectly—with multiple non-classic binding partners in BV2 microglia, suggesting potentially diverse, non-canonical roles for RGS10.

3.3.2. RGS10-STIM2 interaction

Of the potential novel RGS10-interacting proteins, STIM2 was of particular interest because of its prominent role in Ca^{2+} signaling in immune cells and its implicated role in regulating inflammatory responses in microglia and macrophages. In particular, STIM2 in macrophages facilitate LPS-induced production of multiple pro-inflammatory genes in macrophages, including TNFα, IL-6, and IL-1β (Sogkas et al., 2015), and these cytokines are also known to be regulated by RGS10 in microglia (Alqinyah et al., 2018; Alqinyah et al., 2017; Lee et al., 2011). To characterize RGS10 interaction with STIM2, we first assessed the specificity of the co-immunoprecipitation experiment. We performed RGS10 immunoprecipitation (IP) in RGS10-null BV2 microglia in which RGS10 expression has been disrupted using CRISPR ($RGS10^{-/-}$) and in control CRISPR BV2 cells (control) which express a normal level of endogenous RGS10 using both RGS10 and control IgG antibodies. We observed no STIM2 or RGS10 immunopreactivity precipitating with RGS10 antibody in knockout lysates, or with control IgG in control lysates, thereby ruling out non-specific immunoprecipitation (**Figure 3.1A**). We also observed RGS10-STIM2 co-immunoprecipitation (co-IP) in N9 microglia and RAW264.7 macrophage cell lines,

and in primary mouse peritoneal macrophages (**Figure 3.1B**). Collectively, these data suggest that endogenous RGS10 specifically interacts with STIM2 *in vitro* and in primary immune cells.

STIM2 shares approximately 50% identity with its homolog STIM1 (Williams et al., 2001), which is also expressed in microglia and is implicated in the regulation of inflammatory signaling (Kraft et al., 2015; Michaelis et al., 2015), suggesting a possible interaction of RGS10 with STIM1. However, STIM1 was not identified as an interacting protein in our proteomics results or direct RGS10 co-IP (**Table S3.1** & **Figure 3.1C**), indicating that RGS10 selectively associates with STIM2. In addition to binding calcium ions directly, STIM2 also binds the calcium-binding regulatory protein calmodulin (CaM) , and a Ca^{2+}-dependent interaction between RGS10 and CaM has been reported in other cellular models . Therefore, we predicted that CaM may serve as a bridge between RGS10 and STIM2 to facilitate Ca^{2+}-dependent interaction in microglia. To examine this, we tested whether CaM co-precipitates with RGS10 in BV2 cells and if Ca^{2+}-CaM regulates the RGS10-STIM interaction. We did not observe a difference in the extent of RGS10-STIM2 interaction in co-IP assays performed in the presence of excess calcium or the calcium chelator EGTA, while STIM1 did not co-IP with RGS10 under the conditions tested (**Figure 3.1D**). We also did not detect an interaction between RGS10 and CaM under these conditions, regardless of calcium level. These results suggest that RGS10 interaction with STIM2 does not require calcium or calmodulin. Immunoprecipitations for proteomics analysis and experiments shown in *Figures 1A-D* were performed on total cell lysates containing sodium deoxycholate (SDC), while previous studies that detected RGS10-CaM interaction were performed in the absence of this detergent (Yang & Li, 2007). We confirmed Ca^{2+}-dependent RGS10 interaction with CaM in BV2 cell lysates prepared with lower stringency co-IP buffer lacking SDC (**Figure**

3.1E). Our results collectively suggest a robust, calcium-insensitive interaction between RGS10 and STIM2, and a detergent-sensitive, Ca^{2+}-dependent interaction between RGS10 and CaM.

Given that RGS10 suppresses inflammatory signaling triggered by TLR4 activation, we next determined whether RGS10-STIM2 interaction in microglia is regulated by LPS. We compared RGS10-STIM2 co-IP in resting BV2 cells or cells activated by LPS for 3 hours, a time point that corresponds to the initiation of LPS stimulated expression of proinflammatory mediators (Kang et al., 2006; Rex et al., 2016). We did not observe a difference in RGS10-STIM2 interaction in co-IP experiments, suggesting that the interaction of RGS10 and STIM2 is not impacted by LPS stimulation at this time point (**Figure 3.1F**), although it remains possible that LPS triggers a transient change in this interaction.

3.3.3. Role of STIM2 and Orai-Calcineurin pathway in COX-2 regulation

Previous studies have implicated a role of STIM2 in regulating inflammatory signaling (Sogkas et al., 2015; Yoshikawa et al., 2019). In particular, Sogkas *et al*. (2015) showed that STIM2 knockout mice are resistant to LPS-induced inflammation *in vivo* and that primary macrophages isolated from STIM2 knockout mice display impaired TLR-4 induced expression of pro-inflammatory genes. STIM2 facilitates migration and phagocytosis of microglia in response to extracellular nucleotide (Michaelis et al., 2015), but its role in regulating microglial inflammatory responses has not been explored. Here, we examined the effect of STIM2 on the inflammatory signaling events that are modulated by RGS10, in particular the regulation of COX-2 by TLR4 activation. COX-2 expression is highly inducible in response to inflammatory stimuli including the bacterial epitope LPS (Font-Nieves et al., 2012; Ikeda-Matsuo et al., 2015). We show that transient transfection of STIM2 siRNA in BV2 cells resulted in greater than 75% reduction of

STIM2 protein levels and inhibited LPS-induced COX-2 protein by approximately 50%, indicating that STIM2 is required for maximal LPS stimulated COX-2 expression (**Figure 3.2A-C**). STIM2 siRNA did not affect the expression of the STIM homologue STIM1, ruling out a an off-target effect (**Figure S3.2**). LPS treatment suppressed RGS10 expression as we and others have previously reported (Alqinyah et al., 2017; Alqinyah et al. 2018), but it caused a marked increase in STIM2 protein level (**Figure 3.2A&B**). These results suggest that STIM2 facilitates LPS-stimulated COX-2 expression.

The established role of STIM proteins is to serve as a sensor for endoplasmic reticulum (ER) Ca^{2+} store depletion and to couple this depletion to extracellular Ca^{2+} entry through activation of plasma membrane Orai channels, a mechanism known as store-operated calcium entry (SOCE) (Nelson et al., 2018; Soboloff et al., 2012). Orai channels are strongly coupled to the activation of the Ca^{2+}-dependent phosphatase calcineurin and downstream targets which regulate calcium-dependent inflammatory gene expression (Hogan et al., 2010; Hogan et al., 2015; Kar et al., 2013, Park et al., 2020). To define the role of the Orai-calcineurin function in regulating LPS response, we examined LPS-induced COX-2 gene expression following pharmacologic inhibition of either Orai using YM58483 (YM), or calcineurin using cyclosporin A (CsA). Inhibition of either Orai channels or calcineurin significantly blocked LPS-induced COX-2 production in BV2 microglia (**Figure 3.2D**), suggesting that the SOCE pathway is essential for COX-2 production in response to TLR4 activation. To validate whether this pathway mediates a similar function in other cell lines, we examined the effect of YM and CsA on LPS-induced COX-2 expression in N9 cells, an alternative immortalized cell line (**Figure 3.2E**). We observed a similar effect in N9 cells in which YM and CsA significantly reduced COX-2 expression. In addition to BV2 and N9 cells, we also

confirmed our result in primary microglia in which Orai inhibition blocked LPS-induced COX-2 transcript levels (**Figure 3.2F**). Altogether, our data suggest that components of the SOCE pathway, including STIM2, Orai, and calcineurin, are essential for LPS-induced COX-2 production.

Impact of STIM2 and Orai-Calcineurin signaling axis on RGS10 sensitive COX-2 expression.

The observed effect of STIM2 expression and Orai/calcineurin activity on LPS-stimulated COX-2 expression contrasts our previous observation that loss of RGS10 expression upregulates LPS-induced COX-2 (Alqinyah et al., 2018). This opposing effects of STIM2 and RGS10 on LPS signaling, along with the observed biochemical interaction, suggested a potential functional link between RGS10 and STIM2. To determine the role of STIM2 in RGS10-sensitive COX-2 expression, we performed STIM2 knockdown in Control and $RGS10^{-/-}$ BV2 cells. STIM1, STIM2, and Orai protein levels were unchanged in $RGS10^{-/-}$ cells (data not shown). As expected, LPS-induced COX-2 expression was enhanced in $RGS10^{-/-}$ cells compared to control cells as expected, but this upregulation was significantly inhibited by STIM2 knockdown (**Figure 3.3A-C)**. In cells with STIM2 knockdown, loss of RGS10 did not significantly enhance LPS-stimulated COX-2 expression. Similarly, the observed upregulation of COX-2 mRNA and protein in RGS10 knockout cells was inhibited in the presence of either the Orai inhibitor YM (**Figure 3.3D&E)** or the calcineurin inhibitor CsA **(Figure 3.3F&G)**. Collectively, our data demonstrate that the STIM2-Orai-calcineurin pathway is required for RGS10-mediated regulation of LPS-induced COX-2 production.

3.3.4. Effect of calcium store depletion on LPS stimulated COX-2 expression.

Since the SOCE pathway is activated following ER Ca^{2+} store depletion (Nelson et al., 2018; Soboloff et al., 2012), we examined whether ER calcium depletion itself affects LPS-induced COX-2 production. We pretreated BV-2 cells with the SERCA-Ca^{2+}-ATPase inhibitor Thapsigargin (TG) to trigger ER calcium depletion prior to LPS stimulation and examined its effect on transcript and protein levels of COX-2 and RGS10. A short-term (20 min) pretreatment with TG before LPS (PreTG) enhanced LPS-mediated induction of COX-2 transcript and protein levels more than fivefold over the effect seen with LPS alone (**Figure 3.4A & B**). TG pre-treatment also enhanced LPS-induced downregulation of RGS10 protein level (**Figure 3.4A)**, suggesting that ER calcium depletion amplifies positive regulation of COX-2 and negative regulation of RGS10 expression in response to LPS. To delineate whether the TG-induced transient calcium elevation or the secondary SOCE response is responsible for enhancing LPS-stimulated COX-2 expression, we co-treated cells with LPS and either the Orai inhibitor (YM) or the calcineurin inhibitor (CsA), following TG pretreatment. Both YM and CsA significantly suppressed TG-mediated upregulation of LPS-induced COX-2 expression (**Figure 3.4C**), indicating that the effect of thapsigargin on COX-2 expression is dependent on the SOCE pathway. Altogether, these results suggest that the STIM2-Orai-calcineurin mediated SOCE pathway, which is triggered by ER depletion, amplifies LPS-stimulated COX-2 expression.

3.3.5. SOCE effect in RGS10-regulated pro-inflammatory genes

Although we focused on COX-2 as a known target of RGS10 regulation, both RGS10 and STIM2 also regulate other pro-inflammatory cytokines in response to LPS (Alqinyah et al., 2018; Alqinyah et al., 2017; Lee et al., 2011; Sogkas et al., 2015). To examine the dual effect of RGS10

and SOCE on additional genes, we analyzed the effect of Orai inhibitor on tumor-necrosis factor-alpha (TNFα), interleukin-6 (IL-6), and inducible nitric oxide synthase (iNOS) expression in BV2 cells after treatment with different LPS doses (1 ng/mL and 10 ng/mL). Similar to the effect for COX-2 (**Figure S3.3A)**, loss of RGS10 enhanced LPS-induced TNFα and IL-6 transcripts at both LPS doses tested, and this upregulation was blunted by Orai inhibition (**Figure 3.5A & B**). Similar regulation of iNOS expression was observed, but only at the lower LPS dose (**Figure S3.3B**). To further validate the role of SOCE on RGS10 function, we performed similar experiments in primary microglia isolated from wild type and RGS10 knockout mice. As expected, RGS10 transcript was depleted in RGS10 knockout primary microglia compared to wild type cells, and LPS suppressed RGS10 transcript in cells expressing RGS10 (**Figure 3.5C**). Consistent with our BV2 data, we observed that primary microglia lacking RGS10 had greater LPS-stimulated COX-2 and IL-6 expression, and this effect was fully inhibited in the presence of Orai inhibitor (**Figure 3.5D & E**). Orai inhibition also significantly inhibited TNFα expression in RGS10 knockout primary microglia, although the upregulation of TNFα in RGS10 knockout primary microglia compared to wildtype cells was not significant (**Figure 3.5F**). Altogether, these data suggest that RGS10 regulates LPS-stimulated pro-inflammatory gene expression in microglia through a mechanism that requires SOCE.

3.3.6. RGS10 and SOCE role in thrombin signaling

LPS is a commonly used stimulus to model neuroinflammation associated with neurodegeneration (Batista et al., 2019; Lively et al., 2018), but multiple other mediators are implicated in mediating inflammation in the context of CNS injury. To explore responses associated with CNS injury, we examined the role of RGS10 and SOCE in pro-inflammatory

responses of microglia to thrombin, a physiologically relevant endogenous stimulus (Krenzlin et al., 2016). We observed significant upregulation of COX-2, TNFα, and IL-6 transcript expression in RGS10 knockout BV2 cells compared to control cells in response to thrombin treatment (**Figure 3.6A-C**). Similar to the effect observed for LPS, the Orai-inhibitor restored RGS10 loss-mediated upregulation of COX-2 and IL-6 expression (**Figure 3.6A & B**). Orai inhibition also significantly suppressed thrombin-induced TNFα expression in RGS10 knockout cells, yet it did not fully restore TNFα upregulation (**Figure 3.6C**). We also observed a similar trend for iNOS transcript, yet the effect of both RGS10 and Orai was not statistically significant (data not shown). Overall, our results suggest that RGS10 regulates thrombin-stimulated pro-inflammatory gene expression in BV2 microglia through a mechanism involving SOCE.

3.3.7. RGS10 effect on store-operated calcium entry (SOCE)

Given the opposing involvement of the STIM2/SOCE pathway in mediating RGS10-sensitive pro-inflammatory gene expression, we hypothesized that RGS10 may also regulate store-operated calcium entry. To evaluate the role of RGS10 in SOCE, we conducted live cell calcium imaging of control and RGS10$^{-/-}$ BV2 cells loaded with the fluorescent Ca^{2+} indicator Cal-520-AM. A transient rise in cytoplasmic calcium was triggered upon ER calcium depletion using thapsigargin (TG) in the absence of extracellular calcium. Following a return to baseline cytoplasmic calcium levels, extracellular Ca^{2+} was added to allow store-operated calcium entry (SOCE) (**Figure 3.7A and B**). Compared to control BV2 cells, RGS10$^{-/-}$ cells displayed a reduced initial TG-induced calcium transient**,** while the SOCE peak was significantly enhanced (**Figure 3.7B and C).** This resulted in a SOCE:TG peak height ratio of 1.1 for control cells and 2.0 for RGS10$^{-/-}$ cells. This suggests a closer coupling of ER calcium depletion and extracellular calcium

entry in the absence of RGS10 compared to control cells, and the ability of endogenous RGS10 to blunt extracellular calcium entry in response to ER calcium depletion.

3.4. Discussion

Chronic activation of microglia is a driving factor in the progression of neuroinflammatory diseases (Hickman et al., 2018), and mechanisms that regulate microglial inflammatory signaling are potential targets for novel therapeutics (Fatoba et al., 2020; Subramaniam & Federoff, 2017). The small Regulator of G-protein Signaling 10 protein (RGS10) impacts the pathophysiology of diverse diseases (Almutairi et al., 2020), as demonstrated in various animal and cellular disease models (Ali et al., 2013; Alqinyah et al., 2018; Hooks et al., 2010; Hooks & Murph, 2015; Lee et al., 2011; Lee et al., 2016; Miao et al., 2016; Yang & Li, 2007). Among these broad effects, the role of RGS10 in microglia stands out as the most pronounced and most clearly tied to pathology. Specifically, microglial RGS10 suppresses the expression of multiple pro-inflammatory genes, including a particularly profound negative regulation of COX-2 and other pro-inflammatory cytokines downstream of LPS/TLR4 activation (Alqinyah et al., 2018; Lee et al., 2008; Lee et al., 2011). While RGS10 holds great promise as an anti-inflammatory drug target, its mechanism of action is mediated through an unknown G protein-independent mechanism (Alqinyah et al., 2018).

In this study, we identified a non-canonical interaction of microglial RGS10 with STIM2, an ER-resident calcium sensor and component of the store-operated calcium entry (SOCE) machinery (Berna-Erro et al., 2017; Hoth & Niemeyer, 2013; Ong et al., 2015). Our collective findings revealed a bi-directional and opposing regulation of LPS-stimulated inflammatory gene expression by RGS10 and STIM2. The regulation of inflammatory gene expression is mediated by multiple pathways and components. Recently, a direct link between LPS signaling and store-

operated calcium entry has been explored in microglia. Mizuma and colleagues (2019) demonstrated that LPS induces SOCE in BV2 cells, and inhibition of SOCE suppresses downstream inflammatory responses including the activation of NF_kB and NFAT, suggesting the importance of microglial SOCE to LPS signaling (Mizuma et al., 2019). Our data extend this finding to implicate STIM2, Orai, and calcineurin in facilitating LPS-stimulated response and in mediating RGS10-sensitive pro-inflammatory gene expression. In particular, we demonstrated the requirement of the STIM2-Orai-Calcineurin signaling axis for RGS10-mediated regulation of COX-2 expression in response to LPS. We also determined that the upstream trigger of SOCE, the depletion of store calcium, amplifies the pro-inflammatory effect of LPS. Additionally, our results revealed a new role of RGS10 in the regulation of SOCE triggered by store depletion. Collectively, our data demonstrate a complex signaling network linking LPS, RGS10, and SOCE which suggests that the ability of RGS10 to form a complex with and/or modulate the activity of the store calcium machinery may account for its G protein-independent anti-inflammatory effects (**Figure 3.8**).

Similar to RGS10-mediated modulation of COX-2, RGS10 also regulated LPS-induced expression of IL-6, TNFα, and to a lesser extent iNOS, in a mechanism that requires SOCE. Multiple receptor stimuli can trigger both calcium depletion from the ER and inflammatory gene expression (Newton et al., 2012). Therefore, the ability of RGS10 to regulate SOCE may impact pro-inflammatory responses downstream of different stimuli besides the TLR4 agonist LPS, in particular regulation of pathways that converge with SOCE. Previous reports showed that the endogenous agonist thrombin elicits cytoplasmic Ca^{2+} release from the ER and triggers SOCE in endothelial cells (Spinelli et al., 2016; Stolwijk et al., 2016; Sundivakkam et al., 2013). Thrombin is a pro-inflammatory agonist that has been shown to activate microglia via G protein-coupled

proteinase-activated receptors (PARs) (Hanisch et al., 2004). We demonstrated that loss of RGS10 in BV2 microglia enhanced thrombin-mediated expression of pro-inflammatory genes including COX-2, TNFα, and IL-6, indicating that RGS10's anti-inflammatory effect is not limited to the regulation of TLR4 response. Inhibition of SOCE also blunted the upregulation of thrombin-stimulated expression of these pro-inflammatory genes in response to RGS10 loss. Therefore, the ability of RGS10 to regulate both thrombin and LPS pro-inflammatory responses through a common downstream mechanism involving SOCE suggests a broad anti-inflammatory role for RGS10. NFAT is a likely candidate for mediating the effect of RGS10 downstream of Orai-calcineurin activation, and multiple NFAT family members; in particular NFATc1 and NFATc2, have been reported to have prominent expression in microglia (Nagamoto-Combs et al., 2010). Ongoing studies will characterize the effect of RGS10 on NFAT expression, actvation, and translocation in response to multiplestimuli. We have previously demonstrated that RGS10 does not regulate acute activation of NFkB, MAPK and AKT pathways following LPS stimulation (Alqinyah et al., 2018).

STIM1 and STIM2 are localized throughout the ER under basal conditions with high ER calcium, but upon ER calcium depletion, the STIM proteins undergo conformational rearrangement and form homo- and/or hetero-dimers that translocate to ER-PM junctions, where they can bind and activate Orai channels, triggering SOCE (Palty et al., 2017; Stathopulos et al., 2009). Despite the close homology between STIM1 and STIM2, our results indicate that RGS10 specifically interacts with STIM2 and not STIM1, and the interaction with STIM2 does not depend on calcium. These results are consistent with a basal interaction of RGS10 and STIM2 that does not include STIM1-STIM2 heterodimers. It is possible that RGS10 interaction with STIM2 may

inhibit formation of STIM1/2 heterodimers, which would allow RGS10 to indirectly impact STIM1 function without physically interact with STIM1. While this study uncovered a functional link between RGS10 and STIM2, it did not delineate the specific role of this biochemical interaction. It is plausible that the anti-inflammatory function of RGS10 and its ability to alter SOCE may be mediated by its interaction with STIM2, which may alter the functional response of STIM2 including conformational activation, dimerization, and/or STIM/Orai coupling (Palty et al., 2017; Stathopulos et al., 2009). Ongoing biochemical and signaling studies are examining the role and biochemical requirements of the RGS10-STIM2 interaction. For example, it is important to determine if STIM2 directly binds RGS10 or if their interaction reflects mutual enrichment in a multi-protein complex regulated by other factors such as subcellular localization, G protein activation, or additional binding partners. Given the lack of defined functional domains in RGS10 other than the highly conserved RGS domain, which is shared among all members of the RGS protein family (Hollinger & Hepler, 2002), further biochemical studies should determine if the RGS10-STIM2 interaction is mediated by the RGS domain and whether STIM2 also associates with this domain in other RGS proteins.

Calcium Release-Activated Calcium (CRAC) proteins including Orai channels represent the primary route for store-operated calcium entry (SOCE). Despite limited knowledge of the role of microglial SOCE, STIM2 and the components of CRAC channels have been implicated in several acute and chronic neuropathological conditions including PD, AD, ischemic stroke, and traumatic brain injury (TBI) (Secondo et al., 2008). Therefore, RGS10's ability to suppress SOCE and its broad anti-inflammatory response in microglia has implications for many neurodegenerative diseases with underlying chronic neuroinflammation. RGS10 is also expressed

in multiple other cells and modulates immune signaling and other functions in macrophages (Lee et al., 2013), osteoclasts (Yang et al., 2013), T-lymphocytes (Garcia-Bernal et al., 2011), cardiomyocytes (Miao et al., 2016), neurons (Lee et al., 2012), and cancer cells (Ali et al., 2013; Hooks et al., 2015). Although many functions of RGS10 have been identified in these systems, the exact molecular mechanisms governing these functions are not understood. Therefore, the involvement of STIM2 and SOCE in RGS10's anti-inflammatory molecular mechanism has implications beyond neuroinflammation, to include diverse pathologies in which RGS10 function is implicated, such as multiple sclerosis (Lee et al., 2016), cancer chemoresistance (Ali et al., 2013; Hooks et al., 2015), cardiac hypertrophy (Miao et al., 2016), and bone disorders (Yang et al., 2007; Yang et al., 2013).

Table 3.1. Proteins enriched by RGS10 immunoprecipitation in BV2 microglia

Protein Name	Uniprot ID	Normalized NSAF score Mean (SEM) RGS10	Normalized NSAF score Mean (SEM) IgG	SAINT score
Regulator of G protein Signaling 10	Q9CQE5	100.02 (0.02)	0.00 (0.00)	1.00
Guanine nucleotide-binding protein (Gi) subunit alpha-2	P08752	36.12 (9.06)	1.48 (1.48)	1.00
Methylosome protein 50	Q99J09	18.56 (1.04)	3.09 (0.29)	0.96
Multifunctional protein ADE2	Q9DCL9	18.26 (0.15)	1.49 (1.00)	1.00
Alanine aminotransferase 1	Q8QZR5	16.09 (3.74)	0.00 (0.00)	0.88
Guanine nucleotide-binding protein (Gi) subunit alpha-3	Q9DC51	12.63 (0.64)	0.59 (0.59)	0.97
Stromal interaction molecule 2 (STIM2)	P83093	10.17 (0.91)	0.49 (0.49)	0.95
NADH dehydrogenase 1 alpha subcomplex subunit 10	Q99LC3	9.64 (0.44)	0.00 (0.00)	1.00
Tyrosine-protein phosphatase non-receptor type 2	Q06180	6.98 (1.82)	0.00 (0.00)	1.00
E3 ubiquitin-protein ligase RNF146	Q9CZW6	6.08 (0.48)	0.00 (0.00)	1.00
Malectin	Q6ZQI3	5.89 (1.28)	0.00 (0.00)	0.96
STIP1 homology and U box-containing protein 1	Q9WUD1	5.58 (0.43)	0.00 (0.00)	1.00
DDB1- and CUL4-associated factor 7	P61963	5.23 (0.65)	0.31 (0.31)	0.99
Anion exchange protein 2	P13808	5.06 (0.73)	0.08 (0.08)	1.00
Nitric oxide-associated protein 1	Q9JJG9	4.99 (0.48)	0.00 (0.00)	0.88
Syntaxin-5	Q8K1E0	4.85 (0.81)	0.00 (0.00)	1.00
cAMP-specific 3',5'-cyclic phosphodiesterase 4A	O89084	4.57 (0.07)	0.18 (0.18)	1.00
Methylosome subunit pICln	Q61189	4.53 (2.64)	0.00 (0.00)	0.88
Sec1 family domain-containing protein 1	Q8BRF7	4.42 (2.58)	0.00 (0.00)	0.87
rRNA methyltransferase 1, mitochondrial	Q99J25	4.01 (1.58)	0.00 (0.00)	0.99
Golgi membrane protein 1	Q91XA2	3.75 (0.90)	0.00 (0.00)	0.86
Dual specificity tyrosine-phosphorylation-regulated kinase 1A	Q61214	2.69 (0.05)	0.00 (0.00)	1.00
G patch domain-containing protein 2	Q7TQC7	2.13 (0.41)	0.00 (0.00)	0.98
Malonyl-CoA decarboxylase, mitochondrial	Q99J39	2.06 (0.21)	0.00 (0.00)	0.97
Choromodomain-helicase-DNA-binding protein 1-like	Q9CXF7	2.05 (1.18)	0.00 (0.00)	1.00
Arf-GAP with coiled-coil, ANK repeat and PH domain-containing protein 1	Q8K2H4	1.97 (0.15)	0.00 (0.00)	0.87

Proteins enriched in RGS10 immunoprecipitated samples compared to control IgG samples were determined from LC-MS/MS analysis and filtered using a probability-based SAINT score. Biological replicates from two independent co-immunoprecipitation experiments were used for peptide identification and data analysis, and hits with a SAINT score above 0.8 are listed ranked by normalized spectral abundance factor (NSAF) in RGS10 co-IP samples, represented as a percentage of RGS10 NSAF score (100%).

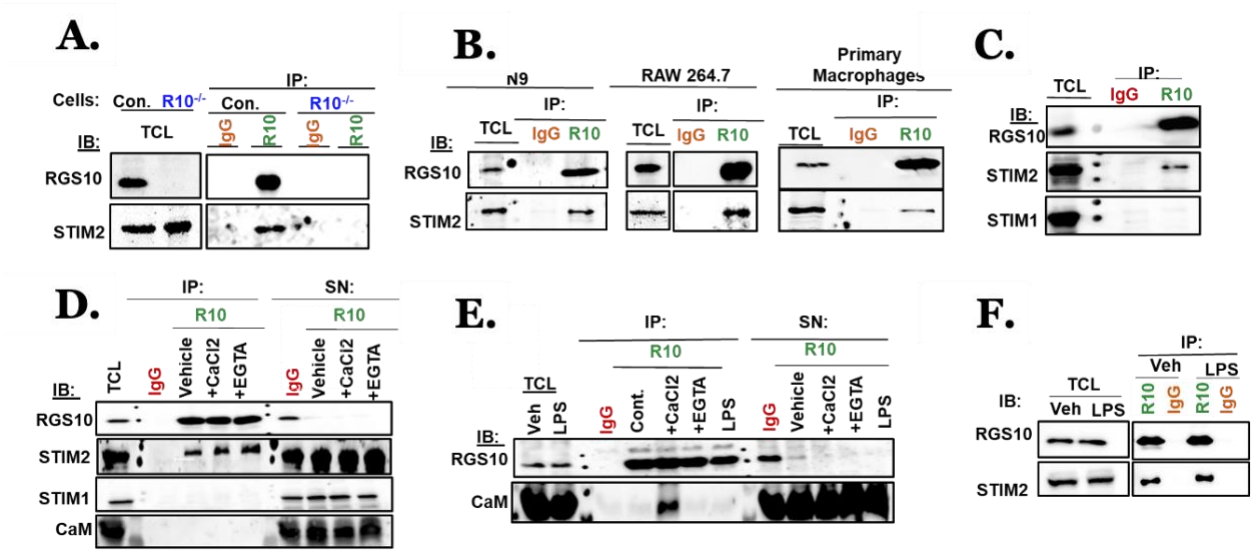

Figure 3.1. Specificity and regulation of RGS10-STIM2 interaction. **A)** Control (Con.) and RGS10 knockout ($R10^{-/-}$) BV2 total cell lysate (TCL) immunoprecipitated (IP) with RGS10 (R10) and control (IgG) antibodies followed by immunoblotting (IB) for RGS10 and STIM2. **B)** RGS10 IP in N9 microglia (left panel), RAW264.7 macrophages (middle panel), and primary peritoneal macrophages (right panel), followed by IB for RGS10 and STIM2. **C)** RGS10 IP in wild type BV2 cells followed by IB for RGS10, STIM2, and STIM1. **D.** RGS10 and control IP from BV2 cells incubated for 1 hour with lysis buffer alone (Veh) or in the presence of either $CaCl_2$ (1mM) or EGTA (0.5mM), followed by IB for RGS10, STIM1, STIM2, and CaM. **E)** RGS10 IP conducted as in (D) but in the absence of sodium deoxycholate. **F)** RGS10 IP from BV2 cells treated with vehicle or LPS (10 ng/mL) for 3 h, followed by IB for RGS10 and STIM2. All figures are representative of three independent experiments.

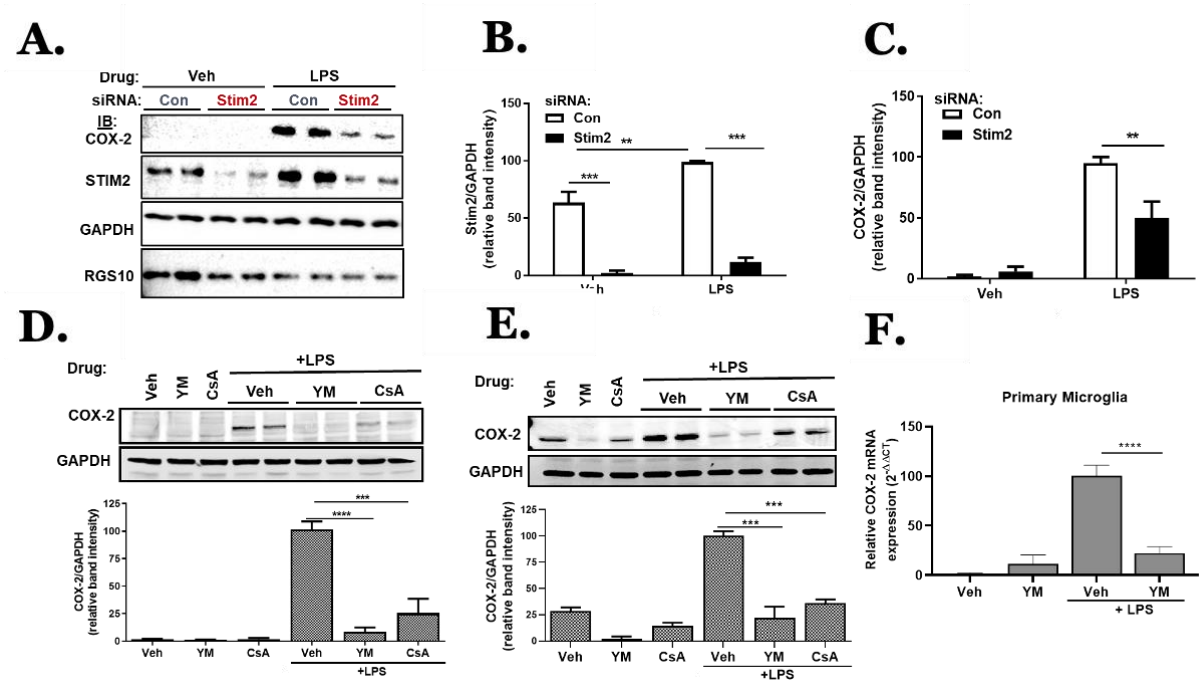

Figure 3.2. STIM2 and the Orai-calcineurin signaling axis is required for LPS-stimulated COX-2 expression. **A-C)** BV2 cells were transfected with control siRNA (Con) or STIM2-targeted siRNA (Stim2). 24 hours after transfection, cells were treated with either serum-free media (Veh) or LPS (10 ng/mL) for additional 24 hours. **A)** Immunoblot (IB) of BV2 cells probed for COX-2, STIM2, RGS10, and GAPDH. **B)** Densitometry analysis of Stim2 data in (A) normalized to GAPDH. **C)** Normalized densitometry analysis of COX-2 data in (A). **D)** BV2 cells were pre-treated with Veh, or media containing either the Orai inhibitor YM58483 (YM) (10 uM) or the calcineurin inhibitor cyclosporin (CsA) (100 ng/mL) for 1 hour prior to a 24-hour incubation with Veh or LPS (10 ng/mL). COX-2 and GAPDH protein level was analyzed by IB (top panel), and quantified figures are shown (bottom panel). **E)** IB data of N9 cells treated as in (D), but with a modified LPS dose (100 ng/mL). **F)** Primary microglia isolated from postnatal mouse pups were pretreated with a Veh or YM (10 uM) for 1 hour, followed by treatment with Veh or LPS (10 ng/mL) for 24 h. Relative COX-2 mRNA expression analyzed by quantitative real-time PCR (qRT-PCR) normalized to an endogenous control β-actin ($2^{-\Delta\Delta Ct}$). qRT-PCR and western blot data were normalized to the lowest values, and representative data are presented as mean ± SEM pooled from three independent experiments. *p < 0.05, **p<0.01, and ***p<0.001, determined by one-way ANOVA followed by Tukey post hoc test.

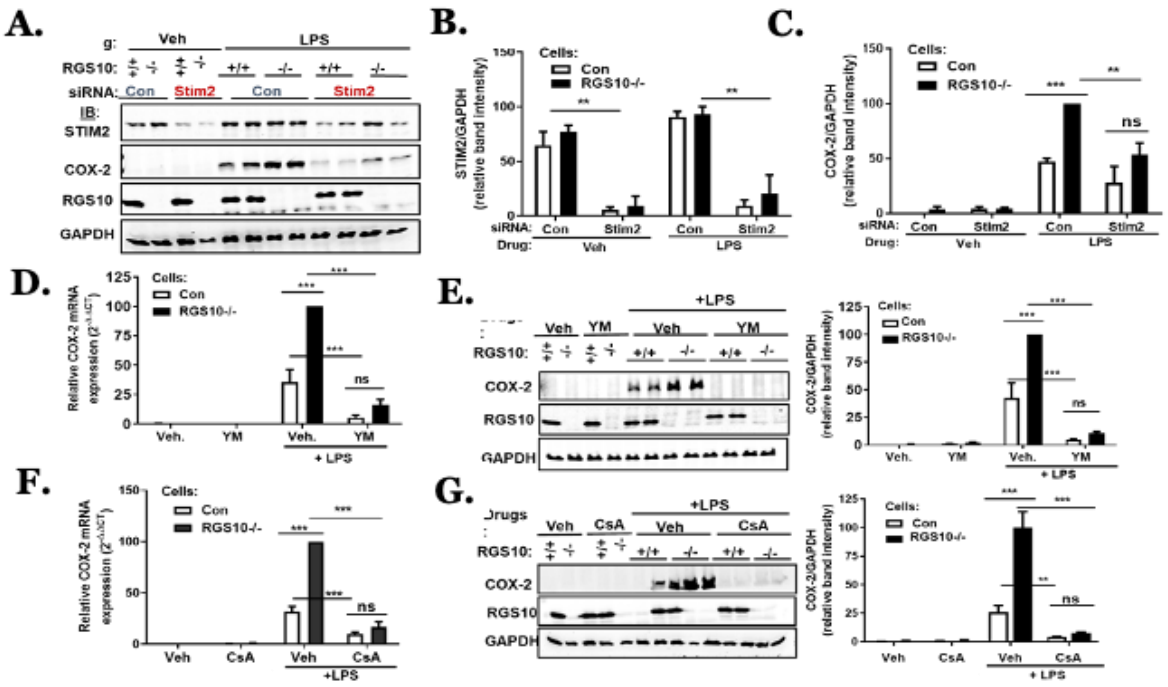

Figure 3.3. The STIM2-Orai-Calcineurin signaling axis mediates RGS10 sensitive COX-2 expression. **A-C)** CRISPR-control (+/+) and RGS10 knockout (-/-) BV2 cells were transfected with control siRNA (Con) or STIM2-targeted siRNA (Stim2). 24 hours after transfection, cells were treated with either serum-free media (Veh) or LPS (10 ng/mL) for additional 24 hours. **A)** Immunoblot (IB) of BV2 cells probed for COX-2, STIM2, RGS10, and GAPDH. **B)** Densitometry analysis of Stim2 data in (A) normalized to GAPDH. **C)** Normalized densitometry analysis of COX-2 data in (A). **D-E)** Control and RGS10 knockout BV2 cells ($RGS10^{-/-}$) were treated with Veh or media containing 10 µM YM58483 (YM) for 1 hour prior to a 24-hour incubation with Veh or LPS (10 ng/mL). Relative COX-2 mRNA expression was analyzed by qRT-PCR **(D)**. IB of COX-2, RGS10, and GAPDH (left panel) and representative densitometry of COX-2 band intensity normalized to GAPDH (right panel) **(E)**. **F-G)** Control and $RGS10^{-/-}$ cells treated with either Veh, 100ng/mL cyclosporine (CsA) and/or LPS (10 ng/mL) for 24 hours. Relative COX-2 mRNA expression was analyzed by qRT-PCR (**F**). Representative IB images of COX-2, RGS10, and GAPDH (left panel) and densitometry of COX-2 band normalized to GAPDH (right panel) (**G**). qRT-PCR data are normalized to endogenous control β-actin ($2^{-\Delta\Delta Ct}$). Fold difference of qRT-PCR and WB densitometry data were calculated after normalizing to a Veh treatment, and data represent mean ± SEM pooled from three independent experiments. *p < 0.05, **p<0.01, and ***p<0.001, determined by one-way ANOVA followed by Tukey post hoc test.

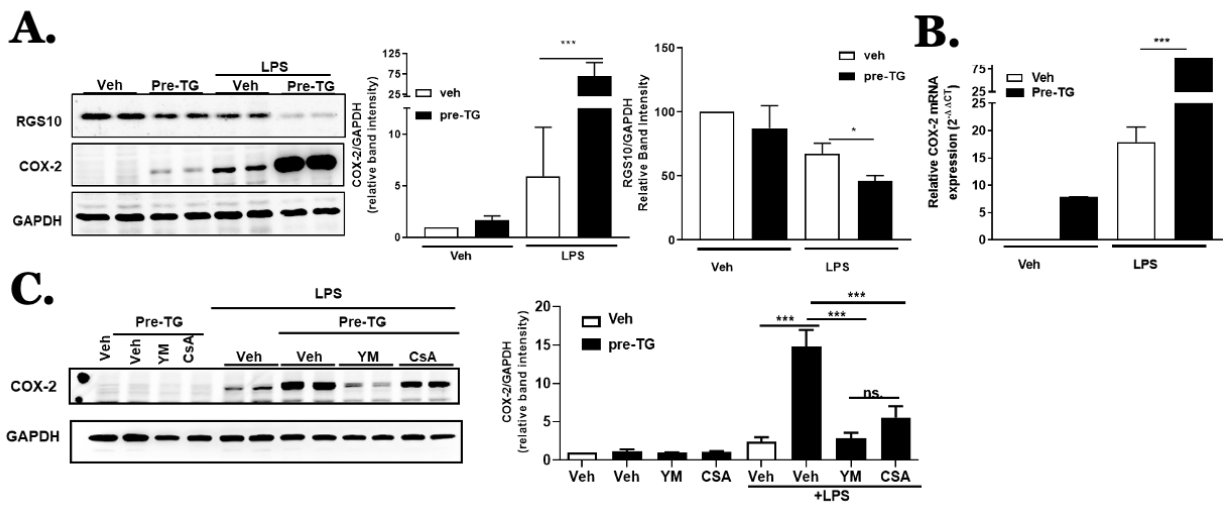

Figure 3.4. Depletion of calcium from intracellular stores amplifies LPS effects on COX-2 and RGS10 expression. A-B) Wildtype BV2 cells were pretreated with vehicle or 1μM thapsigargin (TG) for 20 minutes. TG-containing media was removed and replaced by fresh media containing either vehicle or LPS (10 ng/mL) for 24 hours. **A).** Representative IB images of COX-2, RGS10, and GAPDH (left panel), and densitometry quantification (bar graphs). **B)** Relative COX-2 mRNA expression was analyzed by qRT-PCR. **C)** Representative IB images of COX-2 and GAPDH (left panel), and densitometry quantification (bar graph) of BV2 cells pretreated with TG as in (A-B) followed by LPS, alone or LPS in combination with either Orai inhibitor (YM) and calcineurin inhibitor (CsA). qRT-PCR data are normalized to endogenous control β-actin (2-ΔΔCt). Fold difference of qRT-PCR and WB densitometry data were calculated after normalizing to vehicle conditions, and data represent mean ± SEM pooled from three independent experiments. *p < 0.05, **p<0.01, and ***p<0.001, determined by one-way ANOVA followed by Tukey post hoc test.

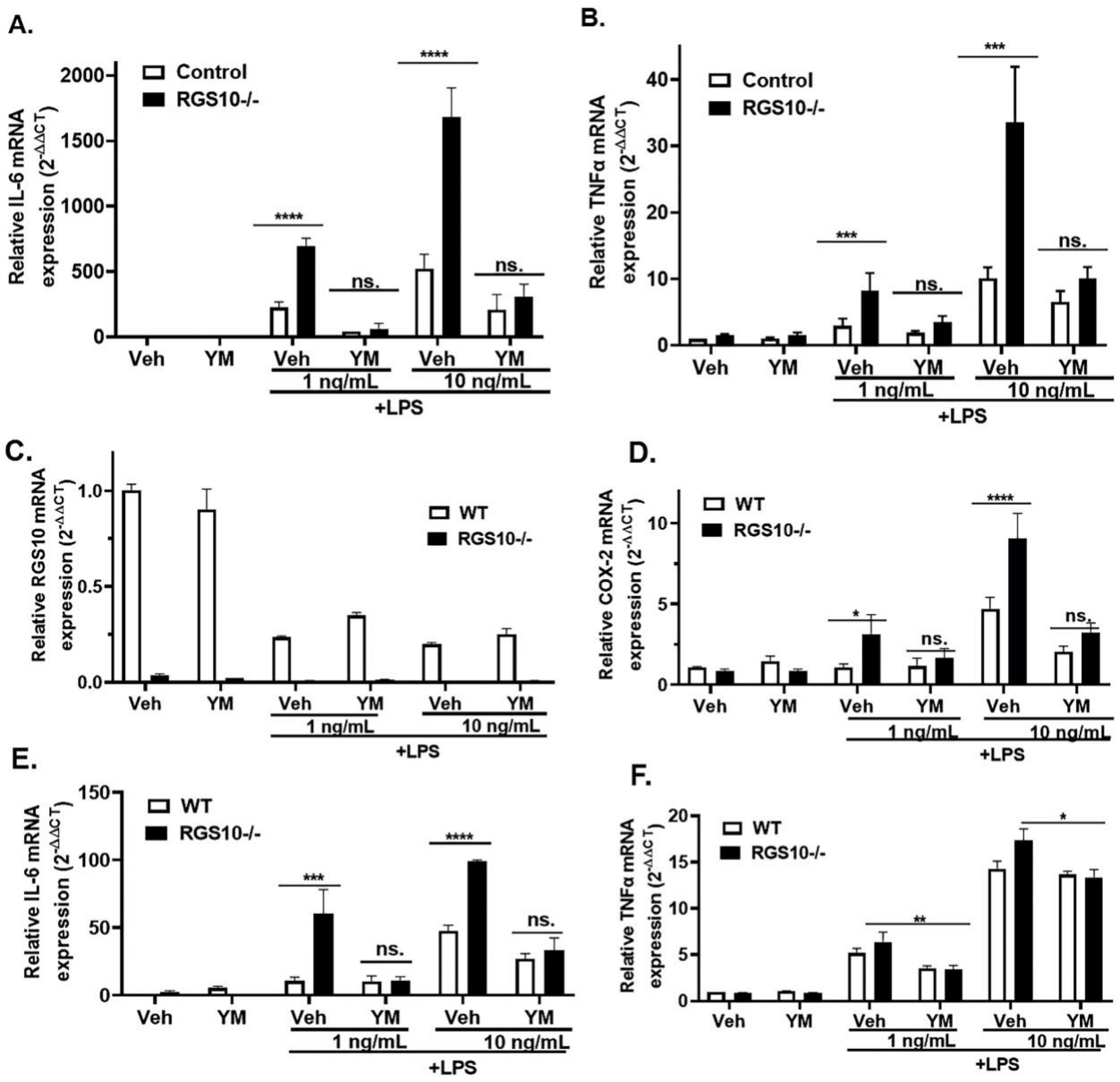

Figure 3.5. RGS10 requires SOCE to regulate LPS-induced pro-inflammatory genes in BV2 and primary microglia. A&B) CRISPR-control (Control) and RGS10 knockout (RGS10-/-) BV2 cells were pretreated for 1 hour with serum-free medium (Veh) or the Orai inhibitor YM58483 (YM) (10 uM) prior to 24-hour incubation with Veh, LPS (1 ng/mL) or LPS (10 ng/mL). Relative expression of IL-6 transcript **(A)** and TNFα transcript **(B)** are analyzed by quantitative real-time PCR (qRT-PCR). **C-F)** Primary microglia from wild type (WT) and RGS10 knockout (RGS10-/-) mice were treated as in (A&B), and relative expression of RGS10 transcript (**C**), COX-2 transcript (**D**), IL-6 transcript (**E**), and TNFα transcript (**F**) are analyzed by qRT-PCR. Data are normalized to endogenous control β-actin ($2^{-\Delta\Delta Ct}$) and fold differences are calculated after normalizing to vehicle treatment groups. Data represent mean ± SEM pooled from 7-8 experiments for BV2 cells (A-B) and three experiments for primary microglia (C-F). *p < 0.05, **p<0.01, and ***p<0.001, determined by one-way ANOVA followed by Tukey post hoc test.

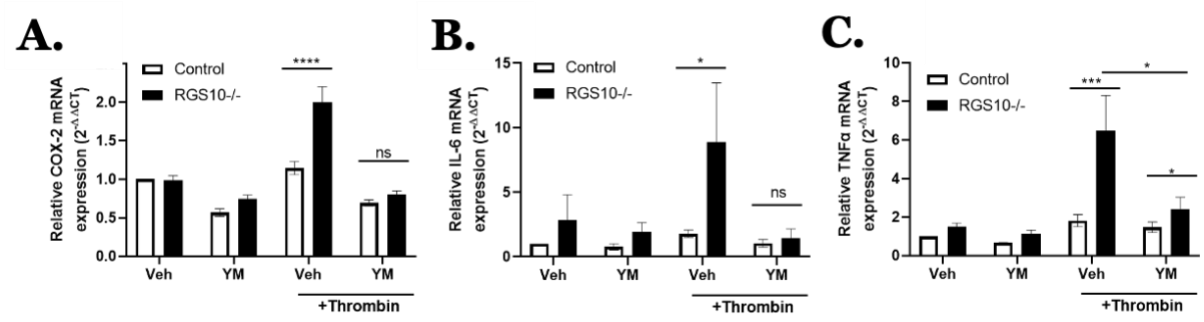

Figure 3.6. Loss of RGS10 upregulates thrombin-stimulated pro-inflammatory genes in BV2 microglia in SOCE-dependent mechanism. CRISPR-control (Control) and RGS10 knockout (RGS10-/-) BV2 cells were treated with Fatty acid-free BSA (Veh) or Thrombin (10 U/mL) for 4 hours with or without a 1-hour pretreatment with Orai inhibitor YM58483 (YM) (10 uM). Relative expression of COX-2 transcript (**A**), IL-6 transcript (**B**), and TNFα transcript (**C**) are analyzed by qRT-PCR. Data are normalized to endogenous control β-actin ($2^{-\Delta\Delta Ct}$) and fold difference is calculated after normalizing to the vehicle treatment group of control cells. Represented data are mean ± SEM pooled from 4-5 independent experiments. *p < 0.05, **p<0.01, and ***p<0.001, determined by ANOVA followed by Tukey post hoc test.

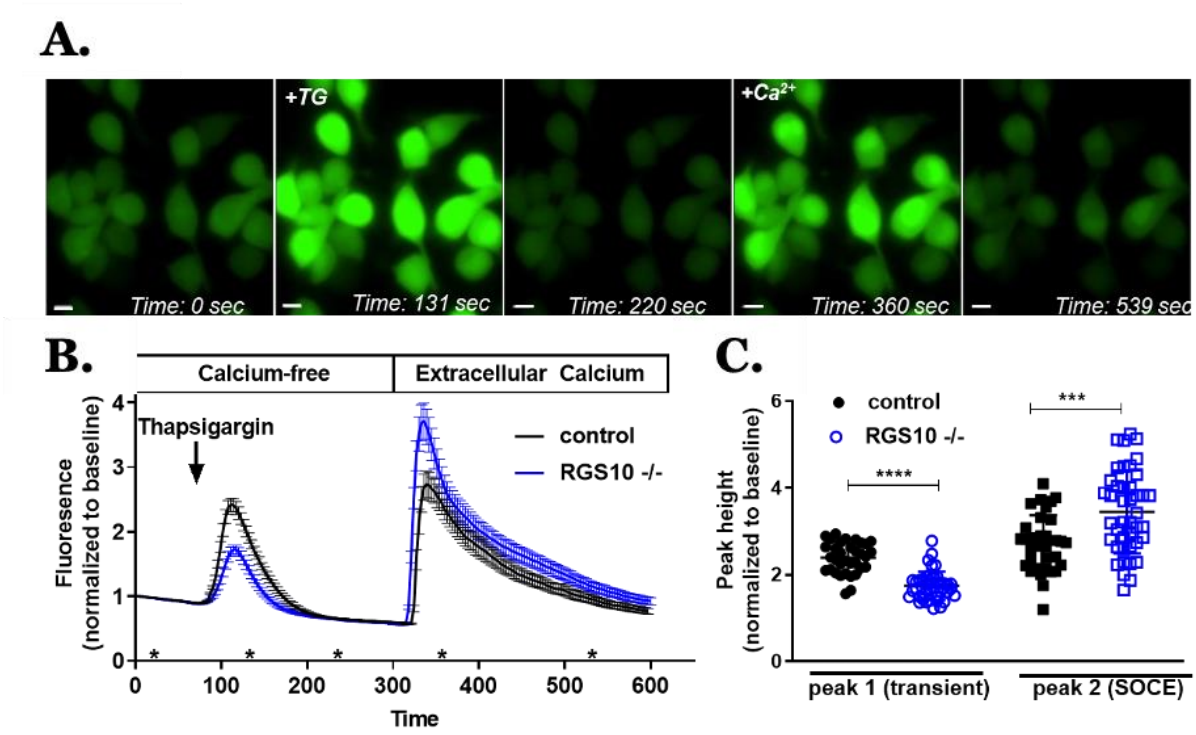

Figure 3.7. Loss of RGS10 enhances store-operated calcium entry (SOCE) triggered by ER depletion. BV2 cells were loaded with 5 µM CAL520-AM for 20 min at 37ºC and incubated in calcium-free buffer containing EGTA. Live cell imaging was initiated at time=0, and TG (1 µM) and Ca^{2+} (1.8 mM) were added at 60 sec and 300 sec, respectively. Images were captured every 3 sec. **A)** Representative fluorescence images of control BV2 cells at indicated time points. **B)** Quantified tracings of average fluorescence intensity in CRISPR-control BV2 cells (black) and RGS10 knockout BV2 cells (blue). Error bars indicate standard deviation from at least ten cells in a single experiment. Asterisks (*) indicate approximate time points corresponding to images shown in (A). **C)** Average peak height of the TG-induced Ca^{2+} transient calcium signal and SOCE signal observed after 1.8 mM Ca^{2+} addition, from three independent experiments, with 10-15 cells quantified from each cell line in each experiment. *p < 0.05, **p<0.01, and ***p<0.001, determined by unpaired student's t-test.

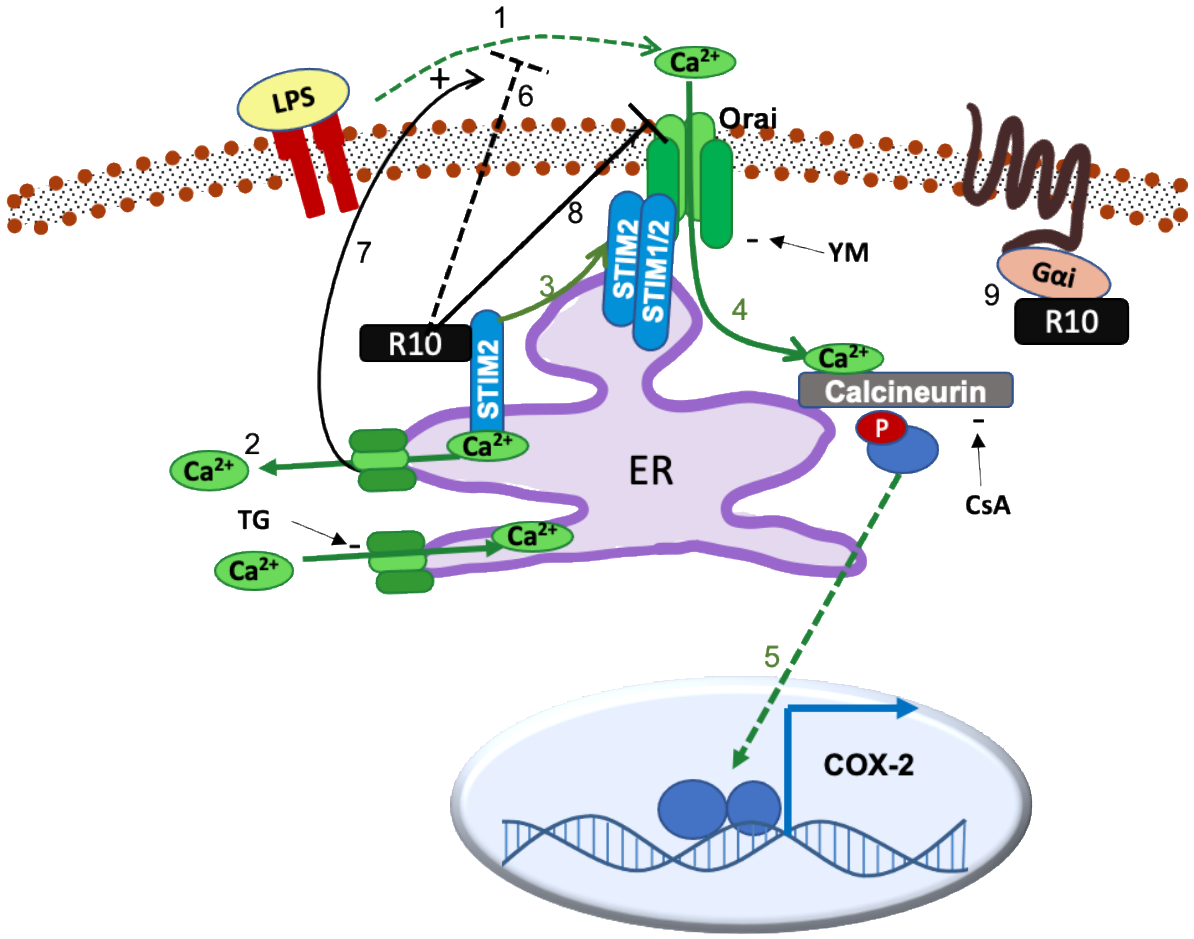

Figure 3.8. Model and Summary: RGS10 regulates pro-inflammatory gene expression through functional interaction with the SOCE machinery. LPS facilitates extracellular calcium entry through plasma membrane Orai channels, a mechanism known as store-operated calcium entry (SOCE) (1). SOCE is activated through an upstream mechanism involving calcium depletion from intracellular stores. Upon ER depletion (2), calcium dissociates from the ER membrane resident calcium sensor STIM2, triggering STIM2 translocation to ER-PM junctions where it forms a complex with STIM1 and Orai subunits to form an active calcium channel (3). SOCE through Orai is tightly coupled to activation of the phosphatase calcineurin (4), which triggers activation of downstream substrates and promotes the expression of pro-inflammatory genes (5). Our data demonstrate that LPS requires an intact SOCE pathway including STIM2, Orai, and calcineurin to trigger pro-inflammatory gene expression through undefined, indirect mechanisms. We previously showed that RGS10 (R10) suppresses LPS-induced pro-inflammatory gene expression in a G-protein independent mechanism. Here, we show that RGS10 selectively interacts with STIM2, and RGS10-mediated regulation of LPS response requires activation of the STIM2-Orai-Calcineurin pathway (6). Depletion of intracellular calcium (2) activates SOCE and enhances LPS response (7), and RGS10 suppresses SOCE triggered by store depletion (8). In addition to G protein-independent regulation of LPS response, RGS10 also mediates signaling in microglia through its canonical interaction with Gαi subunits (9). The interplay of RGS10 co-regulation of these two critical pathways and the specific role of RGS10-STIM2 biochemical interaction is unknown. It is plausible that RGS10 regulates SOCE and downstream pro-inflammatory response by interacting with and/or modulating STIIM2 function such as STIM2 activation, PM translocation, and interaction with STIM1/Orai channel (3). Similar to the regulation of TLR4 response, RGS10 also suppresses thrombin-stimulated pro-inflammatory genes through a mechanism requiring Orai activity, suggesting that RGS10 has the potential to regulate a broad range of inflammatory responses that depend on SOCE. The effects of pharmacological agents Thapsigargin (TG), YM58483 (YM), and cyclosporine A (CsA) are shown.

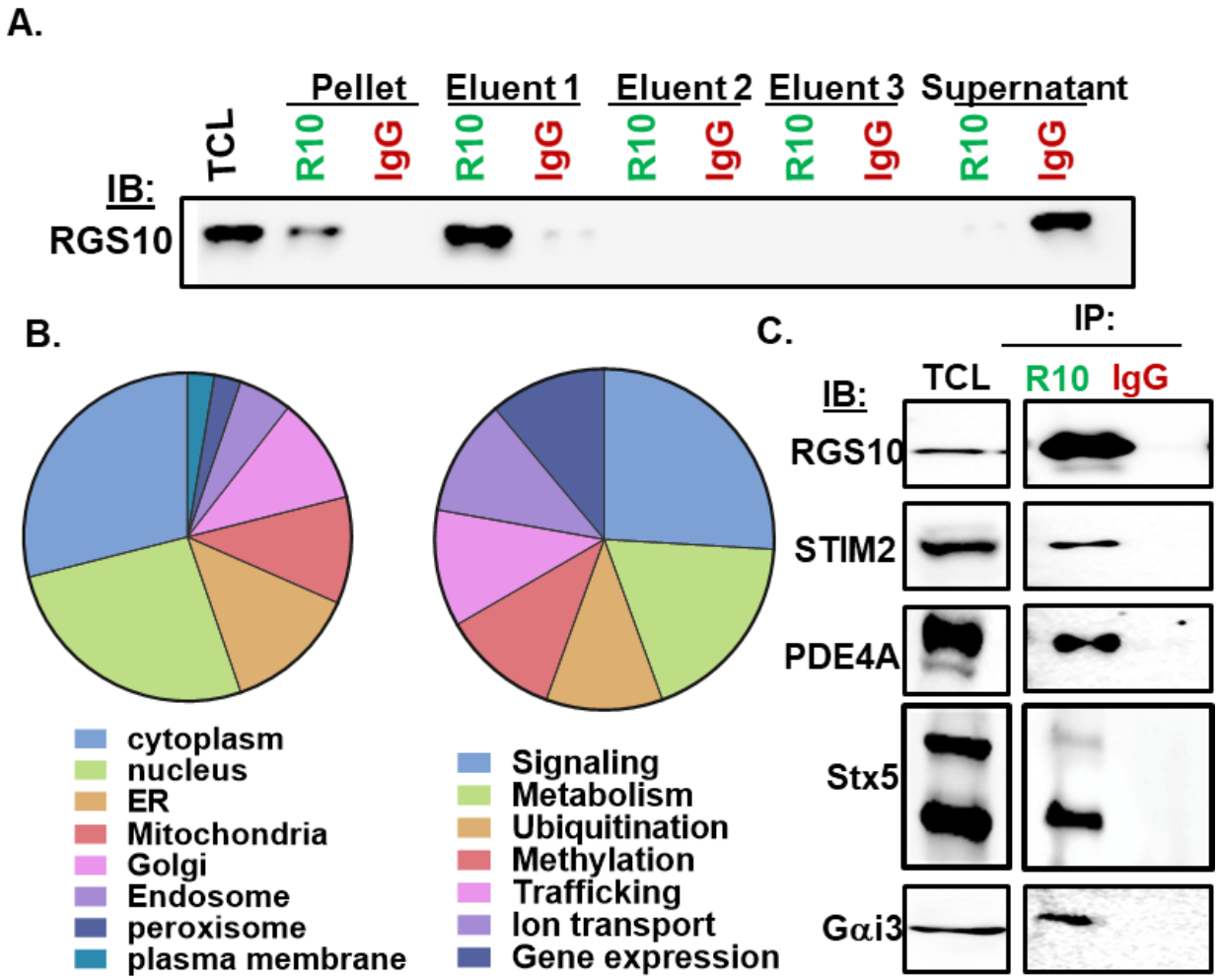

Figure S3.1. RGS10 immunoprecipitation and identification of interacting proteins. A) BV2 total cell lysates (TCL) were immunoprecipitated using RGS10 antibody-conjugated beads or control IgG-conjugated beads, and the resulting supernatant fractions, elution fractions, and final bead pellets were analyzed for RGS10 immunoreactivity by immunoblotting (IB). **B)** Proteins significantly enriched by RGS10 IP were categorized according to their subcellular localization (left panel) and main molecular/biological function (right panel). See Table S1 for further details. **C)** RGS10 interaction with multiple putative interacting partners were confirmed using direct co-immunoprecipitation from BV2 cell lysates with RGS10 (R10) or control IgG (IgG) antibody followed by immunoblotting (IB) for Gαi3, STIM2, syntaxin5, and PDE4A.

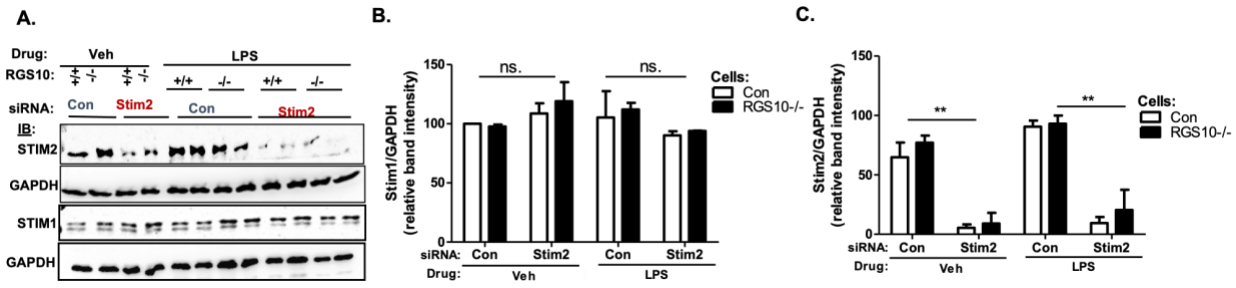

Figure S3.2. STIM2 knockdown does not affect STIM1 expression. CRISPR-control (+/+) and RGS10 knockout (-/-) BV2 cells were transfected with control siRNA (Con) or STIM2-targeted siRNA (Stim2). 24 hours after transfection, cells were treated with either serum-free media (Veh) or LPS (10ng/mL) for additional 24 hours. Representative immunoblot (IB) images of STIM1, STIM2, and GAPDH (left panel), densitometry analysis of Stim1 data normalized to GAPDH (middle panel), and normalized COX-2 data (right panel). Fold differences of densitometry data were calculated after normalizing to a Veh treatment, and data represents mean ± SEM pooled from three independent experiments. *$p < 0.05$, **$p<0.01$, and ***$p<0.001$, determined by one-way ANOVA followed by Tukey post hoc test.

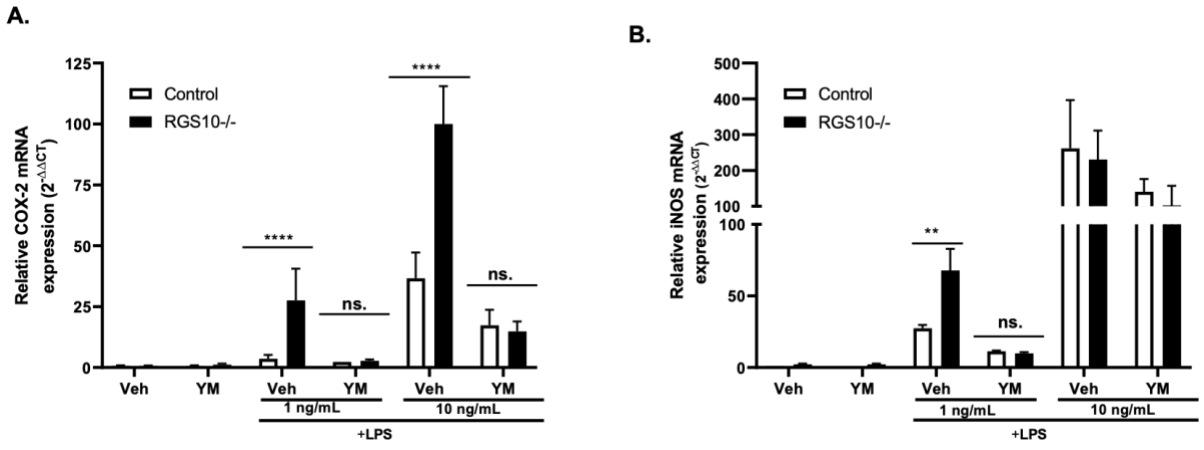

Figure S3.3. RGS10 requires SOCE to regulate LPS-induced COX-2 and iNOS expression in BV2 microglia. CRISPR-control (Control) and RGS10 knockout (RGS10-/-) BV2 cells were pretreated for 1 hour with serum-free medium (Veh) or the Orai inhibitor YM58483 (YM) (10 uM) prior to 24-hour incubation with Veh, LPS (1 ng/mL) or LPS (10 ng/mL). Relative expression of COX-2 transcript **(A)** and iNOS transcript **(B)** are analyzed by quantitative real-time PCR (qRT-PCR). Data are normalized to endogenous control β-actin ($2^{-\Delta\Delta Ct}$) and fold differences are calculated after normalizing to vehicle treatment groups. Data represent mean ± SEM pooled from at least three experiments. *p < 0.05, **p<0.01, and ***p<0.001, determined by one-way ANOVA followed by Tukey post hoc test.

CHAPTER 4

TRANSCRIPTOMIC ANALYSIS OF GENE EXPRESSION BY CRISPR/CAS9-MEDIATED DELETION OF RGS10 IN MICROGLIA

4.1. Introduction

RGS10 is a small member of the RGS protein family, containing only the conserved RGS domain that canonically functions as a GTPase-activating protein (GAP) for Gαi (Hunt et al., 1996). RGS10 exerts protective roles in multiple models, and loss of its expression is implicated in the pathophysiology of various diseases including Parkinson's disease (PD) (Lee et al., 2011), influenza (Almutairi et al., 2021), osteoporosis (Yang & Li, 2007), vascular injury (Hensch et al., 2016; Miao et al., 2016), rheumatoid arthritis (Ren et al., 2021), and periodontitis (Chan et al., 2022). Furthermore, polymorphisms in the RGS10 gene have been associated with human neurological diseases, including schizophrenia (Hishimoto et al., 2004) and age-related neurodegenerative maculopathy (Kannarkat et al., 2015).

Several studies have demonstrated protective functions of RGS10 in central and peripheral immune cells. In particular, RGS10 is abundantly expressed in microglia and mediates anti-inflammatory and neuroprotective functions, as demonstrated in an inflammation model of PD (Lee et al., 2008; Lee et al., 2011). Compared to wild-type mice, RGS10-null mice exhibit chronic microgliosis and enhanced dopaminergic (DA) neuronal death induced by chronic low-dose exposure to lipopolysaccharide (LPS) compared to wild-type mice (Lee et al., 2008). Additionally, primary cell studies indicated that microglial RGS10 protects vulnerable DA neurons from

inflammation-induced neurotoxicity by limiting the release of pro-inflammatory and neurotoxic cytokines from activated microglia (Lee et al., 2008; Lee et al., 2011).

Apart from its role in the central nervous system, RGS10 is also enriched in various peripheral immune cells, including macrophages, platelets, dendritic cells, lymphocytes, and osteoclasts, where it generally mediates protective functions (Almutairi et al., 2020). While RGS10 exerts anti-inflammatory and neuroprotective properties, its expression is downregulated in response to inflammatory stimuli such as LPS and Tumor necrosis factor α (TNFα) (Alqinyah et al., 2017; Lee et al., 2008). Furthermore, age-related loss of RGS10 expression in microglia has been linked to macular degeneration (Kannarkat et al., 2015).

Although the function of RGS10 has been investigated in various cell types and disease models, there is limited knowledge regarding its molecular mechanism. We recently demonstrated that, despite only containing the conserved RGS domain that mediates the canonical interaction with G proteins, RGS10 interacts with multiple non-canonical protein partners (Wendimu et al., 2021), implying that RGS10 may have diverse roles in microglia. Furthermore, we have shown that RGS10 regulates LPS-induced expression of pro-inflammatory genes in BV2 microglia (Wendimu et al., 2021), and transient overexpression of wild-type and a GAP-dead mutant human RGS10-2 (short variant) in TLR4-expressing HEK293 cells suppresses LPS-induced expression of TNFα (Alqinyah et al., 2018). Although the overexpression study revealed a potential G protein-independent role for RGS10, it had a few limitations: 1) it was performed in the HEK293 cell line, which is not an immune cell model; 2) it utilized a transient expression system; and 3) we overexpressed a less dominant variant of human RGS10 (hRGS10-2).

To expand our previous observation in microglia, we generated stable RGS10 knockout and overexpression BV2 microglia models and confirmed the G protein-independent effects of RGS10 in the regulation of LPS-induced expression of cyclooxygenase-2 (COX-2) and interleukin-6 (IL-6). Using RNA-sequencing (RNA-seq), we further investigated transcriptomic alterations induced by CRISPR/Cas9-mediated deletion of RGS10 in resting and LPS-activated BV2 cells to comprehensively examine the role of RGS10 in global gene regulation and identify relevant molecular mechanisms. The identification of altered biological processes and pathways in this study may help to elucidate the functional implications of RGS10 loss during inflammation and in the context of age-related pathologies.

4.2. Method

Cell lines and reagents

Murine BV2 microglia cells, originally generated by Blasi et al. (Blasi et al., 1990), were gifted to our laboratory by G. Hasko at the University of Medicine and Dentistry of New Jersey (Newark, NJ). This cell line was used to generate CRISPR/Cas9 control and RGS10 knockout BV2 cells, and human RGS10 (hRGS10) overexpression BV2 cells, as described below. J.K Lee at the University of Georgia provided us with wild-type and RGS10 knockout breeder mice, which were used for primary microglia isolation, as previously described (Wendimu et al., 2021). Lipopolysaccharide (Sigma-Aldrich: L2880) was used for cell treatment.

Generation of CRISPR/Cas9 RGS10 knockout BV2 cells

Three mouse RGS10 sgRNA CRISPR/Cas9 All-in-One lentivector and scrambled control vector (K010) were purchased (Abm inc. #K4107305). Our detailed protocol for lentivirus packaging, expression, and cell selection is previously outlined (Alqinyah et al., 2018). Briefly,

recombinant lentiviral particles were produced in 293T cells by packaging sgRNA CRISPR/Cas9 vectors with a third-generation lentivirus packaging mix. Two days after transfection, viral media was harvested, and viral particles were isolated by ultracentrifugation. BV2 cells were transfected with different volumes of viral and successful transfectants were selected for stable expression using puromycin (6 ug/mL). Puromycin-resistant cells were expanded and clonal populations were further isolated using a single cell sorter flow cytometer. Changes in RGS10 gene expression in the clonal and heterogeneous population were validated by western blotting and quantitative real-time PCR (RT-PCR). Cells transfected with target 2 sgRNA exhibited high survival in selection medium, and this cell population was used for experiments. The sequences for the gRNA are shown below.

sg *Rgs10* target 1: 43 CGCAACCGCTTACCAGACGG (targeting end of exon 1)

sg *Rgs10* Target 2: 49 TGTTTTGCAGATATCCATGA (targeting beginning of exon 2)

sg *Rgs10* Target 3: 308 CTTCACAAGTCAACGTGGAG (targeting exon 4)

Generation of wild-type and mutant RGS10 overexpressing BV2 cells

The coding DNA sequence of wild-type and E52K mutant human RGS10-1 (hRGS10-1) (long variant: 181 aa) were synthesized and subcloned into Addgene's pLV-EF1a-Blast mammalian expression vector (Addgene: #85133) using custom service from Genescript. Lentivirus packaging and expression was performed same as before (Alqinyah et al., 2018), but using a second-generation lentivirus packaging mix. The isolated viral media was further concentrated using a speedy lentivirus purification kit following the manufacturer's protocol (Abm inc. #LV999). The produced lentivirus containing wild-type and mutant RGS10 and a control background vector was transduced into the CRISPR/Cas9 RGS10 knockout BV2 cells and control

CRISPR/Cas9 cells, and the original puromycin resistant cells were subsequently selected using blasticidin (20 ug/mL). Successful transformants were expanded and the expression level of endogenous RGS10 and overexpressed hRGS10-1 was confirmed by western blotting and RT-PCR.

Co-immunoprecipitation and Western blotting

The co-immunoprecipitation (co-IP) experiment in control, RGS10 knockout, and RGS10 overexpression BV2 cell lysates was performed by isolating cell lysates and following our previously described co-IP and western blot protocol (Alqinyah et al., 2018; Wendimu et al., 2021). Before immunoprecipitation, the lysates were incubated for 30 minutes in a shaking incubator at 4 °C in the presence of GDP (10 uM) alone or with GDP + AlCl3 (100 uM) + NaF (10 mM) to activate G proteins. After G protein activation, cell lysates were immunoprecipitated overnight using rabbit antibodies for Gαi3 (2 ug/mL) and normal IgG (2 ug). Gαi3 IP and RGS10 co-precipitation with Gαi3 was confirmed by western blot using anti-Gαi3 (Proteintech: #21192-1-AP) and goat anti-RGS10 (Santa Cruz Biotechnology: #sc-6206) primary antibodies, and donkey anti-goat IgG HRP (Santa Cruz Biotechnology: #sc-2020) and goat anti-rabbit IgG-HRP (MilliporeSigma: #12-348) secondary antibodies.

RNA extraction and library construction

For RNA sequencing experiments, four biological replicates of cells were harvested after a 24h treatment with LPS (10 ng/mL) or an equivalent volume of serum-free medium. Total RNA was isolated from four different passages of each generated cell line using TRIzol reagent according to a standard protocol (Invitrogen). Total RNA extracted with A260/280 and A260/230 ratio of ~ 2.0 and an RNA integrity number of > 9.5 were used for mRNA purification and library

construction, determined by the Nanodrop™ 8000 Spectrophotometer and the Agilent 2100 Bioanalyzer. Quality control, library construction, and reverse-stranded paired-end 50 (P50) sequencing were performed by the Georgia Genomics and Bioinformatics Core (GGBC) at the University of Georgia. The Kapa mRNA stranded protocol was used for library preparation and the run was sequenced on NextSeq 2000 with a P3 100 cycle kit following a standard Illumina protocol. Approximately 30 million reads were sequenced for each sample.

Quality control and pre-processing of sequencing data

FASTQ files containing raw sequenced reads were obtained from GGBC. A graphical workflow of our data analysis method and programs is shown (***Figure 4.1)***, and detailed data analysis codes can be provided upon request. Sequence quality control, preprocessing, and read counting were all performed using software packages in the Saplo2 interface of the Georgia Advanced Computing Resource Center (GACRC). Briefly, raw FASTQC files were subjected to quality control using the FASTQC v0.11.9 module (Andrew, 2010). All reads had a Phred score > 30, and adapter and overrepresented sequences were trimmed using Trimmomatic v0.39 (Bolger et al., 2014). Total ribosomal RNA contamination was checked by mapping reads to rRNA fasta files using BWA v0.7 (Li & Durbin, 2009), and total rRNA content was confirmed to be < 1.5%. The cleaned sequence reads were mapped to the mouse reference genome (GENCODE GRCm39 release M27 primary assembly sequence) and using the equivalent annotation file. Genome indexing and read mapping was performed using the splice-aware alignment program STAR v2.7.3a (Dobin et al., 2013). Quality control of the mapped BAM files was carried out using Qualimap v2.2.1 (Garcia-Alcalde et al., 2012), which showed high total mapped and uniquely mapped sequences, > 80 and 90%, respectively (**Figure S4.1A**). Most of the mapped reads fell

under the exonic region, and more than 95% of the spliced alignments occurred at known junctions (**Figure S4.1B & C**). Furthermore, the overall mapping rate and the downstream data analysis results were confirmed using an alternative alignment program HISAT2 v2.2.1 (Kim et al., 2019). The mapped data were visualized using Integrative Genomics Viewer v2.8.2 (IGV) (Robinson et al., 2011). For gene expression counts, the BAM alignment files were used as input for three different gene counting programs: STAR –quantMode Genecounts, featureCounts v2.0.1 (Liao et al., 2014), and HTSeq-count v0.91 (Anders et al., 2015). These different tools provided similar gene count data (**Figure S4.1D**), and the HTSeq-count data was used to perform downstream data analysis.

Explorative data analysis and differential gene expression analysis

The summarized expression data table generated from the HTSeq-count program (described above) and the associated metadata, which includes information on sample description and replicates, were used as input to perform explorative data analysis (EDA) and differential gene expression analysis (DGE) using Bioconductor packages in R and the integrated differential expression and pathway analysis (iDEP.93) web application (Ge et al., 2018). Briefly, genes with low expression count were removed and only those that expressed at least 1 count per million (CPM) in at least 4 samples were used for downstream analysis. The filtered read data were further normalized using the DESeq2 median ratios method, which estimates the size factor to account for library size differences between samples. The data used for EDA are transformed using a regularized log to minimize background noise from low-expression genes (**Figure S4.2A & B**), and pair-wise correlations of transformed data between replicates and sample group were validated using linear regression analysis (**Figure S4.2C**). Principal component analysis, hierarchical

clustering, and k-means clustering were performed to observe the overall patterns of gene expression among replicates and sample groups. Pairwise DGE analysis was performed using DESeq2 (Love et al., 2014), with a factorial design model that considers the effect of genotype, treatment, as well as batch-to-batch variability (Model: expression ~ Genotype + Treatment + Batch + Genotype:Treatment). DGE was alternatively assessed using EdgeR (Robinson et al., 2010). Vehicle-treated samples were used as a reference for treatment comparison, and CRISPR-control BV2 samples with normal expression of RGS10 are used as a reference to compare genotypes. Gene expression differences with log2 fold change ≥ 1 and FDR adjusted p-value (q-value) ≤ 0.05 were considered significantly upregulated, and genes with log2 fold change ≤ -1 and q-value ≤ 0.05 were considered significantly downregulated. Differentially expressed gene sets (DEGs) identified from pairwise genotype comparisons were further compared in the basal and LPS-activated samples to determine DEGs differentially regulated in specific treatment groups, with the help of Venny 2.1 (Oliveros, 2010).

Gene ontology and pathway enrichment analysis

Overrepresented gene ontology and pathways are analyzed using the various functional annotation databases within iDEP.93, including the GO Biological Processes, KEGG, and transcription factor (TF) target genes. DEGs are compared with background gene sets to determine enrichment using the hypergeometric test with q-value <0.05. Unbiased gene lists from different comparisons were further analyzed for gene set enrichment analysis and visualized using Enrichr (Chen et al., 2013). Specifically, biological processes, pathway analysis and transcriptional regulatory network analysis were performed using updated gene set libraries from well-known databases, including GO Biological Processes 2021 (Gene ontology consortium)), Molecular

Signature Database (MSigDB) hallmark gene sets 2020 (Liberzon et al., 2015), WikiPathway 2021 Human (Martens et al., 2021), and TRRUST Transcription Factors 2019 (Han et al., 2018). Enriched terms are presented either as a table format containing the top enriched terms along with the respective p-value and q-value and a list of differentially expressed genes that overlap with known gene set belonging to the specific terms. The enrichment results are alternatively presented as a bar graph to visually represent each significant term. Longer and lighter colored bars indicate higher significance.

Quantitative real-time polymerase chain reaction (qRT-PCR)

Total RNA was isolated from clonal and heterogeneous populations of CRISPR/Cas9 control and RGS10 knockout BV2 cells. RNA was extracted using TRIZol reagent as described above, and cDNA synthesis was performed using the High-Capacity Reverse Transcriptase cDNA kit (Applied Biosystems). A select few genes from the RNA-seq data were validated by qRT-PCR. Gene-specific forward and reverse primer sequences were designed using the NCBI primer design tool (**Table 4.1**). Custom primers were purchased from Sigma-Aldrich. qRT-PCR was performed using SYBR Green PCR Master Mix (Applied Biosystems) in both the original samples used for sequencing and freshly harvested cells from heterogeneous CRISPR-modified cells and homogeneous clonal populations. Gene expression was calculated as a fold change relative to vehicle-treated cells from CRISPR-control cells using the $2^{-\Delta\Delta Ct}$ method after normalizing to *β-actin* housekeeping gene. For the qualitative PCR experiment, gel electrophoresis was performed using amplified PCR products on a 3% agarose gel. Statistical analysis of the qRT-PCR data was performed using ANOVA followed by Tukey post hoc analysis. Data are presented as mean ±

SEM pooled from independent experiments. The p-value cutoff ranges are *p < 0.05, **p < 0.01, and ***p < 0.001.

4.3. Results

4.3.1. Exogeneous overexpression of wild-type and GAP-dead mutant RGS10 suppresses LPS-induced upregulation of COX-2 and IL-6 in BV2 microglia

We have previously shown that transient overexpression of human RGS10-2 (hRGS10-2) (short-variant) in HEK293T cells suppresses LPS-induced TNFα expression (Alqinyah et al., 2018). While the overexpression study uncovered a potential G protein-independent role of RGS10, it was carried out in non-immune cells. To validate findings in a suitable cell model, we developed stable BV2 microglia cell lines that overexpress wild-type hRGS10-1 long variant (KO-WT) and the GAP-dead variant E52K (KO-EK) in RGS10 null background cells (KO), which were previously generated using the CRISPR/Cas9 gene editing tool (Alqinyah et al., 2018). As a control, we expressed a background vector in both CRISPR/Cas9 control cells (Con-Con) and RGS10 KO cells (KO-Con) (**Figure 4.2A**). The expression levels of endogenous RGS10 in Con-Con cells and overexpressed RGS10 in KO-WT and KO-EK cells were confirmed (**Figure 4.2B & D**). Although WT and EK RGS10 showed strong expression in KO cells, the relative expression between endogenous and overexpressed RGS10 forms was not directly comparable due to species-specific differences in antibody specificity. The biochemical difference between the overexpressed RGS10 variants was examined using co-IP by comparing the interaction with Gαi (**Figure 4.2C**). Upon activation of G proteins, the transient interaction of RGS proteins with Gα is known to be stabilized, which can be mimicked in vitro using GDP with aluminum fluoride (AMF) (Berman et al., 1996; Tesmer et al., 1997). Specific interactions of Gαi3 with endogenous RGS10 in Con-Con

cells, as well as the reexpressed WT RGS10 in KO-WT cells, were detected in the presence of AMF, with no interaction observed in either KO-EK cells or in inactivated conditions containing GDP without AMF (**Figure 4.2C**). We confirmed that upregulation of COX-2 and IL-6 expression in activated KO-Con cells could be suppressed by reexpressing either WT or EK RGS10, although this effect was not fully restored to control levels (**Figure 4.2D-F).** These results further validate the G protein-independent effect of RGS10 in the regulation of LPS-induced inflammatory genes in microglia.

4.3.2. Explorative data analysis and clustering of samples

To determine changes in global gene expression regulated by RGS10, we performed RNA-sequencing (RNA-seq) analysis in control and KO cells, and in KO cells reexpressing WT and EK RGS10. A crucial first step in RNA-seq analysis is exploratory data analysis to examine the overall similarity between replicates and sample groups (Love et al., 2015). Visualization of sample-to-sample distance correlation using principal component analysis (PCA) revealed separation of samples into four major clusters, showing variation in overall gene expression patterns between treatment groups and between genotypes (**Figure 4.3A**). Principal component 1 (PC1) separated the samples by treatment, which explains ~65 of the overall variation, while PC2 separated the groups by genotype, accounting for ~21% of the overall variation. To our surprise, both the WT and EK hRGS10-1 overexpression samples did not exhibit overall variability compared to the KO samples (**Figure S4.3A**). Hierarchical clustering of the top 1000 most variable genes also showed a clear separation of the control and KO samples, with no obvious variation between the KO and overexpression samples (**Figure S4.3B & C**). These results suggest that the global gene expression changes induced by CRISPR/Cas9-mediated loss of endogenous RGS10 could not be rescued by

reexpression of hRGS10-1, thus prompting us to remove the overexpression samples from our downstream analysis.

Using the unsupervised k-means clustering method, we examined the gene expression patterns of the remaining four groups of samples, Con-Con and KO-Con cells treated with vehicle or LPS, in which the top 1000 most variable genes were divided into four cluster groups with distinct expression patterns (**Figure 4.3B**). For each cluster, we further carried out enrichment analysis to gain insight into the different types of genes and pathways regulated by RGS10 or by LPS treatment. The genes in cluster A were upregulated in the KO samples and this up-regulation pattern was more prominent in LPS-activated cells. The genes within this cluster were implicated in biological responses to external stimuli, cytokine production, and defense response to virus and bacterium. The biological processes upregulated in the KO samples were also enriched in cluster B, which contains genes strongly induced by LPS. Cluster C consisted of genes strongly downregulated by LPS and were related to biological processes important for housekeeping functions, such as migration, differentiation, and development. The last cluster included genes downregulated by RGS10 in both resting and activated cells, and these genes were enriched in biological processes related to synapse pruning, nucleosome assembly, and cell organization and differentiation.

To get insight into the transcriptional regulatory mechanism for the identified gene clusters, we further performed a transcription factor (TF)-target enrichment analysis (**Table 4.2**). Cluster A genes, which are upregulated in KO samples in both basal and activated cells, mostly consisted of target genes for various members of the interferon regulatory factor family (IRF1,2,7, and 9) and STAT1, and these transcription factors are important for innate immune response functions. The

gene sets upregulated by LPS were mostly inflammatory genes and thus were targets for various inflammatory transcription factors including different NF-κB subunits (NFκB1 (p50), NFκB2 (p52), Rela (P65), and Rel (c-Rel)) (**Table 4.2**). Since the clustering algorithm assigns an individual gene to a single cluster, genes known to be regulated by RGS10 such as *Tnf*, *Il6*, and *Ptgs2* were assigned to the LPS-responsive cluster (B) due to their strong induction by LPS. In general, our cluster analysis suggests that RGS10 regulates innate immune responses in basal and LPS activated microglia, most of which were IRF-target genes.

4.3.3. Differential expression of genes in CRISPR/Cas9 RGS10 knockout cells (Figure 4)

Next, we performed differential gene expression (DGE) analysis in both basal and LPS-activated cells and identified a list of genes differentially regulated in resting or LPS-activated KO samples compared to control samples (**Figures 4.4A & B**), as well as genes differentially regulated by LPS in control cells (**Figure 4.4C**). We filtered the list of differentially expressed genes (DEGs) and only considered genes with LogFC of |1| and pAdj < 0.05, as significant. The number of DEGs and the overall DGE pattern are displayed using volcano plots (**Figure 4.4A-C**). Our RNA-seq analysis revealed DEGs in both basal and LPS-activated samples: 540 genes for vehicle and 759 genes for LPS groups were differentially regulated in KO samples. Among them, 237 and 348 genes were downregulated, while 303 and 411 genes were upregulated, in vehicle and activated samples, respectively (**Figures 4.4A & B)**. LPS induced downregulation of 367 genes and upregulation of 762 genes in Con cells (**Figure 4.4C**). From the list of genes regulated by RGS10, we further subcategorized genes whose expression was differentially regulated depending on the treatment group. Of the total number of DEGs upregulated in the KO samples, ~38% were common in both the vehicle and LPS treatment group, while ~41% were exclusively upregulated

in response to LPS (**Figure 4.4D**), and similar results were observed for downregulated gene sets (**Figure 4.4E**). A complete list of all DEGs and their respective LogFC and pAdj values are presented in the Appendix section (**Tables A.2 & A.3**).

4.3.4. Differential gene ontology and pathway enrichment analysis in CRISPR/Cas9 RGS10 knockout cells

To assign biological relevance, the list of DEGs in KO samples was further analyzed for gene set enrichment analysis (GSEA) of gene ontology biological process (GOBP) and pathways. The enriched terms are arranged in a tree format into different groups based on gene overlap (**Figures 4.5 & 4.6**). GSEA showed regulation of various biological processes; most of the upregulated GOBP terms in both vehicle and LPS-activated samples were involved in functions related to immune response to stress, defense response to virus, and various external and biotic stimuli (**Figures 4.5A & B**). These biological processes showed a stronger enrichment in LPS-activated samples indicated by lower p-values. Furthermore, the downregulated biological processes were largely involved in actin filament organization and cell migration (**Figures 4.5A & B**). The GOBP findings for the DEGs were consistent with those identified by the k-means clustering algorithm (**Figure 4.3B**).

We then analyzed the DEGs for enrichment of KEGG and TF-target pathways. In vehicle treated samples, only the upregulated gene sets showed significant enrichment and were largely involved in viral pathways and innate immune responses (**Figure 4.6A**), and these DEGs showed strong enrichment for being targets of IRF7 and IRF9 (**Figure 4.6B**). In LPS activated KO samples, a greater number of enriched pathways were identified, with a stronger upregulation of virus infection pathways and inflammatory signaling pathways such as the TNFα and NOD-like

receptor pathway while the downregulated genes showed slight enrichment in metabolic pathways (**Figure 4.6C**). As expected, DEGs in LPS-activated KO samples were enriched in IRF target genes and other inflammatory transcription factors, including NFκB1, STAT1, MAPK10 (**Figure 4.6D**). We further analyzed the DEGs using the widely used and comprehensive molecular signature database (MSigDB) hallmark gene set collection, which has summarized gene set pathways with less redundancy. In both basal and activated cells, the most enriched pathways in KO DEGs were interferon gamma and interferon alpha response, TNFα signaling via NF-κB, inflammatory response, and IL-2/STAT5 signaling (**Figures 4.7A & B**). These pathways showed stronger enrichment in LPS-activated cells. The summarized MSigDB further identified apoptosis, p53 pathway, and hypoxia pathways as being significantly enriched in the LPS-treated groups (**Figure 4.7B**). In general, our GO and pathway enrichment analyses suggest that RGS10 regulates various innate immune responses and inflammatory response pathways, and this response is more prominent in activated microglia.

4.3.5. Enriched pathways in CRISPR/Cas9 RGS10 knockout cells in response to LPS

To exclusively examine the differential expression of genes in the RGS10 knockout sample in response to LPS, we performed pathway analysis in gene sets that were only upregulated in LPS-treated KO samples using additional pathway data sets. The 214 DEGs exclusively upregulated in activated samples (depicted in Figure 4.4D), showed enrichment in previously identified pathways, as well as other disease-specific responses such as spinal cord injury and lung fibrosis pathways, and responses to cellular stress such as the unfolded protein response (UPR) pathway, according to the WikiPathway 2021 database (**Table 4.3**). Target genes for ATF4, a transcription factor linked to the unfolded protein response pathway (Fusakio et al., 2016), were

also identified as significantly enriched. Furthermore, pathway analysis using the Jensen compartment database (Binder et al., 2014), identified enrichment in various inflammatory complexes, as well as the CHOP-ATF3 complex, the Ire1 complex, and the BAX complex, which are involved in unfolded protein responses and apoptosis. A complete list of these pathways ranked by their adjusted p-value and the respective DEGs belonging to each pathway is presented in **Table 4.3.** These results suggest a potential novel role for RGS10 in the regulation of ER stress and unfolded proteins response pathways in activated microglia.

4.3.6. Differential regulation of LPS signaling in CRISPR/Cas9 RGS10 knockout cells

The previously characterized function RGS10 in microglia and macrophages was mainly attributed to the regulation of TLR4 signaling by examining pro-inflammatory gene expression in response to LPS (Alqinyah et al., 2018; Lee et al., 2008; Lee et al., 2011; Lee et al., 2013; Wendimu et al., 2021). Therefore, we specifically examined the effect of RGS10 on TLR4-signaling by identifying DEGs in LPS-activated control cells and comparing these gene sets with those regulated by RGS10. Of the 762 total upregulated DEGs induced by LPS treatment (depicted in Figure 4.4C), 140 genes (12.6%) were also differentially upregulated in RGS10 KO cells (**Figure 4.8A**). As expected, these hared genes were largely enriched in biological processes related to cytokine signaling and defense response to virus (**Figure 4.8B & Table 4.4**). Analysis of the MSigDB hallmark gene set also showed upregulated pathways such as interferon gamma and alpha signaling pathways, TNFα signaling via NF-κB, inflammatory responses, and apoptosis pathways (**Table 4.4**). TF-target analysis using TRRUST database further showed enrichment of target genes for various inflammatory transcription factor factors, including Rela, NFκB1, CEBPB, Jun, IKBKB, IRF1, and STAT1. The enriched pathways and the DEGs belonging to each enriched term

are presented in **Table 4.4.** Overall, these results suggest that RGS10 negatively regulates LPS-induced upregulation of inflammatory and viral response processes.

We also compared LPS-downregulated DEGs with those downregulated in RGS10 KO samples and identified 37 shared genes (4.8% of the total LPS-downregulated DEGs) (data not shown). These genes were enriched in biological processes related to cell junction disassembly, synapse pruning, classical complement activation, humoral immune response, microglia cell activation, and fiber organization (**Table 4.5**) and enrichment of these pathways was largely driven by a small set of genes such as complement genes (*C1qa, C1qb, C1qc, and Cfh),* and *Apoe*. These data suggested a potential novel role for RGS10 in enhancing complement elements, which mediate humoral immune response and phagocytosis response in microglia.

4.3.7. Validation of expression levels of candidate genes by RT-PCR

To experimentally verify the RNA-seq data, we selected a list of 7 upregulated and 6 downregulated genes in KO samples, which have variable gene expression patterns based on LPS treatment. Some of these genes were selected for being the most differentially regulated based on Log2FC or adjusted p-value (adjP) value ranking (*Apoe, Tmem132a, Slc2a5, Slc47a1, Ppic, Nsmaf, Unc5b*). Other genes were selected for their involvement in the novel RGS10-regulated pathways identified using our enrichment analysis, such as those involved in UPR and ER stress responses, apoptosis, and complement signaling (*Ppp1r15a, Ddit3, Sqstm1, Unc5b, C1qb*). The RT-PCR validation experiment was performed in RNA samples collected for RNA-seq, as well as in freshly treated control and CRISPR/Cas9 RGS10 knockout cells that did not have a background blasticidin vector (which were used in our RNA-seq experiments to control for the RGS10 overexpression samples). Furthermore, these data were confirmed in clonal CRISPR/Cas9 RGS10

knockout cells. The expression patterns of the selected upregulated and downregulated genes in the RT-PCR data (**Figure 4.9: bottom**), showed strong correlation with the normalized expression counts from the RNA-seq analysis (**Figure 4.9**: top). However, validation of the RNA-seq data for a few genes (*Apoe, C1qb, Marco, Ppic, Ppp1r15a, Tmem132a*) in primary microglia did not show RGS10-mediated regulation (data not shown).

4.3.8. Unexpected expression of *Rgs10* transcript in CRISPR/Cas9 RGS10 knockout BV2 cells

Although *Rgs10* was one of the downregulated DEGs in our RNA-seq data, it was not among the top downregulated genes in the KO samples based on both LogFC and adjP ranking (**Table A.2**). Additionally, our initial exploratory data analysis did not reveal global differences in the gene expression pattern between the RGS10 KO and overexpression samples, implying a potential problem in our RGS10 KO BV2 cells. A close look at the mapped sequenced reads between the control and RGS10 KO samples revealed the expressed reads mapped to *Rgs10* gene in both the control and KO samples, although the KO samples lack reads falling on exon 2 (**Figure 4.10A**). We also performed an exon-level counting analysis and confirmed that only exon 2 lacks expressed reads, while the other exons have partial expressions (**Figure 4.10B**). This data was validated using two different read mapping methods (STAR and HISAT2) and three gene counting programs (HTSeq2-count, STAR gene count, and featureCounts), which identified similar numbers of gene counts, confirming that our unexpected result was not caused by problems in the data analysis.

The initial characterization of CRISPR/Cas9 RGS10 knockout cells was performed by RT-PCR using primer sets that amplify exon 2-3 region, as well as by using two different antibodies

to detect RGS10 protein (RGS10 c-20 antibody from Santa Cruz & RGS10 antibody created in collaboration with the Bioexpression and Fermentation Facility at UGA). To further verify the identified *Rgs10* transcripts in KO cells, we designed different primer sets that amplify regions downstream of exon 2 (**Figure 4.10C**). Relative comparison of RGS10 expression across the different exons showed findings similar to the RNA-seq data, suggesting that all exons with the exception of exon 2 have partial expression of the RGS10 transcript compared to control cells that express *Rgs10* in all exons (**Figure 4.10D**).

4.3.9. Comparison of *Rgs10* expression in CRISPR/Cas9-modified BV2 cells and primary microglia

The CRISPR/Cas9 gene editing technology generally introduces frameshift insertion and deletions (indels), which leads to premature termination codon, thereby eliciting nonsense-mediated decay (Asmamaw & Zawdie, 2021; Popp & Maquat, 2016). However, recent studies revealed unexpected outcomes of CRISPR/Cas9 in inducing large genomic deletions, exon skipping, and alternatively splicing (Mou et al., 2017; Sharpe & Cooper, 2017; Tuladhar et al., 2019). Compared to control cells, a close visualization of the exon-exon junctions in our RGS10 knockout cells revealed junctional reads bypassing the sgRNA-targeted exon 2 region (**Figure 4.11A**). Although our RT-PCR analysis in downstream exons showed *Rgs10* in KO samples, it does not show if there is a continuous *Rgs10* transcript bypassing exon 2. Therefore, we designed a forward primer annealing to exon 1 region and a reverse primer annealing to exon 4 region to check if exon 2 is skipped (**Figure 4.11B**). We amplified cDNA from the heterogeneous control and KO cell population (KO-Het), as well as two clonal populations of KO cells (KO-Clone 1 and KO-Clone 2). We also included wild-type and RGS10 knockout primary cells ($RGS10^{-/-}$) as

positive and negative control, respectively. While both the wild-type primary cells and the CRISPR/Cas9 control cells showed the expected amplicon size of ~381bp, all the different populations of the CRISPR/Cas9 KO cells showed a single lower size band, matching the expected amplicon size without the exon 2, in contrast to the RGS10 knockout primary cells which did not have an amplified product (**Figure 4.11C**). These results suggest that CRISPR/Cas9-mediated targeting of *Rgs10* induced exon 2 skipping and produced a shorter *Rgs10* transcript.

4.4. Discussion

In this study, we performed a global transcriptome analysis to identify RGS10-mediated regulation of gene expression in BV2 microglia. Our main findings are: (1) CRISPR/Cas9-mediated deletion of RGS10 in BV2 microglia induced global gene alterations that resulted in significant upregulation of genes involved in various stress responses and innate immune and inflammatory responses, including upregulation of viral defense pathways, type I and II IFN response pathway, and TNFα signaling through NF-κB; (2) These responses are more differentially upregulated in cells activated by LPS, in addition to exclusive enrichment of unfolded protein response and apoptosis pathways in activated microglia; (3) A large subset of the upregulated genes in RGS10 knockout cells are targets of interferon regulatory factors (IRFs) and the NF-κB family of transcription factors; 4) The global gene expression changes induced by loss of endogenous RGS10 could not be rescued by overexpressing a dominant isoform of human RGS10; and 5) CRISPR/Cas9-mediated editing of RGS10 induced exon 2 skipping and resulted in residual expression of truncated *Rgs10* transcripts. While the RNA-seq data and enrichment analysis are generally consistent with previously implicated roles of RGS10 in the regulation of immune and inflammatory responses, we propose that these findings be cross-validated by

performing RNA-seq experiments in primary microglia in order to delineate the specific effect of loss of RGS10 on global gene expressions.

CRISPR/Cas9 genome editing has emerged as a powerful tool for studying gene functions and employs an RNA-guided Cas9 endonuclease to induce double-strand break (DSB) at complementary DNA targets (Asmamaw & Zawdie, 2021). DSB induced by Cas9 is subsequently repaired by non-homologous end joining (NHEJ), which is an error-prone repair mechanism that introduces insertions or deletions (indels), resulting in frameshift mutations that inactivate the target gene (Popp & Maquat, 2016). A considerable problem with CRISPR technology is the possibility of off-target editing in genomic positions that similarly but imperfectly match the sgRNA sequence (Popp & Maquat, 2016; Shao et al., 2016). The sgRNA used in this study is validated to be specific for *Rgs10* and contains a minimum of 3 mismatches with other genomic regions (https://rth.dk/). The RNA-seq expression count for potentially identified off-target sites did not differ between the control and RGS10 knockout samples (data not shown), suggesting that the CRISPR/Cas9 tool specifically targeted *Rgs10*.

Although gene inactivation is the most common consequence of CRISPR technology, recent evidence has provided important insight into the potential unintended consequences of CRISPR at the post-transcriptional level (Mou et al., 2017; Sharpe & Cooper, 2017; Tuladhar et al., 2019). Specifically, there have been reports of alternative splicing and large or small genomic deletions that remove the target exon without generating frameshift mutations (Mou et al., 2017; Tuladhar et al., 2019). PCR assays typically used to genotype CRISPR clones commonly detect short-range amplification, which can miss large genomic deletions (Mou et al., 2017). In our study, the original RT-PCR primers used to detect *Rgs10* contain a forward priming site in the target exon

2 region and therefore failed to detect *Rgs10* transcripts in the knockout samples. However, both our RNA-seq results and RT-PCR validation experiments using various primer sets detected a substantial level of *Rgs10* cDNA in all exons except exon 2, which is the region targeted by the sgRNA.

Although large genomic deletions commonly disrupt gene function, aberrant placement and splicing of exons can induce exon skipping, resulting in neomorphic alleles (Mou et al., 2017). A closer visualization of our RNA-seq data showed that the KO samples have exons 1-3 junctional reads, in contrast to the control cells, which expressed junctional reads that span all exons, implying that exon 2 is skipped in the KO samples. Furthermore, experimental validation using exon 1-4 spanning primers revealed an exon 2 skipped band in the RGS10 KO samples, in contrast to RGS10 knockout primary cells that showed no amplification, and the CRISPR control and wild-type primary cells that have amplicon size matching the intact *Rgs10* cDNA. These results suggest that our presumed CRISPR/Cas9 RGS10 knockout cells express a truncated form of *Rgs10* transcript lacking exon 2.

Although we have not sequenced the exon 1-4 amplified products from the KO samples, it is possible that it may contain a start codon with an open reading frame that translates into a truncated RGS10 protein lacking the epitope detected by the RGS10 antibody. In fact, a recent CRISPR/Cas9 study targeting *Kras* demonstrated a similar pattern of exon skipping with an internal translation initiating site located downstream of the target exon, producing a truncated Kras protein (Mou et al., 2017). Therefore, future sequencing analysis should characterize the CRISPR/Cas9 RGS10 knockout cells to identify potential in-frame mutations or premature termination codon with protein-coding potential. This may result in the production of truncated

RGS10 with a partial functional protein or aberrant gain of function. For example, exon skipping induced by CRISPR-mediated targeting of *Cttnb1* has resulted in a production of a stabilized and constitutively active nuclear β-catenin (Mou et al., 2017; Tuladhar et al., 2019), indicating that exon skipping can produce functional or dysfunctional proteins with distinct phenotypes compared to wild-type protein.

The longest and most dominant *Rgs10* transcript encodes a protein containing 181 amino acids, of which 40 aa are encoded by exon 2 that contains a portion of the RGS domain, as well as several post-translationally modified residues, including three serine phosphorylation sites (Almutairi et al., 2020). Apart from the classic Gαi-RGS10 interaction, which is mediated by the RGS domain, our recent co-IP study identified many other RGS10 interaction partners in BV2 microglia (Wendimu et al., 2021). The specific region of RGS10 that interacts with these proteins has not yet been characterized. However, it is possible that exon 2 of *Rgs10*, which encodes roughly a quarter of the protein, is crucial for mediating the biochemical interactions and various functions of RGS10. In addition, since large deletions of gene regions have a significant effect on the overall structure, regulation, and function of proteins, a truncated form of RGS10 may have a substantial consequence. Furthermore, since the RGS10 c-20 antibody, which recognizes the last 20 amino acids of RGS10, did not detect RGS10 protein in the KO cells, the genomic edition may have resulted in aberrant form of RGS10 protein. Therefore, the transcriptome alterations identified in our study could be the result of a loss of wild-type RGS10 or an aberrant effect generated by gain of function. This may explain why cells with exogenous expression of hRGS10-1 on KO background did not exhibit a significantly different transcriptome profile compared to the RGS10 KO cells.

It is also possible that the absence of transcriptional changes in KO and overexpression samples is due to the species-specific functional difference in RGS10 or overexpression of a single variant of RGS10, which may not substantially compensate for endogenous loss of RGS10. Although the long variant of RGS10 (RGS10-1) is highly conserved between mouse and human, the latest annotation of the ensemble genome released in December 2021 identified three protein-coding hRGS10 transcripts (encoding 181a.a, 167a.a, and 173a.a proteins) (https://useast.ensembl.org/Homo_sapiens/Gene/Summary?g=ENSG00000148908;r=10:119499817-119542719), while the mouse annotation shows the presence of three protein-coding variants (181 a.a, 93 a.a and 85 a.a) (https://useast.ensembl.org/Mus_musculus/Gene/Summary?db=core;g=ENSMUSG00000030844;r=7:127975345-128020482). All three mouse RGS10 variants contain the translated exon 2 region that is targeted by the sgRNA. Therefore, expression of a single hRGS10 variant may not be sufficient to restore functional alterations caused by the loss of endogenous mouse RGS10.

We recently showed that RGS10 deletion enhances expression of LPS-induced COX-2 and IL-6 transcripts in both CRISPR-modified BV2 cells and primary microglia (Wendimu et al., 2021). However, in this study, hRGS10-1 reexpression did not fully rescue COX-2 and IL-6 upregulation caused by loss of RGS10 (**Figure 4.2**), implying that the expression of a human variant of RGS10 or a single isoform may not have a significant phenotype. The stringent parameters used in our RNA-seq data analysis to filter out false positive DEGs may exclude genes that are modestly regulated by hRGS10 overexpression. While previously known RGS10-regulated inflammatory genes exhibited decreased expression counts (RNA-seq analysis) in the overexpression samples compared to RGS10 knockout samples (data not shown), they were not

considered statistically significant for differential gene expression analysis. Taken together, these results suggest that the lack of variation in our gene expression pattern between CRISPR/Cas9 RGS10 knockout cells and overexpression cells could be explained by a partial restoration of RGS10 function because of the expression of a single hRGS10 variant, or due to the inability of exogenously expressed RGS10 to rescue a potential gain-of-function phenotype induced by exon 2 skipping.

Although our study uncovers a potential caveat of using CRISPR/Cas9-modified RGS10 knockout cells, a considerable number of genes identified in our differential gene expression analysis have previously been shown to be regulated by RGS10, including *Ptgs2*, *Tnf*, *Il6*, *Cxcl10*, and others (Almutairi et al., 2021; Alqinyah et al., 2018; Chan et al., 2022; Lee et al., 2008; Wendimu et al., 2021). Substantial evidence from previous studies indicates that RGS10 regulates cytokine and chemokine signaling in immune cells (Almutairi et al., 2021; Lee et al., 2008; Garcia-Bernal et al., 2011). This finding is consistent with our gene set enrichment analysis (GSEA), which identified cytokine production and immune-related cell responses as one of the most enriched biological processes in LPS-activated RGS10 knockout BV2 cells. Lee et al. (2011) previously demonstrated that RGS10 inhibits NF-κB activation in both LPS and TNFα-stimulated microglia (Lee et al., 2011). Our GSEA analysis using the molecular signature hallmark database (MSigDB) also identified TNFα signaling via NF-κB as one of the most enriched biological pathways in our RGS10 knockout samples, and this enrichment was more prominent in LPS-activated cells. Using a luciferase-based NF-κB reporter, it was demonstrated that RGS10 knockout primary microglia have enhanced NF-κB-dependent transcriptional activity and elevated levels of p50 and p65 compared to wild-type microglia (Lee et al., 2011). RGS10-loss mediated

enhanced activation of p65 has also been recently reported in other immune cells (Almutairi et al., 2021; Ren et al., 2022). A large subset of DEGs identified in the LPS-activated RGS10 KO cells were shown to be target genes for various inflammatory transcription factors, including NF-κB subunits, such as p50 (NFκB1) and p65 (RelA). Furthermore, the NF-κB complex was found to be the most enriched subcellular compartment. In addition, consistent with previous findings (Lee et al., 2008), RGS10 regulated the expression of cytokines in both basal and activated microglia.

Defense response to virus and viral-related pathways, such as those involved in influenza, were also among the most enriched biological processes and pathways identified in both basal and LPS-treated RGS10 knockout cells. Specifically, we have identified a significant enrichment of genes involved in type 1 and type II interferon signaling, which are crucial pathways that mediate immune response to virus infection. Furthermore, GSEA using the Wikipathway database identified lung fibrosis as a highly enriched pathway in activated RGS10 knockout cells, implying a role for RGS10 in viral infection and lung injury model. These results are in line with a recent study by Almutairi et al. (2021) that implicated RGS10 in viral response functions, demonstrating that loss of RGS10 enhances immune and inflammatory responses and exacerbates lung damage in severe influenza-infected lungs (Almutairi et al., 2021). Therefore, despite the unexpected result of CRIPSR/Cas9 *Rgs10* editing, our RNA-seq data is generally consistent with previously reported functions of RGS10.

In conclusion, the DEGs that did not change in primary microglia were selected for validation as they were the most regulated according to statistical parameters (fold change or p-value) (*Apoe, Ppic, and Tmem13a*) or were DEGs identified from specific novel pathways where RGS10 function has not previously been implicated (Unfolded protein response pathway

(*Ppp1r15a*) and Synapse pruning and complement signaling (*C1qb*) (data not shown). Therefore, it is important to define which DEGs and enriched biological processes/pathways identified in this study are caused by the loss of wild-type RGS10 and which are the result of a potential gain of function or off-target effects of RGS10 editing by CRISPR/Cas9. Therefore, RNA-seq study in primary microglia should be conducted to better characterize RGS10-mediated transcriptional alterations in microglia, which can also be used to compare the overall difference of primary and CRISPR/Cas9 modified microglia cells. Despite its off-target exon skipping effect, recent reports suggest that CRISPR/Cas9-mediated exon skipping could be used therapeutically to inactivate a specific region of genes (Smith et al., 2018). Therefore, if a subsequent characterization and sequencing of CRISPR/Cas9 RGS10 knockout cells identifies a truncated protein-coding transcript, these cells may be exploited for structure-function studies to infer region-specific function of RGS10. More importantly, our findings, together with recent studies implicating unexpected consequences of CRISPR (Mou et al., 2017; Sharpe & Cooper, 2017; Tuladhar et al., 2019), highlight the need to improve quality control procedures for selecting correct CRISPR/Cas9 mutant alleles. For example, studies should use multiple sgRNAs targeting different exons, and an efficient clone screening method should be adapted that not only examines genomic DNA and wild-type protein levels but also employs RT-PCR screens incorporating multiple upstream and downstream primers to detect potentially modified transcripts.

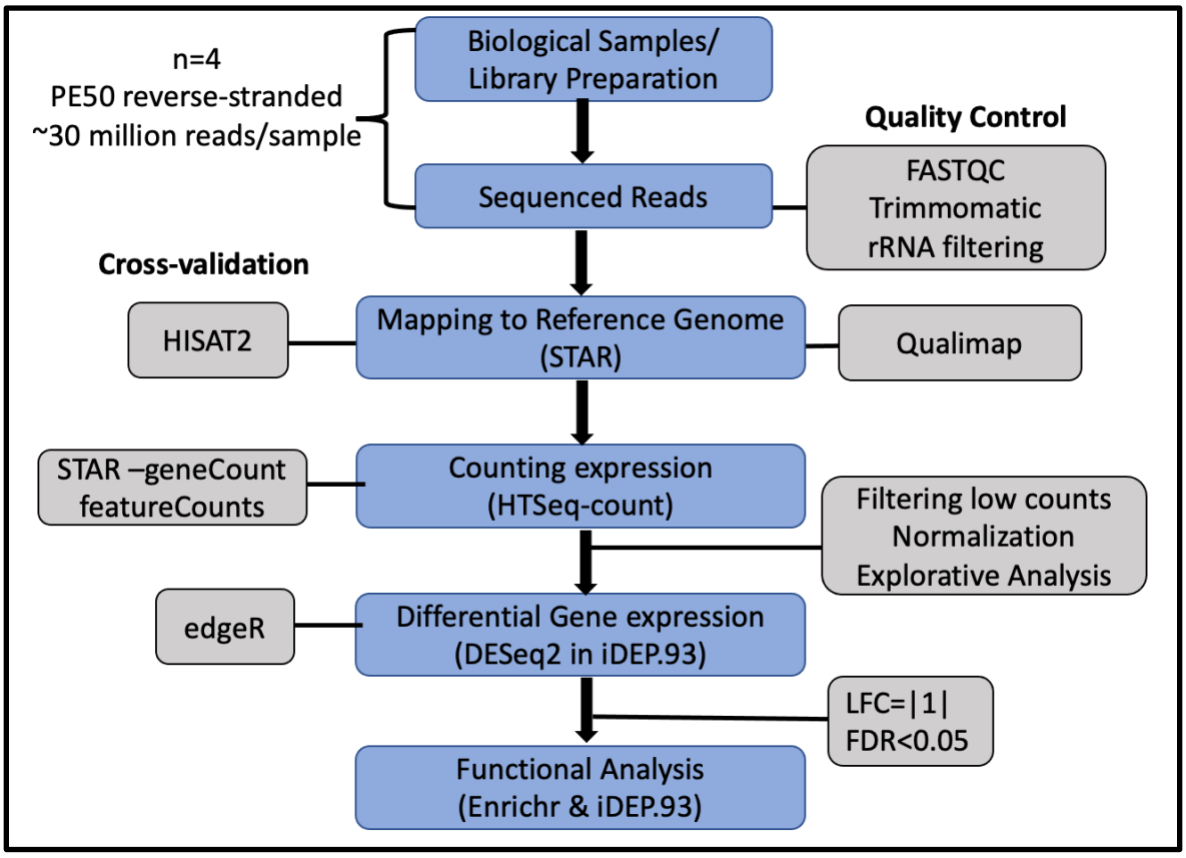

Figure 4.1. RNA-sequencing data analysis workflow

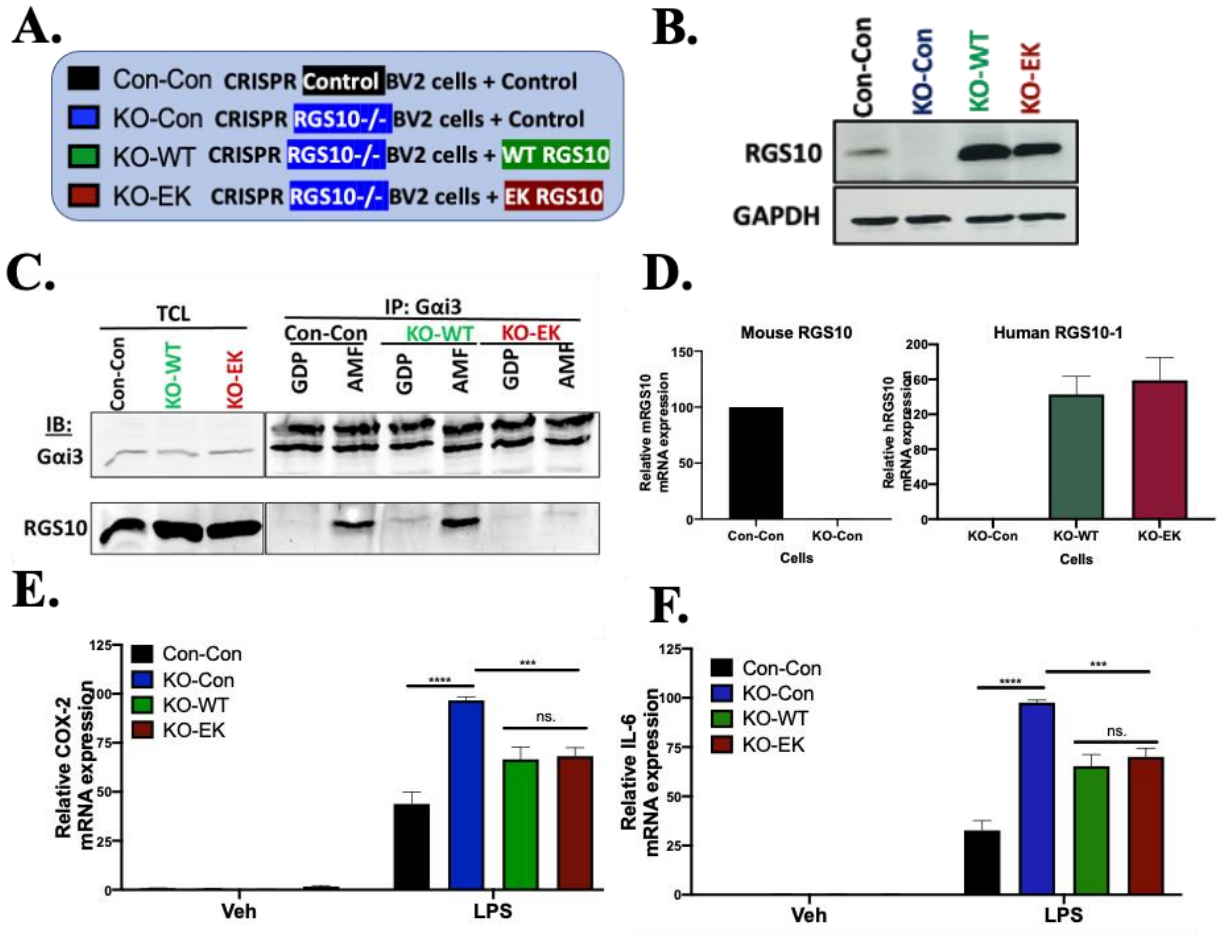

Figure 4.2. **Exogeneous overexpression of wild-type and GAP-dead mutant RGS10 suppresses LPS-induced upregulation of COX-2 and IL-6 in BV2 microglia. A)** Schematic summary of four generated stable BV2 cell lines, in which puromycin-resistant CRISPR/Cas9 RGS10 knockout BV2 cells (KO) are modified by re-expressing either a blasticidin-resistant wild-type human RGS10-1 (KO-WT) or a GAP-dead E52K variant (KO-EK). A background control vector was also transfected in CRISPR/Cas9 control BV2 cells (Con-Con) and KO BV2 cells (KO-Con). **B)** Western blot analysis of endogenous and re-expressed RGS10 and a housekeeping protein GAPDH. **C)** A representative immunoblot of Gai3 and RGS10 in cell lysates immunoprecipitated with Gai3 antibody in basal condition (GDP only) and after G protein activation (GDP with AlF_4^- (AMF)). **D**) qRT-PCR analysis showing mRNA expression of endogenous mouse RGS10 (left) and re-expressed human RGS10-1 (right) normalized relative to Con-Con and KO-Con cells, respectively. **E-F)** qRT-PCR analysis showing mRNA expression of COX-2 (E) and IL-6 (F) in cells treated with vehicle (Veh) or LPS (10 ng/mL) for 24 hours. (B and C) Images are representative of two independent experiments. (D-F) Data are analyzed from 8 independent experiments, with technical duplicates, and statistical differences are analyzed by ANOVA and Tukey's's post hoc test. Data are presented as mean ± SEM., *** $P < 0.001$. ns., not significant.

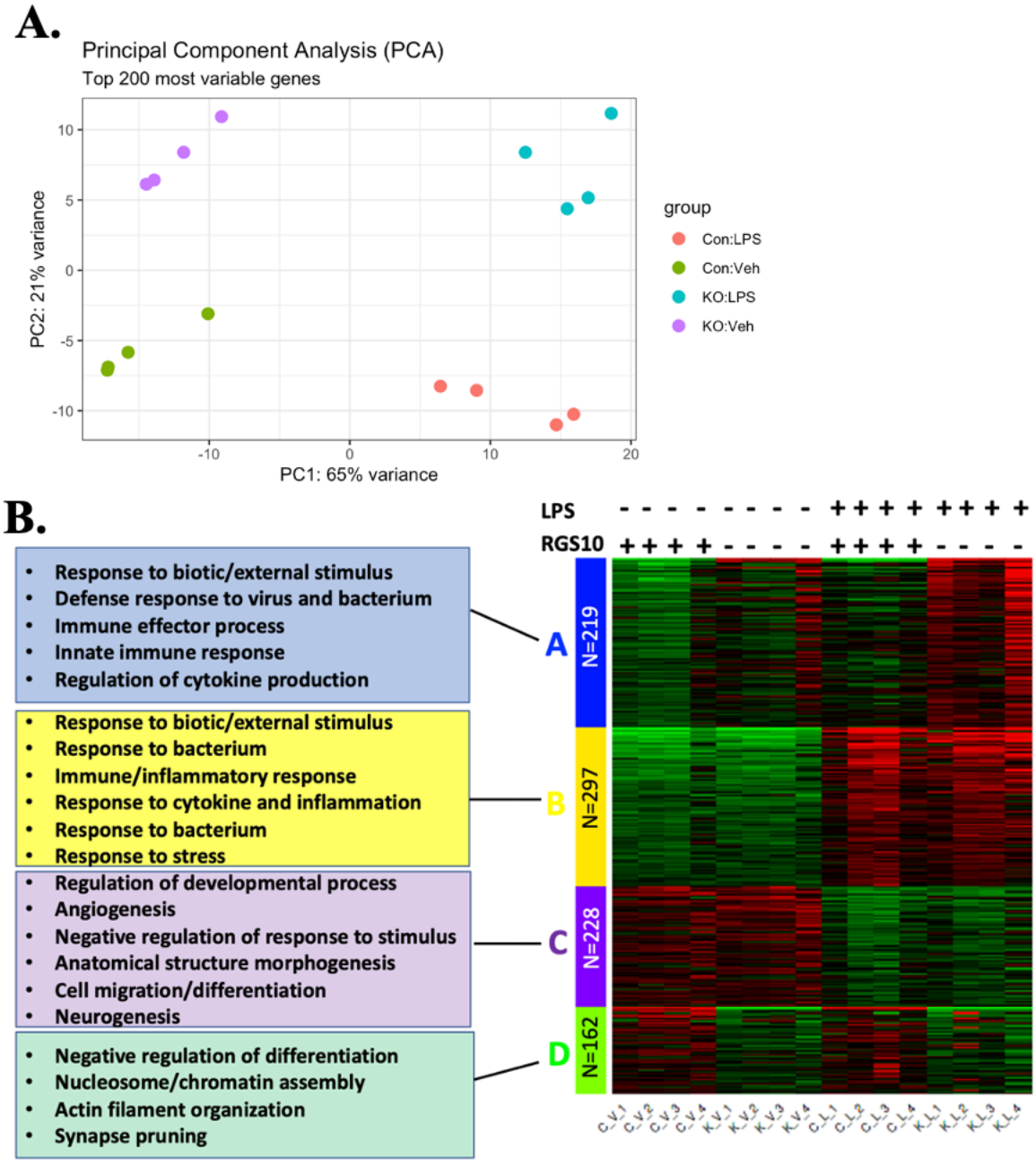

Figure 4.3: Explorative data analysis of CRISPR/Cas9 control and RGS10 knockout BV2 cells. A) A two-dimension principal component analysis plot of the top 200 most variable genes in CRISPR/Cas9 control (Con) and RGS10 knockout (KO) cells treated with either vehicle or LPS (10 ng/mL) for 24h PC1 and PC2 separated the sample groups into clusters based on treatment type and genotype, respectively. **B)** Heatmap showing k-means clustering of the top 1000 most variable genes in Con and KO cells. K-means clustering is performed on mean center-normalized read counts, and rows represent individual genes, and columns represent samples. The colors on the heatmap represent a scaled expression level, with green indicating lowest expression and red indicating highest expression. Selected clusters are analyzed for gene ontology biological process enrichment, and the most enriched categories are presented after removing redundant processes.

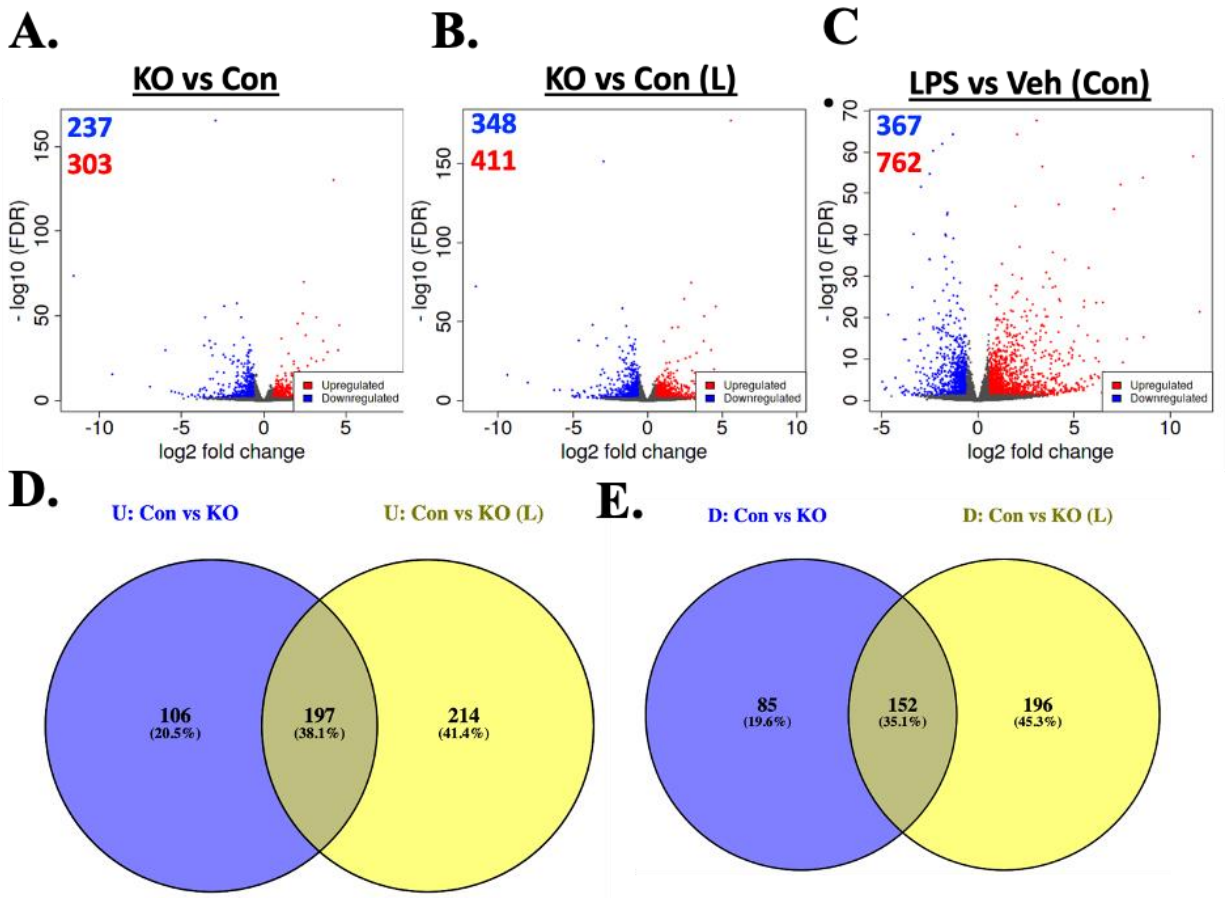

Figure 4.4. Differential gene expression analysis in CRISPR/Cas9 control and RGS10 knockout BV2 cells. Control BV2 cells (Con) and RGS10 knockout cells (KO) were treated with vehicle or LPS (10 ng/mL) (L) for 24h. A-C) Volcano plots of differentially expressed genes (DEGs) from different pairwise comparisons. A volcano plot is depicted to compare DEGs in KO cells in vehicle-treated groups (A) and LPS-treated groups (B), as well as in control cells treated with LPS (C). Signficant DEGs with LogFC $\geq |1|$ and FDR ≤ 0.05 were selected, from n=4 samples. Red dots represent upregulated genes, and blue plots represent downregulated genes, and the number of DEGs is presented in the top left of the volcano plots. D&E) Venn diagram comparing DEGs in KO cells in vehicle-treated cells (purple) and LPS-treated cells (yellow). Comparisons for upregulated and downregulated DEGs are shown in D & E, respectively.

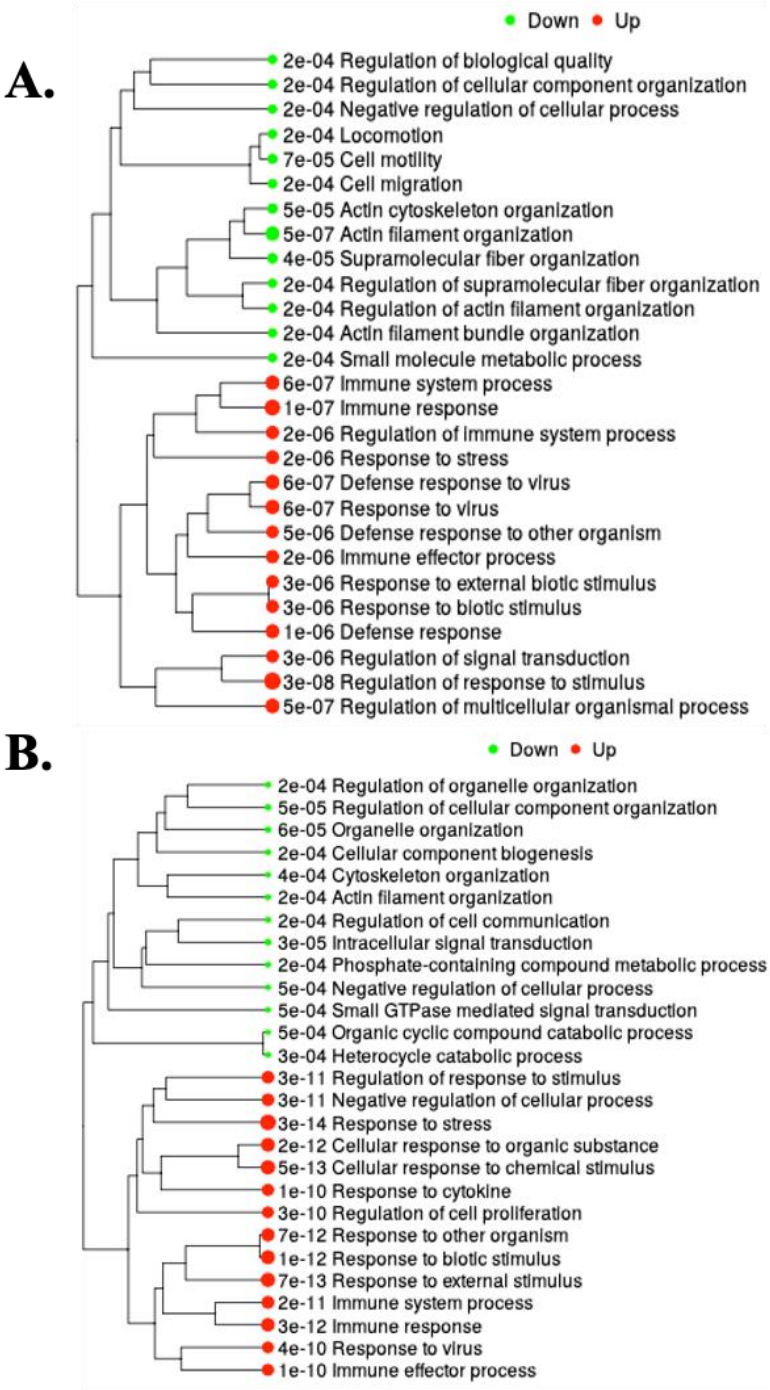

Figure 4.5. Overrepresented GO biological processes in CRISPR/Cas9 RGS10 knockout BV2 cells Differentially expressed genes (DEGs) described in Figure 4.4 legends were analyzed for enrichment of gene ontology (GO) biological processes (BP) in vehicle (**A**) and LPS-treated cells (**B**) A hierarchical clustering tree summarizes the correlation among significant pathways. Upregulated pathways are shown in red and downregulated pathways are shown in green. The circle size indicates more significant P-values, indicating larger number of DEGs.

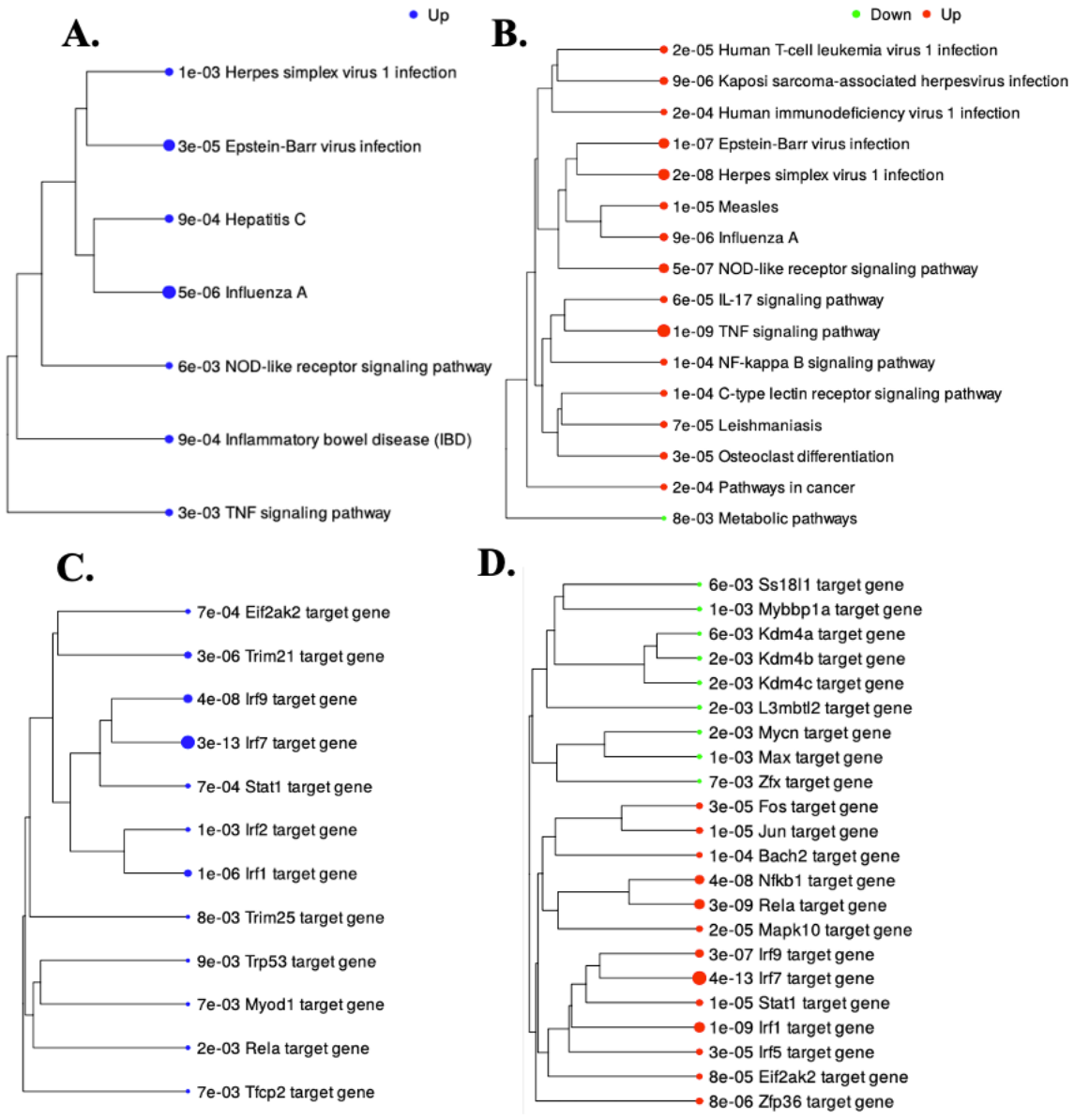

Figure 4.6. Overrepresented KEGG pathways and target gene-transcription factor regulatory networks in CRISPR/Cas9 RGS10 knockout BV2 cells. Significant differentially expressed genes (DEGs) with LogFC ≥ |1 |and FDR ≤ 0.05 were selected, from n=4 samples. DEGs are analyzed for enrichment of KEGG terms in vehicle-treated cells (**A**) and LPS-treated cells (**B**). Enriched gene-transcription factor (TF) regulatory networks (TF.Target.RegNetwork) for vehicle (**C**) and LPS-treated cells (**D**). Hierarchical clustering tree depicts the correlation among significant enriched pathways. For vehicle treated cells only upregulated pathways are enriched and are shown in blue. For LPS-treated cells, upregulated pathways are shown in red and downregulated pathways are shown in green.

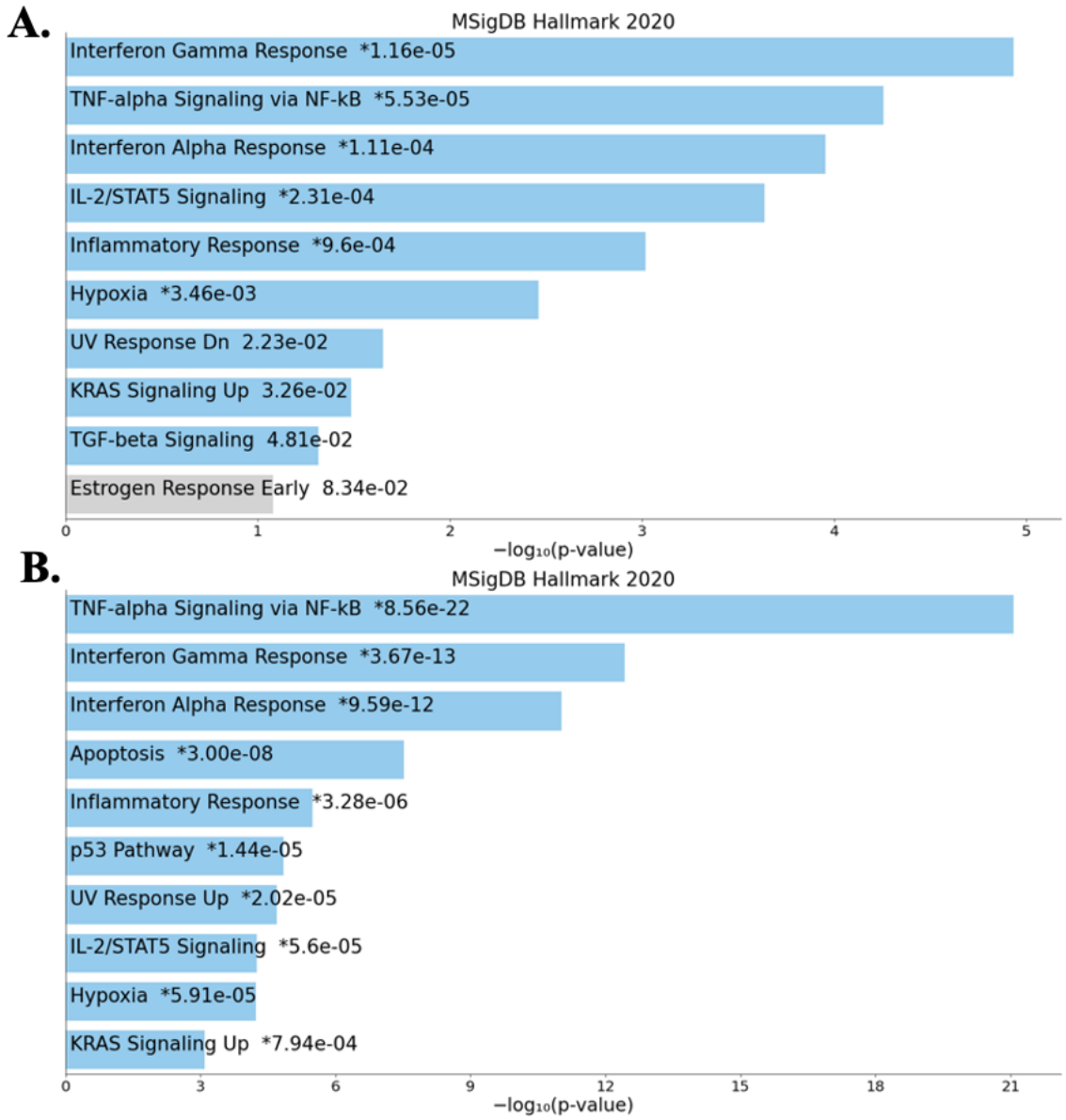

Figure 4.7: Overrepresented molecular signature hallmark pathways in CRISPR/Cas9 RGS10 knockout BV2 cells. Differentially expressed genes (DEGs) were analyzed for enrichment of molecular signature hallmark pathways using the MSigDB Hallmark gene sets 2020 database. Significant DEGs with LogFC ≥ |1 |and FDR ≤ 0.05 were selected, from n=4 samples. Overrepresented pathways are ranked by enrichment score, depicting significance (-log10 (p-value)). The top 10 overrepresented hallmark pathways in basal **(A)** and in LPS-activated RGS10 knockout cells are shown on a bar plot, ranked by significance. Blue bars show significantly enriched terms.

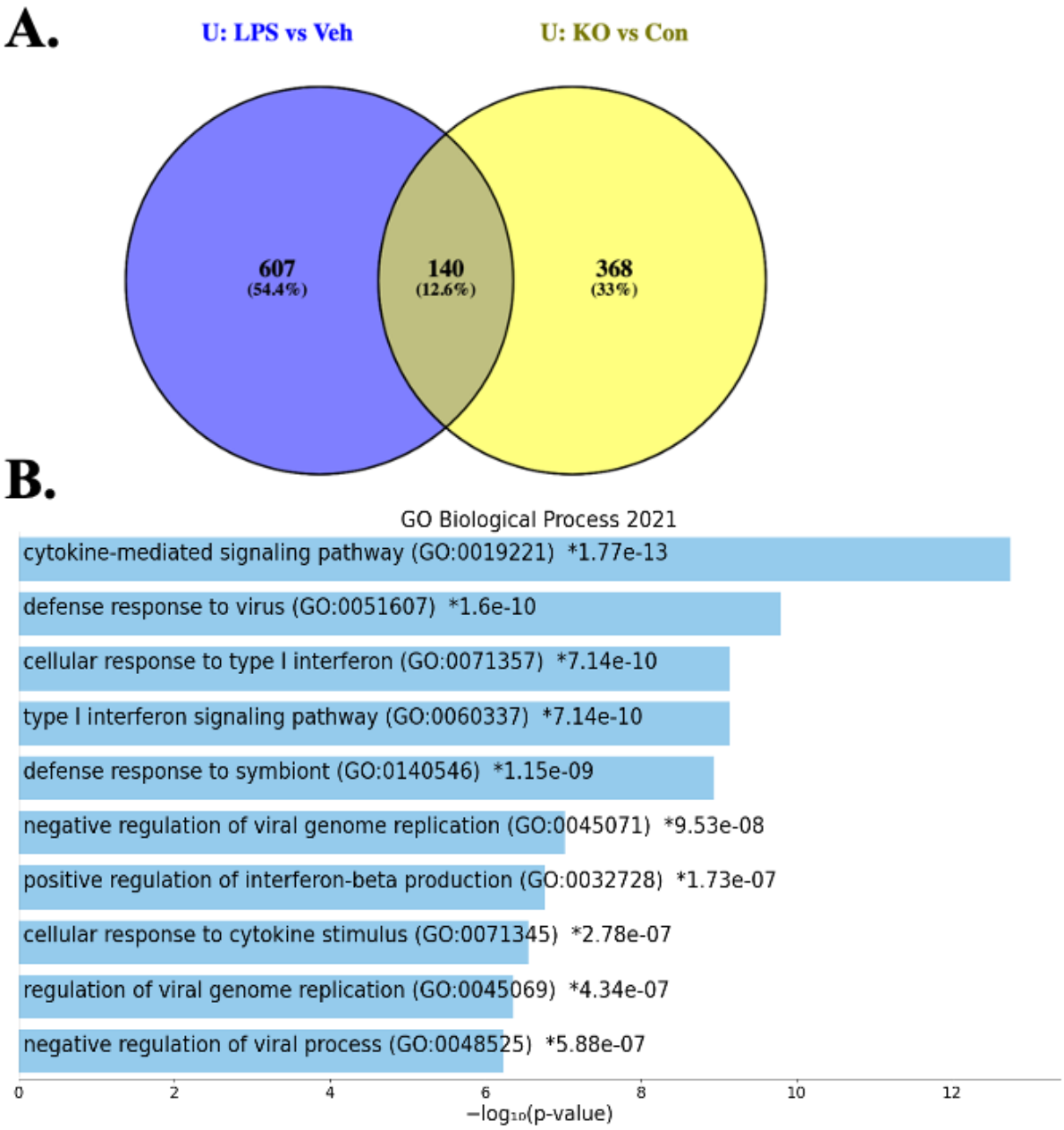

Figure 4.8. Differential regulation of LPS signaling in CRISPR/Cas9 RGS10 knockout cells. Control BV2 cells (Con) and RGS10 knockout cells (KO) were treated with vehicle (Veh) or LPS (10 ng/mL) for 24h. **A)** A volcano plot is depicted to compare the number of upregulated DEGs in KO cells (either in vehicle or LPS treated samples) that are also shared with LPS treatment in Con cells. Significant DEGs with LogFC ≥ |1 |and FDR ≤ 0.05 were selected, from n=4 samples. **B)** Overrepresented biological processes upregulated by LPS and by CRISPR/Cas9-mediated deletion of RGS10. The 140 shared upregulated DEGs were examined for enrichment of GO biological processes to identify biological processes upregulated by LPS and by RGS10 deletion. The top 10 overrepresented biological terms are shown on a bar plot, ranked by significance (-log10 (p-value)).

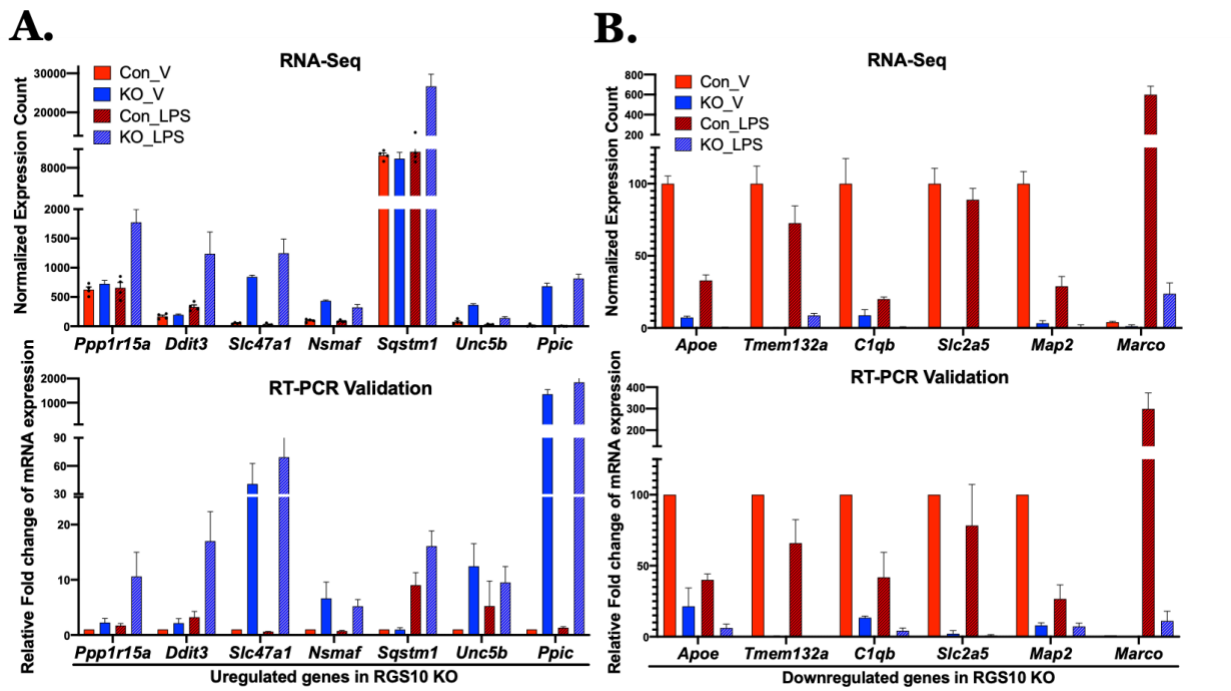

Figure 4.9. Validation of RNA-seq data for differentially expressed genes by RT-PCR. Comparison of normalized expression counts of RNA-seq data (top) and relative fold change of mRNA expression for qRT-PCR analysis (down) for a select few differentially expressed genes (DEGs) identified from RNA-seq analysis. Validation of upregulated DEGs (**A**) and downregulated DEGs (**B**) in RGS10 knockout (KO) cells relative to CRISPR/Cas9 control (Con) cells. Cells are treated with either vehicle (V) or LPS (10 ng/mL) for 24h. RT-PCR validation experiment is performed in freshly treated clonal and heterogeneous cell populations. Data for both RNA-seq expression counts and RT-PCR analysis is analyzed from four independent replicates and presented as mean ± SEM.

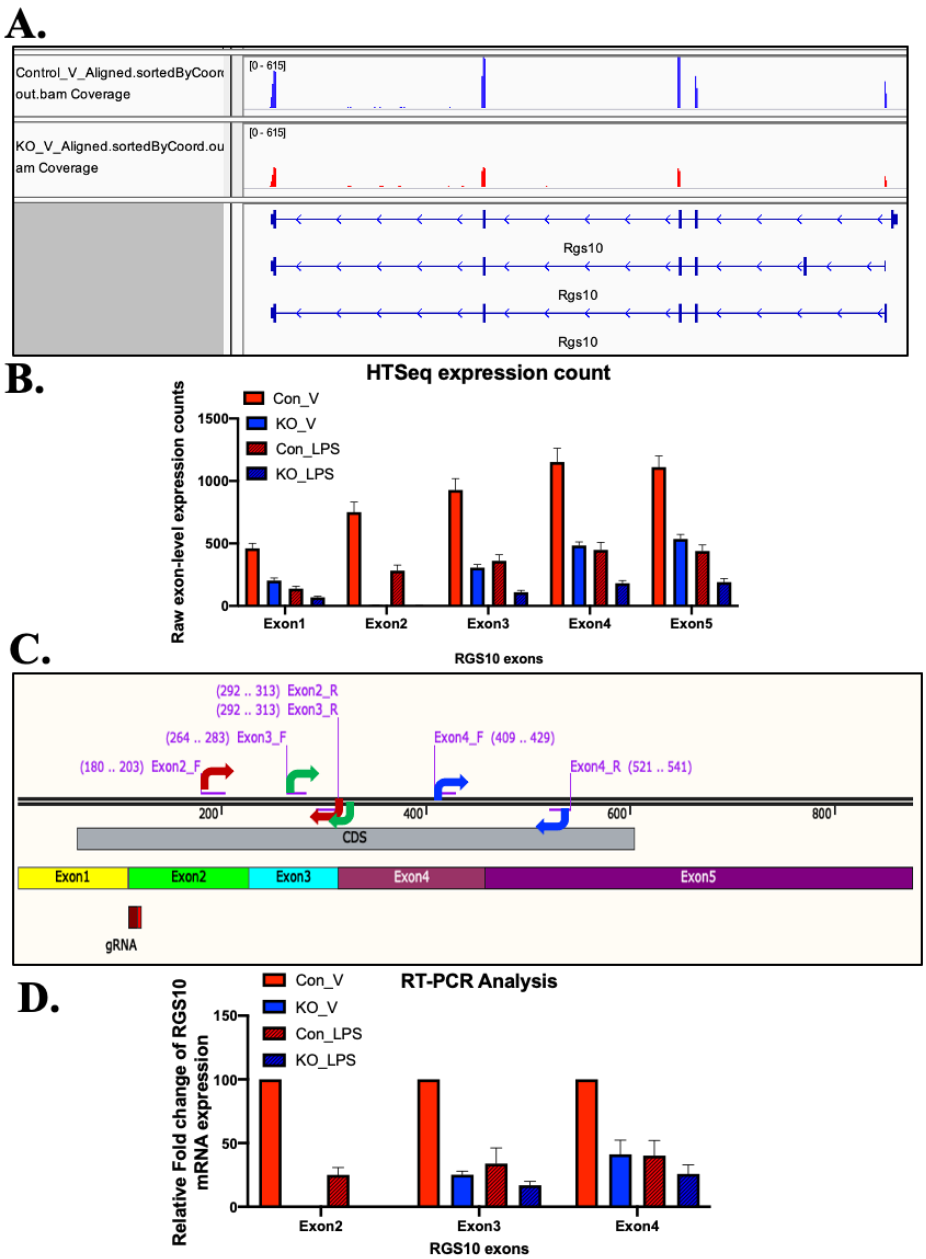

Figure 4.10. Unexpected expression of *Rgs10* transcript in CRISPR/Cas9 RGS10 knockout BV2 cells. **A)** Snapshot taken from integrative genome viewer to visualize sequenced reads mapped to the mouse Rgs10 genomic coordinate. Comparison of mapped reads from CRISPR/Cas9 control (Con) (top: blue color) and RGS10 knockout (KO) (bottom: red color) samples shows Rgs10 transcript expression in all exons except exon 2. **B)** Average raw exon-level expression counts comparing Rgs10 transcript expression for each exons. **C)** Snapshot taken from SnapGene showing the complete coding DNA sequence (CDS) for RGS10 and color-coded exon regions. Three forward/reverse primer sets were designed to amplify different exon regions. The sgRNA target region is located in the intron-exon2 boundary, depicted in the bottom. **D)** qRT-PCR analysis using different primer sets validates the quantified expression data and shows Rgs10 transcript is absent in exon 2 but expressed in other exon regions, suggesting that CRISPR/Cas induced skipping of exon 2. RT-PCR validation experiment is performed in freshly treated clonal and heterogeneous cell populations. Data for both RNA-seq expression counts and RT-PCR analysis is analyzed from four independent replicates and presented as mean ± SEM.

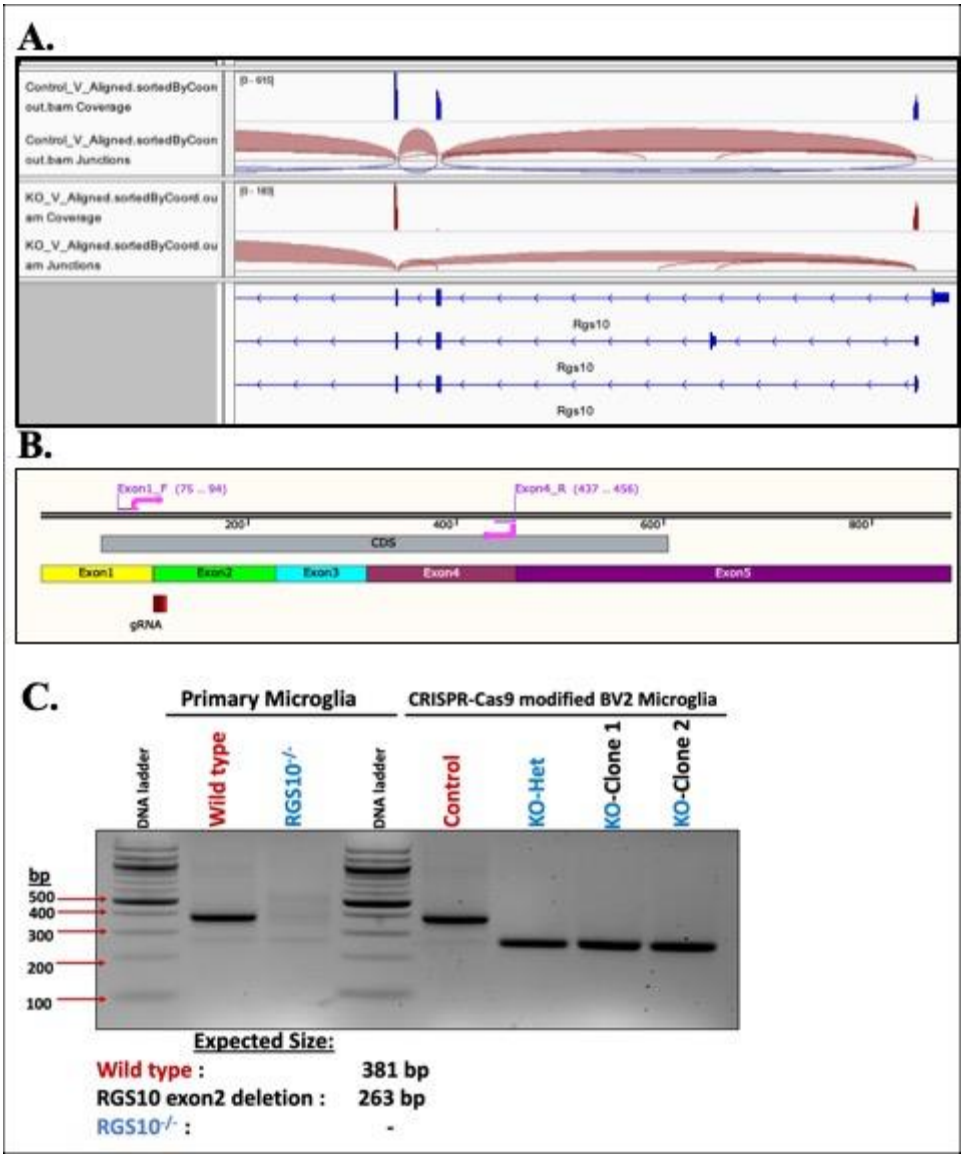

Figure 4.11. *Rgs10* transcript expression in CRISPR/Cas9-modified BV2 cells and primary microglia. A) Snapshot taken from integrative genome viewer to visualize junctional reads between exons 1-3 in CRISPR/Cas9 control (Con) (top: blue color) and RGS10 knockout (KO) (bottom: red color) samples. Visualized junctions show skipping of exon 2 in KO samples. **B)** Snapshot taken from SnapGene showing the complete coding DNA sequence (CDS) for *Rgs10* and color-coded exon regions. A primer set is designed to validate exon 2 skipping in KO samples. A forward primer is designed on upstream exon (exon 1) and reverse primer is designed on downstream exon (exon 4) to amplify exon 1-4 region. The gRNA target region is located in the intron-exon2 boundary, depicted in the bottom. **C)** Amplified cDNA sequence comparison of wild type primary microglia, RGS10 knockout primary cells ($RGS10^{-/-}$), heterogeneous Con CRISPR/Cas9 cells, heterogeneous population of CRISPR/Cas9 RGS10 KO cells (KO-Het), and two clonal populations of KO cells (KO-Clone1 and KO-Clone 2). Amplified transcripts are validated by RT-PCR and gel electrophoresis. Expected amplicon size for wild type, RGS10 knockout, and exon 2 skipped samples are shown in the bottom. The RT-PCR data validates the expression count and junctional analysis and shows that CRISPR/Cas9 induced exon 2 skipping and expression of short *Rgs10* transcript.

Table 4.1. RT-PCR primer sequences used for RNA-seq validation

Gene name	Forward Sequence (5'→3')	Reverse Sequence (5' → 3')
β-actin	GGCTGTATTCCCCTCCATCG	CCAGTTGGTAACAATGCCATGT
Apoe	CAGATCAGCTCGAGTGGCAA	TCCATCAGTGCCGTCAGTTC
C1qb	ACCAGGATTCCATACACAGGAAG	AAGCAGCAGTAACAGGTGTGT
Ddit3	CTGGAAGCCTGGTATGAGGAT	CAGGGTCAAGAGTAGTGAAGGT
Marco	TGTCGCATGCTCGGTTACTC	CTCTGTGCCCCGACAATTCA
Map2	TCTAAAGAACATCCGTCACAGG	GGTGAGCATTGTCAAGTGAGC
Nsmaf	ATGCCTGAGCCAAGATTCAT	GGTGCGATCCTAACGAGGTA
Ppic	ACACCAACGGATCCCAGTTC	GGAATGTACCACAGTCATCCCA
Ppp1r15a	CCTCTAAAAGCTCGGAAGGTACA	TCGATCTCGTGCAAACTGCT
Slc2a5	TTCCTACTCCTCGTCGGCTT	GGTCCTAAGGCGTGTCCTATG
Slc47a1	TGCGGTTATCAATGTCACAGG	CTACGTGCTTTAAGTTCTGGCT
Tmem132a	TCGACACAACTTCACTGCGA	GCCCTTGAAGCGGTCTAACT
Tnfa	CCTGTAGCCCACGTCGTAG	GGGAGTAGACAAGGTACAACCC
Il6	CTGCAAGAGACTTCCATCCAG	AGTGGTATAGACAGGTCTGTTGG
Ptgs2	TGCAAGATCCACAGCCTACC	GCTCAGTTGAACGCCTTTTG
Rgs10 (exon2/3)	CCCGGAGAATCTTCTGGAAGACC	CTGCTTCCTGTCCTCCGTTTTC
Rgs10 (exon3)	TGTTTTGGCTAGCGTGTGAA	CTGCTTCCTGTCCTCCGTTTTC
Rgs10 (exon4/5)	GATTCTGGAAGAGCCACACCC	CTCTTCCTCAGTTCGCTTGGG
Rgs10 (exon1/4)	TGAGCCGACTGAGCAGGAAG	CTCTTCCTCAGTTCGCTTGGG

Table 4.2. Transcription factor target gene enrichment analysis of K-means clusters.

Cluster	adj.Pval	nGenes	Pathways (target genes)	Genes
A	6.81E-14	20	Irf7	[*Dhx58, Cmpk2, Rsad2, Ifih1, Ifi44, Gbp3, Oasl2, Usp18, Trim30a, Oas3, Rtp4, Parp14, H2-Q4 Tap1, Ddx60, Xaf1, Oasl1, Ifit2, Bst2, Irgm1*]
	1.88E-07	11	Irf9	[*Rsad2, Fos, Irf7, Oasl2, Usp18, Oas3, Rtp4, Parp14, H2-Q4, Oasl1, Irgm1*]
	8.55E-06	21	Irf1	[*Il12b, Rcn1, Rgs7bp, Irf7, P2rx3, F3, Gbp3, Usp18, Oas3, Rtp4, Parp14, H2-Q4, Tap1, Dusp10, Oasl1, Agrn, Bst2, Irgm1, Tmem140, Osm, Cdkn2b*]
	4.23E-05	29	Stat1	[*Fosb, Bik, Cmpk2, Rsad2, Fos, Myc, Adamts1, Dusp1, Irf7, Atf3, Ifih1, Ifi44, Gbp3, Oasl2, Usp18, Trim30a, Oas3, Rtp4, Parp14, H2-Q4, H1f2, Tap1, Rras, Oasl1, Dmgdh, Magi1, Ifit2, Irgm1, Osm*]
	5.69E-03	16	Irf2	[*Rcn1, Evl, Irf7, P2rx3, F3, Usp18, Oas3, Rtp4, H2-Q4, Tap1, Dusp10, Oasl1, Agrn, Bst2, Osm, Cdkn2b*]
B	2.73E-13	25	Nfkb1	[*Ccl3, Mmp9, Csf2, Ccl4, Nos2, Nfkbia, Tnf, Fas, Il6, Traf1, Il1rn, Il1b, Il1a, Zbp1, Ptgs2, Cxcl10, Ccl5, Nfkbiz, Acta2, Cd14, Socs3, Cxcl2, Bcl2a1b, Bcl2a1d, Bcl2a1a*]
	4.96E-13	30	Rela	[*Dnmt3l, Ccl3, Ier3, Mmp9, Ccl4, Socs2, Nos2, Nfkbia, Pim1, Tnf, Fas, Il6, Traf1, Il1b, Il1a, Zbp1, Tnfrsf1b, Ccl17, Ptgs2, Cxcl10, Ccl5, Nfkbiz, Ccl2, Csf3, Cd14, Socs3, Cxcl2, Bcl2a1b, Bcl2a1d, Bcl2a1a*]
	2.24E-07	10	Rgs14	[*Ccl9, C3, Ccr1, Cxcl3, Cxcl10, Ccl5, Fpr1, C5ar1, Gpr18, Cxcl2*]
	6.71E-07	10	Nfkb2	[*Nos2, Nfkbia, Tnf, Cd5, Traf1, Il1b, Zbp1, Ptgs2, Nfkbiz, Bcl3*]
	7.43E-07	20	Rel	[*Dnmt3l, Cntnap1, Nos2, Nfkbia, Tiam2, Pim1, Tnf, Ehd1, Il6, Il1a, Tnfrsf1b, Cxcl3, Ccl17, Prr5l, Nfkbiz, Ccl2, Sbno2, Csf3, Stx1, Bcl3*]
	4.86E-06	5	Mapk11	[*Nos2, Tnf, Il6, Il1b, Il1a*]
	1.26E-05	4	Myd88	[*Tnf, Il6, Il1b, Cxcl2*]

Transcription factor target gene enrichment analysis was performed for clusters A and B, visualized in *Figure 4.3B*. Cluster A represents target genes upregulated in CRISPR/Cas9 RGS10 knockout samples compared to control cells, and cluster B represents target genes upregulated by LPS based on unsupervised K-means clustering of the top 1000 most variable genes (described in *Figure 4.3B* legend). Enrichment analysis was performed using transcription factor (TF) target gene set database and ranked based on adjusted p-value.

Table 4.3. Overrepresented pathways exclusively upregulated in activated CRISPR/Cas9 RGS10 knockout BV2 cells.

Table of top 10 significant p-values and q-values for WikiPathway 2021 Human

term	p-value	q-value	overlap_genes
Spinal Cord Injury WP2431	0.000004	0.000364	[*Nr4a1, Cxcl10, Il6, Btg2, Myc, Ptgs2, Tnf, Cxcl2, Rhob*]
Lung fibrosis WP3624	0.000004	0.000364	[*Csf3, Edn1, Il6, Plau, Il12b, Tnf, Cxcl2*]
Unfolded protein response WP4925	0.000004	0.000364	[*Ppp1r15a, Hspa5, Ddit3, Txnip, Bbc3*]
Cytokines and Inflammatory Response WP530	0.000006	0.000405	[*Csf3, Il6, Il12b, Tnf, Cxcl2*]
Photodynamic therapy-induced unfolded protein response WP3613	0.000007	0.000405	[*Ppp1r15a, Hspa5, Ddit3, Atf3, Bbc3*]
COVID-19 adverse outcome pathway WP4891	0.000014	0.000621	[*Cxcl10, Csf3, Il6, Tnf*]
SARS-CoV-2 innate immunity evasion and cell-specific immune response WP5039	0.00006	0.002352	[*Cxcl10, Il6, Stat1, Mx1, Tnf, Cxcl2*]
Acute viral myocarditis WP4298	0.000263	0.00898	[*Edn1, Il6, Stat1, Il12b, Ccr5, Tnf*]
Photodynamic therapy-induced NF-kB survival signaling WP3617	0.000446	0.013518	[*Il6, Ptgs2, Tnf, Cxcl2*]
Type II interferon signaling (IFNG) WP619	0.000553	0.015102	[*Cxcl10, Stat1, Tap1, Isg15*]

Table of top 10 significant p-values and q-values for TRRUST Transcription Factors 2019

term	p-value	q-value	overlap_genes
NFKB1 human	1.75E-08	0.000004	[*Edn1, Btg2, Cd83, Tap2, Tap1, Ptgs2, Tnf, Cxcl2, Cxcl10, Il6, Adora2a, Plau, Myc, Il12b, Ccr5, Sqstm1, Atf3*]
RELA human	9.86E-08	0.000012	[*Edn1, Btg2, Cd83, Stat1, Tap2, Tap1, Ptgs2, Tnf, Cxcl2, Cxcl10, Il6, Adora2a, Plau, Myc, Il12b, Ccr5*]
IRF1 mouse	1.67E-07	0.000014	[*Cxcl10, Tap2, Il12b, Tap1, Il27, Tnf*]
ATF4 human	1.40E-06	0.000086	[*Il6, Hspa5, Plau, Ddit3, Ptgs2, Atf3*]
CEBPB human	2.70E-06	0.000132	[*Il6, Prss50, Gdf15, Ddit3, Prdm1, Ptgs2, Tnf*]
JUN human	3.40E-06	0.000139	[*Il6, Edn1, Plau, Myc, Ddit3, Il12b, Ptgs2, Tnf, Atf3, Rhob*]
CEBPB mouse	4.27E-06	0.00015	[*Btg2, Csf3, Il6, Myc, Ptgs2, Atf3*]
IKBKB mouse	5.07E-06	0.000155	[*Cxcl10, Ptgs2, Cxcl2, Tnf*]
NFKB1 mouse	7.54E-06	0.000205	[*Cxcl10, Egr2, Edn1, Il6, Adora2a, Stat1, Myc, Il12b, Ptgs2, Tnf, Cxcl2*]

JUN mouse	8.76E-06	0.000215	[*Il6, Plau, Il12b, Il27, Prdm1, Eno2, Ptgs2, Tnf, Cxcl2*]

Table of top 10 significant p-values and q-values for Jensen COMPARTMENTS

term	p-value	q-value	overlap_genes
NF-kappaB complex	2.81E-07	0.000221	[*Cx3cr1, Csf3, Cd83, Prdm1, Ptgs2, Tnf, Cxcl2, Plau, Myc, Ccr5, Edn1, Jund, Tnfrsf12a, Hspa5, Stat1, Mx1, Osm, Isg15, Isg20, Cxcl10, Nr4a1, Il6, Ddit3, Lta, Fosb, Sqstm1, Atf3*]
Interferon regulatory factor 7 complex	7.81E-07	0.000307	[*Isg20, Cxcl10, Il6, Stat1, Oas3, Mx1, Ifi44, Isg15, Tnf*]
CHOP-ATF3 complex	1.51E-06	0.000396	[*Nr4a1, Hspa5, Gdf15, Ddit3, Atf3*]
interleukin-23 complex	5.38E-06	0.000975	[*Cx3cr1, Csf3, Cd83, Stat1, Mx1, Il27, Isg15, Prdm1, Ptgs2, Tnf, Cxcl2, Cxcl10, Il6, Myc, Lta, Il12b, Ccr5*]
Interferon regulatory factor complex	6.19E-06	0.000975	[*Isg20, Cxcl10, Il6, Dusp10, Stat1, Oas3, Mx1, Ifi44, Il27, Isg15, Prdm1, Tnf*]
interleukin-12 complex	1.97E-05	0.002274	[*Csf3, Cd83, Stat1, Avil, Mx1, Il27, Isg15, Ptgs2, Tnf, Cxcl2, Cxcl10, Il6, Rgs1, Myc, Lta, Il12b, Ccr5*]
Ire1 complex	2.29E-05	0.002274	[*Ppp1r15a, Il6, Hspa5, Rgs1, Ddit3, Prdm1, Tnf, Sqstm1, Atf3, Bbc3*]
Interferon regulatory factor 3 complex	2.34E-05	0.002274	[*Isg20, Cxcl10, Il6, Dusp10, Stat1, Mx1, Isg15, Il27, Tnf*]
interleukin-6 receptor complex	2.60E-05	0.002274	[*Il6, Stat1, Osm, Il12b, Il27, Tnf*]
BAX complex	3.14E-05	0.002472	[*Ppp1r15a, Prnp, Edn1, Btg2, Cdkn2b, Csf3, Hspa5, Stat1, Gdf15, Ptgs2, Tnf, Bbc3, Nr4a1, Il6, Myc, Ddit3, Txnip, Sqstm1, Atf3, Prkg1*]

Upregulated differentially expressed genes (DEGs) in RGS10 knockout (KO) cells were compared to CRISPR/Cas9 control cells in vehicle treated and LPS (10 ug/mL) treated samples. DEGs exclusively upregulated in KO cells in response to LPS treatment were analyzed for pathway enrichment using three different pathway databases: WikiPathway 2021 Human database (top), TRRUST transcription factor database (middle), and Jensen compartments (bottom). Different enriched terms are presented along with the respective p-value and q-value and a list of DEGs that overlap with known gene set belonging to the specific terms.

Table 4.4. Overrepresented pathways upregulated by LPS and by CRISPR/Cas9-mediated deletion of RGS10.

Upregulated enriched terms

Table of top significant p-values and q-values for GO Biological Process 2021

term	p-value	q-value	overlap_genes
cytokine-mediated signaling pathway (GO:0019221)	1.77E-13	2.09E-10	[*Ifitm3, Csf3, Ptgs2, Tnf, Cxcl2, Il18rap, Myc, Il12b, Ccr5, Rsad2, Mx2, Tnfrsf9, Osm, Isg15, Traf1, F3, Isg20, Cxcl10, Il6, Oas2, Oas3, Irf7, Lta, Rhou, Xaf1, Il7r*]
defense response to virus (GO:0051607)	1.60E-10	9.46E-08	[*Ifitm3, Isg20, Rtp4, Cxcl10, Il6, Rsad2, Ddx58, Oas2, Oas3, Mx2, Irf7, Isg15*]
type I interferon signaling pathway (GO:0060337)	7.14E-10	2.11E-07	[*Ifitm3, Isg20, Rsad2, Oas2, Oas3, Mx2, Irf7, Isg15, Xaf1*]
defense response to symbiont (GO:0140546)	1.15E-09	2.71E-07	[*Ifitm3, Isg20, Rtp4, Il6, Rsad2, Ddx58, Oas2, Oas3, Mx2, Irf7, Isg15*]
negative regulation of viral genome replication (GO:0045071)	9.53E-08	1.88E-05	[*Ifitm3, Isg20, Rsad2, Oas2, Oas3, Isg15, Tnf*]
positive regulation of interferon-beta production (GO:0032728)	1.73E-07	2.93E-05	[*Ddx58, Oas2, Oas3, Dhx58, Irf7, Isg15*]
cellular response to cytokine stimulus (GO:0071345)	2.78E-07	4.11E-05	[*Csf3, Gbp7, Osm, Ptgs2, Tnf, Ptpn14, Cxcl2, F3, Cxcl10, Il6, Myc, Il12b, Rhou, Ccr5, Gbp3, Gsdme*]

Table of top significant p-values and q-values for MSigDB Hallmark 2020

term	p-value	q-value	overlap_genes
Interferon Gamma Response	2.83E-20	1.05E-18	[*Ifitm3, Rtp4, Rsad2, Ddx58, Mx2, Ifi44, Isg15, Ddx60, Ptgs2, Usp18, Isg20, Cxcl10, Il6, Bank1, Oas2, Oas3, Dhx58, Irf7, Cmpk2, Cd69, Xaf1, Gpr18*]
TNF-alpha Signaling via NF-kB	3.38E-15	6.26E-14	[*Edn1, Ddx58, Tnfrsf9, Traf1, Ptgs2, Tnf, Cxcl2, F3, Fosl1, Cxcl10, Il6, Myc, Maff, Il12b, Cd69, Il7r, Sgk1, Phlda1*]
Interferon Alpha Response	1.55E-13	1.91E-12	[*Ifitm3, Rtp4, Rsad2, Ifi44, Isg15, Ddx60, Usp18, Isg20, Cxcl10, Sell, Dhx58, Irf7, Cmpk2*]
Inflammatory Response	7.88E-13	7.29E-12	[*Rtp4, Csf3, Edn1, Tnfrsf9, Osm, F3, Cxcl10, Il6, Il18rap, Sell, Myc, Irf7, Lta, Il12b, Cd69, Il7r*]
IL-2/STAT5 Signaling	1.42E-06	1.05E-05	[*Ifitm3, Cxcl10, Sell, Glipr2, Myc, Tnfrsf9, Maff, Traf1, Phlda1, Igf2r*]

Apoptosis	1.80E-05	1.11E-04	[*Ifitm3, Isg20, Il6, Bik, Ddit3, Cd69, Tnf, Igf2r*]
Allograft Rejection	2.87E-03	1.52E-02	[*Il6, Il18rap, Irf7, Il12b, Ccr5, Tnf*]
KRAS Signaling Up	1.34E-02	5.51E-02	[*Cxcl10, Tnnt2, Traf1, Il7r, Ptgs2*]
Hypoxia	1.34E-02	5.51E-02	[*Isg20, Il6, Ddit3, Maff, F3*]
DNA Repair	2.13E-02	7.81E-02	[*Ak1, Cmpk2, Ccno, Gsdme*]

Table of top significant p-values and q-values for TRRUST Transcription Factors 2019

term	p-value	q-value	overlap_genes
RELA	3.71E-10	3.91E-08	[*Edn1, Tnfrsf9, Traf1, Ptgs2, Tnf, Cxcl2, F3, Cxcl10, Il6, Adora2a, Myc, Irf7, Il12b, Madcam1, Cd69, Ccr5*]
NFKB1	4.09E-10	3.91E-08	[*Edn1, Tnfrsf9, Traf1, Ptgs2, Tnf, Cxcl2, F3, Cxcl10, Il6, Adora2a, Myc, Irf7, Il12b, Madcam1, Cd69, Ccr5*]
CEBPB	2.01E-07	1.28E-05	[*Il6, Prss50, Gdf15, Ddit3, Hp, Ptgs2, Tnf*]
JUN	1.06E-06	4.16E-05	[*Fosl1, Edn1, Il6, Myc, Ddit3, Il12b, Ptgs2, Tnf, F3*]
IKBKB	1.09E-06	4.16E-05	[*Cxcl10, Ptgs2, Cxcl2, Tnf]*
IRF1	2.60E-05	6.55E-04	[*Cxcl10, Sell, Il12b, Tnf*]
STAT1	2.74E-05	6.55E-04	[*Cxcl10, Edn1, Il6, Irf7, Ptgs2, Xaf1*]
EGR1	3.57E-05	7.59E-04	[*Il6, Gdf15, Ptgs2, Tnf, F3, Bcar1*]
APC	7.05E-05	1.35E-03	[*Myc, Ptgs2, Sgk1*]

Upregulated differentially expressed genes (DEGs) in RGS10 knockout cells were compared with those upregulated by LPS treated in CRISPR/Cas9 control cells. 140 shared upregulated DEGs were examined for pathway enrichment using three databases: GO Biological Process 2021 (top), MSigDB Hallmark 2020 (middle) and TRRUST Transcription Factor 2019 (bottom). Different enriched terms are presented along with the respective p-value and q-value and a list of DEGs that overlap with known gene set belonging to the specific terms.

Table 4.5. Overrepresented GO Biological Processes downregulated by LPS and by CRISPR/Cas9-mediated deletion of RGS10.

Downregulated enriched terms Table of top significant p-values and q-values for GO Biological Process 2021			
term	**p-value**	**q-value**	**overlap_genes**
cell junction disassembly (GO:0150146)	1.16E-07	0.000057	[*C1qb*, *C1qa*, *C1qc*]
synapse pruning (GO:0098883)	4.86E-07	0.00008	[*C1qb*, *C1qa*, *C1qc*]
complement activation, classical pathway (GO:0006958)	4.86E-07	0.00008	[*C1qb*, *C1qa*, *C1qc*]
humoral immune response mediated by circulating immunoglobulin (GO:0002455)	9.52E-07	0.000117	[*C1qb*, *C1qa*, *C1qc*]
regulation of complement activation (GO:0030449)	2.15E-06	0.000207	[*C1qb*, *C1qa*, *Cfh*, *C1qc*]
regulation of immune effector process (GO:0002697)	2.72E-06	0.000207	[*C1qb*, *C1qa*, *Cfh*, *C1qc*]
regulation of humoral immune response (GO:0002920)	2.93E-06	0.000207	[*C1qb*, *C1qa*, *Cfh*, *C1qc*]
microglial cell activation (GO:0001774)	7.52E-04	0.045034	[*C1qa*, *Aif1*]
regulation of supramolecular fiber organization (GO:1902903)	8.22E-04	0.045034	[*Map2*, *Apoe*]

Downregulated differentially expressed genes (DEGs) in RGS10 knockout cells were compared with those downregulated by LPS treated in CRISPR/Cas9 control cells. 37 shared downregulated DEGs were examined for GO biological process enrichment using the GO Biological Process 2021 database. Different enriched terms are presented along with the respective p-value and q-value and a list of DEGs that overlap with known gene set belonging to the specific terms.

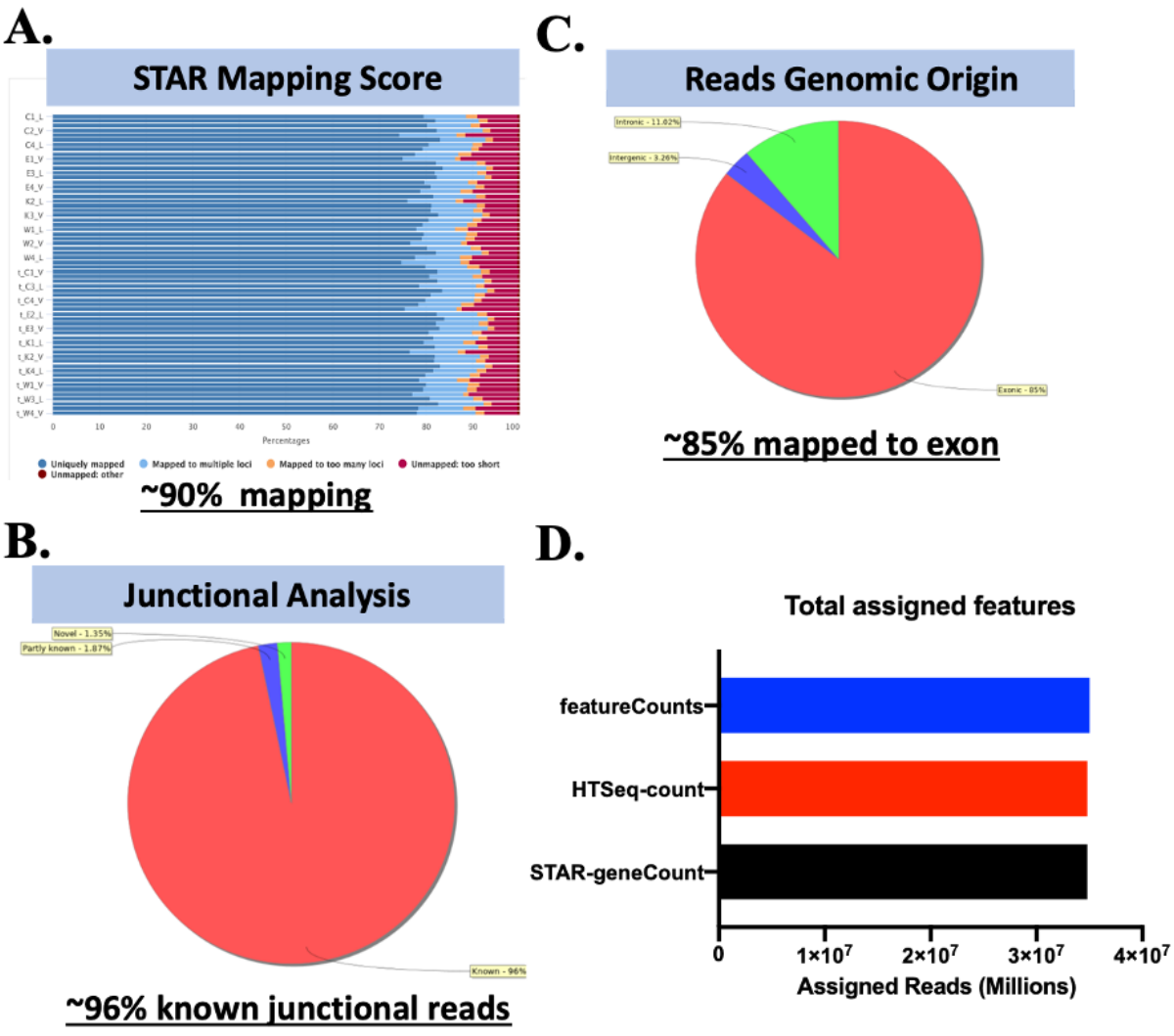

Figure S4.1. Quality control of RNA-seq read mapping and gene counting. A) Mapping of clean transcript sequences using STAR following initial sequence quality control, and subsequent trimming and rRNA filtering. Quality of mapping is assessed using STAR mapping score. Reads have percentage of mapping, uniquely mapped reads were ~80 % and total mapped reads showed ~90% mapping. **B-C)** Representative mapping quality analysis showing high percentage of reads mapped to exons and known exon-intron junctions. **D)** Read count comparison of assigned features performed using three different gene counting programs, showing identical number of assigned features.

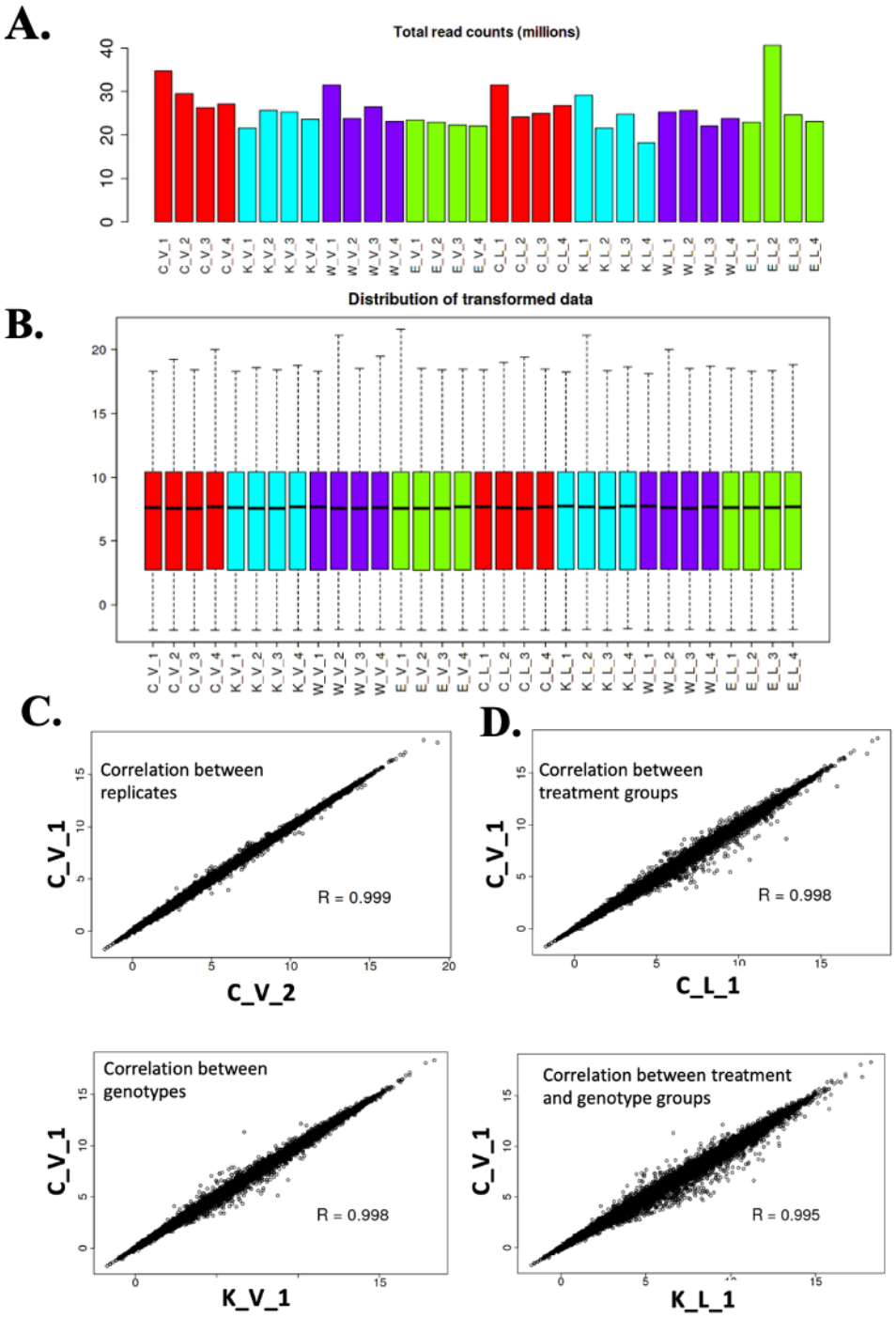

Figure S4.2. Transformation, normalization and sample correlation of expression count. A) Box plots of raw read counts distribution showing difference in library size across samples. **B)** Box plot showing similar distribution of read counts after regularized log (rlog) transformation. **C-F)** Scatterplots showing sample correlations of transformed data between replicate control cells treated with vehicle (**C**), correlation between vehicle and LPS (10ng/ml) treated samples (**D**), correlation between vehicle treated control and RGS10 knockout cells (**E**), and between vehicle treated control cells and LPS treated knockout cells (**F**).

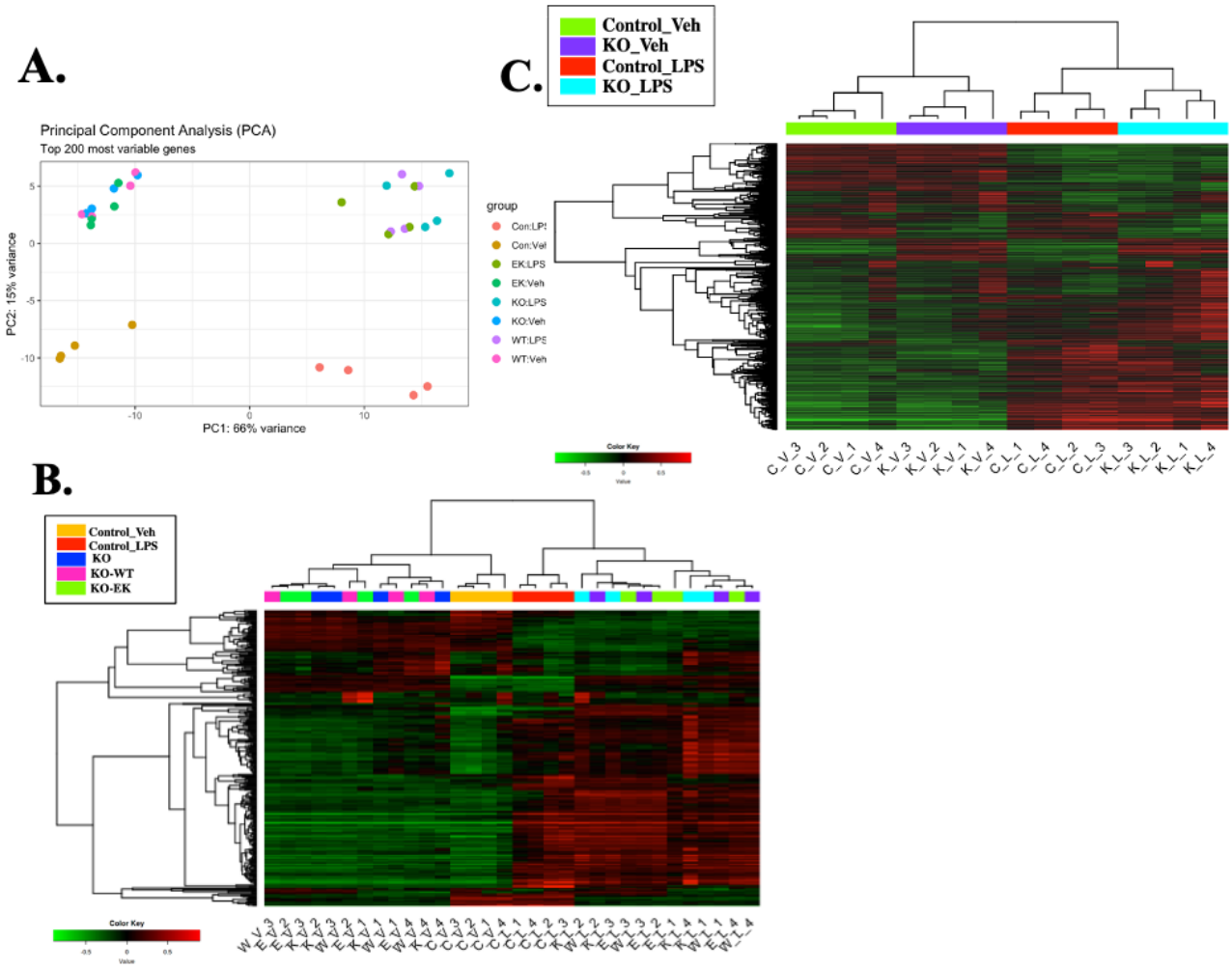

Figure S4.3. Explorative data analysis of CRISPR-Cas9 RGS10 knockout and RGS10 overexpressing BV2 cells. A) Principal component analysis plot of the top 200 most variable genes. PC1 separates clusters based on treatment, while PC2 separates clusters based on genotype. **B-C)** Heatmap showing hierarchical clustering of the top 1000 most variable genes. Rows represent individual genes and columns represent samples arranged into clusters according to structural hierarchy. Heatmap for all sample groups show mixed clustering of genes in RGS10 knockout and RGS10 re-expressing cells (**B**), separate clustering of control and RGS10 knockout cells show two main clusters separated based on treatment group, and a subset of clusters separated based on genotype (**C**). Upregulation and downregulation of genes are represented in red and green, respectively.

CHAPTER 5

DISCUSSION, CONCLUSION, AND FUTURE DIRECTION

Chronic neuroinflammation is an underlying mechanism for the initiation and progression of multiple neurodegenerative diseases such as Alzheimer's disease, Parkinson's disease, and stroke (Hickman et al., 2018). One of the key drivers of inflammatory process in the central nervous system (CNS) is the chronic activation of microglia cells. Activated microglia are a source of several neurotoxic factors, including prostaglandins, pro-inflammatory cytokines, and reactive oxygen species (Hickman et al., 2018; Lull & Block, 2010).

G protein signaling pathways play an important role in inflammatory process in various immune cells. This study focused on the regulator of G protein signaling 10 (RGS10), which is the smallest member of the RGS protein family. RGS10 primarily contains the conserved RGS domain, which functions as a GTPase-activating protein (GAP) for Gα subunit of G proteins (Hunt et al., 1996). Through this canonical role, RGS10 inactivates Gαi family of G proteins and regulates downstream Gi signaling initiated by activation of G protein-coupled receptors (GPCR) (Ghavami et al., 2004; Thelen & Stein, 2008; Xie et al., 2007). RGS10 is abundantly expressed in microglia and mediates important anti-inflammatory and neuroprotective functions (Lee & Tansey, 2015). Most of the previously characterized role of RGS10 in microglia is in the regulation of pro-inflammatory cytokines in response to lipopolysaccharide (LPS) (Lee et al., 2013; Lee et al., 2008), which is a bacterial endotoxin that is commonly used to model inflammation associated with neurodegeneration (Goulopoulou et al., 2016). However, LPS activates microglia through the

toll-like receptor 4 (TLR4) pathway, which is not a GPCR-initiated signaling event that is canonically targeted by GAPs. Therefore, the molecular mechanism by which RGS10 regulates inflammatory response downstream of a non-GPCR receptor is not known.

While microglial RGS10 exerts anti-inflammatory and neuroprotective functions, its expression is downregulated during inflammation and aging (Almutairi et al., 2021; Alqinyah et al., 2017; Kannarkat et al., 2015; Lee et al., 2008). Hence, while the protective functions of RGS10 position it as an anti-inflammatory target for neurodegenerative diseases, the lack of information on its molecular mechanism limits its therapeutic potential. In this study, we used a combination of proteomics, transcriptomics, and signaling approaches to determine the anti-inflammatory molecular mechanism of RGS10 and to further identify novel neuroprotective functions of RGS10 in microglia. A better understanding of the anti-inflammatory molecular mechanism of RGS10 is beneficial for identifying alternative therapeutic targets that can be used to compensate for its functional loss during neuroinflammation.

In our recently published work, we determined that RGS10 negatively regulates the expression of the inflammatory enzyme cyclooxygenase 2 (COX-2) and its downstream neurotoxic product prostaglandin E2 (PGE2) in LPS-activated BV2 microglia (Alqinyah et al., 2018). Although we detected the canonical RGS10-Gαi3 interaction in response to LPS/TLR4 activation (**Figure A.1**), our result showed that the ability of RGS10 to downregulate COX-2 expression is not dependent on its canonical mechanism, as inhibition of Gαi using pertussis toxin does not affect LPS-induced COX-2 production in RGS10 knockdown BV2 cells (**Figure A.2**) (Alqinyah et al., 2018). These results implied a G protein-independent mechanism of RGS10 in microglia.

Some RGS proteins are known to have noncanonical functions; however, many of the previously characterized G protein-independent functions of RGS proteins are mediated through noncanonical protein-protein interactions, most of which occur through defined or undefined motifs outside the conserved RGS domain (Hollinger & Hepler, 2002; Kimple et al., 2001; Shu et al., 2010). Although RGS10 is small and merely contains the conserved GAP domain, we hypothesized that novel binding partners may provide a plausible link between RGS10 and the TLR4 signaling pathway, which may help identify the G protein-independent anti-inflammatory mechanism of RGS10. This hypothesis was tested in **Chapter 3** using a combination of proteomics and mechanistic experiments.

We first investigated non-canonical interactions of RGS10 in BV2 microglia using co-immunoprecipitation (co-IP) and mass spectrometry. Our result identified 23 non-canonical binding partners of RGS10 in BV2 microglia, in addition to the expected canonical Gαi interactions (Gαi3 and Gαi3). These novel interaction partners have diverse subcellular localization and molecular functions, implying potentially diverse noncanonical roles for RGS10 (refer to **Table A.1** for details on the RGS10 interacting partners). Among the list of interacting partners, we identified the stromal interaction molecule 2 (STIM2) as one of the most abundant RGS10 interacting protein, and most closely linked to inflammatory signaling pathways in immune cells (Chang, 2006; Michaelis et al., 2015; Sogkas et al., 2015). By direct co-IP, we validated that the RGS10-STIM2 interaction is not only present in BV2 microglia, but also occurs in an alternative microglia cell line, in peripheral macrophages and in primary cells. These findings suggest that endogenous RGS10 interacts with STIM2 in microglia and peripheral immune cells.

STIM2 is an endoplasmic reticulum (ER)-localized calcium (Ca^{2+}) sensor that detects changes in store calcium levels (Berna-Erro et al., 2017; Hoth & Niemeyer, 2013). There are two known homologues of STIM proteins; both function as ER Ca^{2+} sensors and are involved in positive regulation of inflammatory signaling pathways (Kar & Parekh, 2013). Despite its homology and similar molecular functions, our proteomic and follow-up validation experiments did not identify interaction of RGS10 with STIM1. STIM2 monitors ER Ca^{2+} and couples receptor-mediated store depletion to extracellular Ca^{2+} entry through plasma membrane Ca^{2+}-release-activated calcium (CRAC) channels, a mechanism known as store-operated calcium entry (SOCE) (Berna-Erro et al., 2017; Nelson et al., 2018; Ong et al., 2015). A prominent response after SOCE is the Ca^{2+}/calmodulin-dependent activation of the phosphatase calcineurin (Hogan & Rao, 2015; Kar & Parekh, 2013), which is a molecular target of various immunosuppressive drugs (Crabtree, 2001). Previous evidence implicates pro-inflammatory and neurotoxic functions of STIM2; loss of STIM2 provides protection in preclinical models of traumatic brain injury and multiple sclerosis (Secondo et al., 2018). STIM2 has also been implicated in LPS/TLR4 signaling; STIM2 null mice were shown to be resistant to LPS-induced inflammation, and macrophages isolated from these mice have reduced production of TNFα, IL-6, and IL-1β (Michaelis et al., 2015). However, it is unknown whether STIM2 plays a role in microglial anti-inflammatory response.

Since the SOCE pathway promotes pro-inflammatory responses that are differentially regulated by RGS10, we hypothesized that there is a functional link between RGS10 and the STIM2/SOCE pathway. We tested this hypothesis by inhibiting STIM2, SOCE, or calcineurin and examining the effect on LPS-induced COX-2 production. We confirmed that siRNA-mediated suppression of STIM2, or pharmacological inhibition of SOCE and calcineurin in BV2 microglia,

significantly downregulates LPS-stimulated COX-2 expression, and these findings were validated in an alternative microglia cell line. We further confirmed findings in primary microglia by examining COX-2 transcript suppression in response to cotreatment of LPS with the SOCE inhibitor. These results showed the first evidence of the role of STIM2/SOCE/calcineurin in the regulation of COX-2 in microglia. To determine whether the STIM2/SOCE/calcineurin pathway also mediates the anti-inflammatory effects of RGS10, we performed similar experiments in control and RGS10 knockout BV2 cells where endogenous RGS10 is deleted using CRISPR/Cas9. When STIM2 expression or SOCE/calcineurin function is inhibited, RGS10 was unable to regulate LPS-induced COX-2 production. In addition to COX-2, we further confirmed that inhibition of SOCE reduces the expression of TNFα and IL-6, which were validated in both BV2 and primary microglia. These results suggested that the anti-inflammatory mechanism of RGS10 downstream of TLR4 activation requires the STIM2/SOCE/calcineurin pathway.

If the function of RGS10 is dependent on SITM2, we expected that the anti-inflammatory effect of RGS10 would not be limited to TLR4 signaling and RGS10 may mediate pro-inflammatory responses downstream of other receptors that trigger store $Ca2^{+}$ release. Indeed, our study is the first to identify an anti-inflammatory effect of RGS10 in the regulation of thrombin signaling, which is a physiologically relevant endogenous stimulus that activates protease-activated receptor 1 (PAR-1) (Suo et al., 2002), which is a multifunctional GPCR. Furthermore, we confirmed that SOCE is required for RGS10-mediated regulation of pro-inflammatory genes stimulated by thrombin. Collectively, our findings reveal that RGS10 negatively regulates LPS- and thrombin-mediated pro-inflammatory responses through a common downstream mechanism that involves SOCE, thereby implicating a broad anti-inflammatory effect of RGS10 in microglia.

Given that RGS10 and STIM2/SOCE have an antagonistic effect on pro-inflammatory responses, we hypothesized that RGS10 functions to regulate SOCE in microglia. This hypothesis was tested by monitoring live Ca^{2+} dynamics in control and RGS10 knockout BV2 cells loaded with a cytoplasmic Ca^{2+} indicator. We specifically monitored extracellular Ca^{2+} entry after store calcium depletion using a sarco/ER Ca^{2+}-ATPase (SERCA) channel inhibitor. Our findings indicate that loss of RGS10 enhances SOCE in response to ER depletion, implicating a novel role of RGS10 in SOCE regulation. Our findings from **Chapter 3** collectively indicate that the anti-inflammatory function of RGS10 requires a functional interaction with store calcium machinery and activation of the SOCE pathway.

We have previously shown that the RGS10 E66K GAP-dead mutant (EK), although incapable of interacting with Gαi proteins, can suppress LPS-induced expression of TNFα in TLR4-overexpressing HEK293 cells (HEK-Blue hTLR4), similar to wild-type RGS10 (WT), supporting the G protein-independent role of RGS10 (Alqinyah et al., 2018). However, this study was performed in HEK-Blue hTLR4 cells due to the low expression of endogenous RGS10, and this cell line does not fully mimic inflammatory responses that occur in microglia, such as COX-2 induction. In **Chapter 4**, we extended the previous findings and generated human RGS10-1 overexpression BV2 cell lines in RGS10 knockout BV2 cells to investigate the effect of WT and EK RGS10 on the regulation of TLR4 signaling in microglia. Although endogenous mouse RGS10 was substituted with a human RGS10-1 isoform, we confirmed that both the endogenous RGS10 (in CRISPR-Cas9 control cells) and the reexpressed WT human RGS10 in the knockout background (KO-WT), could interact with activated Gαi. This result is expected since the RGS-Gαi interaction surface is conserved between species (Sierra et al., 2002). We also validated that

the reexpressed EK variant cannot interact with Gαi3. Our signaling results showed that deletion of RGS10 causes upregulation of LPS-induced COX-2 and IL-6 expression, while reexpression of both WT and EK RGS10 similarly suppressed these effects. These results further confirmed that the ability of RGS10 to regulate TLR4 signaling is not mediated by a canonical mechanism that requires interaction with Gαi.

So far, our study focused on the role of RGS10 in the regulation of COX-2, TNFα and IL-6. However, RGS10 may also regulate expression of other genes downstream of TLR4 activation and is also involved in various functions in other cellular and disease models (Almutairi et al., 2020; Lee & Tansey, 2015). The fact that RGS10 interacts with multiple binding partners suggests a potential diverse role for RGS10 in both resting and activated conditions. Therefore, in **Chapter 4,** we also performed a transcriptome analysis to investigate the global effect of RGS10-mediated gene regulation in microglia, which is the first unbiased large-scale study to examine the function of RGS10. Using RNA-sequencing (RNA-seq), we determined transcriptome alterations induced by CRISPR-Cas9-mediated deletion of RGS10 in resting and LPS-activated microglia.

Our RNA-seq analysis identified 576 differentially expressed genes (DEGs) in resting RGS10 knockout BV2cells, and a greater number of DEGs in cells activated with LPS. A large portion of DEGs identified in RGS10 knockout cells were also shared under both resting and activated conditions, and functional enrichment analysis revealed significant upregulation of biological processes involved in viral defense, cytokine production, and immune/inflammatory processes. Pathway analysis further confirmed enrichment of viral defense pathways, type I and II interferon response pathways, and TNFα signaling via NFκB, which were all upregulated in RGS10 knockout cells. While these effects were observed in both resting and activated samples, there was a more

robust enrichment of inflammatory and stress response pathways in cells activated by LPS. We specifically found an enrichment of the unfolded protein response pathway and apoptosis pathways in DEGs exclusively upregulated by RGS10 in LPS-activated microglia. Additional analysis of transcription factor-gene regulatory network pathways identified that a large subset of the upregulated DEGs in RGS10 knockout cells were targets of several members of the interferon regulatory factors (IRFs) and the NFκB family of transcription factors. A select few of the differentially regulated genes were validated using qRT-PCR in control and RGS10 knockout BV2 cells, which showed a strong correlation with the RNA-seq data. Overall, our RNA-seq data and functional enrichment analysis demonstrate that RGS10 has broad effects in regulating innate immune and inflammatory response pathways in both resting and activated cells.

5.1. Limitations and future direction

5.1.1. Unexpected consequence of CRISPR-Cas9 RGS10 knockout

One of the main surprising findings in Chapter 4 is that CRISPR/Cas9-mediated editing of RGS10 induced skipping of the exon targeted by the sgRNA (exon 2). This resulted in the expression of a truncated form of *Rgs10* transcript, as determined by exon-level count analysis, visualization of junctional reads, and experimental validation using primers for upstream and downstream exons. This result suggested that our presumed CRISPR/Cas9 RGS10 knockout cells express a short form of *Rgs10* transcript that lacks exon 2. Although we have not detected RGS10 protein expression using two different antibodies (commercial goat c-20 antibody and antibody generated in collaboration with the UGA bioexpression and fermentation core), it is possible that the short RGS10 transcript may contain a start codon with an open reading frame that translates into a truncated RGS10 protein, which lacks the epitope detected by the RGS10 antibodies. Recent

studies have revealed a similar unintended effect of CRISPR-Cas9 where sgRNA-targeted exons are skipped, leading to the production of truncated forms of protein with a distinct gain-of-function phenotype (Mou et al., 2017; Sharpe & Cooper, 2017; Tuladhar et al., 2019). Therefore, future sequencing analysis should characterize the CRISPR/Cas9 RGS10 knockout cells to identify potential in-frame mutations or premature termination codon, with protein-coding potential. This may lead to the production of a truncated form of RGS10 that may have a partial functional protein or aberrant gain of function, as previously reported (Mou et al., 2017; Tuladhar et al., 2019). Our findings, combined with the recent reports showing an unintended effect of CRISPR/Cas9, highlight the need to improve quality control to screen mutant clones and validating data using different approaches, including transient gene silencing, shRNA-based stable knockdown methods, as well as in primary cells isolated from transgenic models.

Given the identified unexpected consequence of CRISPR/Cas9, it is important to define which DEGs and enriched biological processes/pathways identified in this study are caused by the loss of wild-type RGS10, and which are the results of a potential gain of function or off-target effects of exon skipping induced by CRISPR/Cas9. Therefore, this RNA-seq study is currently being repeated in wild-type and RGS10 knockout primary cells to better characterize RGS10-mediated transcriptional alterations in microglia.

5.1.2. RNA-seq validation

One of the most notable observations from our RNA-seq study is the fact that a large portion of the upregulated DEGs in both resting and activated RGS10 knockout cells are enriched in interferon response pathways and are involved in biological processes related to defense response to virus, such as the influenza pathway. Furthermore, the SARS-COV2 innate immune

invasion pathway and lung fibrosis pathway were shown to be enriched in RGS10 knockout cells. These results support a recent study that implicated RGS10 in viral response functions. Almutairi et al. (2021) demonstrated that loss of RGS10 enhances immune and inflammatory responses and exacerbates lung damage in influenza-infected lungs (Almutairi et al., 2021). Pro-inflammatory cytokines (such as TNFα, IL-6 and IL-1β) and interferons are known for their potent antiviral effects (Costela-Ruiz et al., 2020). Microglia secrete pro-inflammatory cytokines and interferons as an antiviral defense mechanism to protect the brain; however, chronic viral infection and associated pro-inflammatory responses are associated with accelerated brain aging and long-term neurodegeneration (Filgueira et al., 2021). Therefore, the anti-inflammatory function of RGS10 may be linked to its role in viral defense response. Given these findings, our currently ongoing RNA-seq study in primary microglia extends our results in Chapter 4 and incorporates interferon-gamma (IFNγ) and IFNγ+LPS as additional treatment groups. IFNγ is a type II interferon that triggers an adaptive and antiviral immune response (Lee & Ashkar, 2018). We included LPS+IFNγ treatment group, as previous studies have shown that it is a suitable model for neuroinflammation, since it can mimic a microglial activation state induced by the co-presence of damage-associated molecular patterns (DAMPs) acting on TLRs, together with the IFNγ secreted by CNS cells (Gresa-Arribas et al., 2012). A recent transcriptome study has further confirmed that the two stimuli generate distinct gene expression patterns and can help induce different inflammation profiles in primary microglia (Pulido-Salgado et al., 2018). Therefore, our ongoing RNA-seq study in primary microglia (incorporating control, LPS, IFNγ and LPS+IFNγ treatment groups) can help identify the different roles and mechanisms of RGS10 in resting microglia and in response to LPS and IFNγ signaling.

One of the most interesting findings from our RNA-seq data was the enrichment of the unfolded protein response (UPR) pathway, which was specifically upregulated in LPS-activated RGS10 knockout cells. The UPR pathway is activated in response to pathological insults that induce misfolded protein buildup, ER stress, and dysregulation (Garcia-Gonzalez et al., 2018). UPR is initially triggered as a protective mechanism to restore cell homeostasis by blocking protein translation to limit misfolding of proteins. When this fails, UPR triggers the pro-apoptotic pathway by upregulating and activating transcription factor effectors, including ATF4/CHOP, and IRE1 (Van Vliet et al., 2018) A subset of DEGs upregulated in LPS-activated RGS10 knockout cells was shown to be targets for activated transcription factor (ATF4), which is involved in biological responses related to ER stress (Van Vliet et al., 2018). The ATF/CHOP complex and the IRE1 complex were also among the most enriched compartments in LPS-activated RGS10 knockout cells. Chronic ER stress and UPR activation promotes neuroinflammation and are implicated in the pathogenesis of various neurodegenerative diseases (Hiramatsu et al., 2015). Activation of the UPR pathway has been shown to be triggered by loss of ER calcium (Preissler et al., 2020), which induces extracellular calcium entry (Preissler et al., 2020). Since our data shows that loss of RGS10 upregulates SOCE in response to ER depletion, the upregulated UPR pathway identified in the RNA-seq data may be related to its role in regulating SOCE. However, the potential involvement of RGS10 in UPR pathway should be determined in a future RNA-seq study in primary microglia, since one of the UPR marker and ATF4-target gene *(Ppp1r15a)*, identified as DEG in LPS-activated CRISPR/Cas9 KO cells, did not show a difference in primary microglia. Therefore, our ongoing RNA-seq studies in primary microglia can help validate if the UPR pathway is linked to the RGS10-STIM2/SOCE pathway.

5.1.3. Functional interaction of RGS10 and STIM2

Given the collective findings of Chapter 3 & 4, future studies should fill the gap in knowledge and address some limitations. The main findings of Chapter 3 are validated in primary microglia, such as the RGS10-STIM2 interaction and the requirement of SOCE for the anti-inflammatory function of RGS10. However, due to the limited supply of primary microglia, gene silencing experiments that evaluated the functional interaction of RGS10 and STIM2 were not validated in primary microglia. To address this limitation and further examine the functional response of RGS10 and STIM2 in an intact system, we recently generated four different transgenic mice with single and double knockout of RGS10 and STIM2. Global STIM2 knockout mice have developmental defects and are known to have a reduced survival rate (4-6 weeks) (Oh-Hora et al., 2008); therefore, we generated a conditional STIM2 fl/fl mouse line with CSF1R-driven Cre expression to induce targeted knockout of STIM2 in the monocyte / macrophage / microglia population. We generated four experimental transgenic lines: 1) RGS10+/+ and STIM2+/+ (RGS10wt/wt, Stim2 fl/fl, Csf1r, cre-), 2) RGS10-/- and STIM2+/+ (RGS10-/-, Stim2 fl/fl, Csf1r, cre-), 3) RGS10+/+ and STIM2-/- (RGS10wt/wt, Stim2 fl/fl, Csf1r, cre+) and 4) RGS10-/- and STIM2-/- (RGS10-/-, Stim2 fl/fl, Csf1r, cre+) (**Figure A.2A**). In a preliminary study, we isolated primary cells from synchronized litters and validated our finding from Chapter 3 by examining LPS-induced expression of COX-2. Consistent with our previous result in the CRISPR-Cas9 control and RGS10 knockout BV2 model, in which STIM2 expression was manipulated by siRNA, Cre-mediated knockdown of STIM2 blocked upregulated expression of COX-2, caused by RGS10 knockout (**Figure A.2B-D**). These results further confirmed that STIM2 is essential for RGS10-mediated regulation of pro-inflammatory genes in response to LPS. Our preliminary analysis of

STIM2 expression demonstrated a partial loss of STIM2, which may be attributed to incomplete Cre induction or microglial contamination. Therefore, ongoing studies are examining the expression of STIM2 in different cell types and optimizing experimental conditions to obtain pure microglia.

Future studies using these single and double knockout transgenic models will help examine the functional interaction of RGS10 and STIM2 in primary microglia and *in vivo*, in a relevant model of neuroinflammation. For example, important biological processes and pathways identified from RNA-seq data in primary microglia can be validated in cells isolated from these four transgenic groups to determine if STIM2 is involved in other functions and pathways regulated by RGS10. Furthermore, our findings showed that RGS10 regulates SOCE in response to ER depletion, and that the STIM2/SOCE pathway is important for the anti-inflammatory function of RGS10. However, it is not clear if these two responses are linked, and if the functional interaction of RGS10 and STIM2 is important for RGS10-mediated regulation of SOCE. This question can be examined in primary microglia isolated from generated transgenic lines by comparing SOCE in single and double RGS10/STIM2 knockout microglia.

5.1.4. Downstream transcription factors

Although we have shown that the anti-inflammatory effect of RGS10 requires the STIM2/SOCE/calcineurin pathway, we do not yet know what transcription factor is essential for RGS10-sensitive gene regulation. The direct transcription target of calcineurin is the nuclear factor of activated T cells (NFAT), which upon dephosphorylation by calcineurin, translocates to the nucleus and activates inflammatory genes (Park et al., 2020). NFAT function is extensively studied in lymphocytes and other immune cells, and at least four Ca^{2+}/calcineurin- activated NFAT

isoforms have been previously been identified (Vaeth & Feske, 2018). We previously examined the effect of a pan-NFAT inhibitor (VIVIT peptide) to determine if NFAT is involved in the anti-inflammatory mechanism of RGS10; however, we only detected NFAT-sensitive inhibition of RGS10 function at a toxic dose (data not shown). Since we were unable to determine the cell permeability of this peptide, future studies should examine whether RGS10 alters nuclear translocation and activation of NFAT isoforms.

Recent evidence in lymphocytes demonstrated that the STIM/SOCE-mediated calcium mechanism plays an essential role in activating NFκB (Berry et al., 2018). Although NFκB is not a direct substrate target for calcineurin, calcineurin inhibitors have previously been shown to have a strong effect in inhibiting NFκB activity through unknown mechanism (Vafadari et al., 2013). Previously, it has been shown that RGS10 inhibits NFκB activation in both LPS and TNFα stimulated microglia (Lee et al., 2011). RGS10-mediated inhibition of NFκB has also been implicated in other immune cells (Almutairi et al., 2021; Ren et al., 2021). In our study, we found that TNFα signaling via NFκB is one of the most enriched pathways in RGS10 knockout cells, and this enrichment was more prominent in activated microglia. Furthermore, many DEGs upregulated in RGS10 knockout cells, particularly in response to LPS, were NFκB-regulated target genes. This implies that the downstream mechanism for the anti-inflammatory effects of RGS10 may involve inhibition of the NFκB transcriptional activity. Therefore, our RNA-seq data showing a strong enrichment of NFκB pathway in RGS10 knockout cells, combined with the previously implicated role of RGS10 in NFκB signaling, indicate that the ability of RGS10 to regulate NFκB-targeted genes may be mediated by its functional interaction with components of the store-operated calcium machinery. NFκB and NFAT have been shown to have biochemical interaction, and the full

transcriptional activation of NFAT requires intact NFκB signaling and p65 transcriptional activity (Liu et al., 2012). A recent study in microglia also showed that LPS induces SOCE and activation of both NFAT and NFκB (Mizuma et al., 2019). Therefore, our RNA-seq data and the previously reported role of RGS10 suggest NFκB as a plausible candidate that links RGS10 and the SOCE pathway, to inflammatory gene expression. However, future studies should examine whether the STIM2/SOCE/calcineurin-sensitive effect of RGS10 is mediated by NFAT and NFκB.

5.1.5. RGS10 role in SOCE

In Chapter 3, the standard experimental approach we used to study the function of RGS10 in SOCE is by blocking SERCA Ca^{2+} ATPase using to trigger strong ER depletion. However, this approach has limitations, as it does not mimic physiological receptor-mediated release of ER Ca^{2+} which occurs through activation of the inositol 1,4,5-trisphosphate receptor (IP3R) (Harden et al., 2011). Furthermore, our co-IP data showed that RGS10 interacts specifically with STIM2 and not STIM1, and its interaction with STIM2 occurs in both basal and activated conditions and is not affected by calcium, indicating a constitutive interaction of RGS10 with STIM2. Compared to STIM1, STIM2 has a lower affinity for Ca^{2+}, making it more sensitive to small fluctuation of store calcium (Shalygin et al., 2015; Soboloff et al., 2012). Therefore, the effect of RGS10 on SOCE should be examined using agonists to activate upstream receptors or using lower doses of the SERCA inhibitor.

It is also important to determine whether RGS10 affects SOCE triggered by TLR4 activation, as a recent study demonstrated that LPS can induce SOCE in microglia (Mizuma et al., 2019). However, studying the effect of RGS10 on SOCE using different agonists and a range of doses may not be feasible in primary microglia due to low yield. Furthermore, the low-throughput

live imaging analysis we performed in this study uses a fluorescent Ca^{2+}-sensitive dye, which did not allow us to conduct a longer time course experiment. To address this limitation, we recently generated a lentivirus containing a genetically encoded Ca^{2+} indicator (GECI), which is advantageous due to its less invasive nature and lower photobleaching property, which is advantageous for long-term calcium imaging studies (Zhong & Schleifenbaum, 2019). We have generated stable control and RGS10 knockout BV2 cells encoding GECI and confirmed our previous finding, which showed that loss of RGS10 enhances SOCE (**Figure A.3**). Given the limitation of using the CRISPR/Cas9 RGS10 knockout cells, stable RGS10 knockdown BV2 cells have been generated using two different shRNAs. The GECI lentivirus can be incorporated into these cells for future high-throughput studies.

5.1.6. RGS10-STIM2 interaction

Although this study identified a biochemical interaction between RGS10 and STIM2, it is not clear whether the anti-inflammatory effect of RGS10 and its functional link to STIM2 is mediated by the physical interaction. Future experiments should address this gap in knowledge by characterizing in detail the nature of RGS10-STIM2 interaction. It is not clear whether RGS10 directly binds to STIM2 or if it exists in a multiprotein complex that requires linker proteins. Future studies can test this hypothesis by native gel electrophoresis.

Although RGS10 interacts with both Gαi and STIM2, our preliminary study in WT and EK mutant RGS10 overexpression BV2 cells showed that mutant RGS10 can interact with STIM2 to the same extent as WT RGS10 (data not shown). This implies that the biochemical interaction of RGS10 and STIM2 and the functional link is likely mediated via GAP-independent mechanism. Additionally, while our current findings showed that TLR4 activation does not affect the

interaction of RGS10 with STIM2, this experiment was carried out at a single time point. Therefore, future time-course experiments should characterize transient/dynamic interactions between RGS10-STIM2 and RGS10-Gαi and the possible functional consequence. Furthermore, structure-function studies with truncated forms of RGS10 and SITM2 should be performed to identify protein domains/regions essential for biochemical and functional interaction.

5.1.7. Regulation of RGS10 expression

Chronic inflammatory stimuli, such as LPS and TNFα, have previously been shown to downregulate the expression of RGS10 in microglia (Almutairi et al., 2021; Alqinyah et al., 2017; Lee et al., 2008). One of the interesting findings of our study is that short-term depletion of ER calcium, induced by a 20-minute treatment with SERCA inhibitor, significantly amplified LPS-induced suppression of RGS10, which was also correlated with significant COX-2 induction. This effect was dependent on LPS, as ER depletion did not affect RGS10 expression in cells that were not stimulated with LPS. These results imply that functional loss of RGS10 in response to ER stress may sensitize cells to inflammatory stimuli, leading to upregulated pro-inflammatory responses.

Previous studies have shown that RGS10 is transcriptionally regulated through epigenetic mechanisms (Almutairi et al., 2021; Alqinyah et al., 2017; Hooks & Murph, 2015). However, in this study, store depletion-induced suppression of RGS10 in LPS activated cells was not observed at the transcript level (data not shown), implying a potential post-translational regulatory mechanism. However, this needs to be investigated through time course experiments, since both the protein-level and transcript-level regulation is examined 24 h after LPS treatment. Therefore, transcriptional suppression may have occurred at earlier time points, and RGS10 transcript may

have recovered at the time point examined for this study. This hypothesis can be tested using time-course experiments, as well as by inhibiting histone deacetylase (HDAC), which has previously been shown to rescue LPS-induced suppression of the *Rgs10* transcript in microglia (Alqinyah et al., 2017). Alternatively, the post-translational RGS10 regulation mechanism can be investigated by inhibiting the ubiquitin-proteasome complex. Zhu et al. (2020) recently identified interactions between RGS10 and the E3 ubiquitin tripartite motif protein 32 (TRIM32) (Zhu et al., 2020). RGS10 protein was shown to be ubiquitinated and subsequently degraded by TRIM32 in lateral/medial ganglionic eminence (L/MGE) progenitor cells which was also validated in Hela cells and in embryonic brain. Therefore, future studies should examine if TRIM32 is involved in regulating RGS10 stability in response to ER-stress and inflammation.

5.1.8. Non-canonical RGS10 interactions

In addition to STIM2, our result identified 22 other non-canonical RG10 interacting partners in microglia that have diverse molecular functions (**Table A.1**). Future studies should determine whether RGS10 affects the function of these proteins, and if these proteins regulate the expression or function of RGS10. Since suppression of RGS10 has detrimental effects in various cellular and disease models, it is important to identify potential mechanisms that stabilize RGS10 protein and rescue its functional loss during inflammation and aging. In our proteomic findings, we identified two RGS10-interacting E3 ligase proteins: STIP1 homology and U box-containing protein 1 (STUB1) and E3 ubiquitin-protein ligase RNF146. RGS10 contains a few post-translational modification sites, including a conserved lysine residue (Lys148) that is a putative ubiquitination site. Since our study identified suppression of RGS10 protein induced by ER stress-related priming of LPS, it is important to determine if either TRIM32 or the identified RGS10-interacting E3

ubiquitin ligase mediate degradation of RGS10. RGS10 is also regulated by phosphorylation; therefore, the identified RGS10-interacting protein kinases and phosphatases may play an essential role in modulating the subcellular localization and function of RGS10.

Furthermore, since RGS10 contains only the conserved RGS domain, it is important to determine if other RGS proteins also interact with these binding partners, or if the interactions are specific to RGS10, which may implicate additional noncanonical GAP-independent functions of RGS10.

5.2. Conclusion and Implications

Neurodegenerative diseases commonly affect people in their mid to late years, and the prevalence is expected to increase as the general population ages. Despite significant progress in basic and clinical research, there are currently no effective treatments for neurodegenerative diseases, and there is an urgent need to identify and target the underlying molecular mechanisms that contribute to the onset and development of neurodegenerative diseases. Growing evidence showed that age-associated changes in microglia activation, such as hypersensitive response and production of pro-inflammatory and neurotoxic mediators, contribute to progressive neurodegeneration. Therefore, mechanisms that regulate chronic microglia activation and inhibit neurotoxic microglia-neuron crosstalk are potential therapeutic targets for neurodegenerative diseases.

RGS10 exerts anti-inflammatory and neuroprotective functions in microglia, but its expression is dynamically suppressed in response to chronic stress, inflammation, and aging. Current drug screening efforts are focusing on stabilizing RGS10 to rescue its functional loss during inflammation. However, strategies that alter RGS10 expression should take into account the

various functions of RGS10 in homeostatic and inflammatory conditions. Therefore, understanding the molecular mechanism of RGS10 allows for alternative modulation of specific pathways involved in important functions of RGS10.

In this study, we show that RGS10 negatively regulates pro-inflammatory gene expression in microglia through a noncanonical mechanism, independent of its GAP function. Our findings demonstrate that RGS10 biochemically and functionally interacts with STIM2, which is a component of the store-operated calcium entry (SOCE) machinery. We also determined that STIM2 and the SOCE pathway are essential for promoting pro-inflammatory gene expression in microglia and that the anti-inflammatory effects of RGS10 require functional interaction with the SOCE machinery.

The SOCE pathway promotes chronic inflammation and is involved in the pathogenesis of various neurodegenerative diseases. Therefore, the ability of RGS10 to interact with STIM2 and regulate SOCE exposes a novel mechanism for RGS10 and provides an additional therapeutic target that can be modulated to compensate for the functional loss of RGS10 during inflammation. Given that RGS10 is small and lacks a functional domain outside the conserved RGS domain, the identified anti-inflammatory mechanism and diverse non-canonical interacting partners also have other implications. It challenges the notion that the RGS domain exclusively mediates G protein-dependent function, and it opens avenues for exploring the functions of RGS10 and other small RGS proteins. Furthermore, the anti-inflammatory mechanism of RGS10 has implication beyond neuroinflammation, including diverse pathologies in which RGS10 functions are implicated, such as Rheumatoid arthritis, multiple sclerosis, vascular injury, viral infection, and bone disorders.

References

Abud, E. M., Ramirez, R. N., Martinez, E. S., Healy, L. M., Nguyen, C. H. H., Newman, S. A., . . . Blurton-Jones, M. (2017). iPSC-Derived Human Microglia-like Cells to Study Neurological Diseases. *Neuron, 94*(2), 278-293 e279. doi:10.1016/j.neuron.2017.03.042

Ajami, B., Bennett, J. L., Krieger, C., Tetzlaff, W., & Rossi, F. M. (2007). Local self-renewal can sustain CNS microglia maintenance and function throughout adult life. *Nat Neurosci, 10*(12), 1538-1543. doi:10.1038/nn2014

Ajit, S. K., & Young, K. H. (2005). Analysis of chimeric RGS proteins in yeast for the functional evaluation of protein domains and their potential use in drug target validation. *Cell Signal, 17*(7), 817-825. doi:10.1016/j.cellsig.2004.11.003

Alawieyah Syed Mortadza, S., Sim, J. A., Neubrand, V. E., & Jiang, L. H. (2018). A critical role of TRPM2 channel in Abeta42 -induced microglial activation and generation of tumor necrosis factor-alpha. *Glia, 66*(3), 562-575. doi:10.1002/glia.23265

Ali, M. W., Cacan, E., Liu, Y., Pierce, J. Y., Creasman, W. T., Murph, M. M., . . . Hooks, S. B. (2013). Transcriptional suppression, DNA methylation, and histone deacetylation of the regulator of G-protein signaling 10 (RGS10) gene in ovarian cancer cells. *PLoS One, 8*(3), e60185. doi:10.1371/journal.pone.0060185

Alliot, F., Godin, I., & Pessac, B. (1999). Microglia derive from progenitors, originating from the yolk sac, and which proliferate in the brain. *Brain Res Dev Brain Res, 117*(2), 145-152. doi:10.1016/s0165-3806(99)00113-3

Almutairi, F., Lee, J. K., & Rada, B. (2020). Regulator of G protein signaling 10: Structure, expression and functions in cellular physiology and diseases. *Cell Signal, 75*, 109765. doi:10.1016/j.cellsig.2020.109765

Almutairi, F., Sarr, D., Tucker, S. L., Fantone, K., Lee, J. K., & Rada, B. (2021). RGS10 Reduces Lethal Influenza Infection and Associated Lung Inflammation in Mice. *Front Immunol, 12*, 772288. doi:10.3389/fimmu.2021.772288

Almutairi, F., Tucker, S. L., Sarr, D., & Rada, B. (2021). PI3K/ NF-kappaB-dependent TNF-alpha and HDAC activities facilitate LPS-induced RGS10 suppression in pulmonary macrophages. *Cell Signal, 86*, 110099. doi:10.1016/j.cellsig.2021.110099

Alqinyah, M., Almutairi, F., Wendimu, M. Y., & Hooks, S. B. (2018). RGS10 Regulates the Expression of Cyclooxygenase-2 and Tumor Necrosis Factor Alpha through a G Protein-Independent Mechanism. *Mol Pharmacol, 94*(4), 1103-1113. doi:10.1124/mol.118.111674

Alqinyah, M., Maganti, N., Ali, M. W., Yadav, R., Gao, M., Cacan, E., . . . Hooks, S. B. (2017). Regulator of G Protein Signaling 10 (Rgs10) Expression Is Transcriptionally Silenced in Activated Microglia by Histone Deacetylase Activity. *Mol Pharmacol, 91*(3), 197-207. doi:10.1124/mol.116.106963

Amici, S. A., Dong, J., & Guerau-de-Arellano, M. (2017). Molecular Mechanisms Modulating the Phenotype of Macrophages and Microglia. *Front Immunol, 8*, 1520. doi:10.3389/fimmu.2017.01520

Aminzadeh, M., Roghani, M., Sarfallah, A., & Riazi, G. H. (2018). TRPM2 dependence of ROS-induced NLRP3 activation in Alzheimer's disease. *Int Immunopharmacol, 54*, 78-85. doi:10.1016/j.intimp.2017.10.024

An, J. Y., Pang, H. G., Huang, T. Q., Song, J. N., Li, D. D., Zhao, Y. L., & Ma, X. D. (2018). AG490 ameliorates early brain injury via inhibition of JAK2/STAT3-mediated regulation of HMGB1 in subarachnoid hemorrhage. *Exp Ther Med, 15*(2), 1330-1338. doi:10.3892/etm.2017.5539

Anders, S., Pyl, P. T., & Huber, W. (2015). HTSeq--a Python framework to work with high-throughput sequencing data. *Bioinformatics, 31*(2), 166-169. doi:10.1093/bioinformatics/btu638

Anderson, C. F., & Mosser, D. M. (2002). Cutting edge: biasing immune responses by directing antigen to macrophage Fc gamma receptors. *J Immunol, 168*(8), 3697-3701. doi:10.4049/jimmunol.168.8.3697

Andrew, S. (2010). FastQC: A Quality Control Tool for High Throughput Sequence Data. Retrieved from http://www.bioinformatics.babraham.ac.uk/projects/fastqc/

Anwar, S., Pons, V., & Rivest, S. (2020). Microglia Purinoceptor P2Y6: An Emerging Therapeutic Target in CNS Diseases. *Cells, 9*(7). doi:10.3390/cells9071595

Anwar, S., & Rivest, S. (2020). Alzheimer's disease: microglia targets and their modulation to promote amyloid phagocytosis and mitigate neuroinflammation. *Expert Opin Ther Targets, 24*(4), 331-344. doi:10.1080/14728222.2020.1738391

Arimoto, T., Choi, D. Y., Lu, X., Liu, M., Nguyen, X. V., Zheng, N., . . . Bing, G. (2007). Interleukin-10 protects against inflammation-mediated degeneration of dopaminergic neurons in substantia nigra. *Neurobiol Aging, 28*(6), 894-906. doi:10.1016/j.neurobiolaging.2006.04.011

Aronowski, J., & Zhao, X. (2011). Molecular pathophysiology of cerebral hemorrhage: secondary brain injury. *Stroke, 42*(6), 1781-1786. doi:10.1161/STROKEAHA.110.596718

Asai, H., Ikezu, S., Tsunoda, S., Medalla, M., Luebke, J., Haydar, T., . . . Ikezu, T. (2015). Depletion of microglia and inhibition of exosome synthesis halt tau propagation. *Nat Neurosci, 18*(11), 1584-1593. doi:10.1038/nn.4132

Askew, K., Li, K., Olmos-Alonso, A., Garcia-Moreno, F., Liang, Y., Richardson, P., . . . Gomez-Nicola, D. (2017). Coupled Proliferation and Apoptosis Maintain the Rapid Turnover of Microglia in the Adult Brain. *Cell Rep, 18*(2), 391-405. doi:10.1016/j.celrep.2016.12.041

Asmamaw, M., & Zawdie, B. (2021). Mechanism and Applications of CRISPR/Cas-9-Mediated Genome Editing. *Biologics, 15*, 353-361. doi:10.2147/BTT.S326422

Au, N. P. B., & Ma, C. H. E. (2017). Recent Advances in the Study of Bipolar/Rod-Shaped Microglia and their Roles in Neurodegeneration. *Front Aging Neurosci, 9*, 128. doi:10.3389/fnagi.2017.00128

Austin, S. A., Floden, A. M., Murphy, E. J., & Combs, C. K. (2006). Alpha-synuclein expression modulates microglial activation phenotype. *J Neurosci, 26*(41), 10558-10563. doi:10.1523/JNEUROSCI.1799-06.2006

Azam, S., Haque, M. E., Jakaria, M., Jo, S. H., Kim, I. S., & Choi, D. K. (2020). G-Protein-Coupled Receptors in CNS: A Potential Therapeutic Target for Intervention in Neurodegenerative Disorders and Associated Cognitive Deficits. *Cells, 9*(2). doi:10.3390/cells9020506

Babu, R., Bagley, J. H., Di, C., Friedman, A. H., & Adamson, C. (2012). Thrombin and hemin as central factors in the mechanisms of intracerebral hemorrhage-induced secondary brain injury and as potential targets for intervention. *Neurosurg Focus, 32*(4), E8. doi:10.3171/2012.1.FOCUS11366

Bachstetter, A. D., Ighodaro, E. T., Hassoun, Y., Aldeiri, D., Neltner, J. H., Patel, E., . . . Nelson, P. T. (2017). Rod-shaped microglia morphology is associated with aging in 2 human autopsy series. *Neurobiol Aging, 52*, 98-105. doi:10.1016/j.neurobiolaging.2016.12.028

Bachstetter, A. D., Morganti, J. M., Jernberg, J., Schlunk, A., Mitchell, S. H., Brewster, K. W., . . . Gemma, C. (2011). Fractalkine and CX 3 CR1 regulate hippocampal neurogenesis in adult and aged rats. *Neurobiol Aging, 32*(11), 2030-2044. doi:10.1016/j.neurobiolaging.2009.11.022

Bachstetter, A. D., Van Eldik, L. J., Schmitt, F. A., Neltner, J. H., Ighodaro, E. T., Webster, S. J., . . . Nelson, P. T. (2015). Disease-related microglia heterogeneity in the hippocampus of Alzheimer's disease, dementia with Lewy bodies, and hippocampal sclerosis of aging. *Acta Neuropathol Commun, 3*, 32. doi:10.1186/s40478-015-0209-z

Balce, D. R., Li, B., Allan, E. R., Rybicka, J. M., Krohn, R. M., & Yates, R. M. (2011). Alternative activation of macrophages by IL-4 enhances the proteolytic capacity of their phagosomes through synergistic mechanisms. *Blood, 118*(15), 4199-4208. doi:10.1182/blood-2011-01-328906

Bang, S., Jeong, S., Choi, N., & Kim, H. N. (2019). Brain-on-a-chip: A history of development and future perspective. *Biomicrofluidics, 13*(5), 051301. doi:10.1063/1.5120555

Bansal, G., Xie, Z., Rao, S., Nocka, K. H., & Druey, K. M. (2008). Suppression of immunoglobulin E-mediated allergic responses by regulator of G protein signaling 13. *Nat Immunol, 9*(1), 73-80. doi:10.1038/ni1533

Batista, C.R.A., et al., *Lipopolysaccharide-Induced Neuroinflammation as a Bridge to Understand Neurodegeneration.* Int J Mol Sci, 2019. **20**(9).

Barbier, P., Zejneli, O., Martinho, M., Lasorsa, A., Belle, V., Smet-Nocca, C., . . . Landrieu, I. (2019). Role of Tau as a Microtubule-Associated Protein: Structural and Functional Aspects. *Front Aging Neurosci, 11*, 204. doi:10.3389/fnagi.2019.00204

Benner, E. J., Mosley, R. L., Destache, C. J., Lewis, T. B., Jackson-Lewis, V., Gorantla, S., . . . Gendelman, H. E. (2004). Therapeutic immunization protects dopaminergic neurons in a mouse model of Parkinson's disease. *Proc Natl Acad Sci U S A, 101*(25), 9435-9440. doi:10.1073/pnas.0400569101

Bennett, M. L., Bennett, F. C., Liddelow, S. A., Ajami, B., Zamanian, J. L., Fernhoff, N. B., . . . Barres, B. A. (2016). New tools for studying microglia in the mouse and human CNS. *Proc Natl Acad Sci U S A, 113*(12), E1738-1746. doi:10.1073/pnas.1525528113

Berman, D. M., Kozasa, T., & Gilman, A. G. (1996). The GTPase-activating protein RGS4 stabilizes the transition state for nucleotide hydrolysis. *J Biol Chem, 271*(44), 27209-27212. doi:10.1074/jbc.271.44.27209

Berna-Erro, A., Jardin, I., Salido, G. M., & Rosado, J. A. (2017). Role of STIM2 in cell function and physiopathology. *J Physiol, 595*(10), 3111-3128. doi:10.1113/JP273889

Berna-Erro, A., Jardin, I., Salido, G. M., & Rosado, J. A. (2017). Role of STIM2 in cell function and physiopathology. *The Journal of physiology*.

Berry, C. T., May, M. J., & Freedman, B. D. (2018). STIM- and Orai-mediated calcium entry controls NF-kappaB activity and function in lymphocytes. *Cell Calcium, 74*, 131-143. doi:10.1016/j.ceca.2018.07.003

Bertram, L. (2009). Alzheimer's disease genetics current status and future perspectives. *Int Rev Neurobiol, 84*, 167-184. doi:10.1016/S0074-7742(09)00409-7

Bhaskar, K., Konerth, M., Kokiko-Cochran, O. N., Cardona, A., Ransohoff, R. M., & Lamb, B. T. (2010). Regulation of tau pathology by the microglial fractalkine receptor. *Neuron, 68*(1), 19-31. doi:10.1016/j.neuron.2010.08.023

Bido, S., Muggeo, S., Massimino, L., Marzi, M. J., Giannelli, S. G., Melacini, E., . . . Broccoli, V. (2021). Microglia-specific overexpression of alpha-synuclein leads to severe dopaminergic neurodegeneration by phagocytic exhaustion and oxidative toxicity. *Nat Commun, 12*(1), 6237. doi:10.1038/s41467-021-26519-x

Binder, J. X., Pletscher-Frankild, S., Tsafou, K., Stolte, C., O'Donoghue, S. I., Schneider, R., & Jensen, L. J. (2014). COMPARTMENTS: unification and visualization of protein subcellular localization evidence. *Database (Oxford), 2014*, bau012. doi:10.1093/database/bau012

Bisht, K., Sharma, K., Lacoste, B., & Tremblay, M. E. (2016). Dark microglia: Why are they dark? *Commun Integr Biol, 9*(6), e1230575. doi:10.1080/19420889.2016.1230575

Bisht, K., Sharma, K. P., Lecours, C., Sanchez, M. G., El Hajj, H., Milior, G., . . . Tremblay, M. E. (2016). Dark microglia: A new phenotype predominantly associated with pathological states. *Glia, 64*(5), 826-839. doi:10.1002/glia.22966

Blasi, E., Barluzzi, R., Bocchini, V., Mazzolla, R., & Bistoni, F. (1990). Immortalization of murine microglial cells by a v-raf/v-myc carrying retrovirus. *J Neuroimmunol, 27*(2-3), 229-237. doi:10.1016/0165-5728(90)90073-v

Boche, D., Perry, V. H., & Nicoll, J. A. (2013). Review: activation patterns of microglia and their identification in the human brain. *Neuropathol Appl Neurobiol, 39*(1), 3-18. doi:10.1111/nan.12011

Boka, G., Anglade, P., Wallach, D., Javoy-Agid, F., Agid, Y., & Hirsch, E. C. (1994). Immunocytochemical analysis of tumor necrosis factor and its receptors in Parkinson's disease. *Neurosci Lett, 172*(1-2), 151-154. doi:10.1016/0304-3940(94)90684-x

Bolger, A. M., Lohse, M., & Usadel, B. (2014). Trimmomatic: a flexible trimmer for Illumina sequence data. *Bioinformatics, 30*(15), 2114-2120. doi:10.1093/bioinformatics/btu170

Bolos, M., Llorens-Martin, M., Jurado-Arjona, J., Hernandez, F., Rabano, A., & Avila, J. (2016). Direct Evidence of Internalization of Tau by Microglia In Vitro and In Vivo. *J Alzheimers Dis, 50*(1), 77-87. doi:10.3233/JAD-150704

Bolos, M., Llorens-Martin, M., Perea, J. R., Jurado-Arjona, J., Rabano, A., Hernandez, F., & Avila, J. (2017). Absence of CX3CR1 impairs the internalization of Tau by microglia. *Mol Neurodegener, 12*(1), 59. doi:10.1186/s13024-017-0200-1

Borghi, R., Marchese, R., Negro, A., Marinelli, L., Forloni, G., Zaccheo, D., . . . Tabaton, M. (2000). Full length alpha-synuclein is present in cerebrospinal fluid from Parkinson's disease and normal subjects. *Neurosci Lett, 287*(1), 65-67. doi:10.1016/s0304-3940(00)01153-8

Branch, M. R., & Hepler, J. R. (2017). Endogenous RGS14 is a cytoplasmic-nuclear shuttling protein that localizes to juxtanuclear membranes and chromatin-rich regions of the nucleus. *PLoS One, 12*(9), e0184497. doi:10.1371/journal.pone.0184497

Brawek, B., & Garaschuk, O. (2013). Microglial calcium signaling in the adult, aged and diseased brain. *Cell Calcium, 53*(3), 159-169. doi:10.1016/j.ceca.2012.12.003

Brawek, B., Liang, Y., Savitska, D., Li, K., Fomin-Thunemann, N., Kovalchuk, Y., . . . Garaschuk, O. (2017). A new approach for ratiometric in vivo calcium imaging of microglia. *Sci Rep, 7*(1), 6030. doi:10.1038/s41598-017-05952-3

Brawek, B., Schwendele, B., Riester, K., Kohsaka, S., Lerdkrai, C., Liang, Y., & Garaschuk, O. (2014). Impairment of in vivo calcium signaling in amyloid plaque-associated microglia. *Acta Neuropathol, 127*(4), 495-505. doi:10.1007/s00401-013-1242-2

Breitwieser, G. E. (1991). G protein-mediated ion channel activation. *Hypertension, 17*(5), 684-692. doi:10.1161/01.hyp.17.5.684

Broggi, A., & Granucci, F. (2015). Microbe- and danger-induced inflammation. *Mol Immunol, 63*(2), 127-133. doi:10.1016/j.molimm.2014.06.037

Burgon, P. G., Lee, W. L., Nixon, A. B., Peralta, E. G., & Casey, P. J. (2001). Phosphorylation and nuclear translocation of a regulator of G protein signaling (RGS10). *J Biol Chem, 276*(35), 32828-32834. doi:10.1074/jbc.M100960200

Burns, A., & Iliffe, S. (2009). Alzheimer's disease. *BMJ, 338*, b158. doi:10.1136/bmj.b158

Bussian, T. J., Aziz, A., Meyer, C. F., Swenson, B. L., van Deursen, J. M., & Baker, D. J. (2018). Clearance of senescent glial cells prevents tau-dependent pathology and cognitive decline. *Nature, 562*(7728), 578-582. doi:10.1038/s41586-018-0543-y

Butovsky, O., Jedrychowski, M. P., Moore, C. S., Cialic, R., Lanser, A. J., Gabriely, G., . . . Weiner, H. L. (2014). Identification of a unique TGF-beta-dependent molecular and functional signature in microglia. *Nat Neurosci, 17*(1), 131-143. doi:10.1038/nn.3599

Butovsky, O., & Weiner, H. L. (2018). Microglial signatures and their role in health and disease. *Nat Rev Neurosci, 19*(10), 622-635. doi:10.1038/s41583-018-0057-5

Buttgereit, A., Lelios, I., Yu, X., Vrohlings, M., Krakoski, N. R., Gautier, E. L., . . . Greter, M. (2016). Sall1 is a transcriptional regulator defining microglia identity and function. *Nat Immunol, 17*(12), 1397-1406. doi:10.1038/ni.3585

Butturini, E., Boriero, D., Carcereri de Prati, A., & Mariotto, S. (2019). STAT1 drives M1 microglia activation and neuroinflammation under hypoxia. *Arch Biochem Biophys, 669*, 22-30. doi:10.1016/j.abb.2019.05.011

Caldeira, C., Cunha, C., Vaz, A. R., Falcao, A. S., Barateiro, A., Seixas, E., . . . Brites, D. (2017). Key Aging-Associated Alterations in Primary Microglia Response to Beta-Amyloid Stimulation. *Front Aging Neurosci, 9*, 277. doi:10.3389/fnagi.2017.00277

Cardona, A. E., Pioro, E. P., Sasse, M. E., Kostenko, V., Cardona, S. M., Dijkstra, I. M., . . . Ransohoff, R. M. (2006). Control of microglial neurotoxicity by the fractalkine receptor. *Nat Neurosci, 9*(7), 917-924. doi:10.1038/nn1715

Carreno-Muller, E., Herrera, A. J., de Pablos, R. M., Tomas-Camardiel, M., Venero, J. L., Cano, J., & Machado, A. (2003). Thrombin induces in vivo degeneration of nigral dopaminergic neurones along with the activation of microglia. *J Neurochem, 84*(5), 1201-1214. doi:10.1046/j.1471-4159.2003.01634.x

Carta, A. R., Frau, L., Pisanu, A., Wardas, J., Spiga, S., & Carboni, E. (2011). Rosiglitazone decreases peroxisome proliferator receptor-gamma levels in microglia and inhibits TNF-alpha production: new evidences on neuroprotection in a progressive Parkinson's disease model. *Neuroscience, 194*, 250-261. doi:10.1016/j.neuroscience.2011.07.046

Castro-Sanchez, S., Garcia-Yague, A. J., Lopez-Royo, T., Casarejos, M., Lanciego, J. L., & Lastres-Becker, I. (2018). Cx3cr1-deficiency exacerbates alpha-synuclein-A53T induced neuroinflammation and neurodegeneration in a mouse model of Parkinson's disease. *Glia, 66*(8), 1752-1762. doi:10.1002/glia.23338

Chakrabarty, P., Ceballos-Diaz, C., Beccard, A., Janus, C., Dickson, D., Golde, T. E., & Das, P. (2010). IFN-gamma promotes complement expression and attenuates amyloid plaque deposition in amyloid beta precursor protein transgenic mice. *J Immunol, 184*(9), 5333-5343. doi:10.4049/jimmunol.0903382

Chakrabarty, P., Herring, A., Ceballos-Diaz, C., Das, P., & Golde, T. E. (2011). Hippocampal expression of murine TNFalpha results in attenuation of amyloid deposition in vivo. *Mol Neurodegener, 6*, 16. doi:10.1186/1750-1326-6-16

Chakrabarty, P., Jansen-West, K., Beccard, A., Ceballos-Diaz, C., Levites, Y., Verbeeck, C., . . . Das, P. (2010). Massive gliosis induced by interleukin-6 suppresses Abeta deposition in vivo: evidence against inflammation as a driving force for amyloid deposition. *FASEB J, 24*(2), 548-559. doi:10.1096/fj.09-141754

Chakrabarty, P., Tianbai, L., Herring, A., Ceballos-Diaz, C., Das, P., & Golde, T. E. (2012). Hippocampal expression of murine IL-4 results in exacerbation of amyloid deposition. *Mol Neurodegener, 7*, 36. doi:10.1186/1750-1326-7-36

Chan, W. C., Tan, L., Liu, J., Yang, Q., Wang, J., Wang, M., . . . Man, Y. (2022). Inhibition of Rgs10 aggravates periodontitis with collagen-induced arthritis via the nuclear factor-kappaB pathway. *Oral Dis*. doi:10.1111/odi.14147

Chandran, R., Kumar, M., Kesavan, L., Jacob, R. S., Gunasekaran, S., Lakshmi, S., . . . Omkumar, R. V. (2019). Cellular calcium signaling in the aging brain. *J Chem Neuroanat, 95*, 95-114. doi:10.1016/j.jchemneu.2017.11.008

Chang, C. F., Wan, J., Li, Q., Renfroe, S. C., Heller, N. M., & Wang, J. (2017). Alternative activation-skewed microglia/macrophages promote hematoma resolution in experimental intracerebral hemorrhage. *Neurobiol Dis, 103*, 54-69. doi:10.1016/j.nbd.2017.03.016

Chang, W. C. (2006). Store-operated calcium channels and pro-inflammatory signals. *Acta Pharmacol Sin, 27*(7), 813-820. doi:10.1111/j.1745-7254.2006.00395.x

Chatterjee, T. K., & Fisher, R. A. (2000). Cytoplasmic, nuclear, and golgi localization of RGS proteins. Evidence for N-terminal and RGS domain sequences as intracellular targeting motifs. *J Biol Chem, 275*(31), 24013-24021. doi:10.1074/jbc.M002082200

Chauhan, P., Sheng, W. S., Hu, S., Prasad, S., & Lokensgard, J. R. (2021). Differential Cytokine-Induced Responses of Polarized Microglia. *Brain Sci, 11*(11). doi:10.3390/brainsci11111482

Chen, E. Y., Tan, C. M., Kou, Y., Duan, Q., Wang, Z., Meirelles, G. V., . . . Ma'ayan, A. (2013). Enrichr: interactive and collaborative HTML5 gene list enrichment analysis tool. *BMC Bioinformatics, 14*, 128. doi:10.1186/1471-2105-14-128

Chen, G. F., Xu, T. H., Yan, Y., Zhou, Y. R., Jiang, Y., Melcher, K., & Xu, H. E. (2017). Amyloid beta: structure, biology and structure-based therapeutic development. *Acta Pharmacol Sin, 38*(9), 1205-1235. doi:10.1038/aps.2017.28

Chen, S., Zeng, L., & Hu, Z. (2014). Progressing haemorrhagic stroke: categories, causes, mechanisms and managements. *J Neurol, 261*(11), 2061-2078. doi:10.1007/s00415-014-7291-1

Chen-Roetling, J., Song, W., Schipper, H. M., Regan, C. S., & Regan, R. F. (2015). Astrocyte overexpression of heme oxygenase-1 improves outcome after intracerebral hemorrhage. *Stroke, 46*(4), 1093-1098. doi:10.1161/STROKEAHA.115.008686

Cheng, Y., Xi, G., Jin, H., Keep, R. F., Feng, J., & Hua, Y. (2014). Thrombin-induced cerebral hemorrhage: role of protease-activated receptor-1. *Transl Stroke Res, 5*(4), 472-475. doi:10.1007/s12975-013-0288-8

Chhor, V., Le Charpentier, T., Lebon, S., Ore, M. V., Celador, I. L., Josserand, J., . . . Fleiss, B. (2013). Characterization of phenotype markers and neuronotoxic potential of polarised primary microglia in vitro. *Brain Behav Immun, 32*, 70-85. doi:10.1016/j.bbi.2013.02.005

Chidambaram, H., Das, R., & Chinnathambi, S. (2020). Interaction of Tau with the chemokine receptor, CX3CR1 and its effect on microglial activation, migration and proliferation. *Cell Biosci, 10*, 109. doi:10.1186/s13578-020-00474-4

Chiu, I. M., Morimoto, E. T., Goodarzi, H., Liao, J. T., O'Keeffe, S., Phatnani, H. P., . . . Maniatis, T. (2013). A neurodegeneration-specific gene-expression signature of acutely isolated microglia from an amyotrophic lateral sclerosis mouse model. *Cell Rep, 4*(2), 385-401. doi:10.1016/j.celrep.2013.06.018

Choi, H., Liu, G., Mellacheruvu, D., Tyers, M., Gingras, A. C., & Nesvizhskii, A. I. (2012). Analyzing protein-protein interactions from affinity purification-mass spectrometry data with SAINT. *Curr Protoc Bioinformatics, Chapter 8*, Unit8 15. doi:10.1002/0471250953.bi0815s39

Choi, I., Zhang, Y., Seegobin, S. P., Pruvost, M., Wang, Q., Purtell, K., . . . Yue, Z. (2020). Microglia clear neuron-released alpha-synuclein via selective autophagy and prevent neurodegeneration. *Nat Commun, 11*(1), 1386. doi:10.1038/s41467-020-15119-w

Choi, S. H., Joe, E. H., Kim, S. U., & Jin, B. K. (2003). Thrombin-induced microglial activation produces degeneration of nigral dopaminergic neurons in vivo. *J Neurosci, 23*(13), 5877-5886. Retrieved from https://www.ncbi.nlm.nih.gov/pubmed/12843292

Chung, C. Y., Koprich, J. B., Siddiqi, H., & Isacson, O. (2009). Dynamic changes in presynaptic and axonal transport proteins combined with striatal neuroinflammation precede dopaminergic neuronal loss in a rat model of AAV alpha-synucleinopathy. *J Neurosci, 29*(11), 3365-3373. doi:10.1523/JNEUROSCI.5427-08.2009

Clynes, R., Maizes, J. S., Guinamard, R., Ono, M., Takai, T., & Ravetch, J. V. (1999). Modulation of immune complex-induced inflammation in vivo by the coordinate expression of activation and inhibitory Fc receptors. *J Exp Med, 189*(1), 179-185. doi:10.1084/jem.189.1.179

Cockey, S. G., McFarland, K. N., Koller, E. J., Brooks, M. M. T., Gonzalez De La Cruz, E., Cruz, P. E., . . . Chakrabarty, P. (2021). Il-10 signaling reduces survival in mouse models of synucleinopathy. *NPJ Parkinsons Dis, 7*(1), 30. doi:10.1038/s41531-021-00169-8

Colton, C. A., Mott, R. T., Sharpe, H., Xu, Q., Van Nostrand, W. E., & Vitek, M. P. (2006). Expression profiles for macrophage alternative activation genes in AD and in mouse models of AD. *J Neuroinflammation, 3*, 27. doi:10.1186/1742-2094-3-27

Condello, C., Yuan, P., Schain, A., & Grutzendler, J. (2015). Microglia constitute a barrier that prevents neurotoxic protofibrillar Abeta42 hotspots around plaques. *Nat Commun, 6*, 6176. doi:10.1038/ncomms7176

Corder, E. H., Saunders, A. M., Strittmatter, W. J., Schmechel, D. E., Gaskell, P. C., Small, G. W., . . . Pericak-Vance, M. A. (1993). Gene dose of apolipoprotein E type 4 allele and the risk of Alzheimer's disease in late onset families. *Science, 261*(5123), 921-923. doi:10.1126/science.8346443

Costela-Ruiz, V. J., Illescas-Montes, R., Puerta-Puerta, J. M., Ruiz, C., & Melguizo-Rodriguez, L. (2020). SARS-CoV-2 infection: The role of cytokines in COVID-19 disease. *Cytokine Growth Factor Rev, 54*, 62-75. doi:10.1016/j.cytogfr.2020.06.001

Coughlin, S. R. (2000). Thrombin signalling and protease-activated receptors. *Nature, 407*(6801), 258-264. doi:10.1038/35025229

Crabtree, G. R. J. J. o. B. C. (2001). Calcium, calcineurin, and the control of transcription. *276*(4), 2313-2316.

Crews, L., & Masliah, E. (2010). Molecular mechanisms of neurodegeneration in Alzheimer's disease. *Hum Mol Genet, 19*(R1), R12-20. doi:10.1093/hmg/ddq160

Crittenden, P. L., & Filipov, N. M. (2008). Manganese-induced potentiation of in vitro proinflammatory cytokine production by activated microglial cells is associated with persistent activation of p38 MAPK. *Toxicology in Vitro, 22*(1), 18-27.

Croisier, E., Moran, L. B., Dexter, D. T., Pearce, R. K., & Graeber, M. B. (2005). Microglial inflammation in the parkinsonian substantia nigra: relationship to alpha-synuclein deposition. *J Neuroinflammation, 2*, 14. doi:10.1186/1742-2094-2-14

Cserep, C., Posfai, B., Lenart, N., Fekete, R., Laszlo, Z. I., Lele, Z., . . . Denes, A. (2020). Microglia monitor and protect neuronal function through specialized somatic purinergic junctions. *Science, 367*(6477), 528-537. doi:10.1126/science.aax6752

Cui, W., Sun, C., Ma, Y., Wang, S., Wang, X., & Zhang, Y. (2020). Inhibition of TLR4 Induces M2 Microglial Polarization and Provides Neuroprotection via the NLRP3 Inflammasome in Alzheimer's Disease. *Front Neurosci, 14*, 444. doi:10.3389/fnins.2020.00444

Daborg, J., Andreasson, U., Pekna, M., Lautner, R., Hanse, E., Minthon, L., . . . Zetterberg, H. (2012). Cerebrospinal fluid levels of complement proteins C3, C4 and CR1 in Alzheimer's disease. *J Neural Transm (Vienna), 119*(7), 789-797. doi:10.1007/s00702-012-0797-8

Daria, A., Colombo, A., Llovera, G., Hampel, H., Willem, M., Liesz, A., . . . Tahirovic, S. (2017). Young microglia restore amyloid plaque clearance of aged microglia. *EMBO J, 36*(5), 583-603. doi:10.15252/embj.201694591

Davalos, D., Grutzendler, J., Yang, G., Kim, J. V., Zuo, Y., Jung, S., . . . Gan, W. B. (2005). ATP mediates rapid microglial response to local brain injury in vivo. *Nat Neurosci, 8*(6), 752-758. doi:10.1038/nn1472

Davies, D. S., Ma, J., Jegathees, T., & Goldsbury, C. (2017). Microglia show altered morphology and reduced arborization in human brain during aging and Alzheimer's disease. *Brain Pathol, 27*(6), 795-808. doi:10.1111/bpa.12456

De Souza, E. E., Hehnly, H., Perez, A. M., Meirelles, G. V., Smetana, J. H., Doxsey, S., & Kobarg, J. (2015). Human Nek7-interactor RGS2 is required for mitotic spindle organization. *Cell Cycle, 14*(4), 656-667. doi:10.4161/15384101.2014.994988

Deane, R., Singh, I., Sagare, A. P., Bell, R. D., Ross, N. T., LaRue, B., . . . Zlokovic, B. V. (2012). A multimodal RAGE-specific inhibitor reduces amyloid beta-mediated brain disorder in a mouse model of Alzheimer disease. *J Clin Invest, 122*(4), 1377-1392. doi:10.1172/JCI58642

Deczkowska, A., Keren-Shaul, H., Weiner, A., Colonna, M., Schwartz, M., & Amit, I. (2018). Disease-Associated Microglia: A Universal Immune Sensor of Neurodegeneration. *Cell, 173*(5), 1073-1081. doi:10.1016/j.cell.2018.05.003

Dela Cruz, C. S., & Kang, M. J. (2018). Mitochondrial dysfunction and damage associated molecular patterns (DAMPs) in chronic inflammatory diseases. *Mitochondrion, 41*, 37-44. doi:10.1016/j.mito.2017.12.001

Dijkstra, A. A., Voorn, P., Berendse, H. W., Groenewegen, H. J., Netherlands Brain, B., Rozemuller, A. J., & van de Berg, W. D. (2014). Stage-dependent nigral neuronal loss in incidental Lewy body and Parkinson's disease. *Mov Disord, 29*(10), 1244-1251. doi:10.1002/mds.25952

Ding, Y., Qian, J., Li, H., Shen, H., Li, X., Kong, Y., . . . Chen, G. (2019). Effects of SC99 on cerebral ischemia-perfusion injury in rats: Selective modulation of microglia polarization to M2 phenotype via inhibiting JAK2-STAT3 pathway. *Neurosci Res, 142*, 58-68. doi:10.1016/j.neures.2018.05.002

Dionisio-Santos, D. A., Olschowka, J. A., & O'Banion, M. K. (2019). Exploiting microglial and peripheral immune cell crosstalk to treat Alzheimer's disease. *J Neuroinflammation, 16*(1), 74. doi:10.1186/s12974-019-1453-0

Dobin, A., Davis, C. A., Schlesinger, F., Drenkow, J., Zaleski, C., Jha, S., . . . Gingeras, T. R. (2013). STAR: ultrafast universal RNA-seq aligner. *Bioinformatics, 29*(1), 15-21. doi:10.1093/bioinformatics/bts635

Doens, D., & Fernandez, P. L. (2014). Microglia receptors and their implications in the response to amyloid beta for Alzheimer's disease pathogenesis. *J Neuroinflammation, 11*, 48. doi:10.1186/1742-2094-11-48

Dohlman, H. G. (2009). RGS proteins the early days. *Prog Mol Biol Transl Sci, 86*, 1-14. doi:10.1016/S1877-1173(09)86001-8

Doorn, K. J., Moors, T., Drukarch, B., van de Berg, W., Lucassen, P. J., & van Dam, A. M. (2014). Microglial phenotypes and toll-like receptor 2 in the substantia nigra and hippocampus of incidental Lewy body disease cases and Parkinson's disease patients. *Acta Neuropathol Commun, 2*, 90. doi:10.1186/s40478-014-0090-1

Dorszewska, J., Prendecki, M., Oczkowska, A., Dezor, M., & Kozubski, W. (2016). Molecular Basis of Familial and Sporadic Alzheimer's Disease. *Curr Alzheimer Res, 13*(9), 952-963. doi:10.2174/1567205013666160314150501

Dos Santos, S. E., Medeiros, M., Porfirio, J., Tavares, W., Pessoa, L., Grinberg, L., . . . Herculano-Houzel, S. (2020). Similar Microglial Cell Densities across Brain Structures and Mammalian Species: Implications for Brain Tissue Function. *J Neurosci, 40*(24), 4622-4643. doi:10.1523/JNEUROSCI.2339-19.2020

Ducruet, A. F., Zacharia, B. E., Hickman, Z. L., Grobelny, B. T., Yeh, M. L., Sosunov, S. A., & Connolly, E. S., Jr. (2009). The complement cascade as a therapeutic target in intracerebral hemorrhage. *Exp Neurol, 219*(2), 398-403. doi:10.1016/j.expneurol.2009.07.018

Dunn, B., Stein, P., & Cavazzoni, P. (2021). Approval of Aducanumab for Alzheimer Disease-The FDA's Perspective. *JAMA Intern Med, 181*(10), 1276-1278. doi:10.1001/jamainternmed.2021.4607

Dusonchet, J., Li, H., Guillily, M., Liu, M., Stafa, K., Derada Troletti, C., . . . Wolozin, B. (2014). A Parkinson's disease gene regulatory network identifies the signaling protein RGS2 as a modulator of LRRK2 activity and neuronal toxicity. *Hum Mol Genet, 23*(18), 4887-4905. doi:10.1093/hmg/ddu202

Easley-Neal, C., Foreman, O., Sharma, N., Zarrin, A. A., & Weimer, R. M. (2019). CSF1R Ligands IL-34 and CSF1 Are Differentially Required for Microglia Development and Maintenance in White and Gray Matter Brain Regions. *Front Immunol, 10*, 2199. doi:10.3389/fimmu.2019.02199

Edwards, J. P., Zhang, X., Frauwirth, K. A., & Mosser, D. M. (2006). Biochemical and functional characterization of three activated macrophage populations. *J Leukoc Biol, 80*(6), 1298-1307. doi:10.1189/jlb.0406249

Eichhoff, G., Brawek, B., & Garaschuk, O. (2011). Microglial calcium signal acts as a rapid sensor of single neuron damage in vivo. *Biochim Biophys Acta, 1813*(5), 1014-1024. doi:10.1016/j.bbamcr.2010.10.018

El-Agnaf, O. M., Salem, S. A., Paleologou, K. E., Cooper, L. J., Fullwood, N. J., Gibson, M. J., . . . Allsop, D. (2003). Alpha-synuclein implicated in Parkinson's disease is present in extracellular biological fluids, including human plasma. *FASEB J, 17*(13), 1945-1947. doi:10.1096/fj.03-0098fje

El-Zayat, S. R., Sibaii, H., & Mannaa, F. A. (2019). Toll-like receptors activation, signaling, and targeting: an overview. *Bull Natl Res Cent, 43*(187).

Elgayar, S. A. M., Abdel-Hafez, A. A. M., Gomaa, A. M. S., & Elsherif, R. (2018). Vulnerability of glia and vessels of rat substantia nigra in rotenone Parkinson model. *Ultrastruct Pathol, 42*(2), 181-192. doi:10.1080/01913123.2017.1422066

Elmore, M. R., Najafi, A. R., Koike, M. A., Dagher, N. N., Spangenberg, E. E., Rice, R. A., . . . Green, K. N. (2014). Colony-stimulating factor 1 receptor signaling is necessary for microglia viability, unmasking a microglia progenitor cell in the adult brain. *Neuron, 82*(2), 380-397. doi:10.1016/j.neuron.2014.02.040

Eme-Scolan, E., & Dando, S. J. (2020). Tools and Approaches for Studying Microglia In vivo. *Front Immunol, 11*, 583647. doi:10.3389/fimmu.2020.583647

English, C., & Aloi, J. J. (2015). New FDA-Approved Disease-Modifying Therapies for Multiple Sclerosis. *Clin Ther, 37*(4), 691-715. doi:10.1016/j.clinthera.2015.03.001

Eyo, U. B., Miner, S. A., Ahlers, K. E., Wu, L. J., & Dailey, M. E. (2013). P2X7 receptor activation regulates microglial cell death during oxygen-glucose deprivation. *Neuropharmacology, 73*, 311-319. doi:10.1016/j.neuropharm.2013.05.032

Fan, Z., Brooks, D. J., Okello, A., & Edison, P. (2017). An early and late peak in microglial activation in Alzheimer's disease trajectory. *Brain, 140*(3), 792-803. doi:10.1093/brain/aww349

Fang, H., Chen, J., Lin, S., Wang, P., Wang, Y., Xiong, X., & Yang, Q. (2014). CD36-mediated hematoma absorption following intracerebral hemorrhage: negative regulation by TLR4 signaling. *J Immunol, 192*(12), 5984-5992. doi:10.4049/jimmunol.1400054

Farber, K., & Kettenmann, H. (2006). Functional role of calcium signals for microglial function. *Glia, 54*(7), 656-665. doi:10.1002/glia.20412

Fateh-Moghadam, S., Htun, P., Tomandl, B., Sander, D., Stellos, K., Geisler, T., . . . Gawaz, M. (2007). Hyperresponsiveness of platelets in ischemic stroke. *Thromb Haemost, 97*(6), 974-978. Retrieved from https://www.ncbi.nlm.nih.gov/pubmed/17549300

Fatoba, O., T. Itokazu, and T. Yamashita, *Microglia as therapeutic target in central nervous system disorders.* J Pharmacol Sci, 2020. **144**(3): p. 102-118.

Feng, W., Zhang, Y., Wang, Z., Xu, H., Wu, T., Marshall, C., . . . Xiao, M. (2020). Microglia prevent beta-amyloid plaque formation in the early stage of an Alzheimer's disease mouse model with suppression of glymphatic clearance. *Alzheimers Res Ther, 12*(1), 125. doi:10.1186/s13195-020-00688-1

Ferrante, C. J., & Leibovich, S. J. (2012). Regulation of Macrophage Polarization and Wound Healing. *Adv Wound Care (New Rochelle), 1*(1), 10-16. doi:10.1089/wound.2011.0307

Ferrante, C. J., Pinhal-Enfield, G., Elson, G., Cronstein, B. N., Hasko, G., Outram, S., & Leibovich, S. J. (2013). The adenosine-dependent angiogenic switch of macrophages to an M2-like phenotype is independent of interleukin-4 receptor alpha (IL-4Ralpha) signaling. *Inflammation, 36*(4), 921-931. doi:10.1007/s10753-013-9621-3

Ferreira, S. A., & Romero-Ramos, M. (2018). Microglia Response During Parkinson's Disease: Alpha-Synuclein Intervention. *Front Cell Neurosci, 12*, 247. doi:10.3389/fncel.2018.00247

Fiebich, B. L., Batista, C. R. A., Saliba, S. W., Yousif, N. M., & de Oliveira, A. C. P. (2018). Role of Microglia TLRs in Neurodegeneration. *Front Cell Neurosci, 12*, 329. doi:10.3389/fncel.2018.00329

Filgueira, L., Larionov, A., & Lannes, N. (2021). The Influence of Virus Infection on Microglia and Accelerated Brain Aging. *Cells, 10*(7). doi:10.3390/cells10071836

Fogg, D. K., Sibon, C., Miled, C., Jung, S., Aucouturier, P., Littman, D. R., . . . Geissmann, F. (2006). A clonogenic bone marrow progenitor specific for macrophages and dendritic cells. *Science, 311*(5757), 83-87. doi:10.1126/science.1117729

Font-Nieves, M., et al., Induction of COX-2 enzyme and down-regulation of COX-1 expression by lipopolysaccharide (LPS) control prostaglandin E2 production in astrocytes. *J Biol Chem*, 2012. **287**(9): p. 6454-68.

Franco, R., & Fernandez-Suarez, D. (2015). Alternatively activated microglia and macrophages in the central nervous system. *Prog Neurobiol, 131*, 65-86. doi:10.1016/j.pneurobio.2015.05.003

Franco-Bocanegra, D. K., Gourari, Y., McAuley, C., Chatelet, D. S., Johnston, D. A., Nicoll, J. A. R., & Boche, D. (2021). Microglial morphology in Alzheimer's disease and after Abeta immunotherapy. *Sci Rep, 11*(1), 15955. doi:10.1038/s41598-021-95535-0

Frank, M. G., Barrientos, R. M., Biedenkapp, J. C., Rudy, J. W., Watkins, L. R., & Maier, S. F. (2006). mRNA up-regulation of MHC II and pivotal pro-inflammatory genes in normal brain aging. *Neurobiol Aging, 27*(5), 717-722. doi:10.1016/j.neurobiolaging.2005.03.013

Fujimoto, S., Katsuki, H., Ohnishi, M., Takagi, M., Kume, T., & Akaike, A. (2007). Thrombin induces striatal neurotoxicity depending on mitogen-activated protein kinase pathways in vivo. *Neuroscience, 144*(2), 694-701. doi:10.1016/j.neuroscience.2006.09.049

Furman, D., Campisi, J., Verdin, E., Carrera-Bastos, P., Targ, S., Franceschi, C., . . . Slavich, G. M. (2019). Chronic inflammation in the etiology of disease across the life span. *Nat Med, 25*(12), 1822-1832. doi:10.1038/s41591-019-0675-0

Fusakio, M. E., Willy, J. A., Wang, Y., Mirek, E. T., Al Baghdadi, R. J., Adams, C. M., . . . Wek, R. C. (2016). Transcription factor ATF4 directs basal and stress-induced gene expression in the unfolded protein response and cholesterol metabolism in the liver. *Mol Biol Cell, 27*(9), 1536-1551. doi:10.1091/mbc.E16-01-0039

Gadani, S. P., Cronk, J. C., Norris, G. T., & Kipnis, J. (2012). IL-4 in the brain: a cytokine to remember. *J Immunol, 189*(9), 4213-4219. doi:10.4049/jimmunol.1202246

Ganbold, T., Bao, Q., Zandan, J., Hasi, A., & Baigude, H. (2020). Modulation of Microglia Polarization through Silencing of NF-kappaB p65 by Functionalized Curdlan Nanoparticle-Mediated RNAi. *ACS Appl Mater Interfaces, 12*(10), 11363-11374. doi:10.1021/acsami.9b23004

Gandhi, K. R., & Saadabadi, A. (2022). Levodopa (L-Dopa). In *StatPearls*. Treasure Island (FL).

Gao, H. M., Jiang, J., Wilson, B., Zhang, W., Hong, J. S., & Liu, B. (2002). Microglial activation-mediated delayed and progressive degeneration of rat nigral dopaminergic neurons: relevance to Parkinson's disease. *J Neurochem, 81*(6), 1285-1297. doi:10.1046/j.1471-4159.2002.00928.x

Gao, H. M., Zhang, F., Zhou, H., Kam, W., Wilson, B., & Hong, J. S. (2011). Neuroinflammation and alpha-synuclein dysfunction potentiate each other, driving chronic progression of neurodegeneration in a mouse model of Parkinson's disease. *Environ Health Perspect, 119*(6), 807-814. doi:10.1289/ehp.1003013

Garcia-Alcalde, F., Okonechnikov, K., Carbonell, J., Cruz, L. M., Gotz, S., Tarazona, S., . . . Conesa, A. (2012). Qualimap: evaluating next-generation sequencing alignment data. *Bioinformatics, 28*(20), 2678-2679. doi:10.1093/bioinformatics/bts503

Garcia-Bernal, D., Dios-Esponera, A., Sotillo-Mallo, E., Garcia-Verdugo, R., Arellano-Sanchez, N., & Teixido, J. (2011). RGS10 restricts upregulation by chemokines of T cell adhesion mediated by alpha4beta1 and alphaLbeta2 integrins. *J Immunol, 187*(3), 1264-1272. doi:10.4049/jimmunol.1002960

Garcia-Gonzalez, P., Cabral-Miranda, F., Hetz, C., & Osorio, F. (2018). Interplay Between the Unfolded Protein Response and Immune Function in the Development of Neurodegenerative Diseases. *Front Immunol, 9*, 2541. doi:10.3389/fimmu.2018.02541

Garwood, C. J., Cooper, J. D., Hanger, D. P., & Noble, W. (2010). Anti-inflammatory impact of minocycline in a mouse model of tauopathy. *Front Psychiatry, 1*, 136. doi:10.3389/fpsyt.2010.00136

Ge, S. X., Son, E. W., & Yao, R. (2018). iDEP: an integrated web application for differential expression and pathway analysis of RNA-Seq data. *BMC Bioinformatics, 19*(1), 534. doi:10.1186/s12859-018-2486-6

Geirsdottir, L., David, E., Keren-Shaul, H., Weiner, A., Bohlen, S. C., Neuber, J., . . . Prinz, M. (2019). Cross-Species Single-Cell Analysis Reveals Divergence of the Primate Microglia Program. *Cell, 179*(7), 1609-1622 e1616. doi:10.1016/j.cell.2019.11.010

Gencoglan, G., Tosun, M., & Aktepe, F. (2009). The molecular mechanism of etanercept, an anti-tumour necrosis factor-alpha receptor-fusion protein, in the treatment of acute generalized exanthematous pustulosis. *J Dermatolog Treat, 20*(4), 241-245. doi:10.1080/09546630802683843

Gerhard, A., Pavese, N., Hotton, G., Turkheimer, F., Es, M., Hammers, A., . . . Brooks, D. J. (2006). In vivo imaging of microglial activation with [11C](R)-PK11195 PET in idiopathic Parkinson's disease. *Neurobiol Dis, 21*(2), 404-412. doi:10.1016/j.nbd.2005.08.002

Gerrits, E., Heng, Y., Boddeke, E., & Eggen, B. J. L. (2020). Transcriptional profiling of microglia; current state of the art and future perspectives. *Glia, 68*(4), 740-755. doi:10.1002/glia.23767

Ghavami, A., Hunt, R. A., Olsen, M. A., Zhang, J., Smith, D. L., Kalgaonkar, S., . . . Young, K. H. (2004). Differential effects of regulator of G protein signaling (RGS) proteins on serotonin 5-HT1A, 5-HT2A, and dopamine D2 receptor-mediated signaling and adenylyl cyclase activity. *Cell Signal, 16*(6), 711-721. doi:10.1016/j.cellsig.2003.11.006

Ginhoux, F., & Garel, S. (2018). The mysterious origins of microglia. *Nat Neurosci, 21*(7), 897-899. doi:10.1038/s41593-018-0176-3

Ginhoux, F., Greter, M., Leboeuf, M., Nandi, S., See, P., Gokhan, S., . . . Merad, M. (2010). Fate mapping analysis reveals that adult microglia derive from primitive macrophages. *Science, 330*(6005), 841-845. doi:10.1126/science.1194637

Go, M., Kou, J., Lim, J. E., Yang, J., & Fukuchi, K. I. (2016). Microglial response to LPS increases in wild-type mice during aging but diminishes in an Alzheimer's mouse model: Implication of TLR4 signaling in disease progression. *Biochem Biophys Res Commun, 479*(2), 331-337. doi:10.1016/j.bbrc.2016.09.073

Godbout, J. P., Chen, J., Abraham, J., Richwine, A. F., Berg, B. M., Kelley, K. W., & Johnson, R. W. (2005). Exaggerated neuroinflammation and sickness behavior in aged mice following activation of the peripheral innate immune system. *FASEB J, 19*(10), 1329-1331. doi:10.1096/fj.05-3776fje

Goldmann, T., Wieghofer, P., Jordao, M. J., Prutek, F., Hagemeyer, N., Frenzel, K., . . . Prinz, M. (2016). Origin, fate and dynamics of macrophages at central nervous system interfaces. *Nat Immunol, 17*(7), 797-805. doi:10.1038/ni.3423

Gomez Perdiguero, E., Klapproth, K., Schulz, C., Busch, K., Azzoni, E., Crozet, L., . . . Rodewald, H. R. (2015). Tissue-resident macrophages originate from yolk-sac-derived erythro-myeloid progenitors. *Nature, 518*(7540), 547-551. doi:10.1038/nature13989

Gong, C., Hoff, J. T., & Keep, R. F. (2000). Acute inflammatory reaction following experimental intracerebral hemorrhage in rat. *Brain Res, 871*(1), 57-65. doi:10.1016/s0006-8993(00)02427-6

Goodwin, J. L., Uemura, E., & Cunnick, J. E. (1995). Microglial release of nitric oxide by the synergistic action of beta-amyloid and IFN-gamma. *Brain Res, 692*(1-2), 207-214. doi:10.1016/0006-8993(95)00646-8

Gosselin, D., Skola, D., Coufal, N. G., Holtman, I. R., Schlachetzki, J. C. M., Sajti, E., . . . Glass, C. K. (2017). An environment-dependent transcriptional network specifies human microglia identity. *Science, 356*(6344). doi:10.1126/science.aal3222

Goulopoulou, S., McCarthy, C. G., & Webb, R. C. (2016). Toll-like Receptors in the Vascular System: Sensing the Dangers Within. *Pharmacol Rev, 68*(1), 142-167. doi:10.1124/pr.114.010090

Grabert, K., Michoel, T., Karavolos, M. H., Clohisey, S., Baillie, J. K., Stevens, M. P., . . . McColl, B. W. (2016). Microglial brain region-dependent diversity and selective regional sensitivities to aging. *Nat Neurosci, 19*(3), 504-516. doi:10.1038/nn.4222

Granholm, V., Kim, S., Navarro, J. C., Sjolund, E., Smith, R. D., & Kall, L. (2014). Fast and accurate database searches with MS-GF+Percolator. *J Proteome Res, 13*(2), 890-897. doi:10.1021/pr400937n

Gratuze, M., Leyns, C. E. G., & Holtzman, D. M. (2018). New insights into the role of TREM2 in Alzheimer's disease. *Mol Neurodegener, 13*(1), 66. doi:10.1186/s13024-018-0298-9

Gresa-Arribas, N., Vieitez, C., Dentesano, G., Serratosa, J., Saura, J., & Sola, C. (2012). Modelling neuroinflammation in vitro: a tool to test the potential neuroprotective effect of anti-inflammatory agents. *PLoS One, 7*(9), e45227. doi:10.1371/journal.pone.0045227

Grubman, A., Choo, X. Y., Chew, G., Ouyang, J. F., Sun, G., Croft, N. P., . . . Polo, J. M. (2021). Transcriptional signature in microglia associated with Abeta plaque phagocytosis. *Nat Commun, 12*(1), 3015. doi:10.1038/s41467-021-23111-1

Gyoneva, S., Hosur, R., Gosselin, D., Zhang, B., Ouyang, Z., Cotleur, A. C., . . . Ransohoff, R. M. (2019). Cx3cr1-deficient microglia exhibit a premature aging transcriptome. *Life Sci Alliance, 2*(6). doi:10.26508/lsa.201900453

Hamelin, L., Lagarde, J., Dorothee, G., Leroy, C., Labit, M., Comley, R. A., . . . Clinical, I. t. (2016). Early and protective microglial activation in Alzheimer's disease: a prospective study using 18F-DPA-714 PET imaging. *Brain, 139*(Pt 4), 1252-1264. doi:10.1093/brain/aww017

Han, H., Cho, J. W., Lee, S., Yun, A., Kim, H., Bae, D., . . . Lee, I. (2018). TRRUST v2: an expanded reference database of human and mouse transcriptional regulatory interactions. *Nucleic Acids Res, 46*(D1), D380-D386. doi:10.1093/nar/gkx1013

Hanisch, U.K., et al., *The microglia-activating potential of thrombin: the protease is not involved in the induction of proinflammatory cytokines and chemokines.* J Biol Chem, 2004. **279**(50): p. 51880-7.

Hansen, D. V., Hanson, J. E., & Sheng, M. (2018). Microglia in Alzheimer's disease. *J Cell Biol, 217*(2), 459-472. doi:10.1083/jcb.201709069

Hanslik, K. L., & Ulland, T. K. (2020). The Role of Microglia and the Nlrp3 Inflammasome in Alzheimer's Disease. *Front Neurol, 11*, 570711. doi:10.3389/fneur.2020.570711

Haque, M. E., Kim, I. S., Jakaria, M., Akther, M., & Choi, D. K. (2018). Importance of GPCR-Mediated Microglial Activation in Alzheimer's Disease. *Front Cell Neurosci, 12*, 258. doi:10.3389/fncel.2018.00258

Harden, T. K., Waldo, G. L., Hicks, S. N., & Sondek, J. (2011). Mechanism of activation and inactivation of Gq/phospholipase C-beta signaling nodes. *Chem Rev, 111*(10), 6120-6129. doi:10.1021/cr200209p

Hart, A. D., Wyttenbach, A., Perry, V. H., & Teeling, J. L. (2012). Age related changes in microglial phenotype vary between CNS regions: grey versus white matter differences. *Brain Behav Immun, 26*(5), 754-765. doi:10.1016/j.bbi.2011.11.006

Hasselmann, J., Coburn, M. A., England, W., Figueroa Velez, D. X., Kiani Shabestari, S., Tu, C. H., . . . Blurton-Jones, M. (2019). Development of a Chimeric Model to Study and Manipulate Human Microglia In Vivo. *Neuron, 103*(6), 1016-1033 e1010. doi:10.1016/j.neuron.2019.07.002

Hatori, K., Nagai, A., Heisel, R., Ryu, J. K., & Kim, S. U. (2002). Fractalkine and fractalkine receptors in human neurons and glial cells. *J Neurosci Res, 69*(3), 418-426. doi:10.1002/jnr.10304

Hauser, A. S., Attwood, M. M., Rask-Andersen, M., Schioth, H. B., & Gloriam, D. E. (2017). Trends in GPCR drug discovery: new agents, targets and indications. *Nat Rev Drug Discov, 16*(12), 829-842. doi:10.1038/nrd.2017.178

Haynes, S. E., Hollopeter, G., Yang, G., Kurpius, D., Dailey, M. E., Gan, W. B., & Julius, D. (2006). The P2Y12 receptor regulates microglial activation by extracellular nucleotides. *Nat Neurosci, 9*(12), 1512-1519. doi:10.1038/nn1805

He, J., Zhu, G., Wang, G., & Zhang, F. (2020). Oxidative Stress and Neuroinflammation Potentiate Each Other to Promote Progression of Dopamine Neurodegeneration. *Oxid Med Cell Longev, 2020*, 6137521. doi:10.1155/2020/6137521

Hemphill, J. C., 3rd, Bonovich, D. C., Besmertis, L., Manley, G. T., & Johnston, S. C. (2001). The ICH score: a simple, reliable grading scale for intracerebral hemorrhage. *Stroke, 32*(4), 891-897. doi:10.1161/01.str.32.4.891

Hemphill, J. C., 3rd, Greenberg, S. M., Anderson, C. S., Becker, K., Bendok, B. R., Cushman, M., . . . Council on Clinical, C. (2015). Guidelines for the Management of Spontaneous Intracerebral Hemorrhage: A Guideline for Healthcare Professionals From the American Heart Association/American Stroke Association. *Stroke, 46*(7), 2032-2060. doi:10.1161/STR.0000000000000069

Heneka, M. T., Kummer, M. P., Stutz, A., Delekate, A., Schwartz, S., Vieira-Saecker, A., . . . Golenbock, D. T. (2013). NLRP3 is activated in Alzheimer's disease and contributes to pathology in APP/PS1 mice. *Nature, 493*(7434), 674-678. doi:10.1038/nature11729

Henn, A., Lund, S., Hedtjarn, M., Schrattenholz, A., Porzgen, P., & Leist, M. (2009). The suitability of BV2 cells as alternative model system for primary microglia cultures or for animal experiments examining brain inflammation. *Altex, 26*(2), 83-94.

Hensch, N. R., Karim, Z. A., Druey, K. M., Tansey, M. G., & Khasawneh, F. T. (2016). RGS10 Negatively Regulates Platelet Activation and Thrombogenesis. *PLoS One, 11*(11), e0165984. doi:10.1371/journal.pone.0165984

Hickman, S., Izzy, S., Sen, P., Morsett, L., & El Khoury, J. (2018). Microglia in neurodegeneration. *Nat Neurosci, 21*(10), 1359-1369. doi:10.1038/s41593-018-0242-x

Hickman, S. E., Allison, E. K., & El Khoury, J. (2008). Microglial dysfunction and defective beta-amyloid clearance pathways in aging Alzheimer's disease mice. *J Neurosci, 28*(33), 8354-8360. doi:10.1523/JNEUROSCI.0616-08.2008

Hiramatsu, N., Chiang, W. C., Kurt, T. D., Sigurdson, C. J., & Lin, J. H. (2015). Multiple Mechanisms of Unfolded Protein Response-Induced Cell Death. *Am J Pathol, 185*(7), 1800-1808. doi:10.1016/j.ajpath.2015.03.009

Hishimoto, A., Shirakawa, O., Nishiguchi, N., Aoyama, S., Ono, H., Hashimoto, T., & Maeda, K. (2004). Novel missense polymorphism in the regulator of G-protein signaling 10 gene: analysis of association with schizophrenia. *Psychiatry Clin Neurosci, 58*(5), 579-581. doi:10.1111/j.1440-1819.2004.01303.x

Hoenen, C., Gustin, A., Birck, C., Kirchmeyer, M., Beaume, N., Felten, P., . . . Heurtaux, T. (2016). Alpha-Synuclein Proteins Promote Pro-Inflammatory Cascades in Microglia: Stronger Effects of the A53T Mutant. *PLoS One, 11*(9), e0162717. doi:10.1371/journal.pone.0162717

Hogan, P.G., R.S. Lewis, and A. Rao, *Molecular basis of calcium signaling in lymphocytes: STIM and ORAI.* Annu Rev Immunol, 2010. **28**: p. 491-533.

Hogan, P. G., & Rao, A. (2015). Store-operated calcium entry: Mechanisms and modulation. *Biochem Biophys Res Commun, 460*(1), 40-49. doi:10.1016/j.bbrc.2015.02.110

Hollinger, S., & Hepler, J. R. (2002). Cellular regulation of RGS proteins: modulators and integrators of G protein signaling. *Pharmacol Rev, 54*(3), 527-559. doi:10.1124/pr.54.3.527

Holtman, I. R., Raj, D. D., Miller, J. A., Schaafsma, W., Yin, Z., Brouwer, N., . . . Eggen, B. J. (2015). Induction of a common microglia gene expression signature by aging and neurodegenerative conditions: a co-expression meta-analysis. *Acta Neuropathol Commun, 3*, 31. doi:10.1186/s40478-015-0203-5

Honarpisheh, P., Lee, J., Banerjee, A., Blasco-Conesa, M. P., Honarpisheh, P., d'Aigle, J., . . . McCullough, L. D. (2020). Potential caveats of putative microglia-specific markers for assessment of age-related cerebrovascular neuroinflammation. *J Neuroinflammation, 17*(1), 366. doi:10.1186/s12974-020-02019-5

Hong, S., Beja-Glasser, V. F., Nfonoyim, B. M., Frouin, A., Li, S., Ramakrishnan, S., . . . Stevens, B. (2016). Complement and microglia mediate early synapse loss in Alzheimer mouse models. *Science, 352*(6286), 712-716. doi:10.1126/science.aad8373

Hooks, S. B., Callihan, P., Altman, M. K., Hurst, J. H., Ali, M. W., & Murph, M. M. (2010). Regulators of G-Protein signaling RGS10 and RGS17 regulate chemoresistance in ovarian cancer cells. *Mol Cancer, 9*, 289. doi:10.1186/1476-4598-9-289

Hooks, S. B., & Murph, M. M. (2015). Cellular deficiency in the RGS10 protein facilitates chemoresistant ovarian cancer. *Future Med Chem, 7*(12), 1483-1489. doi:10.4155/fmc.15.81

Hoozemans, J. J., Rozemuller, A. J., van Haastert, E. S., Eikelenboom, P., & van Gool, W. A. (2011). Neuroinflammation in Alzheimer's disease wanes with age. *J Neuroinflammation, 8*, 171. doi:10.1186/1742-2094-8-171

Hopp, S. C., Lin, Y., Oakley, D., Roe, A. D., DeVos, S. L., Hanlon, D., & Hyman, B. T. (2018). The role of microglia in processing and spreading of bioactive tau seeds in Alzheimer's disease. *J Neuroinflammation, 15*(1), 269. doi:10.1186/s12974-018-1309-z

Hoth, M., & Niemeyer, B. A. (2013). The neglected CRAC proteins: Orai2, Orai3, and STIM2. In *Current topics in membranes* (Vol. 71, pp. 237-271): Elsevier.

Howard, R., Zubko, O., Bradley, R., Harper, E., Pank, L., O'Brien, J., . . . Minocycline in Alzheimer Disease Efficacy Trialist, G. (2020). Minocycline at 2 Different Dosages vs Placebo for Patients With Mild Alzheimer Disease: A Randomized Clinical Trial. *JAMA Neurol, 77*(2), 164-174. doi:10.1001/jamaneurol.2019.3762

Hu, Y., Fryatt, G. L., Ghorbani, M., Obst, J., Menassa, D. A., Martin-Estebane, M., . . . Gomez-Nicola, D. (2021). Replicative senescence dictates the emergence of disease-associated microglia and contributes to Abeta pathology. *Cell Rep, 35*(10), 109228. doi:10.1016/j.celrep.2021.109228

Hu, Y., Li, C., Wang, X., Chen, W., Qian, Y., & Dai, X. (2021). TREM2, Driving the Microglial Polarization, Has a TLR4 Sensitivity Profile After Subarachnoid Hemorrhage. *Front Cell Dev Biol, 9*, 693342. doi:10.3389/fcell.2021.693342

Huang, C., Ma, R., Sun, S., Wei, G., Fang, Y., Liu, R., & Li, G. (2008). JAK2-STAT3 signaling pathway mediates thrombin-induced proinflammatory actions of microglia in vitro. *J Neuroimmunol, 204*(1-2), 118-125. doi:10.1016/j.jneuroim.2008.07.004

Huang, K. P. (1989). The mechanism of protein kinase C activation. *Trends Neurosci, 12*(11), 425-432. doi:10.1016/0166-2236(89)90091-x

Huang, Y., Todd, N., & Thathiah, A. (2017). The role of GPCRs in neurodegenerative diseases: avenues for therapeutic intervention. *Curr Opin Pharmacol, 32*, 96-110. doi:10.1016/j.coph.2017.02.001

Huber-Lang, M., Sarma, J. V., Zetoune, F. S., Rittirsch, D., Neff, T. A., McGuire, S. R., . . . Ward, P. A. (2006). Generation of C5a in the absence of C3: a new complement activation pathway. *Nat Med, 12*(6), 682-687. doi:10.1038/nm1419

Huhner, L., Rilka, J., Gilsbach, R., Zhou, X., Machado, V., & Spittau, B. (2017). Interleukin-4 Protects Dopaminergic Neurons In vitro but Is Dispensable for MPTP-Induced Neurodegeneration In vivo. *Front Mol Neurosci, 10*, 62. doi:10.3389/fnmol.2017.00062

Hunot, S., Boissiere, F., Faucheux, B., Brugg, B., Mouatt-Prigent, A., Agid, Y., & Hirsch, E. C. (1996). Nitric oxide synthase and neuronal vulnerability in Parkinson's disease. *Neuroscience, 72*(2), 355-363. doi:10.1016/0306-4522(95)00578-1

Hunt, T. W., Fields, T. A., Casey, P. J., & Peralta, E. G. (1996). RGS10 is a selective activator of G alpha i GTPase activity. *Nature, 383*(6596), 175-177. Retrieved from http://www.ncbi.nlm.nih.gov/entrez/query.fcgi?cmd=Retrieve&db=PubMed&dopt=Citation&list_uids=8774883

Iacono, D., Geraci-Erck, M., Rabin, M. L., Adler, C. H., Serrano, G., Beach, T. G., & Kurlan, R. (2015). Parkinson disease and incidental Lewy body disease: Just a question of time? *Neurology, 85*(19), 1670-1679. doi:10.1212/WNL.0000000000002102

Ikeda-Matsuo, Y., et al., *Microglia-specific expression of microsomal prostaglandin E2 synthase-1 contributes to lipopolysaccharide-induced prostaglandin E2 production.* J Neurochem, 2005. **94**(6): p. 1546-58.

Imamura, K., Hishikawa, N., Sawada, M., Nagatsu, T., Yoshida, M., & Hashizume, Y. (2003). Distribution of major histocompatibility complex class II-positive microglia and cytokine profile of Parkinson's disease brains. *Acta Neuropathol, 106*(6), 518-526. doi:10.1007/s00401-003-0766-2

Inoue, K., Morimoto, H., Ohgidani, M., & Ueki, T. (2021). Modulation of inflammatory responses by fractalkine signaling in microglia. *PLoS One, 16*(5), e0252118. doi:10.1371/journal.pone.0252118

Ivashkiv, L. B. (2018). IFNgamma: signalling, epigenetics and roles in immunity, metabolism, disease and cancer immunotherapy. *Nat Rev Immunol, 18*(9), 545-558. doi:10.1038/s41577-018-0029-z

Iwai, A., Masliah, E., Yoshimoto, M., Ge, N., Flanagan, L., de Silva, H. A., . . . Saitoh, T. (1995). The precursor protein of non-A beta component of Alzheimer's disease amyloid is a presynaptic protein of the central nervous system. *Neuron, 14*(2), 467-475. doi:10.1016/0896-6273(95)90302-x

Jain, M., Singh, M. K., Shyam, H., Mishra, A., Kumar, S., Kumar, A., & Kushwaha, J. (2022). Role of JAK/STAT in the Neuroinflammation and its Association with Neurological Disorders. *Annals of Neurosciences*. doi:https://doi.org/10.1177/09727531211070532

Jakobsdottir, J., Conley, Y. P., Weeks, D. E., Mah, T. S., Ferrell, R. E., & Gorin, M. B. (2005). Susceptibility genes for age-related maculopathy on chromosome 10q26. *Am J Hum Genet, 77*(3), 389-407. doi:10.1086/444437

Jimenez, S., Baglietto-Vargas, D., Caballero, C., Moreno-Gonzalez, I., Torres, M., Sanchez-Varo, R., . . . Vitorica, J. (2008). Inflammatory response in the hippocampus of PS1M146L/APP751SL mouse model of Alzheimer's disease: age-dependent switch in the microglial phenotype from alternative to classic. *J Neurosci, 28*(45), 11650-11661. doi:10.1523/JNEUROSCI.3024-08.2008

Joniec-Maciejak, I., Ciesielska, A., Wawer, A., Sznejder-Pacholek, A., Schwenkgrub, J., Cudna, A., . . . Czlonkowski, A. (2014). The influence of AAV2-mediated gene transfer of human IL-10 on neurodegeneration and immune response in a murine model of Parkinson's disease. *Pharmacol Rep, 66*(4), 660-669. doi:10.1016/j.pharep.2014.03.008

Jurga, A. M., Paleczna, M., & Kuter, K. Z. (2020). Overview of General and Discriminating Markers of Differential Microglia Phenotypes. *Front Cell Neurosci, 14*, 198. doi:10.3389/fncel.2020.00198

Kanazawa, M., Ninomiya, I., Hatakeyama, M., Takahashi, T., & Shimohata, T. (2017). Microglia and Monocytes/Macrophages Polarization Reveal Novel Therapeutic Mechanism against Stroke. *Int J Mol Sci, 18*(10). doi:10.3390/ijms18102135

Kang, X., Qiu, J., Li, Q., Bell, K. A., Du, Y., Jung, D. W., . . . Jiang, J. (2017). Cyclooxygenase-2 contributes to oxidopamine-mediated neuronal inflammation and injury via the prostaglandin E2 receptor EP2 subtype. *Sci Rep, 7*(1), 9459. doi:10.1038/s41598-017-09528-z

Kang, Y.J., et al., Cyclooxygenase-2 gene transcription in a macrophage model of inflammation. J *Immunol*, 2006. **177**(11): p. 8111-22.

Kannarkat, G. T., Lee, J. K., Ramsey, C. P., Chung, J., Chang, J., Porter, I., . . . Tansey, M. G. (2015). Age-related changes in regulator of G-protein signaling (RGS)-10 expression in peripheral and central immune cells may influence the risk for age-related degeneration. *Neurobiol Aging, 36*(5), 1982-1993. doi:10.1016/j.neurobiolaging.2015.02.006

Kar, P., & Parekh, A. (2013). STIM proteins, Orai1 and gene expression. *Channels (Austin), 7*(5), 374-378. doi:10.4161/chan.25298

Karpenko, M. N., Vasilishina, A. A., Gromova, E. A., Muruzheva, Z. M., Miliukhina, I. V., & Bernadotte, A. (2018). Interleukin-1beta, interleukin-1 receptor antagonist, interleukin-6, interleukin-10, and tumor necrosis factor-alpha levels in CSF and serum in relation to the clinical diversity of Parkinson's disease. *Cell Immunol, 327*, 77-82. doi:10.1016/j.cellimm.2018.02.011

Kasuya, H., Shimizu, T., & Takakura, K. (1998). Thrombin activity in CSF after SAH is correlated with the degree of SAH the persistence of subarachnoid clot and the development of vasospasm. *Acta Neurochir (Wien), 140*(6), 579-584. doi:10.1007/s007010050143

Kaur, C., Ling, E. A., & Wong, W. C. (1985). Transformation of amoeboid microglial cells into microglia in the corpus callosum of the postnatal rat brain. An electron microscopical study. *Arch Histol Jpn, 48*(1), 17-25. doi:10.1679/aohc.48.17

Kawabori, M., Kacimi, R., Kauppinen, T., Calosing, C., Kim, J. Y., Hsieh, C. L., . . . Yenari, M. A. (2015). Triggering receptor expressed on myeloid cells 2 (TREM2) deficiency attenuates phagocytic activities of microglia and exacerbates ischemic damage in experimental stroke. *J Neurosci, 35*(8), 3384-3396. doi:10.1523/JNEUROSCI.2620-14.2015

Kawahara, K., Suenobu, M., Yoshida, A., Koga, K., Hyodo, A., Ohtsuka, H., . . . Nakayama, H. (2012). Intracerebral microinjection of interleukin-4/interleukin-13 reduces beta-amyloid accumulation in the ipsilateral side and improves cognitive deficits in young amyloid precursor protein 23 mice. *Neuroscience, 207*, 243-260. doi:10.1016/j.neuroscience.2012.01.049

Keren-Shaul, H., Spinrad, A., Weiner, A., Matcovitch-Natan, O., Dvir-Szternfeld, R., Ulland, T. K., . . . Amit, I. (2017). A Unique Microglia Type Associated with Restricting Development of Alzheimer's Disease. *Cell, 169*(7), 1276-1290 e1217. doi:10.1016/j.cell.2017.05.018

Kiffin, R., Kaushik, S., Zeng, M., Bandyopadhyay, U., Zhang, C., Massey, A. C., . . . Cuervo, A. M. (2007). Altered dynamics of the lysosomal receptor for chaperone-mediated autophagy with age. *J Cell Sci, 120*(Pt 5), 782-791. doi:10.1242/jcs.001073

Kim, C., Kwon, S., Iba, M., Spencer, B., Rockenstein, E., Mante, M., . . . Masliah, E. (2021). Effects of innate immune receptor stimulation on extracellular alpha-synuclein uptake and degradation by brain resident cells. *Exp Mol Med, 53*(2), 281-290. doi:10.1038/s12276-021-00562-6

Kim, D., Paggi, J. M., Park, C., Bennett, C., & Salzberg, S. L. (2019). Graph-based genome alignment and genotyping with HISAT2 and HISAT-genotype. *Nat Biotechnol, 37*(8), 907-915. doi:10.1038/s41587-019-0201-4

Kim, W. G., Mohney, R. P., Wilson, B., Jeohn, G. H., Liu, B., & Hong, J. S. (2000). Regional difference in susceptibility to lipopolysaccharide-induced neurotoxicity in the rat brain: role of microglia. *J Neurosci, 20*(16), 6309-6316. Retrieved from https://www.ncbi.nlm.nih.gov/pubmed/10934283

Kimple, A. J., Bosch, D. E., Giguere, P. M., & Siderovski, D. P. (2011). Regulators of G-protein signaling and their Galpha substrates: promises and challenges in their use as drug discovery targets. *Pharmacol Rev, 63*(3), 728-749. doi:10.1124/pr.110.003038

Kimple, R. J., De Vries, L., Tronchere, H., Behe, C. I., Morris, R. A., Gist Farquhar, M., & Siderovski, D. P. (2001). RGS12 and RGS14 GoLoco motifs are G alpha(i) interaction sites with guanine nucleotide dissociation inhibitor Activity. *J Biol Chem, 276*(31), 29275-29281. doi:10.1074/jbc.M103208200

Knott, C., Stern, G., & Wilkin, G. P. (2000). Inflammatory regulators in Parkinson's disease: iNOS, lipocortin-1, and cyclooxygenases-1 and -2. *Mol Cell Neurosci, 16*(6), 724-739. doi:10.1006/mcne.2000.0914

Koellhoffer, E. C., McCullough, L. D., & Ritzel, R. M. (2017). Old Maids: Aging and Its Impact on Microglia Function. *Int J Mol Sci, 18*(4). doi:10.3390/ijms18040769

Koizumi, S., Shigemoto-Mogami, Y., Nasu-Tada, K., Shinozaki, Y., Ohsawa, K., Tsuda, M., . . . Inoue, K. (2007). UDP acting at P2Y6 receptors is a mediator of microglial phagocytosis. *Nature, 446*(7139), 1091-1095. doi:10.1038/nature05704

Kouli, A., Torsney, K. M., & Kuan, W. L. (2018). Parkinson's Disease: Etiology, Neuropathology, and Pathogenesis. In T. B. Stoker & J. C. Greenland (Eds.), *Parkinson's Disease: Pathogenesis and Clinical Aspects*. Brisbane (AU).

Kraft, R., *STIM and ORAI proteins in the nervous system.* Channels (Austin), 2015. **9**(5): p. 245-52.

Krasemann, S., Madore, C., Cialic, R., Baufeld, C., Calcagno, N., El Fatimy, R., . . . Butovsky, O. (2017). The TREM2-APOE Pathway Drives the Transcriptional Phenotype of Dysfunctional Microglia in Neurodegenerative Diseases. *Immunity, 47*(3), 566-581 e569. doi:10.1016/j.immuni.2017.08.008

Krenzlin, H., et al., *The Importance of Thrombin in Cerebral Injury and Disease.* Int J Mol Sci, 2016. **17**(1).

Kumar, A., Alvarez-Croda, D. M., Stoica, B. A., Faden, A. I., & Loane, D. J. (2016). Microglial/Macrophage Polarization Dynamics following Traumatic Brain Injury. *J Neurotrauma, 33*(19), 1732-1750. doi:10.1089/neu.2015.4268

Kummer, M. P., Hermes, M., Delekarte, A., Hammerschmidt, T., Kumar, S., Terwel, D., . . . Heneka, M. T. (2011). Nitration of tyrosine 10 critically enhances amyloid beta aggregation and plaque formation. *Neuron, 71*(5), 833-844. doi:10.1016/j.neuron.2011.07.001

Kummer, M. P., Vogl, T., Axt, D., Griep, A., Vieira-Saecker, A., Jessen, F., . . . Heneka, M. T. (2012). Mrp14 deficiency ameliorates amyloid beta burden by increasing microglial phagocytosis and modulation of amyloid precursor protein processing. *J Neurosci, 32*(49), 17824-17829. doi:10.1523/JNEUROSCI.1504-12.2012

Kuwar, R., Rolfe, A., Di, L., Blevins, H., Xu, Y., Sun, X., . . . Sun, D. (2021). A Novel Inhibitor Targeting NLRP3 Inflammasome Reduces Neuropathology and Improves Cognitive Function in Alzheimer's Disease Transgenic Mice. *J Alzheimers Dis, 82*(4), 1769-1783. doi:10.3233/JAD-210400

L'Episcopo, F., Tirolo, C., Serapide, M. F., Caniglia, S., Testa, N., Leggio, L., . . . Marchetti, B. (2018). Microglia Polarization, Gene-Environment Interactions and Wnt/beta-Catenin Signaling: Emerging Roles of Glia-Neuron and Glia-Stem/Neuroprogenitor Crosstalk for Dopaminergic Neurorestoration in Aged Parkinsonian Brain. *Front Aging Neurosci, 10*, 12. doi:10.3389/fnagi.2018.00012

L'Episcopo, F., Tirolo, C., Testa, N., Caniglia, S., Morale, M. C., Impagnatiello, F., & Marchetti, B. (2011). Switching the microglial harmful phenotype promotes lifelong restoration of subtantia nigra dopaminergic neurons from inflammatory neurodegeneration in aged mice. *Rejuvenation Res, 14*(4), 411-424. doi:10.1089/rej.2010.1134

Lambert, J. C., Ibrahim-Verbaas, C. A., Harold, D., Naj, A. C., Sims, R., Bellenguez, C., . . . Amouyel, P. (2013). Meta-analysis of 74,046 individuals identifies 11 new susceptibility loci for Alzheimer's disease. *Nat Genet, 45*(12), 1452-1458. doi:10.1038/ng.2802

Lan, X., Han, X., Li, Q., Li, Q., Gao, Y., Cheng, T., . . . Wang, J. (2017). Pinocembrin protects hemorrhagic brain primarily by inhibiting toll-like receptor 4 and reducing M1 phenotype microglia. *Brain Behav Immun, 61*, 326-339. doi:10.1016/j.bbi.2016.12.012

Lan, X., Han, X., Li, Q., Yang, Q. W., & Wang, J. (2017). Modulators of microglial activation and polarization after intracerebral haemorrhage. *Nat Rev Neurol, 13*(7), 420-433. doi:10.1038/nrneurol.2017.69

Langston, J. W., Forno, L. S., Tetrud, J., Reeves, A. G., Kaplan, J. A., & Karluk, D. (1999). Evidence of active nerve cell degeneration in the substantia nigra of humans years after 1-methyl-4-phenyl-1,2,3,6-tetrahydropyridine exposure. *Ann Neurol, 46*(4), 598-605. doi:10.1002/1531-8249(199910)46:4<598::aid-ana7>3.0.co;2-f

Lanoiselee, H. M., Nicolas, G., Wallon, D., Rovelet-Lecrux, A., Lacour, M., Rousseau, S., . . . collaborators of the, C. N. R. M. A. J. p. (2017). APP, PSEN1, and PSEN2 mutations in early-

onset Alzheimer disease: A genetic screening study of familial and sporadic cases. *PLoS Med, 14*(3), e1002270. doi:10.1371/journal.pmed.1002270

Lawson, L. J., Perry, V. H., Dri, P., & Gordon, S. (1990). Heterogeneity in the distribution and morphology of microglia in the normal adult mouse brain. *Neuroscience, 39*(1), 151-170. doi:10.1016/0306-4522(90)90229-w

Leclerc, J. L., Lampert, A. S., Loyola Amador, C., Schlakman, B., Vasilopoulos, T., Svendsen, P., . . . Dore, S. (2018). The absence of the CD163 receptor has distinct temporal influences on intracerebral hemorrhage outcomes. *J Cereb Blood Flow Metab, 38*(2), 262-273. doi:10.1177/0271678X17701459

Lee, A. J., & Ashkar, A. A. (2018). The Dual Nature of Type I and Type II Interferons. *Front Immunol, 9*, 2061. doi:10.3389/fimmu.2018.02061

Lee, C. Y., & Landreth, G. E. (2010). The role of microglia in amyloid clearance from the AD brain. *J Neural Transm (Vienna), 117*(8), 949-960. doi:10.1007/s00702-010-0433-4

Lee, D. C., Ruiz, C. R., Lebson, L., Selenica, M. L., Rizer, J., Hunt, J. B., Jr., . . . Morgan, D. (2013). Aging enhances classical activation but mitigates alternative activation in the central nervous system. *Neurobiol Aging, 34*(6), 1610-1620. doi:10.1016/j.neurobiolaging.2012.12.014

Lee, E. J., Woo, M. S., Moon, P. G., Baek, M. C., Choi, I. Y., Kim, W. K., . . . Kim, H. S. (2010). Alpha-synuclein activates microglia by inducing the expressions of matrix metalloproteinases and the subsequent activation of protease-activated receptor-1. *J Immunol, 185*(1), 615-623. doi:10.4049/jimmunol.0903480

Lee, J. K., Chung, J., Druey, K. M., & Tansey, M. G. (2012). RGS10 exerts a neuroprotective role through the PKA/c-AMP response-element (CREB) pathway in dopaminergic neuron-like cells. *J Neurochem, 122*(2), 333-343. doi:10.1111/j.1471-4159.2012.07780.x

Lee, J. K., Chung, J., Kannarkat, G. T., & Tansey, M. G. (2013). Critical Role of Regulator G-Protein Signaling 10 (RGS10) in Modulating Macrophage M1/M2 Activation. *PLoS One, 8*(11), e81785. doi:10.1371/journal.pone.0081785

Lee, J. K., Chung, J., McAlpine, F. E., & Tansey, M. G. (2011). Regulator of G-protein signaling-10 negatively regulates NF-kappaB in microglia and neuroprotects dopaminergic neurons in hemiparkinsonian rats. *J Neurosci, 31*(33), 11879-11888. doi:10.1523/JNEUROSCI.1002-11.2011

Lee, J. K., Kannarkat, G. T., Chung, J., Joon Lee, H., Graham, K. L., & Tansey, M. G. (2016). RGS10 deficiency ameliorates the severity of disease in experimental autoimmune encephalomyelitis. *J Neuroinflammation, 13*, 24. doi:10.1186/s12974-016-0491-0

Lee, J. K., McCoy, M. K., Harms, A. S., Ruhn, K. A., Gold, S. J., & Tansey, M. G. (2008). Regulator of G-protein signaling 10 promotes dopaminergic neuron survival via regulation of the microglial inflammatory response. *J Neurosci, 28*(34), 8517-8528. doi:28/34/8517 [pii] 10.1523/JNEUROSCI.1806-08.2008

Lee, J. K., & Tansey, M. G. (2015). Physiology of RGS10 in Neurons and Immune Cells. *Prog Mol Biol Transl Sci, 133*, 153-167. doi:10.1016/bs.pmbts.2015.01.005

Lehnardt, S. (2010). Innate immunity and neuroinflammation in the CNS: the role of microglia in Toll-like receptor-mediated neuronal injury. *Glia, 58*(3), 253-263. doi:10.1002/glia.20928

Letiembre, M., Hao, W., Liu, Y., Walter, S., Mihaljevic, I., Rivest, S., . . . Fassbender, K. (2007). Innate immune receptor expression in normal brain aging. *Neuroscience, 146*(1), 248-254. doi:10.1016/j.neuroscience.2007.01.004

Li, D., Song, X., Huang, H., Huang, H., & Ye, Z. (2018). Association of Parkinson's disease-related pain with plasma interleukin-1, interleukin-6, interleukin-10, and tumour necrosis factor-alpha. *Neurosci Lett, 683*, 181-184. doi:10.1016/j.neulet.2018.07.027

Li, G., Fan, R. M., Chen, J. L., Wang, C. M., Zeng, Y. C., Han, C., . . . Yao, S. T. (2014). Neuroprotective effects of argatroban and C5a receptor antagonist (PMX53) following intracerebral haemorrhage. *Clin Exp Immunol, 175*(2), 285-295. doi:10.1111/cei.12220

Li, H., & Durbin, R. (2009). Fast and accurate short read alignment with Burrows-Wheeler transform. *Bioinformatics, 25*(14), 1754-1760. doi:10.1093/bioinformatics/btp324

Li, Q., & Barres, B. A. (2018). Microglia and macrophages in brain homeostasis and disease. *Nat Rev Immunol, 18*(4), 225-242. doi:10.1038/nri.2017.125

Li, Q., Lan, X., Han, X., Durham, F., Wan, J., Weiland, A., . . . Wang, J. (2021). Microglia-derived interleukin-10 accelerates post-intracerebral hemorrhage hematoma clearance by regulating CD36. *Brain Behav Immun, 94*, 437-457. doi:10.1016/j.bbi.2021.02.001

Li, Q. Q., Li, L. J., Wang, X. Y., Sun, Y. Y., & Wu, J. (2018). Research Progress in Understanding the Relationship Between Heme Oxygenase-1 and Intracerebral Hemorrhage. *Front Neurol, 9*, 682. doi:10.3389/fneur.2018.00682

Li, R., Liu, W., Yin, J., Chen, Y., Guo, S., Fan, H., . . . Duan, C. (2018). TSG-6 attenuates inflammation-induced brain injury via modulation of microglial polarization in SAH rats through the SOCS3/STAT3 pathway. *J Neuroinflammation, 15*(1), 231. doi:10.1186/s12974-018-1279-1

Li, X., Zhu, Z., Gao, S., Zhang, L., Cheng, X., Li, S., & Li, M. (2019). Inhibition of fibrin formation reduces neuroinflammation and improves long-term outcome after intracerebral hemorrhage. *Int Immunopharmacol, 72*, 473-478. doi:10.1016/j.intimp.2019.04.029

Lian, H., E. Roy, and H. Zheng, *Protocol for Primary Microglial Culture Preparation.* Bio Protoc, 2016. **6**(21)

Liang, G., Bansal, G., Xie, Z., & Druey, K. M. (2009). RGS16 inhibits breast cancer cell growth by mitigating phosphatidylinositol 3-kinase signaling. *J Biol Chem, 284*(32), 21719-21727. doi:10.1074/jbc.M109.028407

Liao, Y., Smyth, G. K., & Shi, W. (2014). featureCounts: an efficient general purpose program for assigning sequence reads to genomic features. *Bioinformatics, 30*(7), 923-930. doi:10.1093/bioinformatics/btt656

Liberzon, A., Birger, C., Thorvaldsdottir, H., Ghandi, M., Mesirov, J. P., & Tamayo, P. (2015). The Molecular Signatures Database (MSigDB) hallmark gene set collection. *Cell Syst, 1*(6), 417-425. doi:10.1016/j.cels.2015.12.004

Lin, L., Yihao, T., Zhou, F., Yin, N., Qiang, T., Haowen, Z., . . . Zhi, C. (2017). Inflammatory Regulation by Driving Microglial M2 Polarization: Neuroprotective Effects of Cannabinoid Receptor-2 Activation in Intracerebral Hemorrhage. *Front Immunol, 8*, 112. doi:10.3389/fimmu.2017.00112

Lin, S., Yin, Q., Zhong, Q., Lv, F. L., Zhou, Y., Li, J. Q., . . . Yang, Q. W. (2012). Heme activates TLR4-mediated inflammatory injury via MyD88/TRIF signaling pathway in intracerebral hemorrhage. *J Neuroinflammation, 9*, 46. doi:10.1186/1742-2094-9-46

Liu, J. T., Wu, S. X., Zhang, H., & Kuang, F. (2018). Inhibition of MyD88 Signaling Skews Microglia/Macrophage Polarization and Attenuates Neuronal Apoptosis in the Hippocampus After Status Epilepticus in Mice. *Neurotherapeutics, 15*(4), 1093-1111. doi:10.1007/s13311-018-0653-0

Liu, Q., Chen, Y., Auger-Messier, M., & Molkentin, J. D. (2012). Interaction between NFkappaB and NFAT coordinates cardiac hypertrophy and pathological remodeling. *Circ Res, 110*(8), 1077-1086. doi:10.1161/CIRCRESAHA.111.260729

Liu, W., Taso, O., Wang, R., Bayram, S., Graham, A. C., Garcia-Reitboeck, P., . . . Salih, D. A. (2020). Trem2 promotes anti-inflammatory responses in microglia and is suppressed under pro-inflammatory conditions. *Hum Mol Genet, 29*(19), 3224-3248. doi:10.1093/hmg/ddaa209

Lively, S. and L.C. Schlichter, *Microglia Responses to Pro-inflammatory Stimuli (LPS, IFNgamma+TNFalpha) and Reprogramming by Resolving Cytokines (IL-4, IL-10).* Front Cell Neurosci, 2018. **12**: p. 215.

Lopes, K. P., Snijders, G. J. L., Humphrey, J., Allan, A., Sneeboer, M. A. M., Navarro, E., . . . Raj, T. (2022). Genetic analysis of the human microglial transcriptome across brain regions, aging and disease pathologies. *Nat Genet, 54*(1), 4-17. doi:10.1038/s41588-021-00976-y

Lopes Pinheiro, M. A., Kooij, G., Mizee, M. R., Kamermans, A., Enzmann, G., Lyck, R., . . . de Vries, H. E. (2016). Immune cell trafficking across the barriers of the central nervous system in multiple sclerosis and stroke. *Biochim Biophys Acta, 1862*(3), 461-471. doi:10.1016/j.bbadis.2015.10.018

Lovaszi, M., Branco Haas, C., Antonioli, L., Pacher, P., & Hasko, G. (2021). The role of P2Y receptors in regulating immunity and metabolism. *Biochem Pharmacol, 187*, 114419. doi:10.1016/j.bcp.2021.114419

Love, M. I., Anders, S., Kim, V., & Huber, W. (2015). RNA-Seq workflow: gene-level exploratory analysis and differential expression. *F1000Res, 4*, 1070. doi:10.12688/f1000research.7035.1

Loving, B. A., & Bruce, K. D. (2020). Lipid and Lipoprotein Metabolism in Microglia. *Front Physiol, 11*, 393. doi:10.3389/fphys.2020.00393

Lucin, K. M., O'Brien, C. E., Bieri, G., Czirr, E., Mosher, K. I., Abbey, R. J., . . . Wyss-Coray, T. (2013). Microglial beclin 1 regulates retromer trafficking and phagocytosis and is impaired in Alzheimer's disease. *Neuron, 79*(5), 873-886. doi:10.1016/j.neuron.2013.06.046

Lull, M. E., & Block, M. L. (2010). Microglial activation and chronic neurodegeneration. *Neurotherapeutics, 7*(4), 354-365. doi:10.1016/j.nurt.2010.05.014

Ma, B., Xu, L., Pan, X., Sun, L., Ding, J., Xie, C., . . . Cai, H. (2016). LRRK2 modulates microglial activity through regulation of chemokine (C-X3-C) receptor 1 -mediated signalling pathways. *Hum Mol Genet, 25*(16), 3515-3523. doi:10.1093/hmg/ddw194

Ma, C., Zhou, W., Yan, Z., Qu, M., & Bu, X. (2015). Toll-like Receptor 4 (TLR4) is Associated with Cerebral Vasospasm and Delayed Cerebral Ischemia in Aneurysmal Subarachnoid Hemorrhage. *Neurol Med Chir (Tokyo), 55*(12), 878-884. doi:10.2176/nmc.oa.2015-0077

Madore, C., Joffre, C., Delpech, J. C., De Smedt-Peyrusse, V., Aubert, A., Coste, L., . . . Nadjar, A. (2013). Early morphofunctional plasticity of microglia in response to acute lipopolysaccharide. *Brain Behav Immun, 34*, 151-158. doi:10.1016/j.bbi.2013.08.008

Madrigal, J. L., Moro, M. A., Lizasoain, I., Lorenzo, P., Fernandez, A. P., Rodrigo, J., . . . Leza, J. C. (2003). Induction of cyclooxygenase-2 accounts for restraint stress-induced oxidative status in rat brain. *Neuropsychopharmacology, 28*(9), 1579-1588. doi:10.1038/sj.npp.1300187

Maeda, J., Minamihisamatsu, T., Shimojo, M., Zhou, X., Ono, M., Matsuba, Y., . . . Sahara, N. (2021). Distinct microglial response against Alzheimer's amyloid and tau pathologies characterized by P2Y12 receptor. *Brain Commun, 3*(1), fcab011. doi:10.1093/braincomms/fcab011

Maiti, P., Manna, J., & Dunbar, G. L. (2017). Current understanding of the molecular mechanisms in Parkinson's disease: Targets for potential treatments. *Transl Neurodegener, 6*, 28. doi:10.1186/s40035-017-0099-z

Majumdar, A., Cruz, D., Asamoah, N., Buxbaum, A., Sohar, I., Lobel, P., & Maxfield, F. R. (2007). Activation of microglia acidifies lysosomes and leads to degradation of Alzheimer amyloid fibrils. *Mol Biol Cell, 18*(4), 1490-1496. doi:10.1091/mbc.e06-10-0975

Makin, S. (2018). The amyloid hypothesis on trial. *Nature, 559*(7715), S4-S7. doi:10.1038/d41586-018-05719-4

Manaenko, A., Chen, H., Zhang, J. H., & Tang, J. (2011). Comparison of different preclinical models of intracerebral hemorrhage. *Acta Neurochir Suppl, 111*, 9-14. doi:10.1007/978-3-7091-0693-8_2

Mancuso, R., Van Den Daele, J., Fattorelli, N., Wolfs, L., Balusu, S., Burton, O., . . . De Strooper, B. (2019). Stem-cell-derived human microglia transplanted in mouse brain to study human disease. *Nat Neurosci, 22*(12), 2111-2116. doi:10.1038/s41593-019-0525-x

Mandrekar-Colucci, S., Karlo, J. C., & Landreth, G. E. (2012). Mechanisms underlying the rapid peroxisome proliferator-activated receptor-gamma-mediated amyloid clearance and reversal of cognitive deficits in a murine model of Alzheimer's disease. *J Neurosci, 32*(30), 10117-10128. doi:10.1523/JNEUROSCI.5268-11.2012

Marinova-Mutafchieva, L., Sadeghian, M., Broom, L., Davis, J. B., Medhurst, A. D., & Dexter, D. T. (2009). Relationship between microglial activation and dopaminergic neuronal loss in the substantia nigra: a time course study in a 6-hydroxydopamine model of Parkinson's disease. *J Neurochem, 110*(3), 966-975. doi:10.1111/j.1471-4159.2009.06189.x

Martens, M., Ammar, A., Riutta, A., Waagmeester, A., Slenter, D. N., Hanspers, K., . . . Kutmon, M. (2021). WikiPathways: connecting communities. *Nucleic Acids Res, 49*(D1), D613-D621. doi:10.1093/nar/gkaa1024

Martin, E., El-Behi, M., Fontaine, B., & Delarasse, C. (2017). Analysis of Microglia and Monocyte-derived Macrophages from the Central Nervous System by Flow Cytometry. *J Vis Exp*(124). doi:10.3791/55781

Martin-McCaffrey, L., Willard, F. S., Pajak, A., Dagnino, L., Siderovski, D. P., & D'Souza, S. J. (2005). RGS14 is a microtubule-associated protein. *Cell Cycle, 4*(7), 953-960. doi:10.4161/cc.4.7.1787

Mastroeni, D., Nolz, J., Sekar, S., Delvaux, E., Serrano, G., Cuyugan, L., . . . Coleman, P. D. (2018). Laser-captured microglia in the Alzheimer's and Parkinson's brain reveal unique regional expression profiles and suggest a potential role for hepatitis B in the Alzheimer's brain. *Neurobiol Aging, 63*, 12-21. doi:10.1016/j.neurobiolaging.2017.10.019

Masuda, T., Sankowski, R., Staszewski, O., Bottcher, C., Amann, L., Sagar, . . . Prinz, M. (2019). Spatial and temporal heterogeneity of mouse and human microglia at single-cell resolution. *Nature, 566*(7744), 388-392. doi:10.1038/s41586-019-0924-x

Masuho, I., Balaji, S., Muntean, B. S., Skamangas, N. K., Chavali, S., Tesmer, J. J. G., . . . Martemyanov, K. A. (2020). A Global Map of G Protein Signaling Regulation by RGS Proteins. *Cell, 183*(2), 503-521 e519. doi:10.1016/j.cell.2020.08.052

Mathys, H., Davila-Velderrain, J., Peng, Z., Gao, F., Mohammadi, S., Young, J. Z., . . . Tsai, L. H. (2019). Single-cell transcriptomic analysis of Alzheimer's disease. *Nature, 570*(7761), 332-337. doi:10.1038/s41586-019-1195-2

Matz, P., Turner, C., Weinstein, P. R., Massa, S. M., Panter, S. S., & Sharp, F. R. (1996). Heme-oxygenase-1 induction in glia throughout rat brain following experimental subarachnoid hemorrhage. *Brain Res, 713*(1-2), 211-222. doi:10.1016/0006-8993(95)01511-6

Mawuenyega, K. G., Sigurdson, W., Ovod, V., Munsell, L., Kasten, T., Morris, J. C., . . . Bateman, R. J. (2010). Decreased clearance of CNS beta-amyloid in Alzheimer's disease. *Science, 330*(6012), 1774. doi:10.1126/science.1197623

McGeer, P. L., Itagaki, S., Boyes, B. E., & McGeer, E. G. (1988). Reactive microglia are positive for HLA-DR in the substantia nigra of Parkinson's and Alzheimer's disease brains. *Neurology, 38*(8), 1285-1291. doi:10.1212/wnl.38.8.1285

Mecha, M., Feliu, A., Carrillo-Salinas, F. J., Rueda-Zubiaurre, A., Ortega-Gutierrez, S., de Sola, R. G., & Guaza, C. (2015). Endocannabinoids drive the acquisition of an alternative phenotype in microglia. *Brain Behav Immun, 49*, 233-245. doi:10.1016/j.bbi.2015.06.002

Melki, R. (2015). Role of Different Alpha-Synuclein Strains in Synucleinopathies, Similarities with other Neurodegenerative Diseases. *J Parkinsons Dis, 5*(2), 217-227. doi:10.3233/JPD-150543

Meng, H. L., Li, X. X., Chen, Y. T., Yu, L. J., Zhang, H., Lao, J. M., . . . Xu, Y. (2016). Neuronal Soluble Fas Ligand Drives M1-Microglia Polarization after Cerebral Ischemia. *CNS Neurosci Ther, 22*(9), 771-781. doi:10.1111/cns.12575

Merlo, S., Spampinato, S. F., Beneventano, M., & Sortino, M. A. (2018). The contribution of microglia to early synaptic compensatory responses that precede beta-amyloid-induced neuronal death. *Sci Rep, 8*(1), 7297. doi:10.1038/s41598-018-25453-1

Miao, R., Lu, Y., Xing, X., Li, Y., Huang, Z., Zhong, H., . . . Yuan, H. (2016). Regulator of G-Protein Signaling 10 Negatively Regulates Cardiac Remodeling by Blocking Mitogen-Activated Protein Kinase-Extracellular Signal-Regulated Protein Kinase 1/2 Signaling. *Hypertension, 67*(1), 86-98. doi:10.1161/HYPERTENSIONAHA.115.05957

Michaelis, M., Nieswandt, B., Stegner, D., Eilers, J., & Kraft, R. (2015). STIM1, STIM2, and Orai1 regulate store-operated calcium entry and purinergic activation of microglia. *Glia, 63*(4), 652-663. doi:10.1002/glia.22775

Michelucci, A., Heurtaux, T., Grandbarbe, L., Morga, E., & Heuschling, P. (2009). Characterization of the microglial phenotype under specific pro-inflammatory and anti-inflammatory conditions: Effects of oligomeric and fibrillar amyloid-beta. *J Neuroimmunol, 210*(1-2), 3-12. doi:10.1016/j.jneuroim.2009.02.003

Miron, V. E., & Priller, J. (2020). Investigating Microglia in Health and Disease: Challenges and Opportunities. *Trends Immunol, 41*(9), 785-793. doi:10.1016/j.it.2020.07.002

Mittelbronn, M., Dietz, K., Schluesener, H. J., & Meyermann, R. (2001). Local distribution of microglia in the normal adult human central nervous system differs by up to one order of magnitude. *Acta Neuropathol, 101*(3), 249-255. doi:10.1007/s004010000284

Mizuma, A., Kim, J. Y., Kacimi, R., Stauderman, K., Dunn, M., Hebbar, S., & Yenari, M. A. (2019). Microglial Calcium Release-Activated Calcium Channel Inhibition Improves Outcome from Experimental Traumatic Brain Injury and Microglia-Induced Neuronal Death. *Journal of Neurotrauma, 36*(7), 996-1007.

Mizuno, T., Kawanokuchi, J., Numata, K., & Suzumura, A. (2003). Production and neuroprotective functions of fractalkine in the central nervous system. *Brain Res, 979*(1-2), 65-70. doi:10.1016/s0006-8993(03)02867-1

Moller, T., Hanisch, U. K., & Ransom, B. R. (2000). Thrombin-induced activation of cultured rodent microglia. *J Neurochem, 75*(4), 1539-1547. doi:10.1046/j.1471-4159.2000.0751539.x

Monier, A., Adle-Biassette, H., Delezoide, A. L., Evrard, P., Gressens, P., & Verney, C. (2007). Entry and distribution of microglial cells in human embryonic and fetal cerebral cortex. *J Neuropathol Exp Neurol, 66*(5), 372-382. doi:10.1097/nen.0b013e3180517b46

Montano, A., Hanley, D. F., & Hemphill, J. C., 3rd. (2021). Hemorrhagic stroke. *Handb Clin Neurol, 176*, 229-248. doi:10.1016/B978-0-444-64034-5.00019-5

Morganti, J. M., Nash, K. R., Grimmig, B. A., Ranjit, S., Small, B., Bickford, P. C., & Gemma, C. (2012). The soluble isoform of CX3CL1 is necessary for neuroprotection in a mouse model of Parkinson's disease. *J Neurosci, 32*(42), 14592-14601. doi:10.1523/JNEUROSCI.0539-12.2012

Mosser, D. M., & Edwards, J. P. (2008). Exploring the full spectrum of macrophage activation. *Nat Rev Immunol, 8*(12), 958-969. doi:10.1038/nri2448

Mou, H., Smith, J. L., Peng, L., Yin, H., Moore, J., Zhang, X. O., . . . Xue, W. (2017). CRISPR/Cas9-mediated genome editing induces exon skipping by alternative splicing or exon deletion. *Genome Biol, 18*(1), 108. doi:10.1186/s13059-017-1237-8

Mukhopadhyay, S., & Ross, E. M. (1999). Rapid GTP binding and hydrolysis by G(q) promoted by receptor and GTPase-activating proteins. *Proc Natl Acad Sci U S A, 96*(17), 9539-9544. doi:10.1073/pnas.96.17.9539

Murakami, K., Koide, M., Dumont, T. M., Russell, S. R., Tranmer, B. I., & Wellman, G. C. (2011). Subarachnoid Hemorrhage Induces Gliosis and Increased Expression of the Pro-inflammatory Cytokine High Mobility Group Box 1 Protein. *Transl Stroke Res, 2*(1), 72-79. doi:10.1007/s12975-010-0052-2

Nagamoto-Combs, K. and C.K. Combs, *Microglial phenotype is regulated by activity of the transcription factor, NFAT (nuclear factor of activated T cells).* J Neurosci, 2010. **30**(28): p. 9641-6.

Nakagawa, Y., & Chiba, K. (2015). Diversity and plasticity of microglial cells in psychiatric and neurological disorders. *Pharmacol Ther, 154*, 21-35. doi:10.1016/j.pharmthera.2015.06.010

Nakano, T., Nakamura, Y., Irie, K., Okano, S., Morimoto, M., Yamashita, Y., . . . Mishima, K. (2020). Antithrombin gamma attenuates macrophage/microglial activation and brain damage after transient focal cerebral ischemia in mice. *Life Sci, 252*, 117665. doi:10.1016/j.lfs.2020.117665

Nakaso, K., Kitayama, M., Mizuta, E., Fukuda, H., Ishii, T., Nakashima, K., & Yamada, K. (2000). Co-induction of heme oxygenase-1 and peroxiredoxin I in astrocytes and microglia around hemorrhagic region in the rat brain. *Neurosci Lett, 293*(1), 49-52. doi:10.1016/s0304-3940(00)01491-9

Nance, M. R., Kreutz, B., Tesmer, V. M., Sterne-Marr, R., Kozasa, T., & Tesmer, J. J. (2013). Structural and functional analysis of the regulator of G protein signaling 2-galphaq complex. *Structure, 21*(3), 438-448. doi:10.1016/j.str.2012.12.016

Nash, K. R., Moran, P., Finneran, D. J., Hudson, C., Robinson, J., Morgan, D., & Bickford, P. C. (2015). Fractalkine over expression suppresses alpha-synuclein-mediated neurodegeneration. *Mol Ther, 23*(1), 17-23. doi:10.1038/mt.2014.175

Natochin, M., & Artemyev, N. O. (1998). A single mutation Asp229 --> Ser confers upon Gs alpha the ability to interact with regulators of G protein signaling. *Biochemistry, 37*(39), 13776-13780. doi:10.1021/bi981155a

Nelson, H. A., Leech, C. A., Kopp, R. F., & Roe, M. W. (2018). Interplay between ER Ca(2+) Binding Proteins, STIM1 and STIM2, Is Required for Store-Operated Ca(2+) Entry. *Int J Mol Sci, 19*(5). doi:10.3390/ijms19051522

Newton, K. and V.M. Dixit, *Signaling in innate immunity and inflammation.* Cold Spring Harb Perspect Biol, 2012. **4**(3).

Nguyen, C. H., Ming, H., Zhao, P., Hugendubler, L., Gros, R., Kimball, S. R., & Chidiac, P. (2009). Translational control by RGS2. *J Cell Biol, 186*(5), 755-765. doi:10.1083/jcb.200811058

Nimmerjahn, A., Kirchhoff, F., & Helmchen, F. (2005). Resting microglial cells are highly dynamic surveillants of brain parenchyma in vivo. *Science, 308*(5726), 1314-1318. doi:10.1126/science.1110647

Nonnekes, J., Post, B., Tetrud, J. W., Langston, J. W., & Bloem, B. R. (2018). MPTP-induced parkinsonism: an historical case series. *Lancet Neurol, 17*(4), 300-301. doi:10.1016/S1474-4422(18)30072-3

Norden, D. M., & Godbout, J. P. (2013). Review: microglia of the aged brain: primed to be activated and resistant to regulation. *Neuropathol Appl Neurobiol, 39*(1), 19-34. doi:10.1111/j.1365-2990.2012.01306.x

O'Hara, D. M., Pawar, G., Kalia, S. K., & Kalia, L. V. (2020). LRRK2 and alpha-Synuclein: Distinct or Synergistic Players in Parkinson's Disease? *Front Neurosci, 14*, 577. doi:10.3389/fnins.2020.00577

Oh-Hora, M., Yamashita, M., Hogan, P. G., Sharma, S., Lamperti, E., Chung, W., . . . Rao, A. (2008). Dual functions for the endoplasmic reticulum calcium sensors STIM1 and STIM2 in T cell activation and tolerance. *Nat Immunol, 9*(4), 432-443. doi:10.1038/ni1574

Ohnishi, M., Katsuki, H., Fujimoto, S., Takagi, M., Kume, T., & Akaike, A. (2007). Involvement of thrombin and mitogen-activated protein kinase pathways in hemorrhagic brain injury. *Exp Neurol, 206*(1), 43-52. doi:10.1016/j.expneurol.2007.03.030

Olah, M., Menon, V., Habib, N., Taga, M. F., Ma, Y., Yung, C. J., . . . De Jager, P. L. (2020). Single cell RNA sequencing of human microglia uncovers a subset associated with Alzheimer's disease. *Nat Commun, 11*(1), 6129. doi:10.1038/s41467-020-19737-2

Oliveros, J. C. (2010). Venny: An interactive tool for comparing lists with Venn’s diagrams. Retrieved from http://bioinfogp.cnb.csic.es/tools/venny/index.html

Olmedillas Del Moral, M., Asavapanumas, N., Uzcategui, N. L., & Garaschuk, O. (2019). Healthy Brain Aging Modifies Microglial Calcium Signaling In Vivo. *Int J Mol Sci, 20*(3). doi:10.3390/ijms20030589

Olsson, F., Schmidt, S., Althoff, V., Munter, L. M., Jin, S., Rosqvist, S., . . . Lundkvist, J. (2014). Characterization of intermediate steps in amyloid beta (Abeta) production under near-native conditions. *J Biol Chem, 289*(3), 1540-1550. doi:10.1074/jbc.M113.498246

Ong, H. L., de Souza, L. B., Zheng, C., Cheng, K. T., Liu, X., Goldsmith, C. M., . . . Ambudkar, I. S. (2015). STIM2 enhances receptor-stimulated Ca²⁺ signaling by promoting recruitment of STIM1 to the endoplasmic reticulum–plasma membrane junctions. *Science Signaling, 8*(359), ra3-ra3. doi:10.1126/scisignal.2005748

Ormel, P. R., Vieira de Sa, R., van Bodegraven, E. J., Karst, H., Harschnitz, O., Sneeboer, M. A. M., . . . Pasterkamp, R. J. (2018). Microglia innately develop within cerebral organoids. *Nat Commun, 9*(1), 4167. doi:10.1038/s41467-018-06684-2

Orre, M., Kamphuis, W., Osborn, L. M., Melief, J., Kooijman, L., Huitinga, I., . . . Hol, E. M. (2014). Acute isolation and transcriptome characterization of cortical astrocytes and microglia from young and aged mice. *Neurobiol Aging, 35*(1), 1-14. doi:10.1016/j.neurobiolaging.2013.07.008

Ostapchenko, V. G., Chen, M., Guzman, M. S., Xie, Y. F., Lavine, N., Fan, J., . . . Jackson, M. F. (2015). The Transient Receptor Potential Melastatin 2 (TRPM2) Channel Contributes to beta-Amyloid Oligomer-Related Neurotoxicity and Memory Impairment. *J Neurosci, 35*(45), 15157-15169. doi:10.1523/JNEUROSCI.4081-14.2015

Ouchi, Y., Yagi, S., Yokokura, M., & Sakamoto, M. (2009). Neuroinflammation in the living brain of Parkinson's disease. *Parkinsonism Relat Disord, 15 Suppl 3*, S200-204. doi:10.1016/S1353-8020(09)70814-4

Pabon, M. M., Bachstetter, A. D., Hudson, C. E., Gemma, C., & Bickford, P. C. (2011). CX3CL1 reduces neurotoxicity and microglial activation in a rat model of Parkinson's disease. *J Neuroinflammation, 8*, 9. doi:10.1186/1742-2094-8-9

Palty, R., Fu, Z., & Isacoff, E. Y. (2017). Sequential Steps of CRAC Channel Activation. *Cell Rep, 19*(9), 1929-1939. doi:10.1016/j.celrep.2017.05.025

Pan, J., Jin, J. L., Ge, H. M., Yin, K. L., Chen, X., Han, L. J., . . . Xu, Y. (2015). Malibatol A regulates microglia M1/M2 polarization in experimental stroke in a PPARgamma-dependent manner. *J Neuroinflammation, 12*, 51. doi:10.1186/s12974-015-0270-3

Parakalan, R., Jiang, B., Nimmi, B., Janani, M., Jayapal, M., Lu, J., . . . Dheen, S. T. (2012). Transcriptome analysis of amoeboid and ramified microglia isolated from the corpus callosum of rat brain. *BMC Neurosci, 13*, 64. doi:10.1186/1471-2202-13-64

Parhizkar, S., Arzberger, T., Brendel, M., Kleinberger, G., Deussing, M., Focke, C., . . . Haass, C. (2019). Loss of TREM2 function increases amyloid seeding but reduces plaque-associated ApoE. *Nat Neurosci, 22*(2), 191-204. doi:10.1038/s41593-018-0296-9

Park, Y. J., Yoo, S. A., Kim, M., & Kim, W. U. (2020). The Role of Calcium-Calcineurin-NFAT Signaling Pathway in Health and Autoimmune Diseases. *Front Immunol, 11*, 195. doi:10.3389/fimmu.2020.00195

Parkhurst, C. N., Yang, G., Ninan, I., Savas, J. N., Yates, J. R., 3rd, Lafaille, J. J., . . . Gan, W. B. (2013). Microglia promote learning-dependent synapse formation through brain-derived neurotrophic factor. *Cell, 155*(7), 1596-1609. doi:10.1016/j.cell.2013.11.030

Pawelec, P., Ziemka-Nalecz, M., Sypecka, J., & Zalewska, T. (2020). The Impact of the CX3CL1/CX3CR1 Axis in Neurological Disorders. *Cells, 9*(10). doi:10.3390/cells9102277

Pereira, J. B., Ossenkoppele, R., Palmqvist, S., Strandberg, T. O., Smith, R., Westman, E., & Hansson, O. (2019). Amyloid and tau accumulate across distinct spatial networks and are differentially associated with brain connectivity. *Elife, 8*. doi:10.7554/eLife.50830

Pickford, F., Masliah, E., Britschgi, M., Lucin, K., Narasimhan, R., Jaeger, P. A., . . . Wyss-Coray, T. (2008). The autophagy-related protein beclin 1 shows reduced expression in early Alzheimer disease and regulates amyloid beta accumulation in mice. *J Clin Invest, 118*(6), 2190-2199. doi:10.1172/JCI33585

Pisanu, A., Lecca, D., Mulas, G., Wardas, J., Simbula, G., Spiga, S., & Carta, A. R. (2014). Dynamic changes in pro- and anti-inflammatory cytokines in microglia after PPAR-gamma agonist neuroprotective treatment in the MPTPp mouse model of progressive Parkinson's disease. *Neurobiol Dis, 71*, 280-291. doi:10.1016/j.nbd.2014.08.011

Platanitis, E., & Decker, T. (2018). Regulatory Networks Involving STATs, IRFs, and NFkappaB in Inflammation. *Front Immunol, 9*, 2542. doi:10.3389/fimmu.2018.02542

Plescher, M., Seifert, G., Hansen, J. N., Bedner, P., Steinhauser, C., & Halle, A. (2018). Plaque-dependent morphological and electrophysiological heterogeneity of microglia in an Alzheimer's disease mouse model. *Glia, 66*(7), 1464-1480. doi:10.1002/glia.23318

Poewe, W., Seppi, K., Tanner, C. M., Halliday, G. M., Brundin, P., Volkmann, J., . . . Lang, A. E. (2017). Parkinson disease. *Nat Rev Dis Primers, 3*, 17013. doi:10.1038/nrdp.2017.13

Polazzi, E., Altamira, L. E., Eleuteri, S., Barbaro, R., Casadio, C., Contestabile, A., & Monti, B. (2009). Neuroprotection of microglial conditioned medium on 6-hydroxydopamine-induced neuronal death: role of transforming growth factor beta-2. *J Neurochem, 110*(2), 545-556. doi:10.1111/j.1471-4159.2009.06117.x

Popov, S., Yu, K., Kozasa, T., & Wilkie, T. M. (1997). The regulators of G protein signaling (RGS) domains of RGS4, RGS10, and GAIP retain GTPase activating protein activity in vitro. *Proc Natl Acad Sci U S A, 94*(14), 7216-7220. Retrieved from http://www.ncbi.nlm.nih.gov/entrez/query.fcgi?cmd=Retrieve&db=PubMed&dopt=Citation&list_uids=9207071

Popp, M. W., & Maquat, L. E. (2016). Leveraging Rules of Nonsense-Mediated mRNA Decay for Genome Engineering and Personalized Medicine. *Cell, 165*(6), 1319-1322. doi:10.1016/j.cell.2016.05.053

Pozner, A., Xu, B., Palumbos, S., Gee, J. M., Tvrdik, P., & Capecchi, M. R. (2015). Intracellular calcium dynamics in cortical microglia responding to focal laser injury in the PC::G5-tdT reporter mouse. *Front Mol Neurosci, 8*, 12. doi:10.3389/fnmol.2015.00012

Pradhan, S., & Andreasson, K. (2013). Commentary: Progressive inflammation as a contributing factor to early development of Parkinson's disease. *Exp Neurol, 241*, 148-155. doi:10.1016/j.expneurol.2012.12.008

Preissler, S., Rato, C., Yan, Y., Perera, L. A., Czako, A., & Ron, D. (2020). Calcium depletion challenges endoplasmic reticulum proteostasis by destabilising BiP-substrate complexes. *Elife, 9*. doi:10.7554/eLife.62601

Probert, L. (2015). TNF and its receptors in the CNS: The essential, the desirable and the deleterious effects. *Neuroscience, 302*, 2-22. doi:10.1016/j.neuroscience.2015.06.038

Puigdellivol, M., Milde, S., Vilalta, A., Cockram, T. O. J., Allendorf, D. H., Lee, J. Y., . . . Brown, G. C. (2021). The microglial P2Y6 receptor mediates neuronal loss and memory deficits in neurodegeneration. *Cell Rep, 37*(13), 110148. doi:10.1016/j.celrep.2021.110148

Pulido-Salgado, M., Vidal-Taboada, J. M., Barriga, G. G., Sola, C., & Saura, J. (2018). RNA-Seq transcriptomic profiling of primary murine microglia treated with LPS or LPS + IFNgamma. *Sci Rep, 8*(1), 16096. doi:10.1038/s41598-018-34412-9

Qin, C., Fan, W. H., Liu, Q., Shang, K., Murugan, M., Wu, L. J., . . . Tian, D. S. (2017). Fingolimod Protects Against Ischemic White Matter Damage by Modulating Microglia Toward M2 Polarization via STAT3 Pathway. *Stroke, 48*(12), 3336-3346. doi:10.1161/STROKEAHA.117.018505

Qin, H., Buckley, J. A., Li, X., Liu, Y., Fox, T. H., 3rd, Meares, G. P., . . . Benveniste, E. N. (2016). Inhibition of the JAK/STAT Pathway Protects Against alpha-Synuclein-Induced Neuroinflammation and Dopaminergic Neurodegeneration. *J Neurosci, 36*(18), 5144-5159. doi:10.1523/JNEUROSCI.4658-15.2016

Raffaele, S., Lombardi, M., Verderio, C., & Fumagalli, M. (2020). TNF Production and Release from Microglia via Extracellular Vesicles: Impact on Brain Functions. *Cells, 9*(10). doi:10.3390/cells9102145

Ramirez, A. I., de Hoz, R., Salobrar-Garcia, E., Salazar, J. J., Rojas, B., Ajoy, D., . . . Ramirez, J. M. (2017). The Role of Microglia in Retinal Neurodegeneration: Alzheimer's Disease, Parkinson, and Glaucoma. *Front Aging Neurosci, 9*, 214. doi:10.3389/fnagi.2017.00214

Ransohoff, R. M., & Brown, M. A. (2012). Innate immunity in the central nervous system. *J Clin Invest, 122*(4), 1164-1171. doi:10.1172/JCI58644

Rechsteiner, M., & Rogers, S. W. (1996). PEST sequences and regulation by proteolysis. *Trends Biochem Sci, 21*(7), 267-271. Retrieved from https://www.ncbi.nlm.nih.gov/pubmed/8755249

Reichwald, J., Danner, S., Wiederhold, K. H., & Staufenbiel, M. (2009). Expression of complement system components during aging and amyloid deposition in APP transgenic mice. *J Neuroinflammation, 6*, 35. doi:10.1186/1742-2094-6-35

Ren, J., Wei, W., Tan, L., Yang, Q., Lu, Q., Ding, H., . . . Li, J. (2021). Inhibition of regulator of G protein signaling 10, aggravates rheumatoid arthritis progression by promoting NF-kappaB signaling pathway. *Mol Immunol, 134*, 236-246. doi:10.1016/j.molimm.2021.03.024

Rex, J., et al., *Model-Based Characterization of Inflammatory Gene Expression Patterns of Activated Macrophages.* PLoS Comput Biol, 2016. **12**(7): p. e1005018.

Rhee, S. G., & Bae, Y. S. (1997). Regulation of phosphoinositide-specific phospholipase C isozymes. *J Biol Chem, 272*(24), 15045-15048. doi:10.1074/jbc.272.24.15045

Ricciotti, E., & FitzGerald, G. A. (2011). Prostaglandins and inflammation. *Arterioscler Thromb Vasc Biol, 31*(5), 986-1000. doi:10.1161/ATVBAHA.110.207449

Righy, C., Turon, R., Freitas, G., Japiassu, A. M., Faria Neto, H. C. C., Bozza, M., . . . Bozza, F. A. (2018). Hemoglobin metabolism by-products are associated with an inflammatory response in patients with hemorrhagic stroke. *Rev Bras Ter Intensiva, 30*(1), 21-27. doi:10.5935/0103-507x.20180003

Robinson, J. T., Thorvaldsdottir, H., Winckler, W., Guttman, M., Lander, E. S., Getz, G., & Mesirov, J. P. (2011). Integrative genomics viewer. *Nat Biotechnol, 29*(1), 24-26. doi:10.1038/nbt.1754

Robinson, S. R., Dang, T. N., Dringen, R., & Bishop, G. M. (2009). Hemin toxicity: a preventable source of brain damage following hemorrhagic stroke. *Redox Rep, 14*(6), 228-235. doi:10.1179/135100009X12525712409931

Rodriguez-Yanez, M., Brea, D., Arias, S., Blanco, M., Pumar, J. M., Castillo, J., & Sobrino, T. (2012). Increased expression of Toll-like receptors 2 and 4 is associated with poor outcome in intracerebral hemorrhage. *J Neuroimmunol, 247*(1-2), 75-80. doi:10.1016/j.jneuroim.2012.03.019

Rogers, J. T., Morganti, J. M., Bachstetter, A. D., Hudson, C. E., Peters, M. M., Grimmig, B. A., . . . Gemma, C. (2011). CX3CR1 deficiency leads to impairment of hippocampal cognitive function and synaptic plasticity. *J Neurosci, 31*(45), 16241-16250. doi:10.1523/JNEUROSCI.3667-11.2011

Ruan, Z., Pathak, D., Venkatesan Kalavai, S., Yoshii-Kitahara, A., Muraoka, S., Bhatt, N., . . . Ikezu, T. (2021). Alzheimer's disease brain-derived extracellular vesicles spread tau pathology in interneurons. *Brain, 144*(1), 288-309. doi:10.1093/brain/awaa376

Rupprecht, C., Rupprecht, R., & Rammes, G. (2021). C1q, a small molecule with high impact on brain development: putative role for aging processes and the occurrence of Alzheimer's disease. *Eur Arch Psychiatry Clin Neurosci, 271*(5), 809-812. doi:10.1007/s00406-021-01273-9

Rutar, M., Valter, K., Natoli, R., & Provis, J. M. (2014). Synthesis and propagation of complement C3 by microglia/monocytes in the aging retina. *PLoS One, 9*(4), e93343. doi:10.1371/journal.pone.0093343

Ryu, J., Pyo, H., Jou, I., & Joe, E. (2000). Thrombin induces NO release from cultured rat microglia via protein kinase C, mitogen-activated protein kinase, and NF-kappa B. *J Biol Chem, 275*(39), 29955-29959. doi:10.1074/jbc.M001220200

Safieh, M., Korczyn, A. D., & Michaelson, D. M. (2019). ApoE4: an emerging therapeutic target for Alzheimer's disease. *BMC Med, 17*(1), 64. doi:10.1186/s12916-019-1299-4

Salim, S., Sinnarajah, S., Kehrl, J. H., & Dessauer, C. W. (2003). Identification of RGS2 and type V adenylyl cyclase interaction sites. *J Biol Chem, 278*(18), 15842-15849. doi:10.1074/jbc.M210663200

Sansing, L. H., Harris, T. H., Welsh, F. A., Kasner, S. E., Hunter, C. A., & Kariko, K. (2011). Toll-like receptor 4 contributes to poor outcome after intracerebral hemorrhage. *Ann Neurol, 70*(4), 646-656. doi:10.1002/ana.22528

Sassone-Corsi, P. (2012). The cyclic AMP pathway. *Cold Spring Harb Perspect Biol, 4*(12). doi:10.1101/cshperspect.a011148

Saunders, A. M., Burns, D. K., & Gottschalk, W. K. (2021). Reassessment of Pioglitazone for Alzheimer's Disease. *Front Neurosci, 15*, 666958. doi:10.3389/fnins.2021.666958

Savage, J. C., Picard, K., Gonzalez-Ibanez, F., & Tremblay, M. E. (2018). A Brief History of Microglial Ultrastructure: Distinctive Features, Phenotypes, and Functions Discovered Over the Past 60 Years by Electron Microscopy. *Front Immunol, 9*, 803. doi:10.3389/fimmu.2018.00803

Schartz, N. D., & Tenner, A. J. (2020). The good, the bad, and the opportunities of the complement system in neurodegenerative disease. *J Neuroinflammation, 17*(1), 354. doi:10.1186/s12974-020-02024-8

Schindelin, J., Arganda-Carreras, I., Frise, E., Kaynig, V., Longair, M., Pietzsch, T., . . . Cardona, A. (2012). Fiji: an open-source platform for biological-image analysis. *Nat Methods, 9*(7), 676-682. doi:10.1038/nmeth.2019

Schoeber, J. P., Topala, C. N., Wang, X., Diepens, R. J., Lambers, T. T., Hoenderop, J. G., & Bindels, R. J. (2006). RGS2 inhibits the epithelial Ca2+ channel TRPV6. *J Biol Chem, 281*(40), 29669-29674. doi:10.1074/jbc.M606233200

Schuitemaker, A., van der Doef, T. F., Boellaard, R., van der Flier, W. M., Yaqub, M., Windhorst, A. D., . . . van Berckel, B. N. (2012). Microglial activation in healthy aging. *Neurobiol Aging, 33*(6), 1067-1072. doi:10.1016/j.neurobiolaging.2010.09.016

Schwartz, M., Kipnis, J., Rivest, S., & Prat, A. (2013). How do immune cells support and shape the brain in health, disease, and aging? *J Neurosci, 33*(45), 17587-17596. doi:10.1523/JNEUROSCI.3241-13.2013

Secondo, A., Bagetta, G., & Amantea, D. (2018). On the role of store-operated calcium entry in acute and chronic neurodegenerative diseases. *Frontiers in molecular neuroscience, 11*, 87.

Serang, O., & Noble, W. S. (2012). Faster mass spectrometry-based protein inference: junction trees are more efficient than sampling and marginalization by enumeration. *IEEE/ACM Trans Comput Biol Bioinform, 9*(3), 809-817. doi:10.1109/TCBB.2012.26

Shalygin, A., Skopin, A., Kalinina, V., Zimina, O., Glushankova, L., Mozhayeva, G. N., & Kaznacheyeva, E. (2015). STIM1 and STIM2 proteins differently regulate endogenous store-

operated channels in HEK293 cells. *J Biol Chem, 290*(8), 4717-4727. doi:10.1074/jbc.M114.601856

Shao, M., Xu, T. R., & Chen, C. S. (2016). The big bang of genome editing technology: development and application of the CRISPR/Cas9 system in disease animal models. *Dongwuxue Yanjiu, 37*(4), 191-204. doi:10.13918/j.issn.2095-8137.2016.4.191

Sharpe, J. J., & Cooper, T. A. (2017). Unexpected consequences: exon skipping caused by CRISPR-generated mutations. *Genome Biol, 18*(1), 109. doi:10.1186/s13059-017-1240-0

Shavali, S., Combs, C. K., & Ebadi, M. (2006). Reactive macrophages increase oxidative stress and alpha-synuclein nitration during death of dopaminergic neuronal cells in co-culture: relevance to Parkinson's disease. *Neurochem Res, 31*(1), 85-94. doi:10.1007/s11064-005-9233-x

Sheffield, L. G., Marquis, J. G., & Berman, N. E. (2000). Regional distribution of cortical microglia parallels that of neurofibrillary tangles in Alzheimer's disease. *Neurosci Lett, 285*(3), 165-168. doi:10.1016/s0304-3940(00)01037-5

Shen, Z., Bao, X., & Wang, R. (2018). Clinical PET Imaging of Microglial Activation: Implications for Microglial Therapeutics in Alzheimer's Disease. *Front Aging Neurosci, 10*, 314. doi:10.3389/fnagi.2018.00314

Sheng, L., Chen, M., Cai, K., Song, Y., Yu, D., Zhang, H., & Xu, G. (2019). Microglial Trem2 induces synaptic impairment at early stage and prevents amyloidosis at late stage in APP/PS1 mice. *FASEB J, 33*(9), 10425-10442. doi:10.1096/fj.201900527R

Shu, F. J., Ramineni, S., & Hepler, J. R. (2010). RGS14 is a multifunctional scaffold that integrates G protein and Ras/Raf MAPkinase signalling pathways. *Cell Signal, 22*(3), 366-376. doi:10.1016/j.cellsig.2009.10.005

Shu, L., Liang, D., Pan, H., Xu, Q., Yan, X., Tang, B., & Sun, Q. (2018). Gastrointestinal Dysfunctions Are Associated with IL-10 Variants in Parkinson's Disease. *Parkinsons Dis, 2018*, 5908359. doi:10.1155/2018/5908359

Siderovski, D. P., & Willard, F. S. (2005). The GAPs, GEFs, and GDIs of heterotrimeric G-protein alpha subunits. *Int J Biol Sci, 1*(2), 51-66. doi:10.7150/ijbs.1.51

Sierra, A., de Castro, F., Del Rio-Hortega, J., Rafael Iglesias-Rozas, J., Garrosa, M., & Kettenmann, H. (2016). The "Big-Bang" for modern glial biology: Translation and comments on Pio del Rio-Hortega 1919 series of papers on microglia. *Glia, 64*(11), 1801-1840. doi:10.1002/glia.23046

Sierra, D. A., Gilbert, D. J., Householder, D., Grishin, N. V., Yu, K., Ukidwe, P., . . . Wilkie, T. M. (2002). Evolution of the regulators of G-protein signaling multigene family in mouse and human. *Genomics, 79*(2), 177-185. doi:10.1006/geno.2002.6693

Smajic, S., Prada-Medina, C. A., Landoulsi, Z., Ghelfi, J., Delcambre, S., Dietrich, C., . . . Spielmann, M. (2021). Single-cell sequencing of human midbrain reveals glial activation and a Parkinson-specific neuronal state. *Brain*. doi:10.1093/brain/awab446

Smith, J. L., Mou, H., & Xue, W. (2018). Understanding and repurposing CRISPR-mediated alternative splicing. *Genome Biol, 19*(1), 184. doi:10.1186/s13059-018-1565-3

Spinelli, A.M. and M. Trebak, *Orai channel-mediated Ca2+ signals in vascular and airway smooth muscle.* Am J Physiol Cell Physiol, 2016. **310**(6): p. C402-13.

Soboloff, J., Rothberg, B. S., Madesh, M., & Gill, D. L. (2012). STIM proteins: dynamic calcium signal transducers. *Nat Rev Mol Cell Biol, 13*(9), 549-565. doi:10.1038/nrm3414

Sogkas, G., Stegner, D., Syed, S. N., Vogtle, T., Rau, E., Gewecke, B., . . . Gessner, J. E. (2015). Cooperative and alternate functions for STIM1 and STIM2 in macrophage activation and in the context of inflammation. *Immun Inflamm Dis, 3*(3), 154-170. doi:10.1002/iid3.56

Song, G. J., & Suk, K. (2017). Pharmacological Modulation of Functional Phenotypes of Microglia in Neurodegenerative Diseases. *Front Aging Neurosci, 9*, 139. doi:10.3389/fnagi.2017.00139

Song, M., Jin, J., Lim, J. E., Kou, J., Pattanayak, A., Rehman, J. A., . . . Fukuchi, K. (2011). TLR4 mutation reduces microglial activation, increases Abeta deposits and exacerbates cognitive deficits in a mouse model of Alzheimer's disease. *J Neuroinflammation, 8*, 92. doi:10.1186/1742-2094-8-92

Soreq, L., Consortium, U. K. B. E., North American Brain Expression, C., Rose, J., Soreq, E., Hardy, J., . . . Ule, J. (2017). Major Shifts in Glial Regional Identity Are a Transcriptional Hallmark of Human Brain Aging. *Cell Rep, 18*(2), 557-570. doi:10.1016/j.celrep.2016.12.011

Soundararajan, M., Willard, F. S., Kimple, A. J., Turnbull, A. P., Ball, L. J., Schoch, G. A., . . . Siderovski, D. P. (2008). Structural diversity in the RGS domain and its interaction with heterotrimeric G protein alpha-subunits. *Proc Natl Acad Sci U S A, 105*(17), 6457-6462. doi:10.1073/pnas.0801508105

Spittau, B. (2017). Aging Microglia-Phenotypes, Functions and Implications for Age-Related Neurodegenerative Diseases. *Front Aging Neurosci, 9*, 194. doi:10.3389/fnagi.2017.00194

Sprang, S. R. (2016). Invited review: Activation of G proteins by GTP and the mechanism of Galpha-catalyzed GTP hydrolysis. *Biopolymers, 105*(8), 449-462. doi:10.1002/bip.22836

Srinivasan, K., Friedman, B. A., Etxeberria, A., Huntley, M. A., van der Brug, M. P., Foreman, O., . . . Hansen, D. V. (2020). Alzheimer's Patient Microglia Exhibit Enhanced Aging and Unique Transcriptional Activation. *Cell Rep, 31*(13), 107843. doi:10.1016/j.celrep.2020.107843

Srinivasan, K., Friedman, B. A., Larson, J. L., Lauffer, B. E., Goldstein, L. D., Appling, L. L., . . . Hansen, D. V. (2016). Untangling the brain's neuroinflammatory and neurodegenerative transcriptional responses. *Nat Commun, 7*, 11295. doi:10.1038/ncomms11295

Stathopulos, P. B., Zheng, L., & Ikura, M. (2009). Stromal interaction molecule (STIM) 1 and STIM2 calcium sensing regions exhibit distinct unfolding and oligomerization kinetics. *J Biol Chem, 284*(2), 728-732. doi:10.1074/jbc.C800178200

Stehling, O., Vashisht, A. A., Mascarenhas, J., Jonsson, Z. O., Sharma, T., Netz, D. J., . . . Lill, R. (2012). MMS19 assembles iron-sulfur proteins required for DNA metabolism and genomic integrity. *Science, 337*(6091), 195-199. doi:10.1126/science.1219723

Stephan, A. H., Madison, D. V., Mateos, J. M., Fraser, D. A., Lovelett, E. A., Coutellier, L., . . . Barres, B. A. (2013). A dramatic increase of C1q protein in the CNS during normal aging. *J Neurosci, 33*(33), 13460-13474. doi:10.1523/JNEUROSCI.1333-13.2013

Stevens, B., Allen, N. J., Vazquez, L. E., Howell, G. R., Christopherson, K. S., Nouri, N., . . . Barres, B. A. (2007). The classical complement cascade mediates CNS synapse elimination. *Cell, 131*(6), 1164-1178. doi:10.1016/j.cell.2007.10.036

Stewart, C. R., Stuart, L. M., Wilkinson, K., van Gils, J. M., Deng, J., Halle, A., . . . Moore, K. J. (2010). CD36 ligands promote sterile inflammation through assembly of a Toll-like receptor 4 and 6 heterodimer. *Nat Immunol, 11*(2), 155-161. doi:10.1038/ni.1836

Stirling, D. P., Cummins, K., Mishra, M., Teo, W., Yong, V. W., & Stys, P. (2014). Toll-like receptor 2-mediated alternative activation of microglia is protective after spinal cord injury. *Brain, 137*(Pt 3), 707-723. doi:10.1093/brain/awt341

Stokholm, M. G., Iranzo, A., Ostergaard, K., Serradell, M., Otto, M., Svendsen, K. B., . . . Pavese, N. (2017). Assessment of neuroinflammation in patients with idiopathic rapid-eye-movement sleep behaviour disorder: a case-control study. *Lancet Neurol, 16*(10), 789-796. doi:10.1016/S1474-4422(17)30173-4

Stolwijk, J.A., et al., *Calcium Signaling Is Dispensable for Receptor Regulation of Endothelial Barrier Function.* J Biol Chem, 2016. **291**(44): p. 22894-22912.

Streit, W. J., Sammons, N. W., Kuhns, A. J., & Sparks, D. L. (2004). Dystrophic microglia in the aging human brain. *Glia, 45*(2), 208-212. doi:10.1002/glia.10319

Subramaniam, S. R., & Federoff, H. J. (2017). Targeting Microglial Activation States as a Therapeutic Avenue in Parkinson's Disease. *Front Aging Neurosci, 9*, 176. doi:10.3389/fnagi.2017.00176

Sundivakkam, P.C., et al., *Store-operated Ca2+ entry (SOCE) induced by protease-activated receptor-1 mediates STIM1 protein phosphorylation to inhibit SOCE in endothelial cells through AMP-activated protein kinase and p38beta mitogen-activated protein kinase.* J Biol Chem, 2013. **288**(23): p. 17030-41.

Suo, Z., Wu, M., Ameenuddin, S., Anderson, H. E., Zoloty, J. E., Citron, B. A., . . . Festoff, B. W. (2002). Participation of protease-activated receptor-1 in thrombin-induced microglial activation. *J Neurochem, 80*(4), 655-666. doi:10.1046/j.0022-3042.2001.00745.x

Suzumura, A., Marunouchi, T., & Yamamoto, H. (1991). Morphological transformation of microglia in vitro. *Brain Res, 545*(1-2), 301-306. doi:10.1016/0006-8993(91)91302-h

Svoboda, D. S., Barrasa, M. I., Shu, J., Rietjens, R., Zhang, S., Mitalipova, M., . . . Jaenisch, R. (2019). Human iPSC-derived microglia assume a primary microglia-like state after transplantation into the neonatal mouse brain. *Proc Natl Acad Sci U S A, 116*(50), 25293-25303. doi:10.1073/pnas.1913541116

Swisher, J. F., Haddad, D. A., McGrath, A. G., Boekhoudt, G. H., & Feldman, G. M. (2014). IgG4 can induce an M2-like phenotype in human monocyte-derived macrophages through FcgammaRI. *MAbs, 6*(6), 1377-1384. doi:10.4161/19420862.2014.975657

Syrovatkina, V., Alegre, K. O., Dey, R., & Huang, X. Y. (2016). Regulation, Signaling, and Physiological Functions of G-Proteins. *J Mol Biol, 428*(19), 3850-3868. doi:10.1016/j.jmb.2016.08.002

Tam, W. Y., Au, N. P., & Ma, C. H. (2016). The association between laminin and microglial morphology in vitro. *Sci Rep, 6*, 28580. doi:10.1038/srep28580

Tam, W. Y., & Ma, C. H. (2014). Bipolar/rod-shaped microglia are proliferating microglia with distinct M1/M2 phenotypes. *Sci Rep, 4*, 7279. doi:10.1038/srep07279

Tampi, R. R., Forester, B. P., & Agronin, M. (2021). Aducanumab: evidence from clinical trial data and controversies. *Drugs Context, 10*. doi:10.7573/dic.2021-7-3

Tang, M., Harrison, J., Deaton, C. A., & Johnson, G. V. W. (2019). Tau Clearance Mechanisms. *Adv Exp Med Biol, 1184*, 57-68. doi:10.1007/978-981-32-9358-8_5

Tang, Y., & Le, W. (2016). Differential Roles of M1 and M2 Microglia in Neurodegenerative Diseases. *Mol Neurobiol, 53*(2), 1181-1194. doi:10.1007/s12035-014-9070-5

Taupenot, L., Ciesielski-Treska, J., Ulrich, G., Chasserot-Golaz, S., Aunis, D., & Bader, M. F. (1996). Chromogranin A triggers a phenotypic transformation and the generation of nitric oxide in brain microglial cells. *Neuroscience, 72*(2), 377-389. doi:10.1016/0306-4522(96)83172-1

Taylor, R. A., Chang, C. F., Goods, B. A., Hammond, M. D., Mac Grory, B., Ai, Y., . . . Sansing, L. H. (2017). TGF-beta1 modulates microglial phenotype and promotes recovery after intracerebral hemorrhage. *J Clin Invest, 127*(1), 280-292. doi:10.1172/JCI88647

Taylor, R. A., & Sansing, L. H. (2013). Microglial responses after ischemic stroke and intracerebral hemorrhage. *Clin Dev Immunol, 2013*, 746068. doi:10.1155/2013/746068

Taylor, S. E., Morganti-Kossmann, C., Lifshitz, J., & Ziebell, J. M. (2014). Rod microglia: a morphological definition. *PLoS One, 9*(5), e97096. doi:10.1371/journal.pone.0097096

Taylor, V. G., Bommarito, P. A., & Tesmer, J. J. (2016). Structure of the Regulator of G Protein Signaling 8 (RGS8)-Galphaq Complex: MOLECULAR BASIS FOR Galpha SELECTIVITY. *J Biol Chem, 291*(10), 5138-5145. doi:10.1074/jbc.M115.712075

Teng, W., Wang, L., Xue, W., & Guan, C. (2009). Activation of TLR4-mediated NFkappaB signaling in hemorrhagic brain in rats. *Mediators Inflamm, 2009*, 473276. doi:10.1155/2009/473276

Terada, T., Yokokura, M., Yoshikawa, E., Futatsubashi, M., Kono, S., Konishi, T., . . . Ouchi, Y. (2016). Extrastriatal spreading of microglial activation in Parkinson's disease: a positron emission tomography study. *Ann Nucl Med, 30*(8), 579-587. doi:10.1007/s12149-016-1099-2

Tesmer, J. J., Berman, D. M., Gilman, A. G., & Sprang, S. R. (1997). Structure of RGS4 bound to AlF4--activated G(i alpha1): stabilization of the transition state for GTP hydrolysis. *Cell, 89*(2), 251-261. doi:10.1016/s0092-8674(00)80204-4

Tesseur, I., Nguyen, A., Chang, B., Li, L., Woodling, N. S., Wyss-Coray, T., & Luo, J. (2017). Deficiency in Neuronal TGF-beta Signaling Leads to Nigrostriatal Degeneration and Activation of TGF-beta Signaling Protects against MPTP Neurotoxicity in Mice. *J Neurosci, 37*(17), 4584-4592. doi:10.1523/JNEUROSCI.2952-16.2017

Thabet, A. M., Kottapally, M., & Hemphill, J. C., 3rd. (2017). Management of intracerebral hemorrhage. *Handb Clin Neurol, 140*, 177-194. doi:10.1016/B978-0-444-63600-3.00011-8

Thelen, M., & Stein, J. V. (2008). How chemokines invite leukocytes to dance. *Nat Immunol, 9*(9), 953-959. doi:10.1038/ni.f.207

Theodore, S., Cao, S., McLean, P. J., & Standaert, D. G. (2008). Targeted overexpression of human alpha-synuclein triggers microglial activation and an adaptive immune response in a mouse model of Parkinson disease. *J Neuropathol Exp Neurol, 67*(12), 1149-1158. doi:10.1097/NEN.0b013e31818e5e99

Tichauer, J. E., Flores, B., Soler, B., Eugenin-von Bernhardi, L., Ramirez, G., & von Bernhardi, R. (2014). Age-dependent changes on TGFbeta1 Smad3 pathway modify the pattern of microglial cell activation. *Brain Behav Immun, 37*, 187-196. doi:10.1016/j.bbi.2013.12.018

Trudler, D., Nazor, K. L., Eisele, Y. S., Grabauskas, T., Dolatabadi, N., Parker, J., . . . Lipton, S. A. (2021). Soluble alpha-synuclein-antibody complexes activate the NLRP3 inflammasome in hiPSC-derived microglia. *Proc Natl Acad Sci U S A, 118*(15). doi:10.1073/pnas.2025847118

Tschoe, C., Bushnell, C. D., Duncan, P. W., Alexander-Miller, M. A., & Wolfe, S. Q. (2020). Neuroinflammation after Intracerebral Hemorrhage and Potential Therapeutic Targets. *J Stroke, 22*(1), 29-46. doi:10.5853/jos.2019.02236

Tu, Y., Popov, S., Slaughter, C., & Ross, E. M. (1999). Palmitoylation of a conserved cysteine in the regulator of G protein signaling (RGS) domain modulates the GTPase-activating activity of RGS4 and RGS10. *J Biol Chem, 274*(53), 38260-38267. doi:10.1074/jbc.274.53.38260

Tuggle, K., Ali, M. W., Salazar, H., & Hooks, S. B. (2014). Regulator of G protein signaling transcript expression in human neural progenitor differentiation: R7 subfamily regulation by DNA methylation. *Neurosignals, 22*(1), 43-51. doi:10.1159/000362128

Tuladhar, R., Yeu, Y., Tyler Piazza, J., Tan, Z., Rene Clemenceau, J., Wu, X., . . . Lum, L. (2019). CRISPR-Cas9-based mutagenesis frequently provokes on-target mRNA misregulation. *Nat Commun, 10*(1), 4056. doi:10.1038/s41467-019-12028-5

Tyagi, S., Gupta, P., Saini, A. S., Kaushal, C., & Sharma, S. (2011). The peroxisome proliferator-activated receptor: A family of nuclear receptors role in various diseases. *J Adv Pharm Technol Res, 2*(4), 236-240. doi:10.4103/2231-4040.90879

Ueno, M., Fujita, Y., Tanaka, T., Nakamura, Y., Kikuta, J., Ishii, M., & Yamashita, T. (2013). Layer V cortical neurons require microglial support for survival during postnatal development. *Nat Neurosci, 16*(5), 543-551. doi:10.1038/nn.3358

Unnithan, A. K. A., & Mehta, P. (2022). Hemorrhagic Stroke. In *StatPearls*. Treasure Island (FL).

Uranova, N. A., Vikhreva, O. V., Rakhmanova, V. I., & Orlovskaya, D. D. (2018). Ultrastructural pathology of oligodendrocytes adjacent to microglia in prefrontal white matter in schizophrenia. *NPJ Schizophr, 4*(1), 26. doi:10.1038/s41537-018-0068-2

Uriarte Huarte, O., Kyriakis, D., Heurtaux, T., Pires-Afonso, Y., Grzyb, K., Halder, R., . . . Michelucci, A. (2021). Single-Cell Transcriptomics and In Situ Morphological Analyses Reveal Microglia Heterogeneity Across the Nigrostriatal Pathway. *Front Immunol, 12*, 639613. doi:10.3389/fimmu.2021.639613

V., Z. Z., & C., W. K. (2019). Microglial activation and polarization after subarachnoid hemorrhage. *Neuroimmunology and Neuroinflammation, 6*(1). Retrieved from 10.20517/2347-8659.2018.52

Vaeth, M., & Feske, S. (2018). NFAT control of immune function: New Frontiers for an Abiding Trooper. *F1000Res, 7*, 260. doi:10.12688/f1000research.13426.1

Vafadari, R., Kraaijeveld, R., Weimar, W., & Baan, C. C. (2013). Tacrolimus inhibits NF-kappaB activation in peripheral human T cells. *PLoS One, 8*(4), e60784. doi:10.1371/journal.pone.0060784

van Wageningen, T. A., Vlaar, E., Kooij, G., Jongenelen, C. A. M., Geurts, J. J. G., & van Dam, A. M. (2019). Regulation of microglial TMEM119 and P2RY12 immunoreactivity in multiple sclerosis white and grey matter lesions is dependent on their inflammatory environment. *Acta Neuropathol Commun, 7*(1), 206. doi:10.1186/s40478-019-0850-z

Van Vliet, A. R., Sassano, M. L., & Agostinis, P. (2018). The unfolded protein response and membrane contact sites: Tethering as a matter of life and death? *Contact, 1*, 251525641877051. https://doi.org/10.1177/2515256418770512

VanGuilder, H. D., Bixler, G. V., Brucklacher, R. M., Farley, J. A., Yan, H., Warrington, J. P., . . . Freeman, W. M. (2011). Concurrent hippocampal induction of MHC II pathway components and glial activation with advanced aging is not correlated with cognitive impairment. *J Neuroinflammation, 8*, 138. doi:10.1186/1742-2094-8-138

Vawter, M. P., Dillon-Carter, O., Tourtellotte, W. W., Carvey, P., & Freed, W. J. (1996). TGFbeta1 and TGFbeta2 concentrations are elevated in Parkinson's disease in ventricular cerebrospinal fluid. *Exp Neurol, 142*(2), 313-322. doi:10.1006/exnr.1996.0200

Venegas, C., Kumar, S., Franklin, B. S., Dierkes, T., Brinkschulte, R., Tejera, D., . . . Heneka, M. T. (2017). Microglia-derived ASC specks cross-seed amyloid-beta in Alzheimer's disease. *Nature, 552*(7685), 355-361. doi:10.1038/nature25158

Vijitruth, R., Liu, M., Choi, D. Y., Nguyen, X. V., Hunter, R. L., & Bing, G. (2006). Cyclooxygenase-2 mediates microglial activation and secondary dopaminergic cell death in the mouse MPTP model of Parkinson's disease. *J Neuroinflammation, 3*, 6. doi:10.1186/1742-2094-3-6

Vitek, M. P., Araujo, J. A., Fossel, M., Greenberg, B. D., Howell, G. R., Rizzo, S. J. S., . . . Edelmayer, R. M. (2020). Translational animal models for Alzheimer's disease: An Alzheimer's Association Business Consortium Think Tank. *Alzheimers Dement (N Y), 6*(1), e12114. doi:10.1002/trc2.12114

Vodovotz, Y., Lucia, M. S., Flanders, K. C., Chesler, L., Xie, Q. W., Smith, T. W., . . . Sporn, M. B. (1996). Inducible nitric oxide synthase in tangle-bearing neurons of patients with Alzheimer's disease. *J Exp Med, 184*(4), 1425-1433. doi:10.1084/jem.184.4.1425

Wan, S., Cheng, Y., Jin, H., Guo, D., Hua, Y., Keep, R. F., & Xi, G. (2016). Microglia Activation and Polarization After Intracerebral Hemorrhage in Mice: the Role of Protease-Activated Receptor-1. *Transl Stroke Res, 7*(6), 478-487. doi:10.1007/s12975-016-0472-8

Wang, C. J., & Chidiac, P. (2019). RGS2 promotes the translation of stress-associated proteins ATF4 and CHOP via its eIF2B-inhibitory domain. *Cell Signal, 59*, 163-170. doi:10.1016/j.cellsig.2019.02.007

Wang, G., Li, T., Duan, S. N., Dong, L., Sun, X. G., & Xue, F. (2018). PPAR-gamma Promotes Hematoma Clearance through Haptoglobin-Hemoglobin-CD163 in a Rat Model of Intracerebral Hemorrhage. *Behav Neurol, 2018*, 7646104. doi:10.1155/2018/7646104

Wang, G., Zhou, Y., Wang, Y., Li, D., Liu, J., & Zhang, F. (2019). Age-Associated Dopaminergic Neuron Loss and Midbrain Glia Cell Phenotypic Polarization. *Neuroscience, 415*, 89-96. doi:10.1016/j.neuroscience.2019.07.021

Wang, J., & Dore, S. (2007). Inflammation after intracerebral hemorrhage. *J Cereb Blood Flow Metab, 27*(5), 894-908. doi:10.1038/sj.jcbfm.9600403

Wang, J., Rogove, A. D., Tsirka, A. E., & Tsirka, S. E. (2003). Protective role of tuftsin fragment 1-3 in an animal model of intracerebral hemorrhage. *Ann Neurol, 54*(5), 655-664. doi:10.1002/ana.10750

Wang, J., & Tsirka, S. E. (2005). Tuftsin fragment 1-3 is beneficial when delivered after the induction of intracerebral hemorrhage. *Stroke, 36*(3), 613-618. doi:10.1161/01.STR.0000155729.12931.8f

Wang, L., Li, D., Yang, K., Hu, Y., & Zeng, Q. (2008). Toll-like receptor-4 and mitogen-activated protein kinase signal system are involved in activation of dendritic cells in patients with acute coronary syndrome. *Immunology, 125*(1), 122-130. doi:10.1111/j.1365-2567.2008.02827.x

Wang, Q., Yao, H., Liu, W., Ya, B., Cheng, H., Xing, Z., & Wu, Y. (2021). Microglia Polarization in Alzheimer's Disease: Mechanisms and a Potential Therapeutic Target. *Front Aging Neurosci, 13*, 772717. doi:10.3389/fnagi.2021.772717

Wang, W. Y., Tan, M. S., Yu, J. T., & Tan, L. (2015). Role of pro-inflammatory cytokines released from microglia in Alzheimer's disease. *Ann Transl Med, 3*(10), 136. doi:10.3978/j.issn.2305-5839.2015.03.49

Wang, X., Huang, G., Luo, X., Penninger, J. M., & Muallem, S. (2004). Role of regulator of G protein signaling 2 (RGS2) in Ca(2+) oscillations and adaptation of Ca(2+) signaling to reduce excitability of RGS2-/- cells. *J Biol Chem, 279*(40), 41642-41649. doi:10.1074/jbc.M406450200

Wang, Y., Cella, M., Mallinson, K., Ulrich, J. D., Young, K. L., Robinette, M. L., . . . Colonna, M. (2015). TREM2 lipid sensing sustains the microglial response in an Alzheimer's disease model. *Cell, 160*(6), 1061-1071. doi:10.1016/j.cell.2015.01.049

Wang, Y., Szretter, K. J., Vermi, W., Gilfillan, S., Rossini, C., Cella, M., . . . Colonna, M. (2012). IL-34 is a tissue-restricted ligand of CSF1R required for the development of Langerhans cells and microglia. *Nat Immunol, 13*(8), 753-760. doi:10.1038/ni.2360

Wang, Y., Ulland, T. K., Ulrich, J. D., Song, W., Tzaferis, J. A., Hole, J. T., . . . Colonna, M. (2016). TREM2-mediated early microglial response limits diffusion and toxicity of amyloid plaques. *J Exp Med, 213*(5), 667-675. doi:10.1084/jem.20151948

Wang, Y. C., Wang, P. F., Fang, H., Chen, J., Xiong, X. Y., & Yang, Q. W. (2013). Toll-like receptor 4 antagonist attenuates intracerebral hemorrhage-induced brain injury. *Stroke, 44*(9), 2545-2552. doi:10.1161/STROKEAHA.113.001038

Watson, M. B., Richter, F., Lee, S. K., Gabby, L., Wu, J., Masliah, E., . . . Chesselet, M. F. (2012). Regionally-specific microglial activation in young mice over-expressing human wildtype alpha-synuclein. *Exp Neurol, 237*(2), 318-334. doi:10.1016/j.expneurol.2012.06.025

Watson, N., Linder, M. E., Druey, K. M., Kehrl, J. H., & Blumer, K. J. (1996). RGS family members: GTPase-activating proteins for heterotrimeric G-protein alpha-subunits. *Nature, 383*(6596), 172-175. Retrieved from http://www.ncbi.nlm.nih.gov/entrez/query.fcgi?cmd=Retrieve&db=PubMed&dopt=Citation&list_uids=8774882

Webb, J. L., Ravikumar, B., Atkins, J., Skepper, J. N., & Rubinsztein, D. C. (2003). Alpha-Synuclein is degraded by both autophagy and the proteasome. *J Biol Chem, 278*(27), 25009-25013. doi:10.1074/jbc.M300227200

Wei, S., Luo, C., Yu, S., Gao, J., Liu, C., Wei, Z., . . . Yi, B. (2017). Erythropoietin ameliorates early brain injury after subarachnoid haemorrhage by modulating microglia polarization via the EPOR/JAK2-STAT3 pathway. *Exp Cell Res, 361*(2), 342-352. doi:10.1016/j.yexcr.2017.11.002

Wen, L., You, W., Wang, H., Meng, Y., Feng, J., & Yang, X. (2018). Polarization of Microglia to the M2 Phenotype in a Peroxisome Proliferator-Activated Receptor Gamma-Dependent Manner Attenuates Axonal Injury Induced by Traumatic Brain Injury in Mice. *J Neurotrauma, 35*(19), 2330-2340. doi:10.1089/neu.2017.5540

Wen, R. X., Shen, H., Huang, S. X., Wang, L. P., Li, Z. W., Peng, P., . . . Zhang, Z. J. (2020). P2Y6 receptor inhibition aggravates ischemic brain injury by reducing microglial phagocytosis. *CNS Neurosci Ther, 26*(4), 416-429. doi:10.1111/cns.13296

Wendimu, M. Y., Alqinyah, M., Vella, S., Dean, P., Almutairi, F., Davila-Rivera, R., . . . Hooks, S. B. (2021). RGS10 physically and functionally interacts with STIM2 and requires store-operated calcium entry to regulate pro-inflammatory gene expression in microglia. *Cell Signal, 83*, 109974. doi:10.1016/j.cellsig.2021.109974

Wes, P. D., Holtman, I. R., Boddeke, E. W., Moller, T., & Eggen, B. J. (2016). Next generation transcriptomics and genomics elucidate biological complexity of microglia in health and disease. *Glia, 64*(2), 197-213. doi:10.1002/glia.22866

Wettschureck, N., & Offermanns, S. (2005). Mammalian G proteins and their cell type specific functions. *Physiol Rev, 85*(4), 1159-1204. doi:10.1152/physrev.00003.2005

Wierzba-Bobrowicz, T., Gwiazda, E., Kosno-Kruszewska, E., Lewandowska, E., Lechowicz, W., Bertrand, E., . . . Schmidt-Sidor, B. (2002). Morphological analysis of active microglia--rod and ramified microglia in human brains affected by some neurological diseases (SSPE, Alzheimer's disease and Wilson's disease). *Folia Neuropathol, 40*(3), 125-131. Retrieved from https://www.ncbi.nlm.nih.gov/pubmed/12572918

Williams, R.T., et al., *Identification and characterization of the STIM (stromal interaction molecule) gene family: coding for a novel class of transmembrane proteins.* Biochem J, 2001. **357**(Pt 3): p. 673-85.

Wilquet, V., & De Strooper, B. (2004). Amyloid-beta precursor protein processing in neurodegeneration. *Curr Opin Neurobiol, 14*(5), 582-588. doi:10.1016/j.conb.2004.08.001

Wohlschlegel, J. A. (2009). Identification of SUMO-conjugated proteins and their SUMO attachment sites using proteomic mass spectrometry. *Methods Mol Biol, 497*, 33-49. doi:10.1007/978-1-59745-566-4_3

Wong, Y. C., & Krainc, D. (2017). alpha-synuclein toxicity in neurodegeneration: mechanism and therapeutic strategies. *Nat Med, 23*(2), 1-13. doi:10.1038/nm.4269

Wootten, D., Christopoulos, A., Marti-Solano, M., Babu, M. M., & Sexton, P. M. (2018). Mechanisms of signalling and biased agonism in G protein-coupled receptors. *Nat Rev Mol Cell Biol, 19*(10), 638-653. doi:10.1038/s41580-018-0049-3

Wu, H., Wu, T., Xu, X., Wang, J., & Wang, J. (2011). Iron toxicity in mice with collagenase-induced intracerebral hemorrhage. *J Cereb Blood Flow Metab, 31*(5), 1243-1250. doi:10.1038/jcbfm.2010.209

Xie, G. X., & Palmer, P. P. (2007). How regulators of G protein signaling achieve selective regulation. *J Mol Biol, 366*(2), 349-365. doi:10.1016/j.jmb.2006.11.045

Xie, Z., Geiger, T. R., Johnson, E. N., Nyborg, J. K., & Druey, K. M. (2008). RGS13 acts as a nuclear repressor of CREB. *Mol Cell, 31*(5), 660-670. doi:10.1016/j.molcel.2008.06.024

Xue, M., & Del Bigio, M. R. (2000). Intracerebral injection of autologous whole blood in rats: time course of inflammation and cell death. *Neurosci Lett, 283*(3), 230-232. doi:10.1016/s0304-3940(00)00971-x

Xue, M., & Del Bigio, M. R. (2003). Comparison of brain cell death and inflammatory reaction in three models of intracerebral hemorrhage in adult rats. *J Stroke Cerebrovasc Dis, 12*(3), 152-159. doi:10.1016/S1052-3057(03)00036-3

Yamamoto, M., Kiyota, T., Walsh, S. M., Liu, J., Kipnis, J., & Ikezu, T. (2008). Cytokine-mediated inhibition of fibrillar amyloid-beta peptide degradation by human mononuclear phagocytes. *J Immunol, 181*(6), 3877-3886. doi:10.4049/jimmunol.181.6.3877

Yamanaka, M., Ishikawa, T., Griep, A., Axt, D., Kummer, M. P., & Heneka, M. T. (2012). PPARgamma/RXRalpha-induced and CD36-mediated microglial amyloid-beta phagocytosis results in cognitive improvement in amyloid precursor protein/presenilin 1 mice. *J Neurosci, 32*(48), 17321-17331. doi:10.1523/JNEUROSCI.1569-12.2012

Yang, J., Ding, S., Huang, W., Hu, J., Huang, S., Zhang, Y., & Zhuge, Q. (2016). Interleukin-4 Ameliorates the Functional Recovery of Intracerebral Hemorrhage Through the Alternative Activation of Microglia/Macrophage. *Front Neurosci, 10*, 61. doi:10.3389/fnins.2016.00061

Yang, Q., Wang, G., & Zhang, F. (2020). Role of Peripheral Immune Cells-Mediated Inflammation on the Process of Neurodegenerative Diseases. *Front Immunol, 11*, 582825. doi:10.3389/fimmu.2020.582825

Yang, S., & Li, Y. P. (2007). RGS10-null mutation impairs osteoclast differentiation resulting from the loss of [Ca2+]i oscillation regulation. *Genes Dev, 21*(14), 1803-1816. doi:10.1101/gad.1544107

Yang, S., Nakamura, T., Hua, Y., Keep, R. F., Younger, J. G., Hoff, J. T., & Xi, G. (2006). Intracerebral hemorrhage in complement C3-deficient mice. *Acta Neurochir Suppl, 96*, 227-231. doi:10.1007/3-211-30714-1_49

Yang, X., Lou, Y., Liu, G., Wang, X., Qian, Y., Ding, J., . . . Xiao, Q. (2017). Microglia P2Y6 receptor is related to Parkinson's disease through neuroinflammatory process. *J Neuroinflammation, 14*(1), 38. doi:10.1186/s12974-017-0795-8

Yang, Z., Liu, B., Zhong, L., Shen, H., Lin, C., Lin, L., . . . Yuan, B. (2015). Toll-like receptor-4-mediated autophagy contributes to microglial activation and inflammatory injury in mouse models of intracerebral haemorrhage. *Neuropathol Appl Neurobiol, 41*(4), e95-106. doi:10.1111/nan.12177

Yang, Z., Zhong, S., Liu, Y., Shen, H., & Yuan, B. (2015). Scavenger receptor SRA attenuates microglia activation and protects neuroinflammatory injury in intracerebral hemorrhage. *J Neuroimmunol, 278*, 232-238. doi:10.1016/j.jneuroim.2014.11.010

Yanguas-Casás, N. (2020). Physiological sex differences in microglia and their relevance in neurological disorders. *Neuroimmunology and Neuroinflammation*(7).

Yao, K., & Zu, H. B. (2020). Microglial polarization: novel therapeutic mechanism against Alzheimer's disease. *Inflammopharmacology, 28*(1), 95-110. doi:10.1007/s10787-019-00613-5

Yao, X., Liu, S., Ding, W., Yue, P., Jiang, Q., Zhao, M., . . . Zhang, H. (2017). TLR4 signal ablation attenuated neurological deficits by regulating microglial M1/M2 phenotype after traumatic brain injury in mice. *J Neuroimmunol, 310*, 38-45. doi:10.1016/j.jneuroim.2017.06.006

Yao, Y. and S.E. Tsirka, *The C terminus of mouse monocyte chemoattractant protein 1 (MCP1) mediates MCP1 dimerization while blocking its chemotactic potency.* J Biol Chem, 2010. **285**(41): p. 31509-16.

Yau, D. M., Sethakorn, N., Taurin, S., Kregel, S., Sandbo, N., Camoretti-Mercado, B., . . . Dulin, N. O. (2008). Regulation of Smad-mediated gene transcription by RGS3. *Mol Pharmacol, 73*(5), 1356-1361. doi:10.1124/mol.108.044990

Yeh, F. L., Wang, Y., Tom, I., Gonzalez, L. C., & Sheng, M. (2016). TREM2 Binds to Apolipoproteins, Including APOE and CLU/APOJ, and Thereby Facilitates Uptake of Amyloid-Beta by Microglia. *Neuron, 91*(2), 328-340. doi:10.1016/j.neuron.2016.06.015

Yoshikawa, S., et al., *Pivotal role of STIM2, but not STIM1, in IL-4 production by IL-3-stimulated murine basophils.* Sci Signal, 2019. **12**(576).

Yoshiyama, Y., Higuchi, M., Zhang, B., Huang, S. M., Iwata, N., Saido, T. C., . . . Lee, V. M. (2007). Synapse loss and microglial activation precede tangles in a P301S tauopathy mouse model. *Neuron, 53*(3), 337-351. doi:10.1016/j.neuron.2007.01.010

Yu, Y., & Ye, R. D. (2015). Microglial Abeta receptors in Alzheimer's disease. *Cell Mol Neurobiol, 35*(1), 71-83. doi:10.1007/s10571-014-0101-6

Zhang, J., Li, X., & Li, J. D. (2019). The Roles of Post-translational Modifications on alpha-Synuclein in the Pathogenesis of Parkinson's Diseases. *Front Neurosci, 13*, 381. doi:10.3389/fnins.2019.00381

Zhang, J., Song, L., Pedersen, D. V., Li, A., Lambris, J. D., Andersen, G. R., . . . Garred, P. (2020). Soluble collectin-12 mediates C3-independent docking of properdin that activates the alternative pathway of complement. *Elife, 9*. doi:10.7554/eLife.60908

Zhang, Q. S., Heng, Y., Yuan, Y. H., & Chen, N. H. (2017). Pathological alpha-synuclein exacerbates the progression of Parkinson's disease through microglial activation. *Toxicol Lett, 265*, 30-37. doi:10.1016/j.toxlet.2016.11.002

Zhang, S. (2019). Microglial activation after ischaemic stroke. *Stroke Vasc Neurol, 4*(2), 71-74. doi:10.1136/svn-2018-000196

Zhang, W., Wang, T., Pei, Z., Miller, D. S., Wu, X., Block, M. L., . . . Zhang, J. (2005). Aggregated alpha-synuclein activates microglia: a process leading to disease progression in Parkinson's disease. *FASEB J, 19*(6), 533-542. doi:10.1096/fj.04-2751com

Zhang, Y., Feng, S., Nie, K., Li, Y., Gao, Y., Gan, R., . . . Zhang, Y. (2018). TREM2 modulates microglia phenotypes in the neuroinflammation of Parkinson's disease. *Biochem Biophys Res Commun, 499*(4), 797-802. doi:10.1016/j.bbrc.2018.03.226

Zhang, Z., Song, Y., Zhang, Z., Li, D., Zhu, H., Liang, R., . . . Wang, J. (2017). Distinct role of heme oxygenase-1 in early- and late-stage intracerebral hemorrhage in 12-month-old mice. *J Cereb Blood Flow Metab, 37*(1), 25-38. doi:10.1177/0271678X16655814

Zhao, F., Hua, Y., He, Y., Keep, R. F., & Xi, G. (2011). Minocycline-induced attenuation of iron overload and brain injury after experimental intracerebral hemorrhage. *Stroke, 42*(12), 3587-3593. doi:10.1161/STROKEAHA.111.623926

Zhao, S. C., Ma, L. S., Chu, Z. H., Xu, H., Wu, W. Q., & Liu, F. (2017). Regulation of microglial activation in stroke. *Acta Pharmacol Sin, 38*(4), 445-458. doi:10.1038/aps.2016.162

Zhao, X., Grotta, J., Gonzales, N., & Aronowski, J. (2009). Hematoma resolution as a therapeutic target: the role of microglia/macrophages. *Stroke, 40*(3 Suppl), S92-94. doi:10.1161/STROKEAHA.108.533158

Zhao, X., Sun, G., Zhang, J., Strong, R., Song, W., Gonzales, N., . . . Aronowski, J. (2007). Hematoma resolution as a target for intracerebral hemorrhage treatment: role for peroxisome proliferator-activated receptor gamma in microglia/macrophages. *Ann Neurol, 61*(4), 352-362. doi:10.1002/ana.21097

Zhao, Y., Wu, X., Li, X., Jiang, L. L., Gui, X., Liu, Y., . . . Xu, H. (2018). TREM2 Is a Receptor for beta-Amyloid that Mediates Microglial Function. *Neuron, 97*(5), 1023-1031 e1027. doi:10.1016/j.neuron.2018.01.031

Zhong, C., & Schleifenbaum, J. (2019). Genetically Encoded Calcium Indicators: A New Tool in Renal Hypertension Research. *Front Med (Lausanne), 6*, 128. doi:10.3389/fmed.2019.00128

Zhong, L., Zhang, Z. L., Li, X., Liao, C., Mou, P., Wang, T., . . . Chen, X. F. (2017). TREM2/DAP12 Complex Regulates Inflammatory Responses in Microglia via the JNK Signaling Pathway. *Front Aging Neurosci, 9*, 204. doi:10.3389/fnagi.2017.00204

Zhou, T., Huang, Z., Sun, X., Zhu, X., Zhou, L., Li, M., . . . He, C. (2017). Microglia Polarization with M1/M2 Phenotype Changes in rd1 Mouse Model of Retinal Degeneration. *Front Neuroanat, 11*, 77. doi:10.3389/fnana.2017.00077

Zhou, X., Zoller, T., Krieglstein, K., & Spittau, B. (2015). TGFbeta1 inhibits IFNgamma-mediated microglia activation and protects mDA neurons from IFNgamma-driven neurotoxicity. *J Neurochem, 134*(1), 125-134. doi:10.1111/jnc.13111

Zhou, Y., Chen, Y., Xu, C., Zhang, H., & Lin, C. (2020). TLR4 Targeting as a Promising Therapeutic Strategy for Alzheimer Disease Treatment. *Front Neurosci, 14*, 602508. doi:10.3389/fnins.2020.602508

Zhou, Y., Wang, Y., Wang, J., Anne Stetler, R., & Yang, Q. W. (2014). Inflammation in intracerebral hemorrhage: from mechanisms to clinical translation. *Prog Neurobiol, 115*, 25-44. doi:10.1016/j.pneurobio.2013.11.003

Zhu, J. W., Zou, M. M., Li, Y. F., Chen, W. J., Liu, J. C., Chen, H., . . . Xu, R. X. (2020). Absence of TRIM32 Leads to Reduced GABAergic Interneuron Generation and Autism-like Behaviors in

Mice via Suppressing mTOR Signaling. *Cereb Cortex, 30*(5), 3240-3258. doi:10.1093/cercor/bhz306

Ziebell, J. M., Taylor, S. E., Cao, T., Harrison, J. L., & Lifshitz, J. (2012). Rod microglia: elongation, alignment, and coupling to form trains across the somatosensory cortex after experimental diffuse brain injury. *J Neuroinflammation, 9*, 247. doi:10.1186/1742-2094-9-247

Zindel, J., & Kubes, P. (2020). DAMPs, PAMPs, and LAMPs in Immunity and Sterile Inflammation. *Annu Rev Pathol, 15*, 493-518. doi:10.1146/annurev-pathmechdis-012419-032847

Zoller, T., Schneider, A., Kleimeyer, C., Masuda, T., Potru, P. S., Pfeifer, D., . . . Spittau, B. (2018). Silencing of TGFbeta signalling in microglia results in impaired homeostasis. *Nat Commun, 9*(1), 4011. doi:10.1038/s41467-018-06224-y

Zrzavy, T., Hametner, S., Wimmer, I., Butovsky, O., Weiner, H. L., & Lassmann, H. (2017). Loss of 'homeostatic' microglia and patterns of their activation in active multiple sclerosis. *Brain, 140*(7), 1900-1913. doi:10.1093/brain/awx113

Zujovic, V., Schussler, N., Jourdain, D., Duverger, D., & Taupin, V. (2001). In vivo neutralization of endogenous brain fractalkine increases hippocampal TNFalpha and 8-isoprostane production induced by intracerebroventricular injection of LPS. *J Neuroimmunol, 115*(1-2), 135-143. doi:10.1016/s0165-5728(01)00259-4

APPENDIX

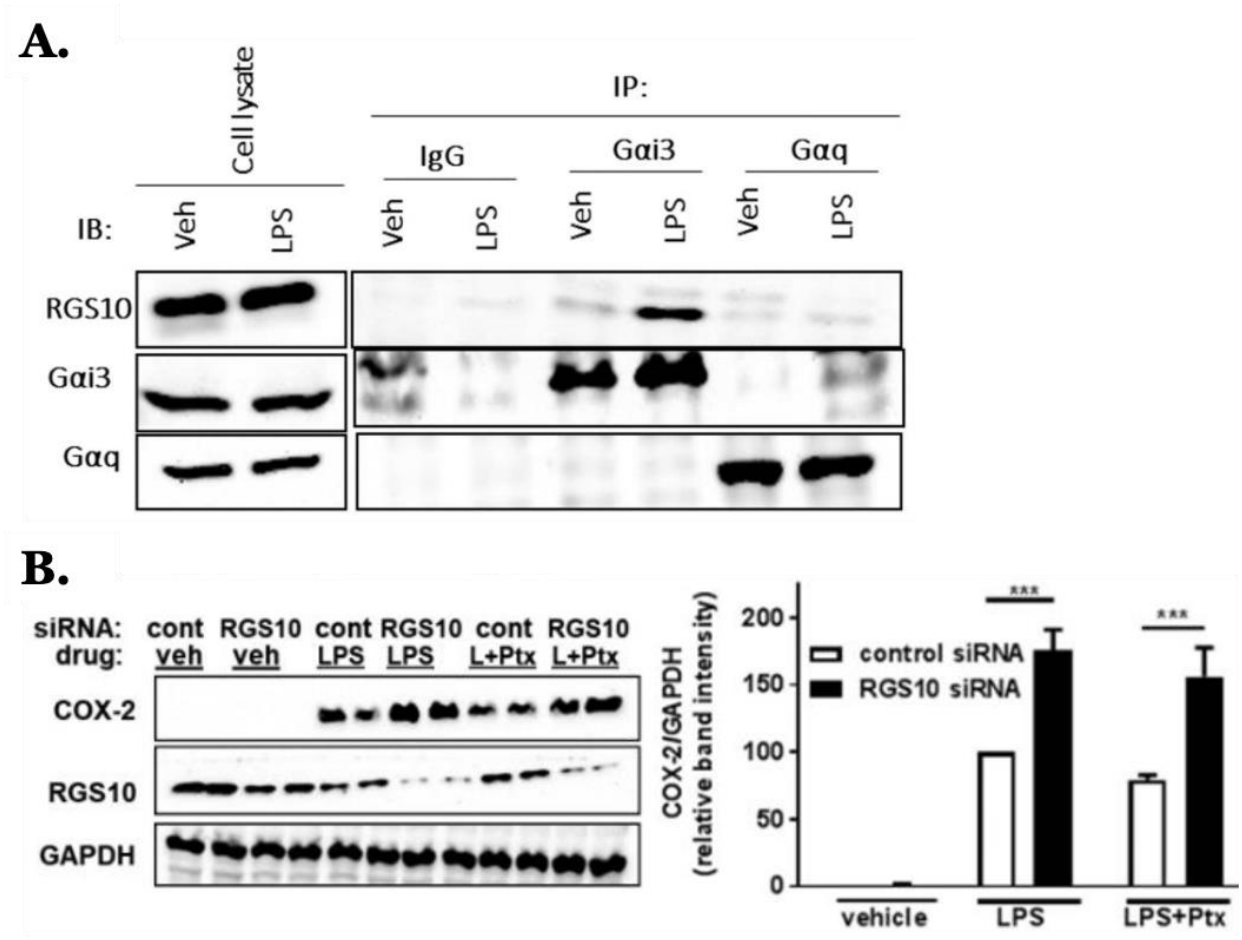

Figure A.1. **Endogenous RGS10 specifically associates with the active form of Gα_i in LPS activated microglia but its ability to downregulate COX-2 does not require Gαi signaling. A)** BV-microglia cells were treated with vehicle (Veh) or 10 ng/ml LPS for 3 hours and cleared lysates were immunoprecipitated (IP) using Gα_i3, Gα_q, or control IgG antibodies. Western blot (IB) was conducted to probe for RGS10, Gα_i3, or Gα_q. **B)** BV-2 microglia cells were transfected with control or RGS10 siRNA. Twenty-four hours after transfection, cells were treated with vehicle (Veh) or LPS for an additional 24 h with or without PTX (100 ng/ml). PTX was added 4 hours prior to LPS and was included throughout the 24 h LPS treatment. Western blotting was performed using specific antibodies against COX-2, RGS10, and the loading control GAPDH. Band intensity was analyzed from three independent experiments and the difference between groups was analyzed by ANOVA, followed by Tukey's test. Data are presented as mean ± S.E.M., where $*P < 0.05$, $**P < 0.01$, and $***P < 0.001$.

Figure adapted from:

Alqinyah, M., Almutairi, F., Wendimu, M. Y., & Hooks, S. B. (2018). RGS10 regulates the expression of cyclooxygenase-2 and tumor necrosis factor Alpha through a G protein–independent mechanism. *Molecular Pharmacology*, *94* (4), 1103-1113. https://doi.org/10.1124/mol.118.111674

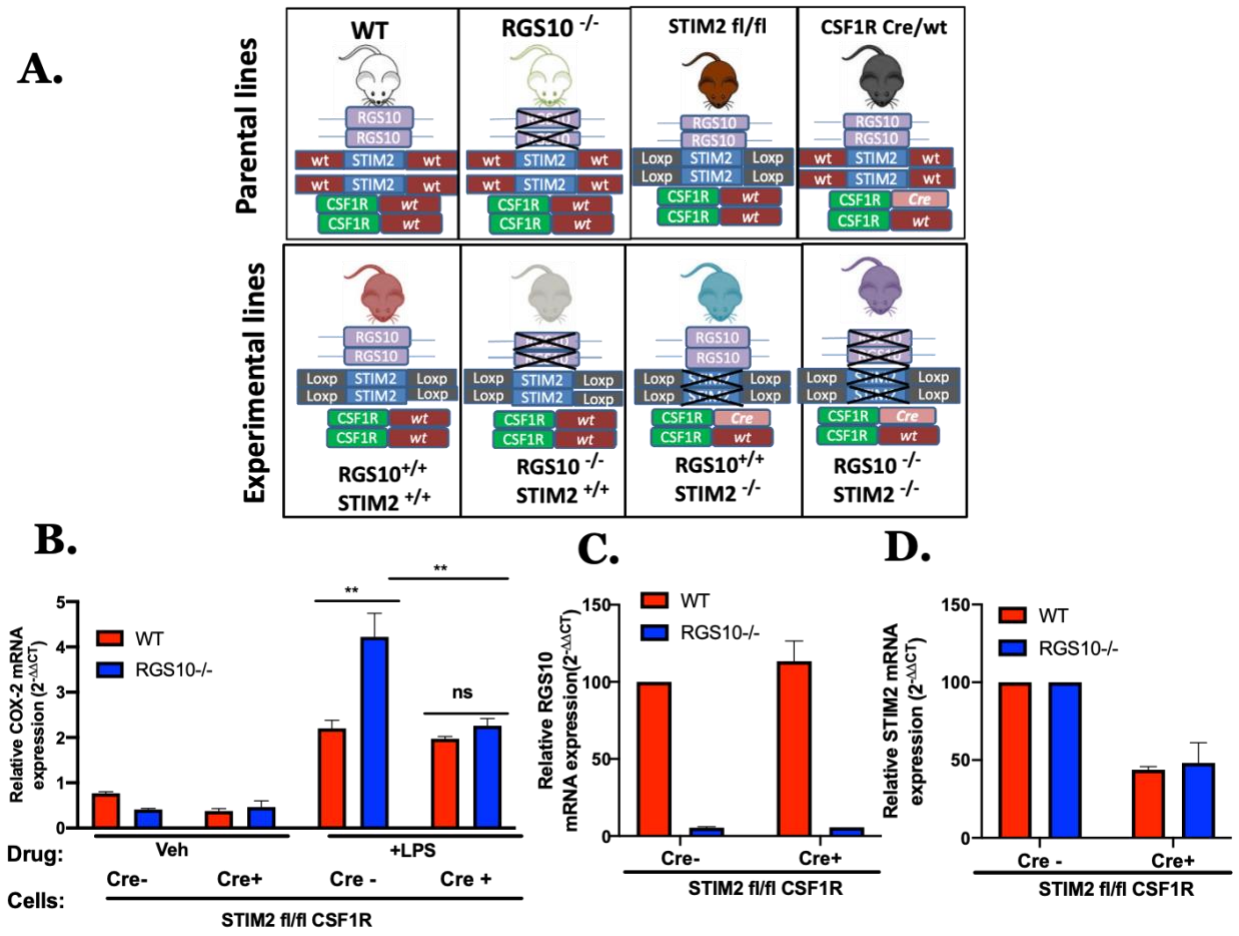

Figure A.2. Generation of RGS10 and STIM2 double knockout transgenic mice. A) Schematic figure depicting parental and experimental transgenic line. STIM2 fl/fl mouse line with CSF1R-driven Cre expression was generated to induce conditional STIM2 knockout in microglia/monocyte population. Experimental lines were generated through genetic crosses from four parental lines*: wild-type (WT), RGS10 knockout (RGS10$^{-/-}$), STIM2 fl/fl, and CSF1R Cre/wt). The four main experimental lines used for study are: 1) RGS10$^{+/+}$ and STIM2$^{+/+}$ (Stim2 $^{fl/fl}$, Csf1r, $^{cre-}$), 2) RGS10$^{-/-}$ and STIM2$^{+/+}$ (Stim2 $^{fl/fl}$, Csf1r, $^{cre-}$), 3) RGS10$^{+/+}$ and STIM2$^{-/-}$ (Stim2 $^{fl/fl}$, Csf1r, $^{cre+}$) and 4) RGS10$^{-/-}$ and STIM2$^{-/-}$ (Stim2 $^{fl/fl}$, Csf1r $^{cre+}$) **B-D)**. Primary microglia were isolated from synchronized litters from the four transgenic groups and treated with LPS (10 ug/mL) for 24 hours. Quantitative RT-PCR was performed to analyze COX-2 mRNA (**B**), RGS10 mRNA (**C**) and STIM2 mRNA (**D**), normalized to endogenous control *β-actin* ($2^{-\Delta\Delta Ct}$). Fold difference was determined by normalizing to vehicle control transgenic group (RGS10$^{+/+}$, Stim2 fl/fl, Csf1r^{cre-}). Data represent mean ± *SEM* pooled from two independent experiments. **p<0.01, determined by one-way ANOVA followed by Tukey post hoc test.

* Wild-type and RGS10 knockout parental lines were obtained from JK. Lee laboratory at the University of Georgia, and STIM2fl/fl and CSF1R Cre/wt mice were purchased from Jackson Laboratory.

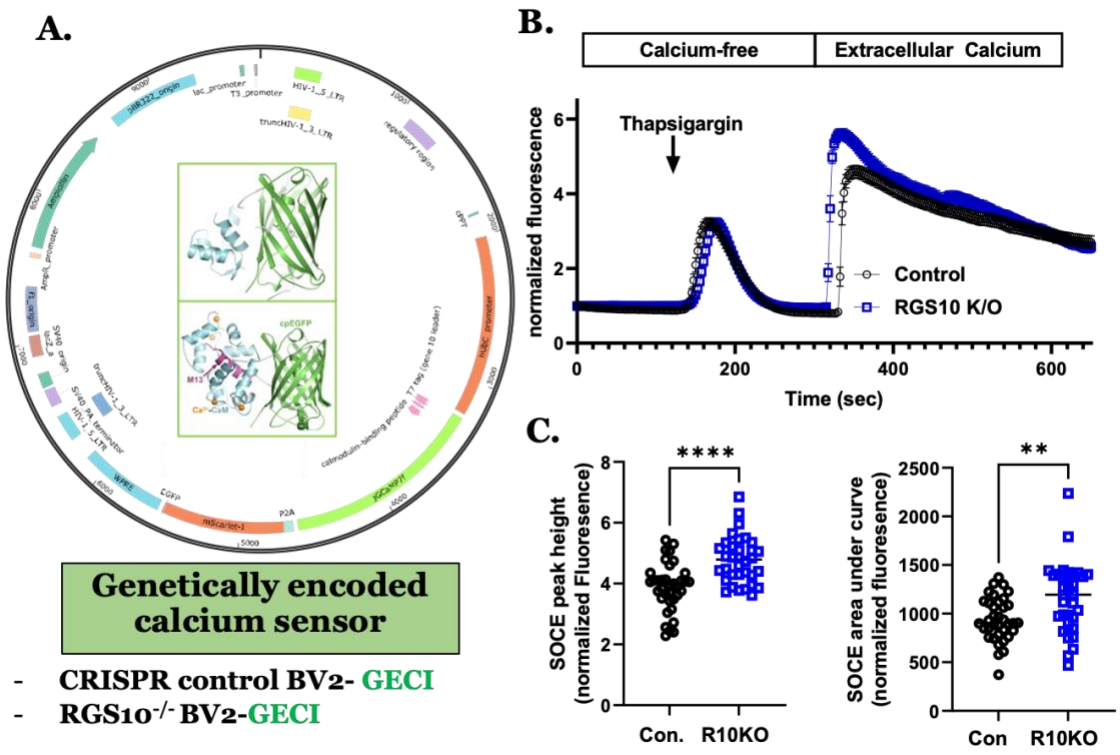

Figure A.3. RGS10 suppresses SOCE in stable GECI-expressing BV2 cells. CRISPR/Cas9 control and RGS10 knockout cells were stably transduced with lentivirus encoding GCaMP7f -mScarlet a genetically encoded calcium sensor which also contains a co-cistronic mScarlet red fluorescent protein used for flow sorting. **A)** Screenshot of plasmid map for JgCamp7f (visualized using SnapGene) and the crystal structure of GCamP in Ca2+ unbound (top) and Ca2+ bound state (bottom).* GCaMP consists of three key domains, a central GFP domain is located in between a cytoplasmic M13 domain and a calmodulin (CaM) domain. The GFP domain is circularly permuted so that it only fluoresces upon conformational change induced in the presence of cytoplasmic calcium. **B)** Fluorescent tracing from live calcium imaging of CRISPR control-GECI (Con) and RGS10 knockout-GECI (KO) BV2 cells. Live cell imaging is initiated at time=0, and 1uM thapsigargin (TG) and 1.8mM Ca2+ were added at 120 sec and 300 sec, respectively. Images were captured every 2.5 sec and average fluorescent intensity was quantified from 30-40 cells. **C-D)** Average peak height (C) and area under the curve (D) comparison of the store-operated calcium entry peak observed after Ca2+ addition, from two independent experiments. **p<0.01, and ****p<0.001, determined by unpaired student's t-test.

*Crystal structure for GCaMP is adapted from:

Akerboom, J., Rivera, J. D., Guilbe, M. M., Malavé, E. C., Hernandez, H. H., Tian, L., Hires, S., Marvin, J. S., Looger, L. L., & Schreiter, E. R. (2009). Crystal structures of the GCaMP calcium sensor reveal the mechanism of fluorescence signal change and aid rational design. *Journal of Biological Chemistry*, *284* (10), 6455-6464. https://doi.org/10.1074/jbc.m807657200

Table A.1. Subcellular localization and molecular function of RGS10 interacting partners.

Cellular Compartments	Protein Names	Molecular Function/ Biological Processes
Cytoplasm	Methylosome protein 50	Methylosome activity; nuclear receptor coactivator
	Alanine aminotransferase 1	Cellular metabolism
	E3 ubiquitin-protein ligase RNF146	Protein ubiquitination ; proteasomal degradation
	STIP1 homology and U box-containing protein 1	protein ubiquitination ; proteasomal degradation
	DDB1- and CUL4-associated factor 7	Substrate recognition for protein ligase; scaffold for kinases
	Methylosome subunit pICln	Chaperon for spliceosome assembly; methylosome activity
	Sec1 family domain-containing protein 1	Membrane fusion; intracellular trafficking
	Serine/threonine-protein kinase RIO1	Protein phosphorylation; rRNA processing
	Malonyl-CoA decarboxylase, mitochondrial	Cellular metabolism
Nucleus	Tyrosine-protein phosphatase non-receptor type 2 (isoform 2)	Protein dephosphorylation
	cAMP-specific 3',5'-cyclic phosphodiesterase 4A (perinuclear)	cAMP regulation/degradation
	Dual specificity tyrosine-phosphorylation-regulated kinase 1A	Protein phosphorylation
	G patch domain-containing protein 2	Nucleic acid binding
	Choromodomain-helicase-DNA-binding protein 1-like	Chromatin remodeling and DNA repair
	Methylosome protein 50	
	Methylosome subunit pICln	
	E3 ubiquitin-protein ligase RNF146	
	DDB1- and CUL4-associated factor 7	
	STIP1 homology and U box-containing protein	
Mitochondria	NADH dehydrogenase [ubiquinone] 1 alpha subcomplex subunit 10, mitochondrial	Mitochondrial electron transport
	Nitric oxide-associated protein 1	Mitochondrial protein translation; cellular respiration
	rRNA methyltransferase 1, mitochondrial	Ribosomal RNA binding and methylation
	Malonyl-CoA decarboxylase, mitochondrial (long isoform)	
Endoplasmic Reticulum	Stromal interaction molecule 2	Regulation of store-operated calcium entry
	Malectin	Carbohydrate metabolism
	Syntaxin-5	Intracellular trafficking; vesicle transport
	Tyrosine-protein phosphatase non-receptor type 2 (isoform 1)	
	Sec1 family domain-containing protein	
Golgi Apparatus	Syntaxin-5	
	cAMP-specific 3',5'-cyclic phosphodiesterase 4A	
	Sec1 family domain-containing protein 1	
	Golgi membrane protein 1	
Endosome	Arf-GAP with coiled-coil, ANK repeat and PH domain-containing protein 1	Intracellular trafficking
	F-BAR and double SH3 domains protein 2	Intracellular trafficking
Peroxisome	Malonyl-CoA decarboxylase, mitochondrial (short isoform)	Peroxisomal fatty acid metabolism
Plasma Membrane	Anion exchange protein 2	Ion transport; pH regulation

Table A.2: Differentially regulated genes in resting CRISPR/Cas9 RGS10 knockout BV2 cells compared to CRISPR/Cas9 control cells.

Upregulated				Downregulated			
Ensembl ID	**Symbol**	**log2 FC**	**Adj.Pval**	**Ensembl ID**	**Symbol**	**log2 FC**	**Adj.Pval**
ENSMUSG00000010122	*Slc47a1*	4.26	1.06E-130	ENSMUSG00000002985	*Apoe*	-2.93	3.82E-168
ENSMUSG00000028245	*Nsmaf*	2.44	1.99E-71	ENSMUSG00000028976	*Slc2a5*	-11.58	2.60E-74
ENSMUSG00000039221	*Rpl22l1*	2.39	4.12E-52	ENSMUSG00000071547	*Nt5dc2*	-1.63	7.48E-59
ENSMUSG00000021719	*Rgs7bp*	3.21	9.76E-50	ENSMUSG00000031709	*Tbc1d9*	-2.40	2.23E-56
ENSMUSG00000006373	*Pgrmc1*	2.07	6.07E-46	ENSMUSG00000028937	*Acot7*	-1.37	1.30E-50
ENSMUSG00000044864	*Ankrd50*	4.61	1.16E-44	ENSMUSG00000009614	*Sardh*	-3.56	7.52E-50
ENSMUSG00000020099	*Unc5b*	2.57	3.73E-39	ENSMUSG00000028766	*Alpl*	-1.25	9.95E-39
ENSMUSG00000054387	*Mdm4*	1.08	1.04E-37	ENSMUSG00000060206	*Zfp462*	-3.29	3.99E-36
ENSMUSG00000031382	*Asb11*	3.63	2.04E-35	ENSMUSG00000040950	*Mgl2*	-2.95	5.27E-34
ENSMUSG00000025558	*Dock9*	4.54	2.76E-30	ENSMUSG00000032554	*Trf*	-1.80	8.62E-34
ENSMUSG00000039200	*Atf7ip2*	3.90	5.16E-29	ENSMUSG00000009376	*Met*	-3.62	5.88E-33
ENSMUSG00000026594	*Ralgps2*	1.52	1.79E-28	ENSMUSG00000014361	*Mertk*	-3.21	1.45E-31
ENSMUSG00000026380	*Tfcp2l1*	2.91	2.71E-25	ENSMUSG00000024736	*Tmem132a*	-5.98	2.59E-30
ENSMUSG00000085456	*Gm15398*	3.64	1.44E-24	ENSMUSG00000040659	*Efhd2*	-1.03	4.99E-28
ENSMUSG00000030108	*Slc6a13*	1.83	9.34E-24	ENSMUSG00000051457	*Spn*	-2.45	1.33E-27
ENSMUSG00000029769	*Ccdc136*	3.21	1.48E-23	ENSMUSG00000036905	*C1qb*	-3.12	4.09E-27
ENSMUSG00000052727	*Map1b*	1.84	5.46E-22	ENSMUSG00000022240	*Ctnnd2*	-1.84	7.06E-27
ENSMUSG00000059900	*Tmem40*	1.09	4.12E-21	ENSMUSG00000028111	*Ctsk*	-2.34	5.44E-26
ENSMUSG00000031647	*Mfap3l*	2.67	7.72E-21	ENSMUSG00000018459	*Slc13a3*	-2.04	5.97E-25
ENSMUSG00000035578	*Iqcg*	2.09	1.43E-19	ENSMUSG00000021676	*Iqgap2*	-1.53	2.45E-24
ENSMUSG00000079017	*Ifi27l2a*	2.16	6.20E-18	ENSMUSG00000039716	*Dock3*	-1.58	2.72E-24
ENSMUSG00000011263	*Exoc3l2*	1.70	6.49E-17	ENSMUSG00000031934	*Panx1*	-1.56	3.75E-24
ENSMUSG00000026675	*Hsd17b7*	1.31	6.49E-17	ENSMUSG00000038244	*Mical2*	-1.84	1.37E-23
ENSMUSG00000055782	*Abcd2*	1.70	1.41E-15	ENSMUSG00000045322	*Tlr9*	-1.15	8.53E-23
ENSMUSG00000034295	*Fhod3*	3.24	2.55E-15	ENSMUSG00000015846	*Rxra*	-1.34	1.05E-22
ENSMUSG00000000244	*Tspan32*	1.33	2.63E-15	ENSMUSG00000032359	*Ctsh*	-1.91	1.85E-22
ENSMUSG00000072572	*Slc39a2*	1.73	3.50E-15	ENSMUSG00000085241	*Snhg3*	-1.22	7.26E-21
ENSMUSG00000030515	*Tarsl2*	5.75	7.26E-14	ENSMUSG00000004633	*Chn2*	-1.60	1.08E-20
ENSMUSG00000024912	*Fosl1*	2.56	2.38E-13	ENSMUSG00000040627	*Aicda*	-2.83	1.89E-17
ENSMUSG00000043207	*Zmpste24*	1.17	3.09E-13	ENSMUSG00000028744	*Pqlc2*	-1.22	2.67E-17
ENSMUSG00000036528	*Ppfibp2*	4.28	4.24E-13	ENSMUSG00000026932	*Nacc2*	-1.59	2.75E-17
ENSMUSG00000058317	*Ube2e2*	1.38	5.98E-13	ENSMUSG00000048376	*F2r*	-2.42	4.13E-17
ENSMUSG00000021136	*Smoc1*	3.95	6.94E-13	ENSMUSG00000040860	*Crocc*	-1.20	6.96E-17
ENSMUSG00000006221	*Hspb7*	1.04	8.48E-13	ENSMUSG00000078517	*Emc1*	-1.07	1.05E-16
ENSMUSG00000029359	*Tesc*	2.22	2.57E-12	ENSMUSG00000037605	*Adgrl3*	-9.22	3.49E-16
ENSMUSG00000022026	*Olfm4*	1.96	2.60E-12	ENSMUSG00000043154	*Ppp2r3a*	-1.57	1.66E-15
ENSMUSG00000023800	*Tiam2*	1.37	5.16E-12	ENSMUSG00000028917	*Plekhm2*	-1.04	4.18E-15
ENSMUSG00000024538	*Ppic*	7.75	5.85E-12	ENSMUSG00000018983	*E2f2*	-1.32	5.00E-15

ENSMUSG00000026815	*Gfi1b*	2.65	1.24E-11	ENSMUSG00000041161	*Otud3*	-1.05	5.30E-15
ENSMUSG00000026817	*Ak1*	3.03	1.31E-11	ENSMUSG00000103174	*Gm37168*	-1.65	6.21E-15
ENSMUSG00000035451	*Foxa1*	1.66	1.94E-11	ENSMUSG00000027002	*Nckap1*	-1.20	5.02E-14
ENSMUSG00000053835	*H2-T24*	2.03	2.59E-11	ENSMUSG00000028948	*Nol9*	-1.00	1.86E-13
ENSMUSG00000102918	*Pcdhgc3*	7.74	2.65E-11	ENSMUSG00000015222	*Map2*	-3.27	2.09E-13
ENSMUSG00000001494	*Sost*	2.45	2.98E-11	ENSMUSG00000005225	*Plekha8*	-1.06	2.37E-13
ENSMUSG00000117465		1.10	7.90E-11	ENSMUSG00000036896	*C1qc*	-3.10	2.64E-13
ENSMUSG00000033214	*Slitrk5*	2.44	8.44E-11	ENSMUSG00000019055	*Plod1*	-1.11	1.19E-12
ENSMUSG00000022514	*Il1rap*	7.43	2.24E-10	ENSMUSG00000028669	*Pithd1*	-1.12	1.33E-12
ENSMUSG00000031410	*Nxf7*	2.75	3.92E-10	ENSMUSG00000028737	*Aldh4a1*	-1.57	1.83E-12
ENSMUSG00000005973	*Rcn1*	1.58	4.65E-10	ENSMUSG00000025277	*Abhd6*	-1.04	6.31E-12
ENSMUSG00000090698	*Apold1*	2.41	4.97E-10	ENSMUSG00000024897	*Apba1*	-1.69	3.71E-11
ENSMUSG00000069171	*Nr2f1*	1.14	5.59E-10	ENSMUSG00000020865	*Abcc3*	-1.60	5.93E-11
ENSMUSG00000028194	*Ddah1*	7.44	5.80E-10	ENSMUSG00000000247	*Lhx2*	-1.37	8.51E-11
ENSMUSG00000055069	*Rab39*	5.41	6.46E-10	ENSMUSG00000069792	*Wfdc17*	-2.08	2.13E-10
ENSMUSG00000046152	*Fut10*	1.48	9.30E-10	ENSMUSG00000020331	*Hcn2*	-1.54	2.13E-10
ENSMUSG00000097177	*9330159M07Rik*	4.84	1.44E-09	ENSMUSG00000029596	*Sdsl*	-2.76	2.24E-10
ENSMUSG00000028133	*Rwdd3*	1.41	1.62E-09	ENSMUSG00000031925	*Maml2*	-1.45	7.07E-10
ENSMUSG00000057337	*Chst3*	1.13	1.62E-09	ENSMUSG00000048332	*Lhfp*	-2.47	8.42E-10
ENSMUSG00000028470	*Hint2*	4.34	2.21E-09	ENSMUSG00000005043	*Sgsh*	-1.14	8.46E-10
ENSMUSG00000047867	*Gimap6*	1.85	2.23E-09	ENSMUSG00000032265	*Fam46a*	-1.24	1.19E-09
ENSMUSG00000032690	*Oas2*	1.40	5.39E-09	ENSMUSG00000021892	*Sh3bp5*	-1.10	1.21E-09
ENSMUSG00000024395	*Lims2*	2.66	5.91E-09	ENSMUSG00000021838	*Samd4*	-1.07	3.42E-09
ENSMUSG00000095253	*Zfp799*	1.02	6.10E-09	ENSMUSG00000030844	*Rgs10*	-1.16	5.05E-09
ENSMUSG00000046598	*Bdh1*	3.17	6.24E-09	ENSMUSG00000077394	*Gm24339*	-1.40	5.44E-09
ENSMUSG00000041827	*Oasl1*	1.10	6.93E-09	ENSMUSG00000017697	*Ada*	-1.42	6.36E-09
ENSMUSG00000026285	*Pdcd1*	2.24	9.25E-09	ENSMUSG00000018927	*Ccl6*	-1.36	6.36E-09
ENSMUSG00000028480	*Glipr2*	1.48	1.13E-08	ENSMUSG00000078490	*Cfap74*	-6.93	7.20E-09
ENSMUSG00000097848	*Gm807*	2.18	1.40E-08	ENSMUSG00000028743	*Akr7a5*	-1.09	1.13E-08
ENSMUSG00000011832	*Evi5l*	6.75	1.42E-08	ENSMUSG00000026712	*Mrc1*	-2.11	1.15E-08
ENSMUSG00000029112	*Nkx1-1*	5.07	1.42E-08	ENSMUSG00000031391	*L1cam*	-1.51	1.42E-08
ENSMUSG00000063450	*Syne2*	3.46	1.55E-08	ENSMUSG00000030600	*Lrfn1*	-1.28	1.72E-08
ENSMUSG00000019970	*Sgk1*	1.64	1.63E-08	ENSMUSG00000024397	*Aif1*	-1.69	1.74E-08
ENSMUSG00000054423	*Cadps*	1.49	1.76E-08	ENSMUSG00000034570	*Inpp5j*	-1.72	3.35E-08
ENSMUSG00000095180	*Rhox5*	2.79	1.87E-08	ENSMUSG00000027864	*Ptgfrn*	-3.59	3.37E-08
ENSMUSG00000033355	*Rtp4*	1.92	1.94E-08	ENSMUSG00000028327	*Stra6l*	-1.08	1.32E-07
ENSMUSG00000020598	*Nrcam*	1.22	1.99E-08	ENSMUSG00000041361	*Myzap*	-3.71	1.75E-07
ENSMUSG00000041075	*Fzd7*	1.12	1.99E-08	ENSMUSG00000087381	*Gm16008*	-3.86	1.98E-07
ENSMUSG00000079554	*Aox2*	3.06	2.21E-08	ENSMUSG00000059401	*Mamld1*	-1.78	3.64E-07
ENSMUSG00000030107	*Usp18*	1.50	2.85E-08	ENSMUSG00000002489	*Tiam1*	-2.57	4.35E-07
ENSMUSG00000078606	*Gm4070*	1.60	3.03E-08	ENSMUSG00000021913	*Ogdhl*	-2.62	5.14E-07
ENSMUSG00000040296	*Ddx58*	1.62	3.18E-08	ENSMUSG00000040570	*Rundc3b*	-1.31	7.90E-07
ENSMUSG00000022018	*Rgcc*	1.38	5.81E-08	ENSMUSG00000103183	*Gm37090*	-3.49	1.06E-06

ENSMUSG00000074794	*Arrdc3*	1.06	7.64E-08	ENSMUSG00000026556	*Vangl2*	-1.21	1.29E-06
ENSMUSG00000036853	*Mcoln3*	1.98	9.26E-08	ENSMUSG00000040522	*Tlr8*	-2.44	1.65E-06
ENSMUSG00000044231	*Nhlrc1*	1.14	1.17E-07	ENSMUSG00000028751	*Pla2g2e*	-1.31	2.74E-06
ENSMUSG00000040086	*Tnni3k*	1.69	1.20E-07	ENSMUSG00000108060	*4921529L05Rik*	-3.89	3.31E-06
ENSMUSG00000027082	*Tfpi*	3.11	1.21E-07	ENSMUSG00000111390	*Gm48796*	-2.63	3.47E-06
ENSMUSG00000091698	*Gm6526*	2.11	1.32E-07	ENSMUSG00000022235	*Cmbl*	-1.53	4.45E-06
ENSMUSG00000060568	*Fam78b*	1.33	1.37E-07	ENSMUSG00000066000	*Zfp979*	-5.62	4.47E-06
ENSMUSG00000040557	*Mettl27*	1.90	1.88E-07	ENSMUSG00000028599	*Tnfrsf1b*	-1.14	4.74E-06
ENSMUSG00000054342	*Kcnn4*	1.53	1.89E-07	ENSMUSG00000041351	*Rap1gap*	-1.39	4.96E-06
ENSMUSG00000033594	*Spata2l*	4.34	2.35E-07	ENSMUSG00000036995	*Asap3*	-1.70	4.97E-06
ENSMUSG00000000266	*Mid2*	2.88	2.46E-07	ENSMUSG00000010051	*Hyal1*	-1.72	5.60E-06
ENSMUSG00000004347	*Pde1c*	3.27	2.74E-07	ENSMUSG00000050493	*Fam167b*	-1.30	6.70E-06
ENSMUSG00000030921	*Trim30a*	1.41	2.77E-07	ENSMUSG00000024743	*Syt7*	-1.04	6.92E-06
ENSMUSG00000115801	*AC160336.1*	1.62	3.23E-07	ENSMUSG00000024247	*Pkdcc*	-1.09	8.93E-06
ENSMUSG00000099375	*Gm28187*	4.07	3.27E-07	ENSMUSG00000039759	*Thap3*	-1.05	1.12E-05
ENSMUSG00000026883	*Dab2ip*	1.27	3.60E-07	ENSMUSG00000012123	*Crybg2*	-5.40	1.42E-05
ENSMUSG00000020396	*Nefh*	4.02	4.27E-07	ENSMUSG00000006205	*Htra1*	-1.64	1.75E-05
ENSMUSG00000042102	*Dmgdh*	5.44	4.47E-07	ENSMUSG00000005045	*Chd5*	-1.18	1.86E-05
ENSMUSG00000096210	*H1f0*	1.06	5.51E-07	ENSMUSG00000019779	*Frk*	-1.36	2.13E-05
ENSMUSG00000035105	*Egln3*	2.50	6.53E-07	ENSMUSG00000027322	*Siglec1*	-1.01	2.44E-05
ENSMUSG00000073902	*Gm1966*	2.58	9.06E-07	ENSMUSG00000078864	*Gm14322*	-3.00	2.59E-05
ENSMUSG00000079243	*Xirp1*	2.12	9.69E-07	ENSMUSG00000031860	*Pbx4*	-1.12	3.16E-05
ENSMUSG00000063354	*Slc39a4*	1.33	9.83E-07	ENSMUSG00000027939	*Nup210l*	-1.41	3.36E-05
ENSMUSG00000026068	*Il18rap*	1.15	9.84E-07	ENSMUSG00000039908	*Slc26a11*	-1.09	3.38E-05
ENSMUSG00000041592	*Sdk2*	2.39	1.02E-06	ENSMUSG00000039043	*Arpin*	-1.28	3.51E-05
ENSMUSG00000054404	*Slfn5*	2.59	1.12E-06	ENSMUSG00000022817	*Itgb5*	-1.08	3.54E-05
ENSMUSG00000100157	*2310034O05Rik*	5.90	1.15E-06	ENSMUSG00000033209	*Ttc28*	-1.32	4.06E-05
ENSMUSG00000000489	*Pdgfb*	1.10	1.85E-06	ENSMUSG00000025357	*Dgka*	-1.86	4.45E-05
ENSMUSG00000021589	*Rhobtb3*	1.37	2.25E-06	ENSMUSG00000024424	*Ttc39c*	-5.15	4.80E-05
ENSMUSG00000001761	*Smo*	3.80	2.86E-06	ENSMUSG00000029553	*Tfec*	-1.15	4.86E-05
ENSMUSG00000040483	*Xaf1*	1.44	3.43E-06	ENSMUSG00000103622	*Gm38391*	-1.04	6.65E-05
ENSMUSG00000040488	*Ltbp4*	2.20	3.47E-06	ENSMUSG00000045777	*Ifitm10*	-2.57	8.32E-05
ENSMUSG00000051124	*Gimap9*	2.95	3.56E-06	ENSMUSG00000032482	*Cspg5*	-1.66	1.02E-04
ENSMUSG00000063286	*Gm8995*	1.00	3.84E-06	ENSMUSG00000036887	*C1qa*	-2.78	1.06E-04
ENSMUSG00000079794	*AC125149.2*	1.89	4.36E-06	ENSMUSG00000097654	*Gm26714*	-1.42	1.72E-04
ENSMUSG00000025498	*Irf7*	1.42	4.36E-06	ENSMUSG00000029718	*Pcolce*	-1.65	1.78E-04
ENSMUSG00000029603	*Dtx1*	2.26	4.46E-06	ENSMUSG00000117079		-2.72	2.14E-04
ENSMUSG00000038602	*Slc35f1*	2.16	4.58E-06	ENSMUSG00000020388	*Pdlim4*	-1.60	2.14E-04
ENSMUSG00000023915	*Tnfrsf21*	5.61	4.68E-06	ENSMUSG00000023868	*Pde10a*	-4.96	2.51E-04
ENSMUSG00000036764	*Dnajc12*	1.17	5.31E-06	ENSMUSG00000024737	*Slc15a3*	-1.10	2.61E-04
ENSMUSG00000054263	*Lifr*	2.08	7.15E-06	ENSMUSG00000050957	*Insl6*	-1.05	2.78E-04
ENSMUSG00000057596	*Trim30d*	2.07	8.11E-06	ENSMUSG00000027329	*Spef1*	-1.03	2.82E-04
ENSMUSG00000044086	*Lmod3*	1.54	8.42E-06	ENSMUSG00000048924	*Ccdc125*	-1.53	2.84E-04

ENSMUSG00000018849	*Wwc1*	1.57	1.00E-05	ENSMUSG00000108239	*Gm19434*	-1.49	2.93E-04
ENSMUSG00000115483	*AC166344.3*	5.53	1.02E-05	ENSMUSG00000079419	*Ms4a6c*	-1.42	3.04E-04
ENSMUSG00000001700	*Gramd3*	3.11	1.12E-05	ENSMUSG00000062515	*Fabp4*	-1.11	3.51E-04
ENSMUSG00000029833	*Trim24*	1.28	1.22E-05	ENSMUSG00000114610	*Cyp2c52-ps*	-4.37	3.64E-04
ENSMUSG00000020577	*Tspan13*	1.34	1.30E-05	ENSMUSG00000074607	*Tox2*	-1.81	4.02E-04
ENSMUSG00000045095	*Magi1*	1.60	1.40E-05	ENSMUSG00000028373	*Astn2*	-2.43	4.05E-04
ENSMUSG00000047409	*Ctdspl*	3.99	1.45E-05	ENSMUSG00000037139	*Myom3*	-1.46	4.26E-04
ENSMUSG00000009654	*Oit3*	1.16	1.48E-05	ENSMUSG00000033419	*Snap91*	-3.64	4.91E-04
ENSMUSG00000020541	*Tom1l1*	1.12	1.62E-05	ENSMUSG00000096740	*Lbhd1*	-1.00	5.11E-04
ENSMUSG00000039765	*Cc2d2a*	6.09	1.72E-05	ENSMUSG00000071604	*Fam189a2*	-1.69	5.46E-04
ENSMUSG00000031955	*Bcar1*	1.26	1.73E-05	ENSMUSG00000079598	*Clec2l*	-3.99	5.84E-04
ENSMUSG00000079267	*Gm5930*	4.46	1.92E-05	ENSMUSG00000008540	*Mgst1*	-4.38	6.95E-04
ENSMUSG00000029821	*Gsdme*	1.46	2.38E-05	ENSMUSG00000084910	*C630043F03Rik*	-1.24	9.29E-04
ENSMUSG00000069855	*Slc47a2*	5.93	2.89E-05	ENSMUSG00000099757	*BE692007*	-1.92	9.76E-04
ENSMUSG00000028268	*Gbp3*	1.51	3.10E-05	ENSMUSG00000079429	*Mroh2a*	-1.26	1.02E-03
ENSMUSG00000029314	*Gpat3*	1.52	3.29E-05	ENSMUSG00000118132		-1.92	1.10E-03
ENSMUSG00000036019	*Tmtc2*	1.15	3.35E-05	ENSMUSG00000111533	*AC137127.1*	-1.38	1.17E-03
ENSMUSG00000104063	*Pcdhgb7*	1.61	3.79E-05	ENSMUSG00000101493	*2810405F17Rik*	-1.16	1.20E-03
ENSMUSG00000028965	*Tnfrsf9*	2.06	4.29E-05	ENSMUSG00000104467	*Gm37660*	-2.09	1.42E-03
ENSMUSG00000020638	*Cmpk2*	1.32	5.73E-05	ENSMUSG00000000409	*Lck*	-1.62	1.42E-03
ENSMUSG00000031722	*Hp*	2.16	5.95E-05	ENSMUSG00000097313	*Gm26569*	-2.11	1.51E-03
ENSMUSG00000041460	*Cacna2d4*	1.18	6.15E-05	ENSMUSG00000074340	*Ovgp1*	-1.02	1.70E-03
ENSMUSG00000031842	*Pde4c*	3.50	6.35E-05	ENSMUSG00000020658	*Efr3b*	-1.04	1.74E-03
ENSMUSG00000078952	*Lncenc1*	3.55	7.77E-05	ENSMUSG00000024677	*Ms4a6b*	-2.18	1.94E-03
ENSMUSG00000063873	*Slc24a3*	3.29	9.24E-05	ENSMUSG00000048534	*Jaml*	-1.75	2.12E-03
ENSMUSG00000045868	*Gvin1*	1.52	9.78E-05	ENSMUSG00000090173	*Fbxw10*	-1.42	2.26E-03
ENSMUSG00000079491	*H2-T10*	4.78	1.02E-04	ENSMUSG00000110730	*Gm19385*	-1.45	2.28E-03
ENSMUSG00000068699	*Flnc*	1.25	1.59E-04	ENSMUSG00000066233	*Tmem42*	-1.16	2.31E-03
ENSMUSG00000034799	*Unc13a*	1.06	1.80E-04	ENSMUSG00000017144	*Rnd3*	-3.24	2.49E-03
ENSMUSG00000049848	*Ceacam19*	4.97	1.83E-04	ENSMUSG00000027805	*Pfn2*	-1.41	2.58E-03
ENSMUSG00000056665	*Them6*	1.29	1.87E-04	ENSMUSG00000019359	*Gdpd2*	-1.96	2.64E-03
ENSMUSG00000027961	*Lrrc39*	1.25	1.87E-04	ENSMUSG00000114584	*Gm47694*	-1.22	2.65E-03
ENSMUSG00000003153	*Slc2a3*	1.11	1.95E-04	ENSMUSG00000030708	*Dnajb13*	-1.03	2.65E-03
ENSMUSG00000037411	*Serpine1*	1.09	2.23E-04	ENSMUSG00000029084	*Cd38*	-1.64	3.04E-03
ENSMUSG00000109829	*Gm45605*	2.53	2.35E-04	ENSMUSG00000018334	*Ksr1*	-1.26	3.13E-03
ENSMUSG00000089822	*Gm15759*	5.32	2.39E-04	ENSMUSG00000020334	*Slc22a4*	-1.04	3.15E-03
ENSMUSG00000025932	*Eya1*	3.11	2.55E-04	ENSMUSG00000021303	*Gng4*	-1.42	3.16E-03
ENSMUSG00000104348	*Gm37691*	1.00	2.58E-04	ENSMUSG00000054510	*Gm14461*	-2.48	3.33E-03
ENSMUSG00000103400	*Gm15853*	1.15	2.60E-04	ENSMUSG00000032232	*Cgnl1*	-1.56	4.41E-03
ENSMUSG00000026679	*Enkur*	1.60	2.65E-04	ENSMUSG00000094447	*9430069I07Rik*	-3.66	4.52E-03
ENSMUSG00000026494	*Kif26b*	2.87	2.67E-04	ENSMUSG00000025804	*Ccr1*	-1.16	4.53E-03
ENSMUSG00000025494	*Sigirr*	3.22	2.73E-04	ENSMUSG00000026579	*F5*	-1.74	4.56E-03
ENSMUSG00000000359	*Rem1*	2.38	2.98E-04	ENSMUSG00000039699	*Batf2*	-3.14	4.66E-03

ENSMUSG00000099470	*Gm29340*	1.02	3.16E-04	ENSMUSG00000112959	*Gm32834*	-1.74	4.66E-03
ENSMUSG00000020641	*Rsad2*	1.18	3.29E-04	ENSMUSG00000002100	*Mybpc3*	-1.78	4.85E-03
ENSMUSG00000024617	*Camk2a*	1.00	3.35E-04	ENSMUSG00000045065	*9930022D16Rik*	-1.14	5.07E-03
ENSMUSG00000049235	*Gm7324*	1.76	3.45E-04	ENSMUSG00000021880	*Rnase6*	-2.78	5.26E-03
ENSMUSG00000048285	*Frmd6*	1.11	4.17E-04	ENSMUSG00000035270	*Impg2*	-2.30	5.31E-03
ENSMUSG00000111752	*Gm38575*	2.50	4.18E-04	ENSMUSG00000038151	*Prdm1*	-1.18	5.50E-03
ENSMUSG00000030589	*Rasgrp4*	1.29	4.18E-04	ENSMUSG00000039787	*Cercam*	-1.11	5.82E-03
ENSMUSG00000108659	*Gm34121*	1.07	6.09E-04	ENSMUSG00000041189	*Chrnb1*	-1.07	5.84E-03
ENSMUSG00000097365	*C030034L19Rik*	1.58	6.11E-04	ENSMUSG00000018566	*Slc2a4*	-1.87	6.09E-03
ENSMUSG00000037664	*Cdkn1c*	2.59	6.94E-04	ENSMUSG00000109953	*5430430B14Rik*	-1.59	6.49E-03
ENSMUSG00000030745	*Il21r*	1.05	9.50E-04	ENSMUSG00000046733	*Gprc5a*	-4.60	6.58E-03
ENSMUSG00000002228	*Ppm1j*	1.05	9.61E-04	ENSMUSG00000016024	*Lbp*	-2.24	6.70E-03
ENSMUSG00000043439	*Epop*	1.36	9.74E-04	ENSMUSG00000007872	*Id3*	-2.39	7.11E-03
ENSMUSG00000020872	*Tac4*	2.19	9.83E-04	ENSMUSG00000027219	*Slc28a2*	-1.21	7.31E-03
ENSMUSG00000017830	*Dhx58*	1.01	1.04E-03	ENSMUSG00000038523	*1700003F12Rik*	-1.78	7.41E-03
ENSMUSG00000002007	*Srpk3*	1.30	1.19E-03	ENSMUSG00000074796	*Slc4a11*	-1.24	7.90E-03
ENSMUSG00000097254	*C430042M11Rik*	1.71	1.34E-03	ENSMUSG00000034438	*Gbp8*	-1.40	7.99E-03
ENSMUSG00000102559	*Gm37570*	1.87	1.35E-03	ENSMUSG00000024770	*Lipn*	-1.59	8.16E-03
ENSMUSG00000063564	*Col23a1*	1.15	1.35E-03	ENSMUSG00000081103	*Rps12-ps26*	-1.06	8.54E-03
ENSMUSG00000030790	*Adm*	2.23	1.38E-03	ENSMUSG00000027546	*Atp9a*	-1.04	8.84E-03
ENSMUSG00000085527	*Gm15535*	1.22	1.61E-03	ENSMUSG00000024672	*Ms4a7*	-1.32	8.89E-03
ENSMUSG00000035041	*Creb3l3*	4.23	1.69E-03	ENSMUSG00000099655	*2310034G01Rik*	-1.36	8.91E-03
ENSMUSG00000113440	*Gm46404*	1.57	1.74E-03	ENSMUSG00000026866	*Kynu*	-1.14	8.99E-03
ENSMUSG00000026581	*Sell*	2.33	1.77E-03	ENSMUSG00000075569	*Rsph10b*	-1.86	9.31E-03
ENSMUSG00000031442	*Mcf2l*	1.00	1.77E-03	ENSMUSG00000066755	*Tnfsf18*	-1.63	9.58E-03
ENSMUSG00000042207	*Kdm5b*	3.01	1.97E-03	ENSMUSG00000040026	*Saa3*	-1.58	1.05E-02
ENSMUSG00000024190	*Dusp1*	1.06	2.25E-03	ENSMUSG00000033967	*Rnf225*	-1.12	1.15E-02
ENSMUSG00000073530	*Pappa2*	1.73	2.32E-03	ENSMUSG00000031963	*Bmper*	-3.87	1.17E-02
ENSMUSG00000030156	*Cd69*	1.15	2.34E-03	ENSMUSG00000045349	*Sh2d5*	-1.08	1.34E-02
ENSMUSG00000041481	*Serpina3g*	1.27	2.48E-03	ENSMUSG00000024990	*Rbp4*	-1.55	1.37E-02
ENSMUSG00000039960	*Rhou*	1.20	2.59E-03	ENSMUSG00000032470	*Mras*	-2.18	1.44E-02
ENSMUSG00000030157	*Clec2d*	1.05	2.59E-03	ENSMUSG00000022504	*Ciita*	-3.23	1.47E-02
ENSMUSG00000028195	*Cyr61*	3.21	2.76E-03	ENSMUSG00000077506	*Scarna9*	-1.69	1.48E-02
ENSMUSG00000029561	*Oasl2*	1.64	2.77E-03	ENSMUSG00000027223	*Mapk8ip1*	-2.54	1.49E-02
ENSMUSG00000053846	*Lipg*	4.72	2.99E-03	ENSMUSG00000074899	*Sptbn5*	-1.47	1.56E-02
ENSMUSG00000079457	*Gm7609*	2.44	3.17E-03	ENSMUSG00000087445	*Gm14286*	-1.18	1.74E-02
ENSMUSG00000079138	*Gm8818*	2.58	3.19E-03	ENSMUSG00000018924	*Alox15*	-1.81	1.77E-02
ENSMUSG00000003882	*Il7r*	1.38	3.21E-03	ENSMUSG00000063652	*Slc22a21*	-1.17	1.81E-02
ENSMUSG00000044770	*Scml4*	1.05	3.21E-03	ENSMUSG00000032375	*Aph1b*	-1.05	1.85E-02
ENSMUSG00000002459	*Rgs20*	1.63	3.22E-03	ENSMUSG00000028602	*Tnfrsf8*	-1.32	1.92E-02
ENSMUSG00000023341	*Mx2*	1.34	3.22E-03	ENSMUSG00000004814	*Ccl24*	-2.20	1.95E-02
ENSMUSG00000073600	*Prob1*	1.01	3.28E-03	ENSMUSG00000110018	*5430437J10Rik*	-1.18	1.95E-02
ENSMUSG00000113131	*Gm48290*	2.37	3.42E-03	ENSMUSG00000021797	*9230112D13Rik*	-1.06	1.95E-02

ENSMUSG00000021974	*Fgf9*	1.18	3.60E-03
ENSMUSG00000055865	*Fam19a3*	1.04	3.89E-03
ENSMUSG00000046447	*Camk2n1*	2.64	4.12E-03
ENSMUSG00000025610	*Map3k7cl*	2.13	4.24E-03
ENSMUSG00000037887	*Dusp8*	1.59	5.00E-03
ENSMUSG00000006362	*Cbfa2t3*	2.12	5.03E-03
ENSMUSG00000032238	*Rora*	1.08	5.22E-03
ENSMUSG00000017314	*Mpp2*	1.57	5.38E-03
ENSMUSG00000022221	*Ripk3*	1.04	5.55E-03
ENSMUSG00000097418	*Mir155hg*	1.83	6.13E-03
ENSMUSG00000060534	*Dcc*	4.79	6.44E-03
ENSMUSG00000021062	*Rab15*	1.72	6.49E-03
ENSMUSG00000023830	*Igf2r*	1.13	6.68E-03
ENSMUSG00000032033	*Barx2*	2.19	6.99E-03
ENSMUSG00000078716	*Tmem8b*	2.23	7.05E-03
ENSMUSG00000107215	*Gm43197*	1.03	7.16E-03
ENSMUSG00000027261	*Hao1*	2.86	7.30E-03
ENSMUSG00000102543	*Pcdhgc5*	3.67	7.55E-03
ENSMUSG00000097104	*Gm26579*	3.55	7.67E-03
ENSMUSG00000029544	*Cabp1*	1.95	7.74E-03
ENSMUSG00000038201	*Kcna7*	1.32	7.83E-03
ENSMUSG00000050967	*Creg2*	1.27	8.73E-03
ENSMUSG00000105940	*Gm42635*	1.48	8.97E-03
ENSMUSG00000041607	*Mbp*	1.41	8.97E-03
ENSMUSG00000104568	*Gm43255*	2.39	9.44E-03
ENSMUSG00000052373	*Mpp3*	1.07	9.66E-03
ENSMUSG00000053963	*Stum*	2.38	1.08E-02
ENSMUSG00000022602	*Arc*	3.23	1.01E-02
ENSMUSG00000029392	*Rilpl1*	2.27	1.15E-02
ENSMUSG00000020310	*Madcam1*	2.22	1.22E-02
ENSMUSG00000019987	*Arg1*	1.76	1.23E-02
ENSMUSG00000037419	*Endod1*	3.38	1.28E-02
ENSMUSG00000075184	*F930017D23Rik*	1.47	1.28E-02
ENSMUSG00000057346	*Apol9a*	3.09	1.31E-02
ENSMUSG00000079244	*Gm5622*	3.23	1.37E-02
ENSMUSG00000052485	*Tmem171*	1.41	1.37E-02
ENSMUSG00000040253	*Gbp7*	1.04	1.41E-02
ENSMUSG00000053101	*Gpr141*	1.85	1.43E-02
ENSMUSG00000005131	*4930550C14Rik*	1.30	1.46E-02
ENSMUSG00000027803	*Wwtr1*	2.77	1.47E-02
ENSMUSG00000044562	*Rasip1*	1.00	1.55E-02
ENSMUSG00000053687	*Dpep2*	1.18	1.57E-02
ENSMUSG00000114279	*Hist1h2bm*	-3.21	1.99E-02
ENSMUSG00000078838	*Gm17382*	-1.16	1.99E-02
ENSMUSG00000055561	*Spink5*	-2.42	2.02E-02
ENSMUSG00000039109	*F13a1*	-1.26	2.15E-02
ENSMUSG00000055360	*Prl2c5*	-3.66	2.21E-02
ENSMUSG00000017412	*Cacnb4*	-1.56	2.26E-02
ENSMUSG00000036641	*Ccdc148*	-1.97	2.27E-02
ENSMUSG00002076074		-1.29	2.30E-02
ENSMUSG00000064899	*Snord118*	-3.32	2.45E-02
ENSMUSG00000039691	*Tspan10*	-1.79	2.48E-02
ENSMUSG00000051984	*Sec31b*	-1.13	2.56E-02
ENSMUSG00000085006	*BC021767*	-4.20	2.61E-02
ENSMUSG00000050357	*Carmil2*	-2.16	2.72E-02
ENSMUSG00000024871	*Doc2g*	-1.25	2.78E-02
ENSMUSG00000095609	*Gm21188*	-2.64	2.81E-02
ENSMUSG00000086657	*Stamos*	-1.22	2.87E-02
ENSMUSG00000111212	*Gm47087*	-2.73	2.91E-02
ENSMUSG00000040828	*Catsperd*	-1.52	2.91E-02
ENSMUSG00000069266	*Hist1h4b*	-2.92	3.03E-02
ENSMUSG00000019768	*Esr1*	-1.18	3.03E-02
ENSMUSG00000089829	*Gm16565*	-1.86	3.22E-02
ENSMUSG00000032012	*Nectin1*	-1.08	3.27E-02
ENSMUSG00000085772	*D630024D03Rik*	-1.21	3.45E-02
ENSMUSG00000108350	*Gm44950*	-1.20	3.94E-02
ENSMUSG00000118839		-3.48	3.99E-02
ENSMUSG00000060093	*Hist1h4a*	-2.90	4.06E-02
ENSMUSG00000097399	*Gm26555*	-1.14	4.98E-02

ENSMUSG00000013974	*Mcemp1*	2.26	1.62E-02
ENSMUSG00000025875	*Tspan17*	1.58	1.70E-02
ENSMUSG00000100217	*9930111H07Rik*	1.29	1.73E-02
ENSMUSG00000037921	*Ddx60*	1.24	1.74E-02
ENSMUSG00000026894	*Morn5*	1.16	1.77E-02
ENSMUSG00000114858	*Gm5790*	1.70	1.90E-02
ENSMUSG00000006930	*Hap1*	1.31	1.99E-02
ENSMUSG00000114624	*Gm48267*	1.33	2.06E-02
ENSMUSG00000032875	*Arhgef17*	1.94	2.09E-02
ENSMUSG00000085912	*Trp53cor1*	1.25	2.16E-02
ENSMUSG00000110588	*Gm45774*	1.33	2.27E-02
ENSMUSG00000022456	*Sept3*	2.56	2.29E-02
ENSMUSG00000026604	*Ptpn14*	2.42	2.31E-02
ENSMUSG00000022836	*Mylk*	2.63	2.48E-02
ENSMUSG00000106968	*C78283*	3.63	2.59E-02
ENSMUSG00000089762	*Ier5l*	1.21	2.73E-02
ENSMUSG00000104213	*Ighd*	2.11	2.77E-02
ENSMUSG00000026255	*Efhd1*	1.13	2.77E-02
ENSMUSG00000051504	*Siglech*	1.90	2.79E-02
ENSMUSG00000037922	*Bank1*	1.08	2.79E-02
ENSMUSG00000102919	*Gm37726*	1.04	2.91E-02
ENSMUSG00000032827	*Ppp1r9a*	2.60	2.92E-02
ENSMUSG00000081723	*Gm15931*	2.04	2.92E-02
ENSMUSG00000076621	*Ighj1*	1.51	2.99E-02
ENSMUSG00000042807	*Hecw2*	1.03	3.06E-02
ENSMUSG00000085957	*Syna*	1.64	3.17E-02
ENSMUSG00000028128	*F3*	1.10	3.17E-02
ENSMUSG00000016758	*Bik*	3.44	3.29E-02
ENSMUSG00000020205	*Phlda1*	1.43	3.37E-02
ENSMUSG00000060512	*0610040J01Rik*	2.63	3.38E-02
ENSMUSG00000025938	*Slco5a1*	1.55	3.44E-02
ENSMUSG00000079584	*Gm364*	2.45	3.45E-02
ENSMUSG00000016028	*Celsr1*	1.35	3.57E-02
ENSMUSG00000074364	*Ehd2*	1.39	3.64E-02
ENSMUSG00000040270	*Bach2*	1.10	3.64E-02
ENSMUSG00000025216	*Lbx1*	2.10	3.74E-02
ENSMUSG00000041538	*H2-Ob*	2.14	3.82E-02
ENSMUSG00000115044	*CT573086.2*	1.59	3.98E-02
ENSMUSG00000100747	*1700084E18Rik*	1.10	4.02E-02
ENSMUSG00000009394	*Syn2*	1.47	4.04E-02
ENSMUSG00000070873	*Lilra5*	2.63	4.18E-02
ENSMUSG00000024399	*Ltb*	1.52	4.21E-02
ENSMUSG00000026875	*Traf1*	1.74	4.25E-02

ENSMUSG00000035095	*Fam167a*	2.55	4.26E-02
ENSMUSG00000042417	*Ccno*	2.20	4.29E-02
ENSMUSG00000104168	*Gm38250*	1.14	4.36E-02
ENSMUSG00000096100	*AC133103.7*	2.91	4.69E-02
ENSMUSG00000079605	*Zbtb9*	1.25	4.84E-02
ENSMUSG00000057370	*Gm8724*	2.16	4.90E-02
ENSMUSG00000106915	*Gm42655*	3.51	4.98E-02
ENSMUSG00000093672	*Gm20655*	1.26	4.99E-02

Table A.3: Differentially regulated genes in LPS-stimulated CRISPR/Cas9 RGS10 knockout BV2 cells compared to CRISPR/Cas9 control cells.

Upregulated				Downregulated			
Ensembl ID	**Symbol**	**log FC**	**Adj.Pval**	**Ensembl ID**	**Symbol**	**log FC**	**Adj.Pval**
ENSMUSG00000010122	*Slc47a1*	5.58	8.4E-178	ENSMUSG00000002985	*Apoe*	-2.94	9.11E-154
ENSMUSG00000039221	*Rpl22l1*	2.93	1.84E-75	ENSMUSG00000028976	*Slc2a5*	-11.50	6.67E-73
ENSMUSG00000006373	*Pgrmc1*	2.46	1.04E-64	ENSMUSG00000071547	*Nt5dc2*	-1.68	1.12E-59
ENSMUSG00000044864	*Ankrd50*	4.57	2.35E-59	ENSMUSG00000028766	*Alpl*	-1.42	1.01E-48
ENSMUSG00000026380	*Tfcp2l1*	3.80	1.89E-53	ENSMUSG00000009376	*Met*	-3.67	3.77E-48
ENSMUSG00000028245	*Nsmaf*	2.06	1.22E-47	ENSMUSG00000028937	*Acot7*	-1.23	2.66E-41
ENSMUSG00000040435	*Ppp1r15a*	1.65	4.51E-47	ENSMUSG00000060206	*Zfp462*	-2.75	2.48E-40
ENSMUSG00000054387	*Mdm4*	1.10	1.26E-38	ENSMUSG00000026390	*Marco*	-4.60	5.09E-38
ENSMUSG00000021719	*Rgs7bp*	3.77	2.78E-38	ENSMUSG00000027199	*Gatm*	-1.15	6.74E-36
ENSMUSG00000031382	*Asb11*	4.27	2.19E-32	ENSMUSG00000040950	*Mgl2*	-3.35	2.56E-35
ENSMUSG00000039200	*Atf7ip2*	3.29	2.27E-30	ENSMUSG00000032554	*Trf*	-1.87	7.2E-35
ENSMUSG00000079017	*Ifi27l2a*	2.86	4.69E-28	ENSMUSG00000032601	*Prkar2a*	-1.01	3.14E-33
ENSMUSG00000020099	*Unc5b*	2.56	2.44E-27	ENSMUSG00000031709	*Tbc1d9*	-1.66	6.2E-32
ENSMUSG00000028459	*Cd72*	2.06	2.31E-25	ENSMUSG00000070691	*Runx3*	-1.27	6.1E-31
ENSMUSG00000006221	*Hspb7*	1.48	8.47E-25	ENSMUSG00000004633	*Chn2*	-1.85	8.27E-28
ENSMUSG00000066861	*Oas1g*	1.26	1.66E-24	ENSMUSG00000085241	*Snhg3*	-1.43	1.17E-27
ENSMUSG00000026594	*Ralgps2*	1.34	6.92E-21	ENSMUSG00000040860	*Crocc*	-1.56	1.41E-26
ENSMUSG00000025558	*Dock9*	4.46	2.18E-20	ENSMUSG00000039716	*Dock3*	-1.67	1.49E-26
ENSMUSG00000052776	*Oas1a*	1.19	1.02E-19	ENSMUSG00000031934	*Panx1*	-1.56	3.35E-25
ENSMUSG00000072572	*Slc39a2*	1.98	1.35E-19	ENSMUSG00000028745	*Capzb*	-1.07	1.66E-24
ENSMUSG00000029769	*Ccdc136*	2.99	2.49E-19	ENSMUSG00000026832	*Cytip*	-1.42	2.37E-24
ENSMUSG00000041827	*Oasl1*	1.56	2.44E-18	ENSMUSG00000039852	*Rere*	-1.10	4.84E-23
ENSMUSG00000085456	*Gm15398*	3.18	4.54E-18	ENSMUSG00000041161	*Otud3*	-1.26	1.04E-21
ENSMUSG00000031770	*Herpud1*	1.40	8.15E-18	ENSMUSG00000039768	*Dnajc11*	-1.07	3.81E-21
ENSMUSG00000021262	*Evl*	1.75	8.35E-18	ENSMUSG00000062995	*Ica1*	-1.28	6.92E-21
ENSMUSG00000036528	*Ppfibp2*	4.41	1.88E-17	ENSMUSG00000028948	*Nol9*	-1.25	6.92E-21
ENSMUSG00000079138	*Gm8818*	4.10	2.92E-17	ENSMUSG00000054843	*Atrnl1*	-1.10	7.74E-21
ENSMUSG00000052727	*Map1b*	1.55	1.19E-16	ENSMUSG00000021676	*Iqgap2*	-1.45	9.09E-21
ENSMUSG00000023952	*Gtpbp2*	1.06	3.16E-16	ENSMUSG00000019055	*Plod1*	-1.43	9.53E-21
ENSMUSG00000095253	*Zfp799*	1.40	3.45E-16	ENSMUSG00000014361	*Mertk*	-3.01	2.92E-20
ENSMUSG00000076617	*Ighm*	1.33	1.73E-15	ENSMUSG00000066037	*Hnrnpr*	-1.08	1.75E-19
ENSMUSG00000040852	*Plekhh2*	1.76	2.37E-15	ENSMUSG00000043154	*Ppp2r3a*	-1.68	6.24E-19
ENSMUSG00000030108	*Slc6a13*	1.40	3.99E-15	ENSMUSG00000028111	*Ctsk*	-1.97	1.56E-18
ENSMUSG00000024538	*Ppic*	9.75	1.06E-14	ENSMUSG00000009614	*Sardh*	-2.89	3.32E-18
ENSMUSG00000096210	*H1f0*	1.54	1.84E-14	ENSMUSG00000015846	*Rxra*	-1.19	9E-18
ENSMUSG00000042216	*Sgsm1*	1.17	3.86E-14	ENSMUSG00000078517	*Emc1*	-1.09	3.03E-17
ENSMUSG00000046718	*Bst2*	1.18	8.21E-14	ENSMUSG00000036905	*C1qb*	-3.13	6.89E-17

ENSMUSG00000046598	*Bdh1*	4.22	2.19E-13	ENSMUSG00000037605	*Adgrl3*	-9.39	7.23E-17
ENSMUSG00000055202	*Zfp811*	3.41	2.24E-13	ENSMUSG00000051457	*Spn*	-1.91	1.27E-16
ENSMUSG00000030107	*Usp18*	1.81	3.27E-13	ENSMUSG00000038811	*Gngt2*	-1.08	1.6E-16
ENSMUSG00000031647	*Mfap3l*	1.92	3.96E-13	ENSMUSG00000103174	*Gm37168*	-1.92	2.04E-16
ENSMUSG00000090698	*Apold1*	2.96	8.14E-13	ENSMUSG00000047250	*Ptgs1*	-1.53	2.22E-16
ENSMUSG00000026285	*Pdcd1*	3.10	8.34E-13	ENSMUSG00000022240	*Ctnnd2*	-1.35	2.88E-16
ENSMUSG00000004837	*Grap*	1.92	1.33E-12	ENSMUSG00000038244	*Mical2*	-1.49	3.92E-16
ENSMUSG00000044231	*Nhlrc1*	1.60	1.35E-12	ENSMUSG00000028744	*Pqlc2*	-1.15	1.12E-15
ENSMUSG00000067212	*H2-T23*	1.17	1.61E-12	ENSMUSG00000024736	*Tmem132a*	-2.62	9.09E-15
ENSMUSG00000026675	*Hsd17b7*	1.10	2.13E-12	ENSMUSG00000032359	*Ctsh*	-1.87	1.85E-14
ENSMUSG00000041075	*Fzd7*	1.37	2.61E-12	ENSMUSG00000028992	*Nmnat1*	-1.00	2.05E-14
ENSMUSG00000102918	*Pcdhgc3*	7.89	6.98E-12	ENSMUSG00000048332	*Lhfp*	-2.39	7.12E-14
ENSMUSG00000022514	*Il1rap*	7.84	1.3E-11	ENSMUSG00000031391	*L1cam*	-2.01	1.4E-13
ENSMUSG00000020641	*Rsad2*	2.00	1.37E-11	ENSMUSG00000000753	*Serpinf1*	-1.69	7.36E-13
ENSMUSG00000000244	*Tspan32*	1.17	1.74E-11	ENSMUSG00000035769	*Xylb*	-1.33	8.34E-13
ENSMUSG00000030515	*Tarsl2*	8.08	1.83E-11	ENSMUSG00000025277	*Abhd6*	-1.09	9.03E-13
ENSMUSG00000024339	*Tap2*	1.01	2.01E-11	ENSMUSG00000042073	*Abhd14b*	-1.04	1.66E-12
ENSMUSG00000071076	*Jund*	1.00	3.24E-11	ENSMUSG00000018927	*Ccl6*	-1.59	2.92E-12
ENSMUSG00000000489	*Pdgfb*	1.47	3.32E-11	ENSMUSG00000059713	*Rcan3*	-1.02	4.31E-12
ENSMUSG00000024190	*Dusp1*	2.03	3.4E-11	ENSMUSG00000078490	*Cfap74*	-8.02	4.97E-12
ENSMUSG00000079554	*Aox2*	3.16	3.61E-11	ENSMUSG00000026932	*Nacc2*	-1.31	3.09E-11
ENSMUSG00000023915	*Tnfrsf21*	7.89	4.08E-11	ENSMUSG00000059401	*Mamld1*	-2.51	4.01E-11
ENSMUSG00000021136	*Smoc1*	3.62	4.16E-11	ENSMUSG00000018459	*Slc13a3*	-2.24	8.63E-11
ENSMUSG00000035451	*Foxa1*	1.63	4.41E-11	ENSMUSG00000028669	*Pithd1*	-1.04	8.65E-11
ENSMUSG00000038518	*Jarid2*	1.02	8.8E-11	ENSMUSG00000103622	*Gm38391*	-1.58	1.21E-10
ENSMUSG00000026311	*Asb1*	1.02	9.77E-11	ENSMUSG00000041362	*Shtn1*	-1.42	1.33E-10
ENSMUSG00000037868	*Egr2*	2.27	1.03E-10	ENSMUSG00000093565	*Rab26os*	-1.06	1.54E-10
ENSMUSG00000004267	*Eno2*	1.46	1.21E-10	ENSMUSG00000052713	*Zfp608*	-1.24	2.24E-10
ENSMUSG00000015837	*Sqstm1*	1.39	1.21E-10	ENSMUSG00000040522	*Tlr8*	-3.17	2.49E-10
ENSMUSG00000043207	*Zmpste24*	1.03	1.79E-10	ENSMUSG00000020032	*Nuak1*	-1.37	3.97E-10
ENSMUSG00000022951	*Rcan1*	1.12	1.9E-10	ENSMUSG00000018983	*E2f2*	-1.07	5.28E-10
ENSMUSG00000058317	*Ube2e2*	1.22	1.96E-10	ENSMUSG00000028737	*Aldh4a1*	-1.42	6.68E-10
ENSMUSG00000118663		1.16	2.03E-10	ENSMUSG00000020331	*Hcn2*	-1.65	7.02E-10
ENSMUSG00000097245	*Gm5421*	1.36	3.75E-10	ENSMUSG00000077394	*Gm24339*	-1.44	7.05E-10
ENSMUSG00000001494	*Sost*	2.47	4.77E-10	ENSMUSG00000061436	*Hipk2*	-1.00	7.31E-10
ENSMUSG00000046169	*Adamts6*	1.20	5.05E-10	ENSMUSG00000030844	*Rgs10*	-1.23	8.22E-10
ENSMUSG00000029112	*Nkx1-1*	6.18	6.05E-10	ENSMUSG00000112963	*Gm6093*	-3.37	8.47E-10
ENSMUSG00000067203	*H2-K2*	1.45	6.77E-10	ENSMUSG00000097855	*A930007I19Rik*	-1.26	1.26E-09
ENSMUSG00000034295	*Fhod3*	2.62	7.26E-10	ENSMUSG00000030600	*Lrfn1*	-1.46	1.6E-09
ENSMUSG00000020577	*Tspan13*	1.83	1.21E-09	ENSMUSG00000028936	*Rpl22*	-1.09	3.91E-09
ENSMUSG00000028133	*Rwdd3*	1.40	1.21E-09	ENSMUSG00000103183	*Gm37090*	-3.76	6.44E-09
ENSMUSG00000020423	*Btg2*	1.22	1.41E-09	ENSMUSG00000024743	*Syt7*	-1.29	7.26E-09
ENSMUSG00000011832	*Evi5l*	6.90	1.77E-09	ENSMUSG00000001089	*Luzp1*	-1.00	7.6E-09

ENSMUSG00000045005	*Fzd5*	1.24	1.89E-09	ENSMUSG00000002489	*Tiam1*	-2.85	8.78E-09
ENSMUSG00000053581	*Zfand2a*	1.13	2.22E-09	ENSMUSG00000048376	*F2r*	-1.63	9.98E-09
ENSMUSG00000097177	*9330159M07Rik*	4.26	2.55E-09	ENSMUSG00000032374	*Plod2*	-1.18	1.29E-08
ENSMUSG00000057596	*Trim30d*	2.28	2.6E-09	ENSMUSG00000021876	*Rnase4*	-1.08	2.42E-08
ENSMUSG00000024395	*Lims2*	2.57	2.77E-09	ENSMUSG00000031727	*Pmfbp1*	-1.94	2.43E-08
ENSMUSG00000026785	*Pkn3*	1.19	2.79E-09	ENSMUSG00000040570	*Rundc3b*	-1.45	2.78E-08
ENSMUSG00000042842	*Serpinb6b*	1.24	4.66E-09	ENSMUSG00000020865	*Abcc3*	-1.38	3.25E-08
ENSMUSG00000029833	*Trim24*	1.62	5.64E-09	ENSMUSG00000040627	*Aicda*	-2.46	4.06E-08
ENSMUSG00000052631	*Sh2d6*	2.57	6.79E-09	ENSMUSG00000034570	*Inpp5j*	-1.76	6.6E-08
ENSMUSG00000045095	*Magi1*	2.00	8.18E-09	ENSMUSG00000029915	*Clec5a*	-1.17	8.25E-08
ENSMUSG00000095180	*Rhox5*	2.79	8.33E-09	ENSMUSG00000027939	*Nup210l*	-1.79	8.39E-08
ENSMUSG00000000266	*Mid2*	2.67	8.36E-09	ENSMUSG00000026365	*Cfh*	-1.25	8.72E-08
ENSMUSG00000004347	*Pde1c*	5.92	8.88E-09	ENSMUSG00000024897	*Apba1*	-1.41	9.51E-08
ENSMUSG00000005580	*Adcy9*	1.07	9.11E-09	ENSMUSG00000117399		-1.37	9.83E-08
ENSMUSG00000035671	*Zswim4*	1.11	0.00000001	ENSMUSG00000005824	*Tnfsf14*	-2.12	9.84E-08
ENSMUSG00000028194	*Ddah1*	6.86	1.12E-08	ENSMUSG00000026556	*Vangl2*	-1.54	1.12E-07
ENSMUSG00000054364	*Rhob*	1.53	1.23E-08	ENSMUSG00000000184	*Ccnd2*	-1.14	1.13E-07
ENSMUSG00000015016	*Acsf3*	1.22	1.62E-08	ENSMUSG00000024974	*Smc3*	-1.03	0.00000013
ENSMUSG00000055069	*Rab39*	6.67	1.74E-08	ENSMUSG00000110945	*Gm9856*	-1.22	1.43E-07
ENSMUSG00000001700	*Gramd3*	3.54	2.22E-08	ENSMUSG00000070583	*Fv1*	-1.02	1.94E-07
ENSMUSG00000038168	*P3h2*	3.57	2.79E-08	ENSMUSG00000032239	*Rp9*	-1.00	2.01E-07
ENSMUSG00000029359	*Tesc*	2.28	2.79E-08	ENSMUSG00000029596	*Sdsl*	-2.39	2.02E-07
ENSMUSG00000100157	*2310034O05Rik*	3.78	3.11E-08	ENSMUSG00000084350	*Znf41-ps*	-1.12	2.12E-07
ENSMUSG00000115801	*AC160336.1*	1.70	3.27E-08	ENSMUSG00000087381	*Gm16008*	-5.87	2.25E-07
ENSMUSG00000052920	*Prkg1*	1.79	3.48E-08	ENSMUSG00000071537	*Klrg2*	-1.11	2.37E-07
ENSMUSG00000079491	*H2-T10*	4.59	4.36E-08	ENSMUSG00000027864	*Ptgfrn*	-6.25	2.57E-07
ENSMUSG00000035105	*Egln3*	2.76	4.55E-08	ENSMUSG00000066000	*Zfp979*	-5.04	2.99E-07
ENSMUSG00000078349	*AW011738*	1.75	4.73E-08	ENSMUSG00000029553	*Tfec*	-1.27	2.99E-07
ENSMUSG00000032487	*Ptgs2*	2.12	5.43E-08	ENSMUSG00000026712	*Mrc1*	-2.12	3.36E-07
ENSMUSG00000036478	*Btg1*	1.15	5.89E-08	ENSMUSG00000073910	*Mob3b*	-1.01	3.51E-07
ENSMUSG00000031953	*Tmem170*	1.01	6.67E-08	ENSMUSG00000078864	*Gm14322*	-3.21	3.86E-07
ENSMUSG00000005973	*Rcn1*	1.40	9.36E-08	ENSMUSG00000111533	*AC137127.1*	-2.33	3.86E-07
ENSMUSG00000029603	*Dtx1*	2.30	1.08E-07	ENSMUSG00000050608	*Minos1*	-1.12	0.00000054
ENSMUSG00000033214	*Slitrk5*	1.89	1.11E-07	ENSMUSG00000036896	*C1qc*	-2.71	6.96E-07
ENSMUSG00000027082	*Tfpi*	3.57	1.12E-07	ENSMUSG00000096655	*1700065D16Rik*	-1.86	0.00000083
ENSMUSG00000069171	*Nr2f1*	1.07	1.21E-07	ENSMUSG00000041361	*Myzap*	-4.24	8.83E-07
ENSMUSG00000024912	*Fosl1*	1.51	1.22E-07	ENSMUSG00000010051	*Hyal1*	-1.98	0.00000116
ENSMUSG00000087579	*Hectd2os*	1.18	1.31E-07	ENSMUSG00000045838	*A430105I19Rik*	-1.09	0.00000116
ENSMUSG00000057337	*Chst3*	1.51	1.37E-07	ENSMUSG00000035835	*Plppr3*	-1.87	0.00000124
ENSMUSG00000034855	*Cxcl10*	1.63	1.59E-07	ENSMUSG00000032174	*Icam5*	-1.58	0.00000148
ENSMUSG00000070031	*Sp140*	1.15	1.59E-07	ENSMUSG00000078862	*Gm14326*	-1.01	0.0000018
ENSMUSG00000026489	*Coq8a*	1.45	1.91E-07	ENSMUSG00000038859	*Baiap2l1*	-1.71	0.00000199
ENSMUSG00000035692	*Isg15*	1.52	2.05E-07	ENSMUSG00000025804	*Ccr1*	-1.57	0.00000204

ENSMUSG00000040877	*Wdr25*	1.02	2.37E-07	ENSMUSG00000018381	*Abi3*	-1.17	0.000003
ENSMUSG00000002083	*Bbc3*	1.16	3.09E-07	ENSMUSG00000029648	*Flt1*	-1.14	0.00000303
ENSMUSG00000028480	*Gliprr2*	1.27	0.0000004	ENSMUSG00000017697	*Ada*	-1.13	0.00000417
ENSMUSG00000046152	*Fut10*	1.31	4.84E-07	ENSMUSG00000027950	*Chrnb2*	-1.14	0.00000487
ENSMUSG00000053835	*H2-T24*	1.49	4.95E-07	ENSMUSG00000008540	*Mgst1*	-4.20	0.00000533
ENSMUSG00000026628	*Atf3*	1.18	5.27E-07	ENSMUSG00000039783	*Kmo*	-1.84	0.00000738
ENSMUSG00000035578	*Iqcg*	1.16	5.82E-07	ENSMUSG00000029718	*Pcolce*	-2.67	0.0000075
ENSMUSG00000025498	*Irf7*	1.45	6.11E-07	ENSMUSG00000115739	*AC101945.4*	-1.72	0.0000108
ENSMUSG00000020638	*Cmpk2*	1.47	7.11E-07	ENSMUSG00000032221	*Mns1*	-1.09	0.0000129
ENSMUSG00000023341	*Mx2*	1.89	7.71E-07	ENSMUSG00000019779	*Frk*	-1.27	0.0000136
ENSMUSG00000024565	*Sall3*	1.06	8.58E-07	ENSMUSG00000015222	*Map2*	-2.36	0.0000148
ENSMUSG00000032661	*Oas3*	1.29	9.47E-07	ENSMUSG00000075225	*Ccdc162*	-1.78	0.000019
ENSMUSG00000102559	*Gm37570*	2.74	0.00000114	ENSMUSG00000032352	*Lrrc1*	-1.21	0.0000197
ENSMUSG00000063450	*Syne2*	2.33	0.00000139	ENSMUSG00000012123	*Crybg2*	-4.66	0.0000215
ENSMUSG00000115483	*AC166344.3*	3.94	0.00000159	ENSMUSG00000069792	*Wfdc17*	-1.31	0.000022
ENSMUSG00000047867	*Gimap6*	1.45	0.00000159	ENSMUSG00000102776	*Gm38162*	-1.89	0.0000283
ENSMUSG00000033594	*Spata2l*	6.07	0.0000018	ENSMUSG00000096740	*Lbhd1*	-1.19	0.0000286
ENSMUSG00000037321	*Tap1*	1.01	0.00000216	ENSMUSG00000079429	*Mroh2a*	-1.41	0.0000348
ENSMUSG00000072620	*Slfn2*	1.02	0.00000229	ENSMUSG00000002797	*Ggct*	-1.12	0.0000394
ENSMUSG00000074466	*Gm15417*	1.18	0.00000303	ENSMUSG00000027546	*Atp9a*	-1.53	0.0000419
ENSMUSG00000037239	*Spred3*	1.07	0.00000346	ENSMUSG00000028751	*Pla2g2e*	-1.05	0.0000559
ENSMUSG00000040483	*Xaf1*	1.34	0.00000373	ENSMUSG00000108239	*Gm19434*	-1.61	0.0000592
ENSMUSG00000031410	*Nxf7*	2.16	0.0000038	ENSMUSG00000118330		-1.35	0.0000748
ENSMUSG00000021822	*Plau*	1.20	0.00000423	ENSMUSG00000024770	*Lipn*	-2.12	0.000097
ENSMUSG00000030921	*Trim30a*	1.23	0.00000504	ENSMUSG00000074607	*Tox2*	-2.03	0.000104
ENSMUSG00000038179	*Slamf7*	3.68	0.00000576	ENSMUSG00000084821	*Gm15880*	-1.06	0.000104
ENSMUSG00000052336	*Cx3cr1*	1.29	0.00000576	ENSMUSG00000058624	*Gda*	-1.66	0.000107
ENSMUSG00000028341	*Nr4a3*	2.05	0.00000672	ENSMUSG00000006205	*Htra1*	-1.33	0.000107
ENSMUSG00000026104	*Stat1*	1.00	0.00000684	ENSMUSG00000056215	*Lrguk*	-1.29	0.000109
ENSMUSG00000039960	*Rhou*	1.33	0.00000735	ENSMUSG00000117662		-1.17	0.000128
ENSMUSG00000116262	*AL589670.3*	1.62	0.00000882	ENSMUSG00000064065	*Ipcef1*	-1.20	0.000134
ENSMUSG00000117231		2.18	0.00000904	ENSMUSG00000032470	*Mras*	-2.46	0.000145
ENSMUSG00000041460	*Cacna2d4*	1.50	0.00000907	ENSMUSG00000021913	*Ogdhl*	-1.82	0.000151
ENSMUSG00000036002	*Fam214b*	1.21	0.00000968	ENSMUSG00000074519	*Zfp971*	-1.19	0.000153
ENSMUSG00000037887	*Dusp8*	2.17	0.00000993	ENSMUSG00000018924	*Alox15*	-2.64	0.000155
ENSMUSG00000090958	*Lrrc32*	3.00	0.0000119	ENSMUSG00000025357	*Dgka*	-1.56	0.000174
ENSMUSG00000032238	*Rora*	1.54	0.0000122	ENSMUSG00000029403	*Cdkl2*	-1.06	0.00018
ENSMUSG00000028195	*Cyr61*	3.66	0.0000123	ENSMUSG00000106219	*5830416I19Rik*	-1.03	0.000205
ENSMUSG00000029158	*Yipf7*	1.06	0.0000123	ENSMUSG00000110218	*Gm20219*	-1.42	0.000231
ENSMUSG00000078606	*Gm4070*	1.07	0.0000126	ENSMUSG00000036995	*Asap3*	-1.51	0.000253
ENSMUSG00000025932	*Eya1*	5.51	0.0000136	ENSMUSG00000074203	*G430095P16Rik*	-1.19	0.00026
ENSMUSG00000018849	*Wwc1*	1.52	0.0000136	ENSMUSG00000048924	*Ccdc125*	-1.24	0.000268
ENSMUSG00000002228	*Ppm1j*	1.32	0.0000138	ENSMUSG00000017144	*Rnd3*	-3.20	0.000271

ENSMUSG00000040557	*Mettl27*	1.57	0.0000159	ENSMUSG00000063245	*Zfp993*	-1.42	0.000308
ENSMUSG00000099375	*Gm28187*	2.61	0.0000164	ENSMUSG00000114584	*Gm47694*	-1.39	0.00033
ENSMUSG00000079267	*Gm5930*	5.69	0.0000166	ENSMUSG00000023868	*Pde10a*	-4.55	0.000366
ENSMUSG00000033355	*Rtp4*	1.44	0.0000195	ENSMUSG00000019359	*Gdpd2*	-2.04	0.000383
ENSMUSG00000056708	*Ier5*	1.07	0.0000199	ENSMUSG00000024869	*Nudt8*	-1.37	0.000405
ENSMUSG00000028268	*Gbp3*	1.43	0.0000202	ENSMUSG00000037139	*Myom3*	-1.53	0.000412
ENSMUSG00000028680	*Plk3*	1.20	0.0000217	ENSMUSG00000031963	*Bmper*	-4.57	0.000428
ENSMUSG00000022026	*Olfm4*	1.78	0.0000228	ENSMUSG00000049699	*Ucn2*	-1.10	0.000478
ENSMUSG00000056144	*Trim34a*	1.57	0.0000242	ENSMUSG00000090093	*Gm14399*	-1.14	0.000502
ENSMUSG00000044086	*Lmod3*	1.50	0.0000243	ENSMUSG00000111390	*Gm48796*	-2.00	0.000517
ENSMUSG00000000359	*Rem1*	3.18	0.0000246	ENSMUSG00000108060	*4921529L05Rik*	-2.06	0.000539
ENSMUSG00000031842	*Pde4c*	3.40	0.0000253	ENSMUSG00000047898	*Ccr4*	-2.88	0.00054
ENSMUSG00000025408	*Ddit3*	1.93	0.0000278	ENSMUSG00000064370	*mt-Cytb*	-1.42	0.000548
ENSMUSG00000028470	*Hint2*	4.04	0.0000285	ENSMUSG00000078861	*Zfp931*	-1.04	0.000589
ENSMUSG00000027078	*Ube2l6*	1.05	0.0000285	ENSMUSG00000070385	*Ampd1*	-2.78	0.000605
ENSMUSG00000069855	*Slc47a2*	5.79	0.0000318	ENSMUSG00000078838	*Gm17382*	-1.56	0.000614
ENSMUSG00000009654	*Oit3*	1.07	0.0000331	ENSMUSG00000097635	*Gm26826*	-1.20	0.000614
ENSMUSG00000020758	*Itgb4*	1.12	0.0000351	ENSMUSG00000039043	*Arpin*	-1.09	0.000614
ENSMUSG00000021367	*Edn1*	2.12	0.0000366	ENSMUSG00000006800	*Sulf2*	-1.06	0.00062
ENSMUSG00000063354	*Slc39a4*	1.11	0.000044	ENSMUSG00000086682	*Gm16023*	-1.16	0.000662
ENSMUSG00000057346	*Apol9a*	2.56	0.0000491	ENSMUSG00000045349	*Sh2d5*	-1.44	0.000688
ENSMUSG00000054423	*Cadps*	1.09	0.0000495	ENSMUSG00000079598	*Clec2l*	-3.05	0.000694
ENSMUSG00000030745	*Il21r*	1.62	0.0000501	ENSMUSG00000066233	*Tmem42*	-1.27	0.0007
ENSMUSG00000079190	*AC133103.1*	1.34	0.000051	ENSMUSG00000107761	*2010008C14Rik*	-1.01	0.000704
ENSMUSG00000002007	*Srpk3*	1.74	0.0000521	ENSMUSG00000039713	*Plekhg5*	-1.09	0.00071
ENSMUSG00000100213	*Gm28151*	1.25	0.0000526	ENSMUSG00000086993	*Rsf1os2*	-1.08	0.00074
ENSMUSG00000030410	*Dmwd*	1.02	0.0000693	ENSMUSG00000117079		-1.97	0.000773
ENSMUSG00000055865	*Fam19a3*	1.54	0.0000702	ENSMUSG00000039787	*Cercam*	-1.30	0.000834
ENSMUSG00000116165	*Pdxp*	1.06	0.0000736	ENSMUSG00000032482	*Cspg5*	-1.50	0.000945
ENSMUSG00000040296	*Ddx58*	1.18	0.0000764	ENSMUSG00000019768	*Esr1*	-1.69	0.000961
ENSMUSG00000099470	*Gm29340*	1.20	0.000078	ENSMUSG00000031780	*Ccl17*	-2.08	0.00103
ENSMUSG00000045868	*Gvin1*	1.32	0.0000789	ENSMUSG00000110730	*Gm19385*	-1.54	0.00105
ENSMUSG00000073600	*Prob1*	1.07	0.0000793	ENSMUSG00000046733	*Gprc5a*	-4.75	0.00106
ENSMUSG00000079794	*AC125149.2*	1.40	0.0000812	ENSMUSG00000036887	*C1qa*	-2.84	0.00113
ENSMUSG00000026358	*Rgs1*	2.26	0.0000816	ENSMUSG00000096233	*Gm13238*	-1.59	0.00114
ENSMUSG00000038602	*Slc35f1*	1.42	0.000086	ENSMUSG00000054304	*D130007C19Rik*	-1.09	0.00118
ENSMUSG00000026864	*Hspa5*	1.01	0.0000868	ENSMUSG00000020961	*Ston2*	-5.02	0.0014
ENSMUSG00000031289	*Il13ra2*	5.40	0.000087	ENSMUSG00000045725	*Prr15*	-3.57	0.00149
ENSMUSG00000043439	*Epop*	1.56	0.000099	ENSMUSG00000079481	*Nhsl2*	-1.09	0.00152
ENSMUSG00000054409	*Tmem74*	1.09	0.0000998	ENSMUSG00000064341	*mt-Nd1*	-1.48	0.00156
ENSMUSG00000037594	*BC022687*	1.07	0.000104	ENSMUSG00000097557	*C130060C02Rik*	-1.32	0.00156
ENSMUSG00000022440	*C1qtnf6*	2.86	0.000108	ENSMUSG00000099722	*Gm29154*	-1.54	0.00159
ENSMUSG00000031442	*Mcf2l*	1.13	0.000113	ENSMUSG00000028396	*2310002L09Rik*	-1.08	0.00165

ENSMUSG00000026494	*Kif26b*	3.05	0.000115	ENSMUSG00000033209	*Ttc28*	-1.11	0.00177
ENSMUSG00000073802	*Cdkn2b*	1.44	0.000116	ENSMUSG00000031549	*Ido2*	-2.06	0.00178
ENSMUSG00000023034	*Nr4a1*	1.47	0.000131	ENSMUSG00000106025	*Gm42940*	-1.34	0.00182
ENSMUSG00000025875	*Tspan17*	2.50	0.000133	ENSMUSG00000097316	*Gm10516*	-1.29	0.00188
ENSMUSG00000029821	*Gsdme*	1.19	0.000133	ENSMUSG00000036362	*P2ry13*	-1.29	0.00213
ENSMUSG00000019970	*Sgk1*	1.12	0.000136	ENSMUSG00000059040	*Eno1b*	-1.31	0.0022
ENSMUSG00000006930	*Hap1*	2.02	0.000137	ENSMUSG00000086606	*Gm13205*	-1.03	0.0022
ENSMUSG00000042102	*Dmgdh*	4.67	0.000151	ENSMUSG00000056904	*Gm5620*	-1.41	0.00228
ENSMUSG00000020396	*Nefh*	4.15	0.000152	ENSMUSG00000101493	*2810405F17Rik*	-1.03	0.0023
ENSMUSG00000039384	*Dusp10*	1.19	0.000155	ENSMUSG00000101655	*2310040G24Rik*	-1.06	0.00234
ENSMUSG00000074141	*Il4i1*	1.02	0.000155	ENSMUSG00000085525	*Gm13166*	-1.62	0.00264
ENSMUSG00000042207	*Kdm5b*	2.69	0.000158	ENSMUSG00000091845	*Rpl36-ps12*	-1.62	0.00281
ENSMUSG00000035041	*Creb3l3*	4.96	0.000159	ENSMUSG00000086806	*Gm13054*	-2.44	0.00285
ENSMUSG00000079808	*AC168977.1*	1.28	0.000174	ENSMUSG00000118314		-1.06	0.003
ENSMUSG00000068699	*Flnc*	1.34	0.000177	ENSMUSG00000039699	*Batf2*	-2.30	0.00301
ENSMUSG00000063564	*Col23a1*	1.15	0.000191	ENSMUSG00000099655	*2310034G01Rik*	-1.55	0.00302
ENSMUSG00000003545	*Fosb*	1.92	0.000195	ENSMUSG00000020461	*Clhc1*	-1.29	0.00306
ENSMUSG00000116657		1.19	0.000199	ENSMUSG00000035390	*Brsk1*	-3.11	0.00307
ENSMUSG00000057137	*Tmem140*	1.19	0.000209	ENSMUSG00000064363	*mt-Nd4*	-1.32	0.00307
ENSMUSG00000059708	*Akap17b*	4.10	0.00021	ENSMUSG00000081103	*Rps12-ps26*	-1.15	0.00332
ENSMUSG00000104394	*Gm37254*	1.00	0.000229	ENSMUSG00000047222	*Rnase2a*	-4.90	0.00358
ENSMUSG00000044770	*Scml4*	1.28	0.000231	ENSMUSG00000035246	*Pcyt1b*	-2.50	0.00363
ENSMUSG00000045875	*Adra1a*	1.75	0.000268	ENSMUSG00000022235	*Cmbl*	-1.22	0.00413
ENSMUSG00000035095	*Fam167a*	3.55	0.000296	ENSMUSG00000064147	*Rab44*	-1.38	0.00419
ENSMUSG00000073409	*H2-Q6*	2.00	0.000298	ENSMUSG00000045777	*Ifitm10*	-1.75	0.00421
ENSMUSG00000054404	*Slfn5*	1.88	0.000329	ENSMUSG00000040424	*Hipk4*	-1.96	0.00438
ENSMUSG00000023266	*Frs3*	1.14	0.000339	ENSMUSG00000091844	*Gm8251*	-1.06	0.00445
ENSMUSG00000042622	*Maff*	1.18	0.000347	ENSMUSG00000085006	*BC021767*	-4.87	0.00446
ENSMUSG00000063873	*Slc24a3*	3.42	0.000384	ENSMUSG00000085378	*Gm11415*	-1.04	0.00462
ENSMUSG00000047409	*Ctdspl*	4.66	0.000388	ENSMUSG00000021303	*Gng4*	-1.32	0.00464
ENSMUSG00000073530	*Pappa2*	1.52	0.000403	ENSMUSG00000002104	*Rapsn*	-1.60	0.00465
ENSMUSG00000043953	*Ccrl2*	1.30	0.000428	ENSMUSG00000051832	*E230016K23Rik*	-1.36	0.00477
ENSMUSG00000025492	*Ifitm3*	2.10	0.000444	ENSMUSG00000021880	*Rnase6*	-2.71	0.00495
ENSMUSG00000053846	*Lipg*	4.12	0.000449	ENSMUSG00000021797	*9230112D13Rik*	-1.22	0.00501
ENSMUSG00000058755	*Osm*	1.06	0.000455	ENSMUSG00000084910	*C630043F03Rik*	-1.06	0.00518
ENSMUSG00000023905	*Tnfrsf12a*	1.18	0.000456	ENSMUSG00000064345	*mt-Nd2*	-1.51	0.00529
ENSMUSG00000054342	*Kcnn4*	1.09	0.000561	ENSMUSG00000070282	*3000002C10Rik*	-1.16	0.00532
ENSMUSG00000106475	*Gm43011*	1.73	0.000593	ENSMUSG00000083340	*Gm13156*	-2.60	0.00551
ENSMUSG00000116908		1.17	0.000615	ENSMUSG00000026866	*Kynu*	-1.23	0.00566
ENSMUSG00000107546	*Gm20560*	1.28	0.000628	ENSMUSG00000050578	*Mmp13*	-2.20	0.00578
ENSMUSG00000102543	*Pcdhgc5*	3.66	0.000631	ENSMUSG00000081778	*Gm6325*	-1.66	0.00579
ENSMUSG00000086196	*Gm13571*	2.32	0.000652	ENSMUSG00000091742	*Gm5093*	-4.88	0.00643
ENSMUSG00000023830	*Igf2r*	1.18	0.000716	ENSMUSG00000117315		-1.84	0.00684

ENSMUSG00000028278	*Rragd*	1.35	0.000739	ENSMUSG00000094447	*9430069I07Rik*	-2.66	0.0069
ENSMUSG00000026791	*Slc2a8*	1.25	0.000739	ENSMUSG00000035126	*Wdr78*	-1.12	0.0072
ENSMUSG00000020178	*Adora2a*	1.75	0.000747	ENSMUSG00000040666	*Sh3bgr*	-1.34	0.00762
ENSMUSG00000116813		4.89	0.00082	ENSMUSG00000108897	*Gm44861*	-2.59	0.00841
ENSMUSG00000079547	*H2-DMb1*	1.09	0.00082	ENSMUSG00000055833	*1700034H15Rik*	-1.43	0.0085
ENSMUSG00000024401	*Tnf*	1.77	0.000989	ENSMUSG00000090173	*Fbxw10*	-1.23	0.00871
ENSMUSG00000026894	*Morn5*	1.69	0.00115	ENSMUSG00000075463	*4930594M22Rik*	-1.44	0.0088
ENSMUSG00000079033	*Mef2b*	1.31	0.00116	ENSMUSG00000026579	*F5*	-1.32	0.00886
ENSMUSG00000056665	*Them6*	1.12	0.00117	ENSMUSG00000022504	*Ciita*	-3.99	0.00923
ENSMUSG00000001761	*Smo*	2.90	0.00126	ENSMUSG00000022123	*Scel*	-1.24	0.00932
ENSMUSG00000070873	*Lilra5*	3.20	0.00133	ENSMUSG00000020798	*Spns3*	-1.59	0.00976
ENSMUSG00000021701	*Plk2*	1.73	0.00133	ENSMUSG00000021684	*Pde8b*	-1.11	0.00989
ENSMUSG00000000386	*Mx1*	2.70	0.00135	ENSMUSG00000078127	*Fam170b*	-1.62	0.00997
ENSMUSG00000036853	*Mcoln3*	1.43	0.00135	ENSMUSG00000053552	*Ebf4*	-1.57	0.0102
ENSMUSG00000089822	*Gm15759*	4.35	0.00137	ENSMUSG00000072115	*Ang*	-1.05	0.0103
ENSMUSG00000027261	*Hao1*	1.88	0.00137	ENSMUSG00000086453	*Gm11457*	-1.06	0.0106
ENSMUSG00000038508	*Gdf15*	1.21	0.00137	ENSMUSG00000064367	*mt-Nd5*	-1.28	0.0107
ENSMUSG00000037921	*Ddx60*	1.35	0.0014	ENSMUSG00000041189	*Chrnb1*	-1.11	0.0107
ENSMUSG00000022221	*Ripk3*	1.13	0.0014	ENSMUSG00000040828	*Catsperd*	-1.45	0.0116
ENSMUSG00000090641	*Zfp712*	1.15	0.00151	ENSMUSG00000032841	*Prr5l*	-1.09	0.0116
ENSMUSG00000095440	*Fignl2*	1.10	0.00151	ENSMUSG00000091370	*5730435O14Rik*	-2.64	0.0119
ENSMUSG00000026815	*Gfi1b*	2.24	0.00161	ENSMUSG00000111094	*Gm34425*	-1.88	0.0119
ENSMUSG00000107215	*Gm43197*	1.10	0.00166	ENSMUSG00000075569	*Rsph10b*	-1.69	0.0119
ENSMUSG00000072844	*G530011O06Rik*	1.00	0.00166	ENSMUSG00000043312	*Olfr131*	-1.20	0.0119
ENSMUSG00000015396	*Cd83*	1.45	0.00168	ENSMUSG00000004814	*Ccl24*	-3.06	0.0121
ENSMUSG00000091698	*Gm6526*	1.27	0.00175	ENSMUSG00000078439	*Smim24*	-2.15	0.0125
ENSMUSG00000113010	*Gm34084*	3.39	0.00177	ENSMUSG00000037217	*Syn1*	-1.70	0.0126
ENSMUSG00000040624	*Plekhg1*	2.96	0.00189	ENSMUSG00000105107	*Gm43412*	-1.50	0.0126
ENSMUSG00000044716	*Dok7*	1.11	0.00193	ENSMUSG00000032232	*Cgnl1*	-1.46	0.0129
ENSMUSG00000054072	*Iigp1*	2.54	0.00194	ENSMUSG00000112959	*Gm32834*	-1.59	0.013
ENSMUSG00000097848	*Gm807*	1.21	0.00197	ENSMUSG00000005493	*Msh4*	-1.58	0.0134
ENSMUSG00000060534	*Dcc*	5.09	0.00199	ENSMUSG00000002100	*Mybpc3*	-1.47	0.014
ENSMUSG00000027803	*Wwtr1*	1.86	0.00227	ENSMUSG00000068587	*Mgam*	-1.68	0.0142
ENSMUSG00000078716	*Tmem8b*	2.85	0.00228	ENSMUSG00000117903		-1.18	0.0147
ENSMUSG00000025432	*Avil*	2.23	0.00232	ENSMUSG00000025934	*Gsta3*	-1.67	0.0155
ENSMUSG00000079243	*Xirp1*	2.24	0.00238	ENSMUSG00000086657	*Stamos*	-1.25	0.0155
ENSMUSG00000112716	*4930471E19Rik*	1.64	0.00244	ENSMUSG00000096923	*A730071L15Rik*	-1.77	0.0158
ENSMUSG00000103901	*Gm37499*	1.33	0.00263	ENSMUSG00000004359	*Spic*	-2.83	0.0162
ENSMUSG00000079584	*Gm364*	1.61	0.00264	ENSMUSG00000044083	*Efcab8*	-2.01	0.0162
ENSMUSG00000048752	*Prss50*	1.14	0.00264	ENSMUSG00000099094	*Gm19569*	-1.87	0.0162
ENSMUSG00000040270	*Bach2*	2.36	0.00271	ENSMUSG00000003341	*Atp8b3*	-1.54	0.0165
ENSMUSG00000022286	*Grhl2*	4.20	0.00279	ENSMUSG00000109724	*Gm18194*	-1.60	0.0167
ENSMUSG00000029392	*Rilpl1*	1.90	0.00279	ENSMUSG00000041205	*Map6d1*	-1.72	0.0174

ENSMUSG00000016758	*Bik*	1.78	0.00279	ENSMUSG00000030219	*Erp27*	-1.40	0.0185
ENSMUSG00000073274	*Gm14636*	1.31	0.00285	ENSMUSG00000079467	*Gm14966*	-1.15	0.0191
ENSMUSG00000058252	*Tcp11x2*	4.40	0.00298	ENSMUSG00000114610	*Cyp2c52-ps*	-1.91	0.0193
ENSMUSG00000087259	*2610035D17Rik*	1.18	0.00302	ENSMUSG00000055360	*Prl2c5*	-2.58	0.0198
ENSMUSG00000048388	*Fam171b*	1.52	0.00326	ENSMUSG00000024793	*Tnfrsf25*	-2.96	0.0201
ENSMUSG00000020310	*Madcam1*	1.77	0.00338	ENSMUSG00000073739	*Gm16287*	-1.00	0.0202
ENSMUSG00000082292	*Gm12250*	1.62	0.00351	ENSMUSG00000104379	*Gm37509*	-1.86	0.0203
ENSMUSG00000033227	*Wnt6*	1.32	0.00362	ENSMUSG00000052955	*Cpvl*	-1.61	0.0204
ENSMUSG00000079457	*Gm7609*	1.49	0.00365	ENSMUSG00000104218	*Gm9134*	-1.42	0.0206
ENSMUSG00000025993	*Slc40a1*	1.03	0.00373	ENSMUSG00000016024	*Lbp*	-1.74	0.0208
ENSMUSG00000037801	*Iqch*	1.91	0.00402	ENSMUSG00000015579	*Nkx2-5*	-3.64	0.021
ENSMUSG00000046447	*Camk2n1*	2.12	0.00427	ENSMUSG00000105449	*Gm43379*	-1.17	0.021
ENSMUSG00000050350	*Gpr18*	1.85	0.00432	ENSMUSG00000037003	*Tns2*	-1.02	0.021
ENSMUSG00000118590		1.65	0.0045	ENSMUSG00000058794	*Nfe2*	-1.07	0.0218
ENSMUSG00000028211	*Trp53inp1*	1.16	0.00453	ENSMUSG00002076074		-1.26	0.0219
ENSMUSG00000003882	*Il7r*	1.26	0.00487	ENSMUSG00000097313	*Gm26569*	-1.34	0.0221
ENSMUSG00000038151	*Prdm1*	1.09	0.00491	ENSMUSG00000118134		-1.78	0.0224
ENSMUSG00000068246	*Apol9b*	2.11	0.00506	ENSMUSG00000089849	*Runx2os2*	-1.32	0.0224
ENSMUSG00000025481	*Urah*	4.04	0.00532	ENSMUSG00000032198	*Dock6*	-2.91	0.0233
ENSMUSG00000058427	*Cxcl2*	2.41	0.00567	ENSMUSG00000098120	*Gm5914*	-1.21	0.0236
ENSMUSG00000022346	*Myc*	1.28	0.00596	ENSMUSG00000101166	*Gm28496*	-1.13	0.0238
ENSMUSG00000038393	*Txnip*	1.25	0.00602	ENSMUSG00000099757	*BE692007*	-1.11	0.0241
ENSMUSG00000020732	*Rab37*	1.86	0.00604	ENSMUSG00000074252	*Gm10654*	-1.08	0.0244
ENSMUSG00000034460	*Six4*	4.23	0.00623	ENSMUSG00000005800	*Mmp8*	-1.77	0.0249
ENSMUSG00000085431	*4930440I19Rik*	1.97	0.00662	ENSMUSG00000022665	*Ccdc80*	-1.32	0.0252
ENSMUSG00000025746	*Il6*	2.20	0.0069	ENSMUSG00000086736	*Gm14902*	-1.15	0.0253
ENSMUSG00000041592	*Sdk2*	1.36	0.00697	ENSMUSG00000105283	*Gm33370*	-1.07	0.0284
ENSMUSG00000049235	*Gm7324*	1.33	0.00718	ENSMUSG00000033967	*Rnf225*	-1.07	0.0288
ENSMUSG00000020205	*Phlda1*	1.62	0.00722	ENSMUSG00000036469	*March1*	-1.72	0.0289
ENSMUSG00000029561	*Oasl2*	1.43	0.00722	ENSMUSG00000074899	*Sptbn5*	-1.39	0.03
ENSMUSG00000043460	*Elfn2*	1.33	0.00728	ENSMUSG00000026581	*Sell*	-1.03	0.0301
ENSMUSG00000039236	*Isg20*	1.28	0.00728	ENSMUSG00000036168	*Ccdc38*	-1.36	0.0303
ENSMUSG00000096100	*AC133103.7*	3.41	0.00794	ENSMUSG00000104649	*Gm43712*	-1.17	0.0309
ENSMUSG00000038201	*Kcna7*	1.32	0.00854	ENSMUSG00000024990	*Rbp4*	-1.30	0.0326
ENSMUSG00000031951	*Tmem231*	1.09	0.00897	ENSMUSG00000107385	*C330024D21Rik*	-2.09	0.0343
ENSMUSG00000049848	*Ceacam19*	2.11	0.00943	ENSMUSG00000054510	*Gm14461*	-2.13	0.035
ENSMUSG00000060716	*Plekhh1*	1.31	0.01	ENSMUSG00000118377		-1.15	0.0357
ENSMUSG00000027748	*Trpc4*	1.46	0.0103	ENSMUSG00000108350	*Gm44950*	-1.20	0.0363
ENSMUSG00000107120	*Gm43059*	1.13	0.0105	ENSMUSG00000020669	*Sh3yl1*	-1.04	0.0366
ENSMUSG00000118426		1.86	0.0106	ENSMUSG00000103957	*Gm10766*	-1.26	0.0372
ENSMUSG00000087006	*Gm13889*	1.55	0.0106	ENSMUSG00000114554	*5430425K12Rik*	-1.50	0.0373
ENSMUSG00000034226	*Rhov*	1.54	0.0108	ENSMUSG00000024677	*Ms4a6b*	-1.46	0.0379
ENSMUSG00000042189	*Tekt3*	2.09	0.0111	ENSMUSG00000059606	*Rnase2b*	-3.94	0.0394

ENSMUSG00000118342		2.11	0.0115
ENSMUSG00000085912	*Trp53cor1*	1.19	0.0115
ENSMUSG00000106968	*C78283*	3.13	0.0116
ENSMUSG00000024402	*Lta*	1.62	0.0116
ENSMUSG00000027603	*Ggt7*	2.21	0.0117
ENSMUSG00000022836	*Mylk*	3.04	0.012
ENSMUSG00000026817	*Ak1*	1.06	0.0125
ENSMUSG00000103845	*Gm19026*	1.86	0.0126
ENSMUSG00000097503	*3110045C21Rik*	1.68	0.0134
ENSMUSG00000064620	*Gm22303*	1.16	0.0136
ENSMUSG00000000126	*Wnt9a*	2.75	0.0137
ENSMUSG00000052131	*Akr1b7*	1.66	0.0138
ENSMUSG00000006576	*Slc4a3*	1.33	0.0139
ENSMUSG00000000204	*Slfn4*	1.56	0.0152
ENSMUSG00000079445	*B3gnt7*	3.12	0.0153
ENSMUSG00000109829	*Gm45605*	1.84	0.0154
ENSMUSG00000044701	*Il27*	3.42	0.016
ENSMUSG00000051627	*Hist1h1e*	1.47	0.016
ENSMUSG00000021974	*Fgf9*	1.15	0.016
ENSMUSG00000095620	*2010005H15Rik*	1.58	0.0164
ENSMUSG00000114104	*Gm47585*	1.96	0.0165
ENSMUSG00000004296	*Il12b*	1.98	0.0171
ENSMUSG00000034391	*Fbxo15*	1.36	0.0171
ENSMUSG00000104168	*Gm38250*	1.27	0.0177
ENSMUSG00000052749	*Trim30b*	3.06	0.0178
ENSMUSG00000111752	*Gm38575*	1.30	0.0189
ENSMUSG00000014303	*Glis2*	1.29	0.0192
ENSMUSG00000095588	*Gm12350*	1.15	0.0194
ENSMUSG00000028037	*Ifi44*	1.65	0.0203
ENSMUSG00000001039	*B9d1*	1.01	0.021
ENSMUSG00000024352	*Spata24*	1.05	0.0215
ENSMUSG00000114255	*Gm10734*	1.86	0.0217
ENSMUSG00000079227	*Ccr5*	1.11	0.0217
ENSMUSG00000084408	*Gm11870*	1.09	0.0219
ENSMUSG00000003534	*Ddr1*	1.15	0.0227
ENSMUSG00000079037	*Prnp*	1.71	0.023
ENSMUSG00000040488	*Ltbp4*	1.50	0.0237
ENSMUSG00000069265	*Hist1h3a*	3.53	0.025
ENSMUSG00000039765	*Cc2d2a*	2.40	0.0253
ENSMUSG00000114858	*Gm5790*	1.64	0.0259
ENSMUSG00000113775	*Gm48027*	1.18	0.026
ENSMUSG00000089844	*A530032D15Rik*	1.14	0.0267
ENSMUSG00000046057	*Gm15428*	-1.55	0.0396
ENSMUSG00000118129		-1.19	0.0398
ENSMUSG00000037849	*Ifi206*	-1.60	0.0404
ENSMUSG00000040537	*Adam22*	-1.46	0.0404
ENSMUSG00000027257	*Pacsin3*	-1.64	0.0421
ENSMUSG00000083465	*Gm11652*	-2.40	0.0444
ENSMUSG00000088625	*Gm23318*	-1.51	0.0445
ENSMUSG00000054074	*Skida1*	-1.07	0.0458
ENSMUSG00000085397	*Gm13524*	-1.71	0.046
ENSMUSG00000035493	*Tgfbi*	-1.69	0.0489

ENSMUSG00000042564	*Fam227a*	1.12	0.027
ENSMUSG00000104213	*Ighd*	2.75	0.0282
ENSMUSG00000101778	*Gm29488*	3.28	0.0284
ENSMUSG00000064427	*Gm22748*	1.07	0.0284
ENSMUSG00000097104	*Gm26579*	2.11	0.0286
ENSMUSG00000090582	*Gm17024*	1.10	0.0286
ENSMUSG00000089762	*Ier5l*	1.24	0.0291
ENSMUSG00000027298	*Tyro3*	1.68	0.0297
ENSMUSG00000060550	*H2-Q7*	1.12	0.0297
ENSMUSG00000113623	*Gm48691*	2.88	0.0298
ENSMUSG00000089542	*Gm25835*	1.60	0.0299
ENSMUSG00000097216	*4932441J04Rik*	1.09	0.0306
ENSMUSG00000078503	*Zfp990*	1.41	0.0313
ENSMUSG00000047220	*Ccdc36*	1.77	0.0366
ENSMUSG00000114540	*Gm6421*	1.38	0.0367
ENSMUSG00000038067	*Csf3*	2.61	0.037
ENSMUSG00000014602	*Kif1a*	1.63	0.0372
ENSMUSG00000006784	*Ttc25*	1.09	0.038
ENSMUSG00000094338	*Hist1h2bl*	3.93	0.0385
ENSMUSG00000103343	*Gm37052*	1.30	0.0385
ENSMUSG00000040495	*Chrm4*	1.72	0.039
ENSMUSG00000002459	*Rgs20*	1.13	0.0393
ENSMUSG00000026984	*Il1f6*	1.27	0.04
ENSMUSG00000108736	*Gm45151*	1.05	0.041
ENSMUSG00000020788	*Atp2a3*	1.33	0.0411
ENSMUSG00000032033	*Barx2*	2.88	0.0433
ENSMUSG00000053141	*Ptprt*	1.63	0.0443
ENSMUSG00000061852	*Gm7582*	2.02	0.0458
ENSMUSG00000026875	*Traf1*	1.53	0.0478
ENSMUSG00000026414	*Tnnt2*	2.36	0.0487
ENSMUSG00000052485	*Tmem171*	1.00	0.0498